

**Crack Growth Behavior of Pipeline Steels under Variable Pressure Fluctuations in  
a Near-Neutral pH Environment**

by

Mengshan Yu

A thesis submitted in partial fulfillment of the requirements for the degree of

Doctor of Philosophy

in

Materials Engineering

Department of Chemical and Materials Engineering

University of Alberta

© Mengshan Yu, 2015

## **Abstract**

This research aims at understanding the crack propagation behavior of pipeline steels under variable pressure fluctuations in a near-neutral pH environment. Although pressure fluctuations have been recognized as the driving force for crack growth for more than two decades, the mechanisms governing their effects on crack growth have yet to be determined. Existing crack growth models that consider the effect of pressure fluctuations are established primarily by assuming a fatigue loading with constant stress amplitudes. This often yields a predicted life that well exceeds the service lifetime observed in the field. We believe that the significant discrepancies between laboratory findings and field observations could be bridged by modeling crack growth through a consideration of variable amplitude fatigue loadings, which are the conditions in the field.

This investigation has focused on the evaluation of a variable amplitude fatigue waveform consisting of cycles with higher R ratios (minimum stress/maximum stress), termed as minor cycles, and periodic underload cycles with lower R ratios. Such a waveform is typical for the pressure fluctuations in pipeline discharge sections, which was performed both in air and in near-neutral pH solution. Compared with the corresponding constant amplitude loadings, the variable amplitude waveform significantly enhanced fatigue crack growth. The waveform was varied to study the effects of various contributing factors, including loading frequency, maximum stress intensity factor, number of minor cycles, and amplitudes of underload and minor cycles.

By comparing results in near-neutral pH solution with that in air, the role of hydrogen and corrosion in crack growth was characterized and clearly defined.

The obtained results agree with various failure scenarios found in the field, including the high frequency of failures found at the discharge sections of pipelines, and the different crack growth characteristics between oil pipelines and gas pipelines. Based on these findings, practical strategies were proposed for avoiding accelerated crack growth.

## Preface

Part of this thesis involved research collaboration: *Section 3.4.2.2 - Theoretical prediction of critical frequency for hydrogen embrittlement* in Chapter 3 and *Appendix A* were performed by Xiao Xing and Dr. Hao Zhang. Dr. Hao Zhang is the supervisor of Xiao Xing who is a PhD Candidate in Department of Chemical and Materials Engineering, University of Alberta. All other parts of this thesis are the original work of Mengshan Yu.

## Acknowledgments

First of all, my sincerest appreciation goes to my supervisor, Prof. Weixing Chen, for his extraordinary tolerance and patience, systematical guidance and continuous encouragement throughout my studies. I would also like to express many thanks to Dr. Reg Eadie and Dr. Hao Zhang for their valuable discussions. I acknowledge the members of the examining committee, Dr. Thomas R. Jack, Dr. Douglas Ivey, Dr. Jingli Luo, and Dr. Hao Zhang. Special thanks to examining committee chair Dr. Leijun Li.

I'm grateful for the in-time department supports from Lily Laser, Walter Boddez, James McKinnon, Herb Green, Kevin Heidebrecht, Nathan Gerein and George Braybrook. I appreciate my colleagues, Dr. Abdoulmajid Eslami, Dr. Tianfei Wang, Dr. Ziqiang Dong, Dr. Jiaxi Zhao, Dr. Hao Li, Mr. Brett Conrad, Miss Karina Chevil, Miss Zeynab Shirband, Mr. Xiao Xing, Mr. Devin Engel and many others for their kind help during this research. I would especially like to thank Dr. Yongwang Kang, who was a postdoctoral faculty member in the department, for his patient mentoring at the beginning of my studies.

I would like to thank the Natural Science and Engineering Research Council (NSERC), TransCanada Pipeline Limited, Spectra Energy, and the Pipeline Research Council International (PRCI) for financial support.

Last but not the least, special thanks go to my parents, Guangxia Yu and Chunhuan Wang, and brother, Mengyun Yu, for all that they have done and continue to do for me.

# Table of Contents

<b>Chapter 1 Introduction.....</b>	<b>1</b>
<b>1.1 Oil and Gas Transmission Pipelines.....</b>	<b>2</b>
<b>1.2 Stress Corrosion Cracking (SCC) .....</b>	<b>3</b>
1.2.1 High pH SCC .....	6
1.2.2 Near-neutral pH stress corrosion cracking (NNpHSCC).....	6
1.2.2.1 Study of corrosion.....	7
1.2.2.2 Study of mitigating external corrosion .....	7
1.2.2.3 Study of materials .....	9
1.2.2.4 Study of crack initiation.....	10
1.2.2.5 Study of crack propagation .....	10
<b>1.3 Corrosion Fatigue in Near-Neutral pH Environments.....</b>	<b>13</b>
1.3.1 Parameters affecting crack propagation.....	14
1.3.1.1 Stress intensity factor range $\Delta K$ .....	14
1.3.1.2 Maximum stress intensity factor $K_{max}$ .....	18
1.3.1.3 Loading frequency .....	20
1.3.1.4 Hydrogen embrittlement.....	21
1.3.2 Available corrosion fatigue models in near-neutral pH environments .....	22
1.3.2.1 Paris Law .....	22
1.3.2.2 Crack tip strain rate model.....	22
1.3.2.3 Superposition model .....	23
1.3.2.4 Combined factor .....	24

<b>1.4 Variable Amplitude (VA) Fatigue .....</b>	<b>27</b>
1.4.1 Overload cyclic loadings - retardation effect.....	31
1.4.2 Underload cyclic loadings – acceleration effect .....	33
1.4.2.1 Number of minor cycles .....	34
1.4.2.2 Maximum stress.....	36
1.4.2.3 Amplitudes of large (underload) and minor cycles .....	37
1.4.2.4 Environments.....	38
<b>1.5 Mechanisms of Load Interactions .....</b>	<b>39</b>
1.5.1 Crack closure .....	39
1.5.2 Residual stress.....	41
1.5.3 Strain hardening/softening.....	42
1.5.4 Dislocation substructure changes.....	42
<b>1.6 Challenges in Crack Growth Study of Pipeline Steels Exposed to NNpH Environments .....</b>	<b>43</b>
<b>1.7 Research Objectives and Thesis Structure .....</b>	<b>46</b>
<b>References .....</b>	<b>47</b>
<b>Chapter 2 Depressurization-Induced Crack Growth Enhancement for Pipeline Steel Exposed to a Near-Neutral pH Environment.....</b>	<b>62</b>
<b>2.1. Introduction.....</b>	<b>62</b>
<b>2.2 Experimental .....</b>	<b>66</b>
2.2.1 Specimen and near-neutral pH solution.....	66
2.2.2 Loading conditions.....	69
2.2.2.1 Constant amplitude cyclic loading.....	69

2.2.2.2 Variable amplitude cyclic loading .....	70
<b>2.3 Results and Discussion.....</b>	<b>72</b>
2.3.1 The role of minor cycles .....	72
2.3.3 Crack growth behavior at different frequencies.....	75
2.3.3.2 Variable amplitude cyclic loading .....	77
<b>2.4 Practical Strategies for Avoiding Enhanced Crack Growth.....</b>	<b>80</b>
<b>2.5 Conclusions.....</b>	<b>81</b>
<b>References .....</b>	<b>82</b>
<b>Chapter 3 Crack Growth Behavior of Pipeline Steel Exposed to a Near-Neutral pH Environment under Variable Pressure Fluctuations: Effects of Loading</b>	
<b>Frequency .....</b>	<b>86</b>
<b>3.1 Introduction.....</b>	<b>86</b>
<b>3.2 Experimental .....</b>	<b>92</b>
3.2.1 Materials and environment .....	92
3.2.2 Mechanical loading conditions .....	93
3.2.2.1 Effect of loading frequency .....	94
3.2.2.2 Effect of maximum stress .....	96
3.2.3 Determination of crack growth rate .....	96
<b>3.3 Results .....</b>	<b>97</b>
3.3.1 Frequency dependence of crack growth rate under constant amplitude cyclic loading.....	97
3.3.2 Frequency dependence of crack growth rate under variable amplitude cyclic loading.....	101

3.3.3 $K_{max}$ dependence of crack growth rate .....	102
<b>3.4 Discussion.....</b>	<b>103</b>
3.4.1 Acceleration effect caused by underload .....	103
3.4.2 Role of corrosive near-neutral pH environments.....	107
3.4.2.1 Observation of critical frequency .....	108
3.4.2.2 Theoretical prediction of critical frequency for hydrogen embrittlement .....	110
3.4.2.3 Understanding the effect of frequency on crack growth behavior.....	114
3.4.2.4 Understanding the effect of maximum stress on crack growth behavior	118
3.4.3 Study results applied to real cracking in the field.....	118
<b>3.5 Conclusions.....</b>	<b>122</b>
<b>References .....</b>	<b>123</b>
<b>Chapter 4 Crack Growth Behavior of Pipeline Steel Exposed to a Near-Neutral pH Environment under Variable Pressure Fluctuations: Effects of Number of Minor Cycles.....</b>	<b>127</b>
<b>4.1 Introduction.....</b>	<b>127</b>
<b>4.2 Experimental .....</b>	<b>131</b>
4.2.1 Materials and preparation of specimen .....	131
4.2.2 Tests in near-neutral pH solution.....	132
4.2.3 Tests in air.....	135
4.2.4 Determination of crack growth rate and acceleration factor.....	136
<b>4.3 Results .....</b>	<b>137</b>
4.3.1 Tests in air.....	137

4.3.1.1 Constant amplitude test.....	138
4.3.1.2 Periodic underload test.....	140
4.3.2 Periodic underload test in C2 solution.....	143
<b>4.4 Discussion.....</b>	<b>148</b>
4.4.1 The role of minor cycles in fatigue crack propagation .....	149
4.4.2 The role of environments in fatigue crack propagation .....	151
4.4.3 Mechanisms of acceleration effect induced by underloads .....	153
4.4.4 Understanding the field crack behaviors in NNpHSCC .....	156
<b>4.5 Conclusions.....</b>	<b>158</b>
<b>References .....</b>	<b>159</b>
<b>Chapter 5 Crack Growth Behavior of a Pipeline Steel Exposed to a Near-Neutral pH Environment under Variable Pressure Fluctuations: Effects of Amplitudes ...</b>	<b>163</b>
<b>5.1 Introduction.....</b>	<b>163</b>
<b>5.2 Experimental .....</b>	<b>168</b>
5.2.1 Materials and environment .....	168
5.2.2 Determination of crack growth rate and acceleration factor.....	170
5.2.3 Mechanical loading conditions .....	171
<b>5.3 Results .....</b>	<b>173</b>
5.3.1 Dependence of crack growth rate on R ratio of underload .....	173
5.3.2 Dependence of crack growth rate on R ratio of minor cycles.....	175
5.3.3 Dependence of acceleration factor on amplitude ratio .....	180
<b>5.4 Discussion.....</b>	<b>182</b>
5.4.1 Enhanced crack growth rate by underload.....	182

5.4.2 Reduced corrosion fatigue threshold by underload .....	184
5.4.3 Effects of environments on crack growth behaviors.....	186
5.4.4 Understanding NNpHSCC crack growth.....	191
<b>5.5 Conclusions.....</b>	<b>192</b>
<b>References .....</b>	<b>193</b>
<b>Chapter 6 Crack Growth Behavior of a Pipeline Steel Exposed to a Near-Neutral pH Environment under Variable Pressure Fluctuations: the Role of Hydrogen ...</b>	<b>198</b>
<b>6.1 Introduction.....</b>	<b>198</b>
<b>6.2 Experimental .....</b>	<b>202</b>
6.2.1 Environment.....	202
6.2.2 Specimen.....	203
6.2.3 Mechanical loading conditions .....	205
6.2.4 Observation of crack growth, widening and fracture surface .....	206
<b>6.3 Results and Discussion.....</b>	<b>207</b>
6.3.1 Determination of crack growth rate .....	207
6.3.2 Characterization of crack width .....	211
6.3.3 Fracture surface observation .....	216
6.3.4 Process of crack propagation in near-neutral pH environments .....	222
6.4 Conclusions.....	226
<b>References .....</b>	<b>227</b>
<b>Chapter 7 Conclusions, research impact and recommendations .....</b>	<b>232</b>
<b>7.1 Conclusions.....</b>	<b>232</b>
7.1.1 Observation of acceleration effect .....	233

7.1.2 Effects of number of minor cycles on crack growth.....	233
7.1.3 Effects of frequency and maximum stress on crack growth .....	234
7.1.4 Effects of amplitudes of underload and minor cycles on crack growth.....	235
7.1.5 The role of hydrogen in crack growth in near-neutral pH environments .....	235
7.1.6 Practical strategies for avoiding enhanced crack growth.....	236
<b>7.2 Research Impact.....</b>	<b>237</b>
<b>7.3 Recommendations .....</b>	<b>238</b>
<b>Appendix A .....</b>	<b>240</b>
<b>References .....</b>	<b>243</b>
<b>References .....</b>	<b>245</b>

## List of figures

Figure 1.1	Causes, by percent, of NEB-regulated pipeline ruptures [7].....	3
Figure 1.2	Definition of stress corrosion cracking (SCC).....	4
Figure 1.3	Failure of an oil pipeline 800 m downstream of a pump station [11].....	5
Figure 1.4	Schematic showing disbonded coating on pipe surface and reduced cathodic protection toward the bottom of a disbonded holiday [5].....	9
Figure 1.5	Typical morphology of a dormant crack found in a buried pipeline steel exposed to a near-neutral pH soil-water solution in the field [5] .....	11
Figure 1.6	Typical stages of crack growth of pipeline steels exposed to near-neutral pH environments—Bathtub Model. ....	12
Figure 1.7	Pressure fluctuations recorded for a high-pressure gas transmission pipeline .....	13
Figure 1.8	Diagram showing three regimes of fatigue crack growth response.....	15
Figure 1.9	Crack growth rate as a function of $\Delta K$ in near-neutral pH solutions (other conditions may vary) .....	17
Figure 1.10	Crack growth rate as a function of $K_{\max}$ in near-neutral pH solutions (other conditions may vary) .....	19
Figure 1.11	Crack growth rate as a function of loading frequency in near-neutral pH solutions (other conditions may vary) .....	19
Figure 1.12	Correlation of combined factor with crack growth rate in near-neutral pH solutions [4] .....	27

Figure 1.13	Basic loading waveforms in variable amplitude fatigue test (a) overload, (b) underload .....	28
Figure 1.14	Schematic of delayed retardation of crack growth following a single overload .....	30
Figure 1.15	Variables in underload waveform .....	33
Figure 1.16	Effect of the number of minor cycles per block on the acceleration factor (other conditions may vary).....	35
Figure 1.17	Effect of maximum stress on acceleration factor (other conditions may vary).....	36
Figure 1.18	Effect of amplitude ratio on the acceleration factor (other conditions may vary).....	37
Figure 1.19	Effects of environments on acceleration factor [88] .....	39
Figure 1.20	Changes in crack opening stress level after a) overload [91]; and b) underload [77].....	40
Figure 1.21	Spectra of an oil pipeline: OA discharge part; and OB suction part .....	45
Figure 2.1	Pressure fluctuations recorded for a high-pressure gas transmission pipeline .....	64
Figure 2.2	Basic loading waveforms in variable amplitude fatigue test .....	65
Figure 2.3	SEM image (secondary electron SE) of pipeline steel microstructures in the transverse section.....	67
Figure 2.4	Dimension of compact tension (CT) specimen used in the testing .....	67
Figure 2.5	Loading waveform applied in the variable amplitude cyclic loading in C2 solution.....	69

Figure 2.6	Crack propagation response under different loading waveforms in C2 solution.....	71
Figure 2.7	SEM images (SE) of fractured surface of specimens in C2 solution, crack propagating from left to right: a) constant amplitude test; and b) variable amplitude test .....	74
Figure 2.8	Crack growth behavior at different frequency for both constant and variable amplitude cyclic loadings in C2 solution .....	76
Figure 2.9	The crack tip morphology (backscatter electron detector BSD) on the middle plane in the thickness direction on the samples of variable amplitude tests at different frequencies. The arrow marks the position of the pre-cracking tip before test (by comparing with the images taken before test).....	80
Figure 3.1	Pressure fluctuations recorded for a high-pressure gas transmission pipeline (SCADA data).....	92
Figure 3.2	Variable amplitude fatigue waveform designed to simulate the pressure fluctuations in Figure 3.1 .....	94
Figure 3.3	Frequency dependence of constant amplitude crack growth rate in C2 solution and in air.....	100
Figure 3.4	Frequency dependence of variable amplitude crack growth rate in C2 solution and in air.....	100
Figure 3.5	$K_{max}$ dependence of variable amplitude crack growth rate in C2 solution and in air.....	102
Figure 3.6	SEM images showing the striations observed on the specimens after testing in C2 solution: a) under constant amplitude loading; and b) under variable	

	amplitude loading with 300 minor cycles (crack propagation from left to right) [23] .....	105
Figure 3.7	Crack growth rate under different loading frequency of underload: a) in air; and b) in C2 solution .....	106
Figure 3.8	Crack growth rate under different $K_{max}$ : a) in air; and b) in C2 solution...	107
Figure 3.9	A schematic showing hydrogen diffusion from the annulus region with an outer radius $R_{eq}$ to a circular region with the radius $r_p$ ( $r_p$ is the plastic zone size).....	111
Figure 3.10	Understanding crack growth behavior of gas and oil pipelines exposed to near-neutral pH environments. $n$ is the number of minor cycles per block. ....	121
Figure 4.1	(a) Pressure fluctuations recorded for a high-pressure gas transmission pipeline; (b) designed test waveform.....	130
Figure 4.2	Comparison of crack growth rate under different waveforms to demonstrate the importance of minor cycles in the crack growth in C2 solution [18] ..	131
Figure 4.3	Variation of crack growth rate with variable R ratios in air. The tests were performed at $K_{max} = 33$ and frequency = 0.5 Hz.....	139
Figure 4.4	Results of periodic underload tests in air: (a) measured and predicted crack growth rates; and (b) variation of acceleration factor with the number of minor cycles per block.....	142
Figure 4.5	Results of periodic underload tests in C2 solution: (a) measured and predicted crack growth rates; and (b) variation of acceleration factor with the number of minor cycles per block .....	144

Figure 4.6	SEM images (SE) showing the striations observed on the fractured surface of the specimens tested under different numbers of minor cycles per block in solution (crack propagated from left to right) .....	147
Figure 4.7	Crack tip morphology on the middle plane in the thickness direction for specimens tested at a different number of minor cycles per block (n) in C2 solution .....	148
Figure 4.8	Growth rate of minor cycles in C2 solution and in air .....	150
Figure 4.9	Ratio of data in C2 solution over that in air for measured growth rate and calculated minor cycle growth rate.....	152
Figure 5.1	Normalized pressure fluctuations recorded for a high-pressure gas transmission pipeline (SCADA data) .....	166
Figure 5.2	Crack propagation response under different loading waveforms in C2 solution [24].....	167
Figure 5.3	Variable amplitude fatigue waveform designed to simulate the pressure fluctuations in Figure 1 .....	172
Figure 5.4	Crack growth behaviors of test of R ratio of underload in air: a) crack growth rate; and b) acceleration factor .....	174
Figure 5.5	Crack growth behaviors of test of R ratio of underload in C2 solution: a) crack growth rate; and b) acceleration factor .....	177
Figure 5.6	Crack growth behaviors of test of R ratio of minor cycles in air: a) crack growth rate; and b) acceleration factor - R ratio of minor cycles; and c) acceleration factor – amplitude ratio .....	179

Figure 5.7	Crack growth behaviors of test of R ratio of minor cycles in C2 solution: a) crack growth rate; and b) acceleration factor – R ratio of minor cycles; and c) acceleration factor – amplitude ratio .....	182
Figure 5.8	Comparison of crack growth in solution and in air: a) R ratio of underload; and b) R ratio of minor cycles .....	188
Figure 5.9	Ratio of crack growth rate in C2 solution over that in air: a) R ratio of underload; and b) R ratio of minor cycles .....	189
Figure 5.10	A schematic showing the mechanism of crack propagation in pipeline steels exposed to near-neutral pH environments under pressure fluctuations.....	191
Figure 6.1	Experimental (a) surface treated compact tension specimen; and (b) variable amplitude waveform: $K_{max} = 33 \text{ MPa}\sqrt{\text{m}}$ , R ratio of minor cycles = 0.9, R ratio of underload =0.5, frequency of minor cycles = 0.00538 Hz, frequency of underload =0.0000278 Hz (10 h/cycle), number of minor cycles per block $n = 1000$ .....	204
Figure 6.2	SEM images (BSD) of crack morphologies of specimens after tests (crack propagation from left to right): a) on surface (the arrow marks the pre-cracking tip before loading); and b) in the middle .....	208
Figure 6.3	(a) Measured crack growth rate; and (b) effects of number of minor cycles on crack growth rate in C2 solution and in air [42]. The data in the current investigation were shown as colored dots. ....	209
Figure 6.4	Fracture surface images (SE) in the middle (crack propagation). The marked zone is the crack growth (from left to right) during the test. Eleven blocks	

	were applied to the coated specimen in solution at $n = 2000$ , while 17 blocks were performed for others. ....	210
Figure 6.5	Measured crack width behind pre-cracking tip .....	214
Figure 6.6	Comparison of stress-strain curves of an X70 pipeline steel with and without hydrogen charging [45].....	215
Figure 6.7	Fracture surface images near the crack tip after tests (crack propagation from left to right). The insert is a magnified view of the fracture surface. Quasi-cleavage can be seen in the coated specimens. ....	218
Figure 6.8	Observation of fractured surface in Figure 6 (d) at different orientations (SE) The blue square is the reference (the same area) at difference orientations. ....	220
Figure 6.9	Illustration showing the “fish ladder” formation during crack propagation (from left to right).....	221
Figure 6.10	Illustration showing the crack widening behind the pre-cracking tip due to mechanical loading, HELP and corrosion during the corrosion fatigue test	224
Figure 6.11	Comparison of the crack growth rate and corrosion rate in near-neutral pH solutions under variety of loading conditions.....	226

## List of tables

Table 2.1	Summary of tests performed with constant and variable amplitude loading	68
Table 3.1	Crack growth rate obtained at different frequencies and maximum stress in this investigation .....	99
Table 4.1	Chemical compositions of C2 solution .....	133
Table 4.2	Results of periodic underload tests in air .....	141
Table 4.3	Results of periodic underload tests in C2 solution.....	145

# Chapter 1 Introduction

Near-neutral pH stress corrosion cracking (NNpHSCC) was first identified in 1985 through the examination of failed pipe sections [1]. Despite decades of research, its mechanisms are still not fully understood and it continues to be a major threat to oil and gas transmission pipelines worldwide. The pipeline failures cause significant economic loss, environmental pollution and/or casualties.

The characteristics of NNpHSCC are very different from the classic high pH stress corrosion cracking (SCC) that has been extensively studied since the 1960s. NNpHSCC is characterized by wide transgranular cracking in a dilute carbonate-bicarbonate electrolyte with a pH value in the range of 5.5 to 8.5 [2]. The extensive investigations in such simulated near-neutral pH environments show that the crack growth rate under the static tensile stress is too low to be a concern, and thereafter the pressure fluctuations during pipeline routine operations are recognized as the driving force for crack propagation [2, 3]. It has been proven that NNpHSCC cracking occurs through mechanisms of corrosion fatigue [4,5].

However, dilemmas still exist between the established corrosion fatigue models and field findings. For example, the lifetime predicted by these models is much longer than the actual service life of the pipelines with SCC, and there is a wide range of service lives found in the field, which varies significantly from section to section. This might be

caused on one hand by the complex field conditions, and on the other hand by insufficient understanding/consideration of the key factors affecting crack growth. One of the key discrepancies is that constant amplitude cyclic loadings have been applied in laboratory tests, while random pressure fluctuations occur in the field. It is well established that the crack growth behavior under variable amplitude fatigue is very different from that under constant amplitude fatigue. This could be one of the key reasons why the lifetime of a pipeline steel experiencing NNpHSCC is shorter than that predicted by those established models.

The following sections will provide a comprehensive review of literature pertinent to this area of research, especially those areas related to the crack growth behavior of pipeline steels in near-neutral pH environments under constant and variable amplitude cyclic loading conditions.

## **1.1 Oil and Gas Transmission Pipelines**

Alberta, Canada, is one of the major producers of oil and gas in the world. In 2012, Alberta produced 3.7 trillion cubic feet of natural gas, 705 million barrels of crude bitumen, and 203 million barrels of crude oil, most of which was transported through pipelines [6]. Of the more than 450,000 kilometers of buried oil and gas transmission pipelines crisscrossing the province in 2012, about 86% of which were constructed of steels [6].

However, the occurrence of pipeline failures is the risk, economic loss and environmental pollutions. Leaking and ruptures are the two common natural failures. Compared with leakage, pipe ruptures caused by SCC lead to more severe results.

According to the data on the Canadian National Energy Board (NEB)-regulated pipelines, between 1991 and 2007 [7], more than one-third of the ruptures were caused by cracking, as can be seen in Fig. 1.1. Understanding the mechanisms of cracking could significantly help to improve the pipeline integrity management. SCC has been recognized as the primary cause of cracking in high-pressure gas and oil transmission lines since 1960 [8], which will be further reviewed in the following sections.

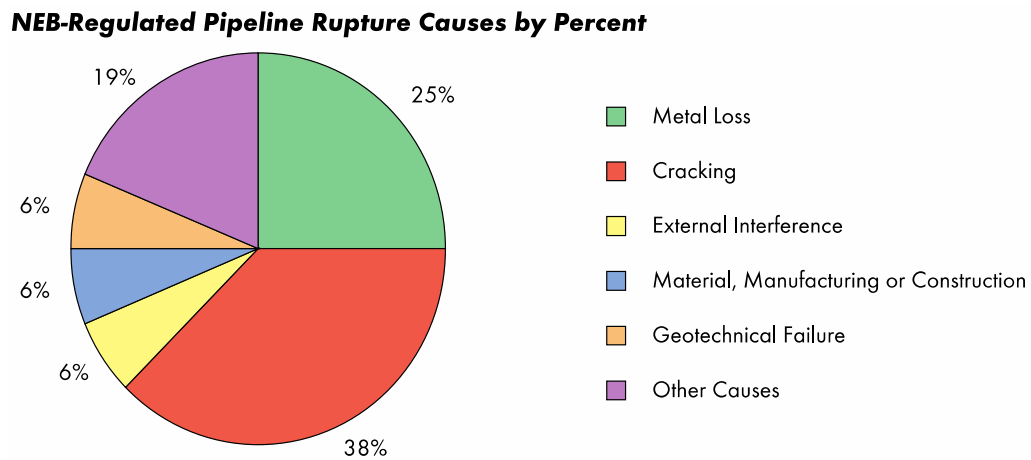


**Figure 1.1 Causes, by percent, of NEB-regulated pipeline ruptures [7]**

## **1.2 Stress Corrosion Cracking (SCC)**

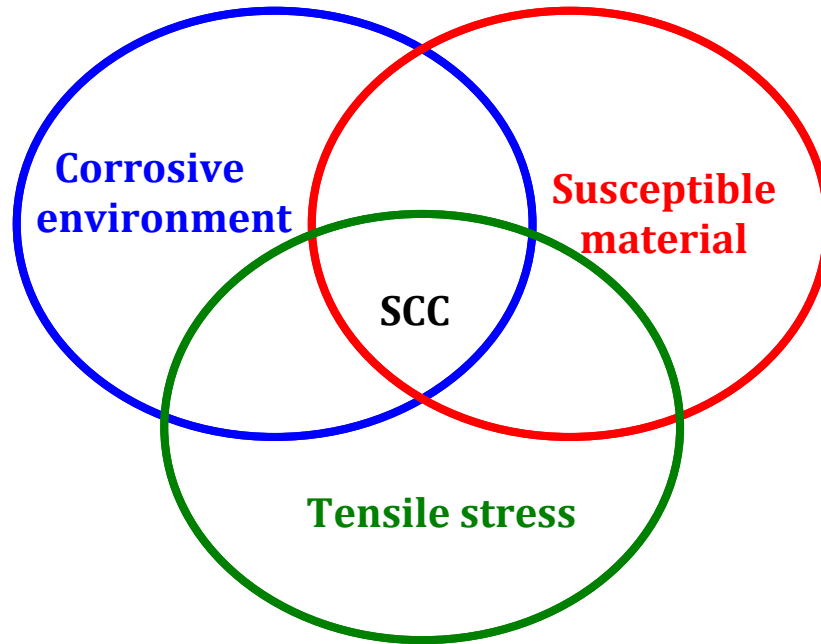


**Figure 1.2 Definition of stress corrosion cracking (SCC)**

SCC is defined as the growth of cracks due to the synergistic effects of non-cyclic tensile stress, a corrosive environment, and susceptible materials [9], as shown in Fig. 1.2.

Usually pipelines are coated with polyethylene (PE), asphalt or fusion bond epoxy to prevent corrosion before being buried underground. However, these coatings can become damaged by external forces and /or disbonded due to the degradation of the coating itself [10]. The damage allows ground water to access the pipe surface and become trapped inside the coating disbondment. If sufficient cathodic potential cannot be applied to this particular location, the pipeline steel will corrode. In addition, the pipelines are operated under high pressure and the steels are susceptible to corrosion by ground water. As a result, SCC occurs. Fig. 1.3 is an example of a pipeline that ruptured due to stress corrosion cracking [11].



**Figure 1.3**                      **Failure of an oil pipeline 800 m downstream of a pump station**  
**[11]**

Based on the range of pH values of the electrolytes at the pipeline surface, SCC of pipeline steels can be categorized as high pH SCC (classical SCC or Intergranular SCC), and near-neutral pH SCC (low pH SCC or Transgranular SCC). Detailed comparisons of these two kinds of SCC was made by R. N. Parkins [2] and John A. Beavers [12]. Concise introduction of the characteristics of the two kinds of SCC will be illustrated below.

### **1.2.1 High pH SCC**

The high pH SCC was first reported in the 1960s [8]. It is characterized as intergranular cracking in concentrated carbonate-bicarbonate soil solutions with pH values above 8.5 [1,8]. In such environments, the cracks propagate in a repeated process of film formation and rupture along the grain boundaries due to the galvanic effect (different potentials between grain boundaries and grain material [13]) under stress, and the passive film is also formed along the crack walls to protect the crack crevice from corrosion [2]. As a result, a sharp and deep SCC crack is seen. It can be reproduced in the laboratory testing environments and thus it is thought to be well understood. This kind of SCC can be controlled by reducing the pipe temperature and controlling the pipe electrochemical potential range [2].

### **1.2.2 Near-neutral pH stress corrosion cracking (NNpHSCC)**

NNpHSCC was first reported in 1985 after an examination of the failed pipe sections [1]. The main characteristics of NNpHSCC is transgranular cracking in a dilute carbonate-bicarbonate soil solution with a pH value in the range of 5.5 to 8.5 [1,2]. As the passive film is not observed in such near-neutral pH solutions, an initially sharp crack will gradually turn into a wide and dormant crack or pitting, as observed in the oil or gas field pipelines [14,15]. Despite decades of research, the mechanisms of NNpHSCC are still open to debate. The work on NNpHSCC will be the focus of this investigation and it will

be further reviewed below in terms of near-neutral pH corrosion, crack initiation and crack propagation.

### **1.2.2.1 Study of corrosion**

The corrosion of pipeline steels occurs when ground water gains access to the pipeline surface after coating disbondment/damage, especially at locations where a sufficient cathodic potential is not reached. The corrosion rate of pipeline steels exposed to near-neutral pH environments is relatively low and could be affected by a number of factors. Flat coupon tests have shown that the general corrosion rate of pipeline steels is about  $1.6 \times 10^{-9}$  mm/s (0.05 mm/year) in a near-neutral pH solution bubbled with 5% CO<sub>2</sub> balanced with N<sub>2</sub> gas [16]. The general corrosion rate could be affected by the CO<sub>2</sub> level [1], temperature [1], soil condition [1], cathodic protection [17], disbondment size [16], position relative to the disbondment open mouth [16], and coating type [1,2,18]. The tape coating disbondment size was well correlated to the corrosion rate of the field data [18]. Although the general corrosion rate, typically 0.05 mm/year, is so low that it may not be an engineering concern, corrosion plays an important role in crack initiation when combined with stress and also in crack propagation through the effects of hydrogen, the by-product of corrosion, which will be described in Section 1.3.1.4.

### **1.2.2.2 Study of mitigating external corrosion**

a) Coating: For the buried pipeline, the protective coating is the first line of defense against external corrosion. However, the coating protection efficiency may be reduced by poor adhesion, mechanical damage, or the aging process, resulting in coating disbondment and thus SCC [19]. Different types of coating affect the magnitude of SCC damage. It was found that even when the epoxy coating and coal tar coating are damaged, cathodic potential (which will be introduced in the following section) can still reach the pipe surface and protect the pipe from corrosion and SCC [20]. On the other hand, near-neutral pH SCC usually occurs under PE and asphalt tape-coated disbondments where cathodic potential (CP) protection is not effective due to the fact that CP cannot reach the bottom of the disbondment (because of the electrolyte conductivity) to protect steel from corrosion due to the geometrical limitation [1,10,21]. The corrosion under PE and asphalt types of coatings in the field was discussed and well correlated to the disbondment size and position relative to the open mouth in laboratory testing [18].

b) Cathodic protection: To mitigate the external corrosion of pipeline steels exposed to ground water solutions after coating disbondment, the pipe can be hooked up to a rectifier and a CP can be applied to prevent corrosion. Applying CP could also lead to an increase in the pH of the electrolyte inside the disbondment and passivate the steel in an alkaline environment [22,23]. The effectiveness of CP depends on several variables, such as steel surface condition and the potential at the coating disbondment [24], alternating current (AC) [25], and coating crevice length [21]. If sufficient CP is not able to reach the bottom of disbondment as shown in Fig. 1.4 [5], NNpHSCC is believed to occur at the pipe

surface. In 2013, the Canadian Gas Association recommended the appropriate practice to control external corrosion [26].

### 1.2.2.3 Study of materials

Pipe steel of all grades are found to be susceptible to NNpHSCC [10]. These steels include American Petroleum Institute (API) X52 [27], X60 [28], X65 [4,5], X70 [29], X80 [30], and X100 [31] (Strong grades have the designation X followed by the specified minimum yield strength, SMYS, measured in ksi), and they vary in strength and microstructure. It is hard to determine which pipe grades are more susceptible to NNpHSCC [32].

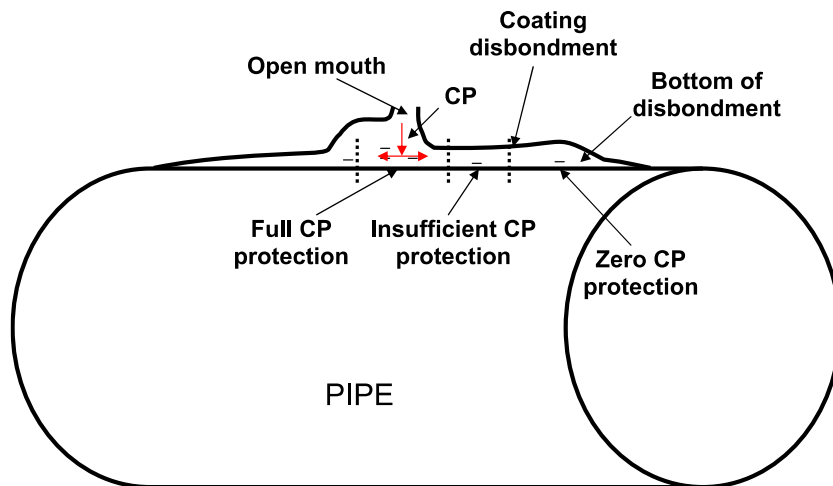


**Figure 1.4 Schematic showing disbonded coating on pipe surface and reduced cathodic protection toward the bottom of a disbonded holiday [5]**

#### **1.2.2.4 Study of crack initiation**

Corrosion at selected locations on the pipe surface can lead to the formation of corrosion pits. The pits could act as stress raisers and cause the formation of micro-cracks at the bottom of the pits. Various mechanisms of crack initiation for NNpHSCC were proposed and summarized in Ref. [5]. Recently, a novel testing setup capable of simulating the synergistic effects of coating disbondment, cathodic protection and cyclic loading on NNpHSCC crack initiation was designed and systematically implemented [33]. Stress, time and the level of CP were found to be the three important factors for increasing the possibility of near-neutral pH SCC crack initiation: old pipes with high levels of stress fluctuations and insufficient (but not totally lacking) CP were more prone to SCC initiation.

#### **1.2.2.5 Study of crack propagation**

From the statistical analysis of thousands of crack colonies, it has been found that 95% of the initiated cracks have a blunt tip, as shown in Fig. 1.5 [5]. Cracks with such a crack tip morphology are considered to be dormant. They are usually less than 1 mm deep and have very small depth/length aspect ratios, around 0.1-0.2. The reason the initiated cracks become dormant is because dissolution at the crack tip and crack wall occurs simultaneously (no passive film formed in NNpH environments as stated before). However, the remaining 5% of cracks can grow continuously or repeatedly, leading to pipeline rupture [5]. Such a process could be described by a modified Bathtub Model

shown in Fig. 1.6. The crack growth rate for the initiated short crack decreases with time to a dormant state. Most of the cracks will be in dormant state until a critical condition is achieved. And then the crack growth rate is enhanced significantly, by the Parkin's Bathtub Model. However, the crack growth rate suddenly increased is nonsense and there should be process for crack growth. Therefore, the model is revised as the blue line in Fig. 1.6.

But one critical question has not been answered: what causes the 5% of the crack population to grow continuously, thus causing the pipe to rupture, while the others become dormant?

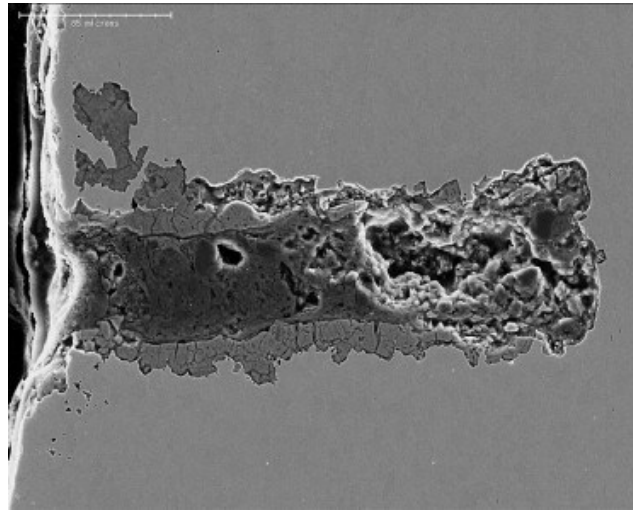


**Figure 1.5** Typical morphology of a dormant crack found in a buried pipeline steel exposed to a near-neutral pH soil-water solution in the field [5]

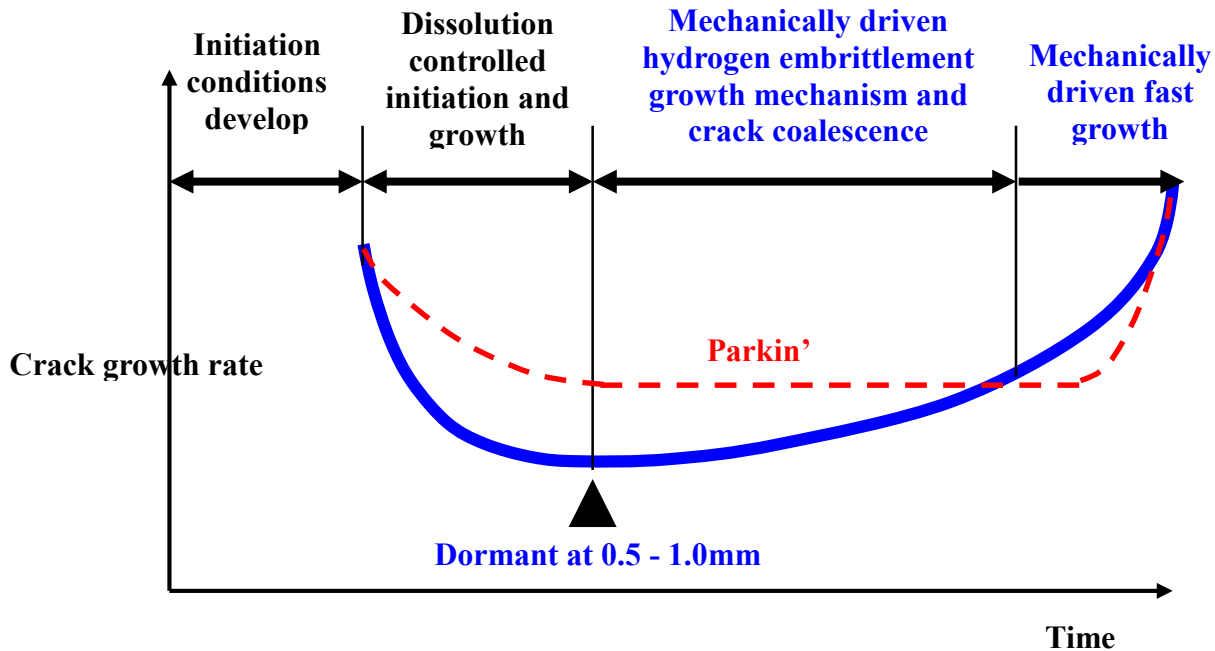


**Figure 1.6 Typical stages of crack growth of pipeline steels exposed to near-neutral pH environments—Bathtub Model.**

Stress is suspected to be the key reason as the steel and environment may be the same within tens of kilometers. The designed pipe hoop stress is usually about 75% of the SMYS. Fig. 1.7 is a typical pressure spectrum from a high-pressure gas transmission pipeline. The spectrum consists of small fluctuations at high R ratios (minimum stress/maximum stress) most of the time. Such minor pressure fluctuations are usually treated as static loading, creating ideal conditions for stress corrosion cracking. However, crack propagation has never been observed under a static loading condition in laboratory testing, even at the high stress intensity factor, except for the initiation of a crack where galvanic corrosion may be predominant [2,4,5]. Even an active crack often ceases to grow under a static hold [5]. In contrast, crack growth is found to grow under cyclic loading above the critical fatigue threshold [1,10].

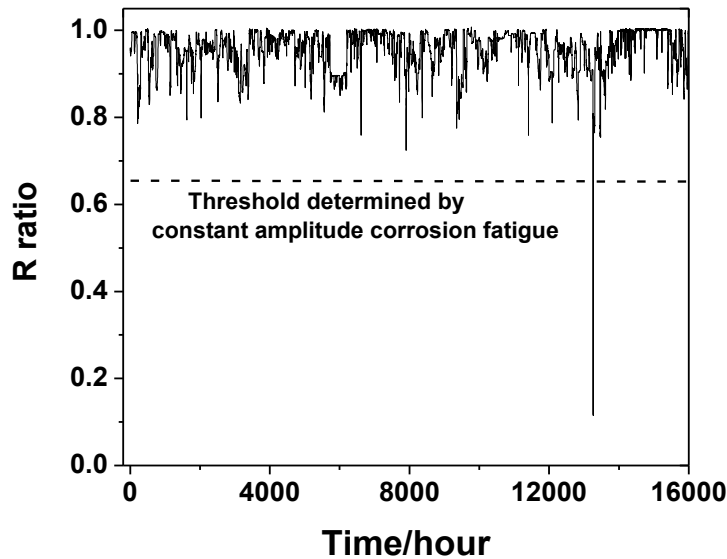


**Figure 1.7** Pressure fluctuations recorded for a high-pressure gas transmission pipeline

### **1.3 Corrosion Fatigue in Near-Neutral pH Environments**

When re-examining the actual pressure spectra obtained from field oil/gas pipelines, it is found that the routine operation pressures are not static as was thought during laboratory testing. Instead, pressure fluctuates randomly during routine operations. These fluctuations may result from planned start/stop, batch pigs passing pump stations, mid-point injections, viscosity changes due to commodity transitions, flow rate changes, and unplanned line outages [34]. Thus, the pressure fluctuations, or cyclic loadings (fatigue), are proposed as the crack propagation driving force [2,3,35], under which the crack

propagation threshold is reduced significantly from non-cyclic SCC [ 36 ]. The combination of the corrosive near-neutral pH environment and fatigue, a scenario of corrosion fatigue instead of SCC, is responsible for crack growth. It has been determined that the NNpHSCC crack growth behavior is consistent with corrosion fatigue mechanisms, even though it was initially termed SCC [4,5]. Corrosion fatigue in the near-neutral pH environment is the main focus in this investigation and therefore the current understanding of corrosion fatigue mechanisms in near-neutral pH environments will be reviewed in the following sections.

Since pressure fluctuations are recognized as the crack propagation driving force, constant amplitude cyclic loading tests have been performed in corrosive near-neutral pH solutions to elucidate the mechanisms of cracking. The effects of fluctuation amplitude (related to stress intensity factor range  $\Delta K$ , or R ratio when  $K_{\max}$  is constant), maximum stress intensity factor  $K_{\max}$ , loading frequency, and hydrogen effects on crack propagation have been studied. Several models have been also proposed to attempt to incorporate the laboratory testing observations and field findings.

### **1.3.1 Parameters affecting crack propagation**

#### **1.3.1.1 Stress intensity factor range $\Delta K$**

The stress intensity factor range,  $\Delta K$  ( $\Delta K=K_{\max}-K_{\min}$ ), has been the most important factor in controlling fatigue crack growth since the relationship between the fatigue crack

growth rate and stress intensity factor range was identified in fracture mechanics [37]. There are three regimes of fatigue crack growth rate that are commonly found when testing in both the inert and corrosive environments, as shown in Fig. 1.8. In Region I, the fatigue crack growth rate decreases rapidly with decreasing  $\Delta K$  until a threshold,  $\Delta K_{th}$ , is reached, below which the fatigue crack growth rate becomes negligibly low. The  $\Delta K_{th}$  threshold is useful in the design of engineering structures that experience cyclic loadings. The linear region of the log-log plot of Fig. 1.8 is the so-called Paris law [38], expressed as

$$\frac{da}{dN} = C \Delta K^m \quad (1 - 1)$$

where  $da/dN$  is the fatigue crack growth rate,  $\Delta K$  is the stress intensity factor range, and  $C$  and  $m$  are material constants that are determined experimentally.

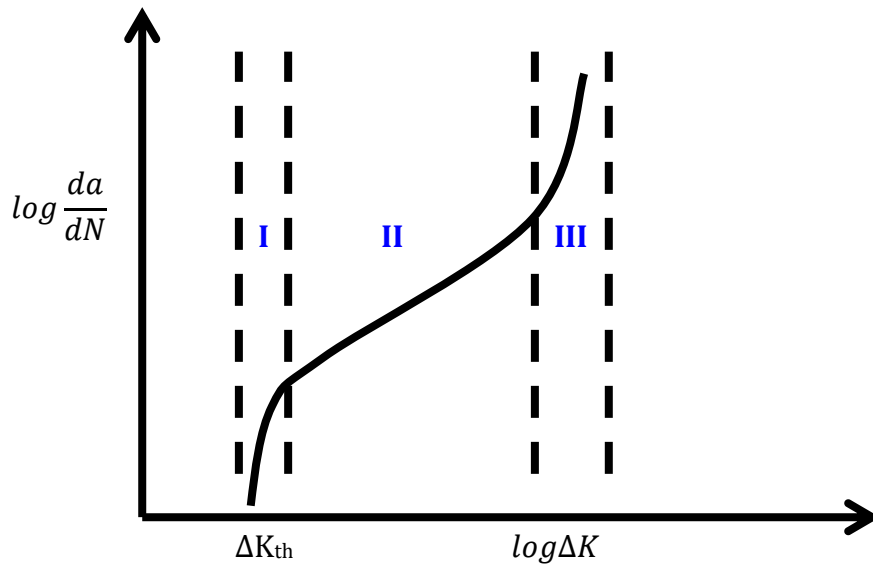


**Figure 1.8** Diagram showing three regimes of fatigue crack growth response

The Law prevails in Region II, which can be applied to predict the remaining life of engineering components and to determine the inspection interval when periodic inspections are required. In Region III, the crack growth rate increases rapidly with  $\Delta K$ , which corresponds to the situation where  $K_{\max}$  approaches the toughness of the material,  $K_c$ . Most of the laboratory tests are performed to obtain the crack growth behavior in Region II and/or to determine  $\Delta K_{th}$  in Region I.

The crack growth behavior in Region II has been specially studied to determine the mechanisms of NNpHSCC. As drawn from different published resources [4,39,40], the representative testing results of crack growth rate as a function of  $\Delta K$  are shown in Fig. 1.9. It can be seen that the linear region of the log-log plot in Fig. 1.9 is primarily governed by the Paris Law. The Paris Law is still valid under high  $\Delta K$  in near-neutral pH environments when all other variables are kept the same. The threshold determined by Been et al. is lower simply because of the higher applied  $K_{\max}$ . Therefore, Paris Law is not sufficient to incorporate the effects of other factors, such as  $K_{\max}$ , loading frequency, environments and cathodic protection.



The pressure fluctuations with cyclic amplitude below  $\Delta K_{th}$  are often considered as near-static loading and non-propagating. However, these minor pressure fluctuations, for example, with  $R \geq 0.9$ , were reported to cause a 72% reduction in the SCC threshold [43]. These minor pressure fluctuations in pipeline operations are usually termed as ripple loads, and are referred to as minor cycles in this investigation. The effect of minor cycles on the crack growth of pipeline steels in near-neutral pH environments has thus far been ignored.

### **1.3.1.2 Maximum stress intensity factor $K_{max}$**

Fig. 1.10 shows some representative results reported on the effect of maximum stress intensity factor  $K_{max}$  on the crack growth rate in near-neutral pH environments [4,39]. It can be seen that the crack growth rate generally increases with increasing  $K_{max}$ , although the data are scattered over several orders of magnitude because of the different  $\Delta K$ . Higher growth rate with increasing  $K_{max}$  may result from the synergistic interaction of enhanced plastic deformation [44] and the corrosive aqueous environments [45], or from effects of hydrogen embrittlement (HE, will be introduced in Section 1.3.1.4) [5,45]. Fig. 1.10 also suggests that a direct application of the Paris Law would be deficient without considering the effect of  $K_{max}$ .

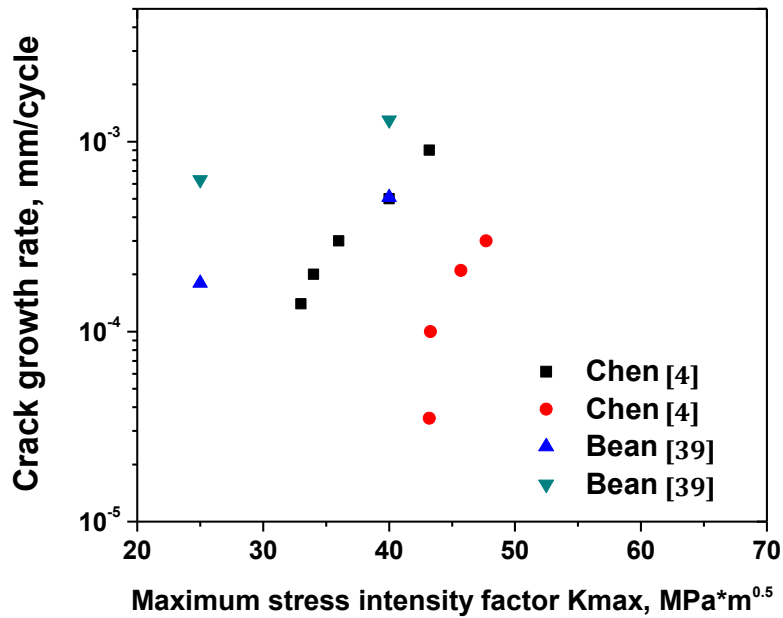


Figure 1.10 Crack growth rate as a function of  $K_{max}$  in near-neutral pH solutions (other conditions may vary)

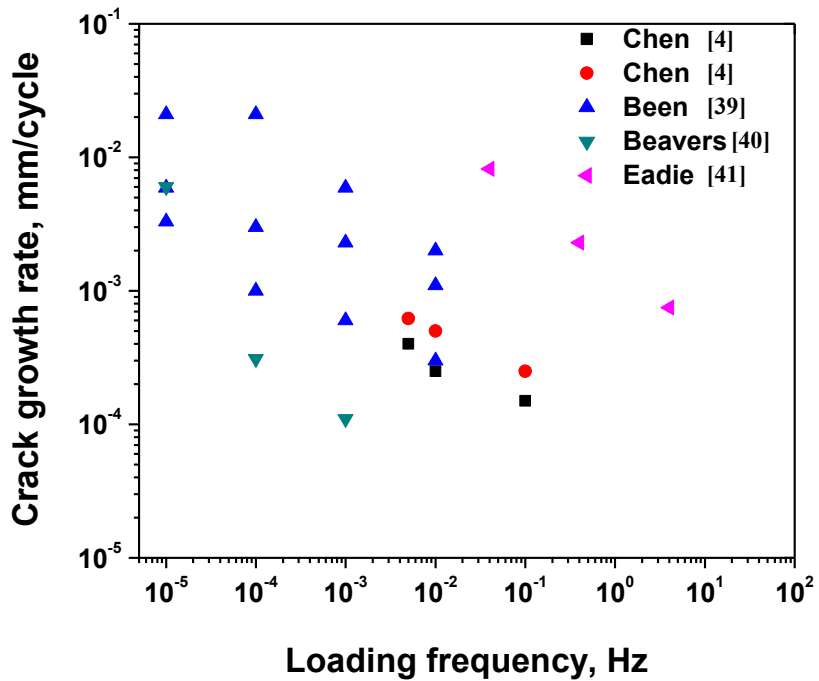


Figure 1.11 Crack growth rate as a function of loading frequency in near-neutral pH solutions (other conditions may vary)

### 1.3.1.3 Loading frequency

The effect of loading frequency on crack growth in near-neutral pH environments [4,39,40,41] is shown in Fig. 1.11. It can be seen that when the frequency is higher than  $10^{-3}$  Hz, the crack growth rate increases as the frequency decreases, as generally believed in corrosion fatigue [45]. This trend can be explained by the increased time for corrosion, or hydrogen diffusion to the crack tip (related to hydrogen embrittlement) with the decrease in the loading frequency [4]. The crack growth rate determined by Eadie et al. [41] is apparently higher than the others because  $H_2S$  was added to the test environments. Many laboratory tests [4,39,41] have been performed at frequencies at or higher than  $10^{-3}$  Hz to reduce the duration of the experiments.

However, the conclusion that the fatigue crack growth rate increases as the loading frequency decreases could not be extended to the frequency range lower than  $10^{-3}$  Hz, because the growth data reported were not complete [39,28] and had not excluded the effect of the maximum stress intensity factor [40,46]. Even for the data shown in Fig. 1.11, the growth rate determined by Been [39] scatters over one order of magnitude at a given loading frequency, despite the fact that such a low loading frequency used in the laboratory simulations is consistent with those found in field. Thus, the crack growth behavior in the frequency range lower than  $10^{-3}$  Hz should be further studied.

#### **1.3.1.4 Hydrogen embrittlement**

Hydrogen embrittlement occurs when atomic hydrogen is introduced into the metal matrix; when this happens, the material toughness and ductility can be reduced dramatically, and subcritical crack growth can occur [47]. Hydrogen embrittlement is well recognized as one of the important failure mechanisms for many engineering components in water vapor [48], aqueous [45,47,49] and hydrogen gaseous [50-52] environments. The magnitude of hydrogen embrittlement is affected by several variables [47], including loading rate, loading history, metal strength, amount of available hydrogen, and system temperature.

Hydrogen embrittlement has been suspected of playing an important role in the crack propagation of pipeline steels [2,12,15,53] exposed to near-neutral pH environments ever since NNpHSCC was identified in 1985 [1]. It is found that hydrogen itself, the by-product of corrosion, may not be an issue for pipeline steels exposed to near-neutral pH environments since the hydrogen content in the pipeline steel matrix is almost one order of magnitude lower than the minimum hydrogen content for forming hydrogen blistering, which is an instant cracking of steels due to the buildup of H<sub>2</sub> pressure at hydrogen traps [54,55].

However, hydrogen embrittlement can occur in the presence of tensile stress and a crack. To lower the chemical potential, hydrogen diffuses and segregates in the high stress zone ahead of the crack tip. Indeed, the role of hydrogen in NNpHSCC was confirmed [5,56],

re-sharpening the dormant cracks under cyclic loadings in near-neutral pH environments [4].

On the other hand, hydrogen in pipeline steels can be generated from the sour gas present in the fluids inside of pipelines [41] or when cathodic potential is applied [4,33,56]. As a result of these additional hydrogen sources, the amount of hydrogen in the steel matrix and thus the degree of hydrogen embrittlement are enhanced [57].

### **1.3.2 Available corrosion fatigue models in near-neutral pH environments**

#### **1.3.2.1 Paris Law**

As expressed by Eq. (1-1), the Paris Law only considers one of the three basic parameters of fatigue, i.e., the stress intensity factor range  $\Delta K$ . It could well model the crack growth behavior in inert environments where  $K_{\max}$  and loading frequency have insignificant influence. As can be seen in Figs. 1.10 and 1.11,  $K_{\max}$  and loading frequency do play an important role in the crack growth rate in the near-neutral pH environments and their effects can not be ignored.

#### **1.3.2.2 Crack tip strain rate model**

The crack tip strain rate was proposed for several corrosion systems under monotonic loading where the crack propagates through the mechanism involving repeated film formation-rupture [58]. The crack tip strain rate for near-neutral pH environments was expressed as [59]:

$$\dot{\epsilon} \approx 4f(1 - R) \quad (1 - 2)$$

where  $\dot{\epsilon}$  is the crack tip strain rate,  $f$  is the loading frequency, and  $R$  is the stress ratio. However, no passive film is observed in near-neutral pH environments [1,2] and models based on the crack tip strain rate showed poor correlation with NNpHSCC crack growth rate data [4]. This may suggest that the crack growth rate is not influenced solely by the strain rate. Other factors should also be considered.

### 1.3.2.3 Superposition model

The superposition model applied in near-neutral pH environments is given as [60,61]:

$$\left(\frac{da}{dN}\right)_{total} = \left(\frac{da}{dN}\right)_{fatigue} + \frac{1}{f} \left(\frac{da}{dt}\right)_{SCC} \quad (1 - 3)$$

where  $(da/dN)_{total}$  is the total crack growth per cycle in a near-neutral pH solution,  $(da/dN)_{fatigue}$  is the crack growth per cycle in air (inert environment),  $f$  is the loading

frequency, and  $(da/dt)_{SCC}$  is the crack growth in terms of time in a near-neutral pH solution by SCC.

However, the crack growth of pipeline steels under static loading in near-neutral pH environments (NNpHSCC) has never been observed, except for the crack initiation resulting from galvanic corrosion [5]. On the other hand, the loading frequency in the field is very low, for example, typically about  $10^{-5}$  Hz for high pressure gas transmission pipelines [62,63]. As a result,  $1/f$  would be very large and could be even larger than the fatigue term. And, as shown in Fig. 1.11, the inverse relationship between the crack growth rate and loading frequency at frequencies lower than  $10^{-3}$  Hz overestimates the crack growth rate. The contribution of the SCC term to the total growth rate in Eq. (1-3) was numerically assumed and had not been experimentally proven.

#### 1.3.2.4 Combined factor

Based on long-term and extensive laboratory crack growth simulations under constant amplitude cyclic loading in near-neutral pH environments, it is found that the crack growth rate can be correlated to a combined factor that incorporates both the mechanical and the environmental driving forces [4] as:

$$\frac{da}{dN} = a \left( \frac{\Delta K^\alpha K_{max}^\beta}{f^\gamma} \right)^n + b \quad (1 - 4)$$

where  $a$ ,  $n$ ,  $\alpha$ ,  $\beta$ , and  $\gamma$  are all constants.  $(\Delta K^\alpha K_{max}^\beta / f^\gamma)$  is termed as the combined factor,  $\Delta K$  is the change in stress intensity at the crack tip due to cyclic loading,  $K_{max}$  is the maximum stress intensity at the crack tip, and  $f$  is the loading frequency. The relative contribution of  $\Delta K$  and  $K_{max}$  to crack growth is represented by  $\alpha$  and  $\beta$ , under the relationship  $\alpha + \beta = 1$  (yielding  $\Delta K^\alpha K_{max}^\beta$  with a unit of  $\text{MPa}\cdot\text{m}^{0.5}$  and reflecting the synergistic role of  $K_{max}$  and  $\Delta K$  in fatigue crack growth).  $\alpha + \beta = 1$   $\gamma$  is a factor representing the influence of the corrosion environment on the crack growth rate, which is found to be around 0.1.  $b$  is the contribution of stress corrosion cracking, which was found to be about one order of magnitude lower than the first term in Stage II crack growth, and it can be ignored.  $\Delta K$  and  $K_{max}$  are strongly dependent on the geometry of the specimen, while  $\gamma$  is dependent on the corrosiveness of the environment. A threshold value of  $(\Delta K^\alpha K_{max}^\beta / f^\gamma)$  ( $(\Delta K)^\alpha (K_{max})^\beta / f^\gamma$ ) is also determined, below which the crack will cease to grow. The relationship is shown in Fig. 1.12.

The combined factor model could correlate well with the constant amplitude fatigue crack growth rate of pipeline steels exposed to near-neutral pH environments in a laboratory. However, when it comes to the field pressure fluctuations, such as those shown in Fig. 1.7, which is a typical example of pressure fluctuations recorded in the high-pressure gas transmission line where NNpHSCC was found, it is found that there are only a limited number of pressure fluctuations with combined factors exceeding the threshold determined by Equation (1-4) (shown as the dash line by assuming that  $K_{max}=33 \text{ MPa}\cdot\text{m}^{0.5}$ ). And it would need hundreds of years for a crack to propagate to the

critical dimension at which instant failure would occur. This contradicts the fact that failure of pipelines by cracking in the field can occur as soon as a few years after the surface of pipeline steels is in direct contact with near-neutral pH environments. This contradiction is also found in the other models.

As shown in Fig. 1.7, pressure fluctuates randomly during routine operations, which is a typical situation of variable amplitude (VA) cyclic loadings, not the constant amplitude (CA) fatigue testing performed in laboratories. To convert the random stress spectra into meaningful fatigue cycles, a number of methods have been developed. They include rainflow counting by the American Society for Testing and Materials (ASTM) Standard E1049-85 [64], level cross counting, peak counting, simple-range counting, range-pair counting and simple range counting. These methods have been applied to model the crack growth in near-neutral pH environments [65]. However, the contradiction as stated above still exists.

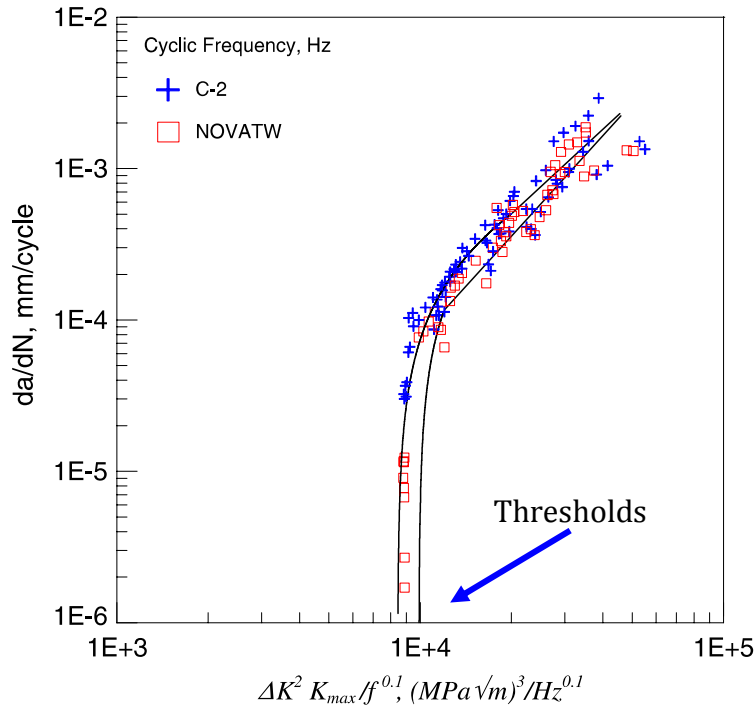


**Figure 1.12 Correlation of combined factor with crack growth rate in near-neutral pH solutions [4]**

In fact, the crack growth behavior under variable amplitude cyclic loadings has been found to be very different from that under constant amplitude fatigue loading. The latter fails to consider the effect of load interactions on crack growth. This might be the key to bridging the discrepancies between laboratory simulations and field observations for NNpHSCC. The variable amplitude fatigue studies will be introduced in the following section.

## 1.4 Variable Amplitude (VA) Fatigue

Engineering components are often operated under variable amplitude cyclic loadings in service, although they are designed by considering the level of static stress or constant amplitude fatigue strength. When a component is subjected to variable amplitude cyclic loadings, the crack growth of the component can be retarded or accelerated through load interactions: that is, the crack growth rate at any given time may depend not only on the current loading conditions, but also on the prior loading history. The fatigue life of engineering structures can be also extended or shortened.

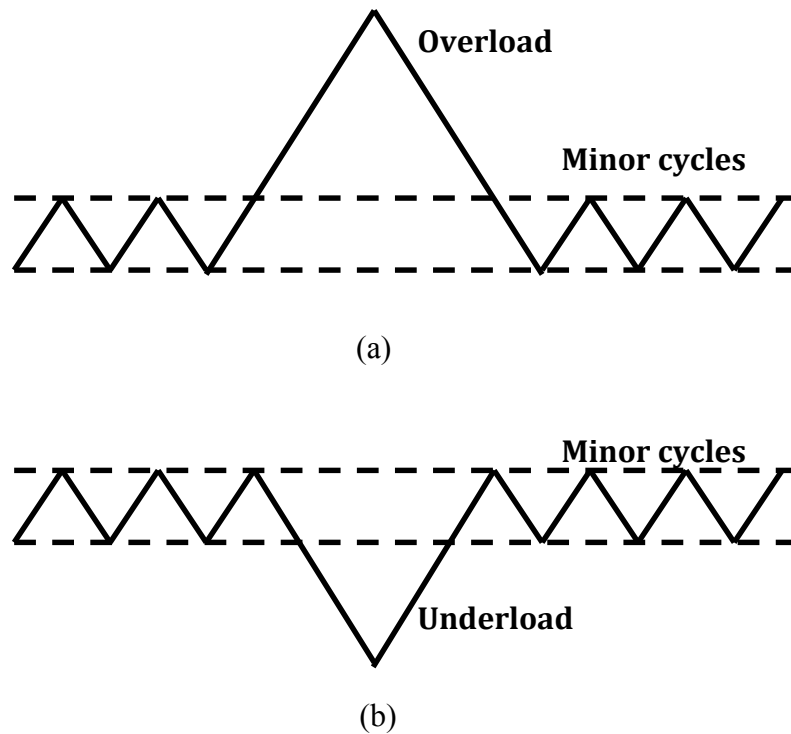


**Figure 1.13 Basic loading waveforms in variable amplitude fatigue test (a) overload, (b) underload**

Underload and overload, as schematically shown in Fig. 1.13, are two common features of variable amplitude cyclic loadings. Any other types of variable amplitude fatigue waveforms can be obtained by combining these two fundamental forms. Underload and overload can accelerate and retard subsequent fatigue crack growth, respectively [66,67]. The obtained growth rates differ from the crack growth predicted by a linear summation of damage of constant amplitude cyclic loadings with magnitudes equal to the variable amplitude. The predicted growth rate by linear summation can be expressed by the following equation:

$$\left(\frac{da}{dN}\right)_{\text{block}} = N_1 \left(\frac{da}{dN}\right)_1 + N_2 \left(\frac{da}{dN}\right)_2 + \dots \quad (1-5)$$

where  $(da/dN)_{\text{total}}$  is the linear summation;  $(da/dN)_1$  is the constant amplitude crack growth rate at amplitude 1, and  $N_1$  is the number of cycles in the block with amplitude 1;  $(da/dN)_2$  is the constant amplitude crack growth rate at amplitude 2, and  $N_2$  is the number of cycles in the block with amplitude 2.

Such variable amplitude fatigue waveforms are performed in the laboratory to simulate the crack growth in many engineering components in service, including turbine blades [68,69], aircraft [70,71], bridges [72], and welded joints [73,74]. The predicted lifetime based on such testing results is much closer to the actual service time of the components. The materials studied under variable amplitude fatigue tests include steels [75-77], titanium alloys [69,78], and especially Al alloys [66, 68,75-77,79,80] that are widely used

in the aircraft industry. The effects of the two basic waveforms, overload and underload, will be introduced in detail in the following section.

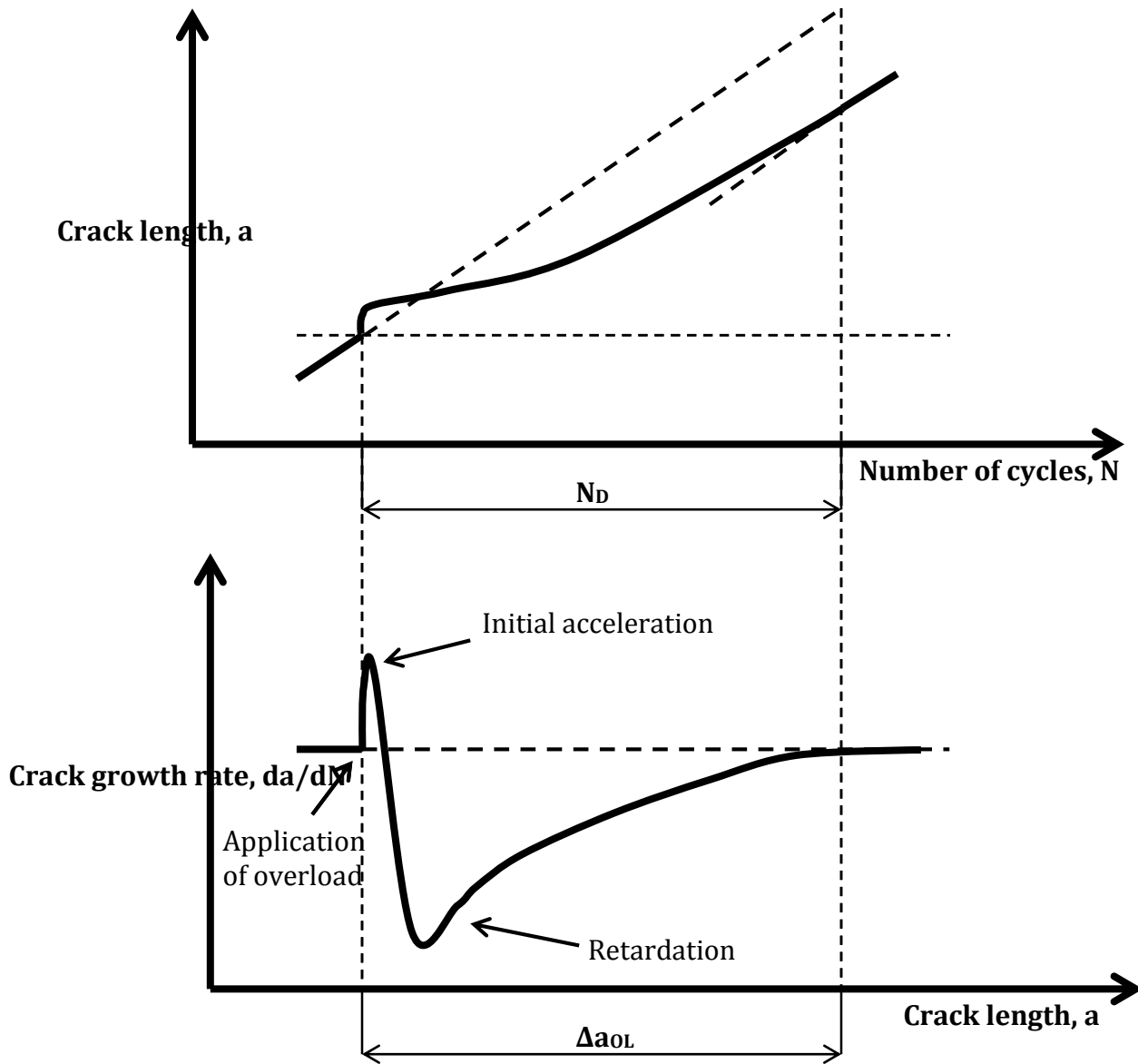


**Figure 1.14** Schematic of delayed retardation of crack growth following a single overload

### **1.4.1 Overload cyclic loadings - retardation effect**

The superposition of a single-peak tensile overload during the constant amplitude cyclic loadings, as shown in Fig. 1.13 (a), can cause the so-called retardation effect. As illustrated in Fig. 1.14, the crack growth rate of the subsequent minor cycles increases initially over a short period of time, but drops by an order of magnitude or more [66,72] afterwards, before gradually increasing to the growth rate prior to the application of the overload cycle. The occurrence of initial acceleration is found to depend on the type of materials [66]. The crack advancement and the applied number of cycles during this retardation effect are defined as the overload-affected crack growth increment ( $\Delta a_{OL}$ ) and the number of delay cycles ( $N_D$ ), respectively, as shown in Fig. 1.14 [66]. The extent of the retardation effect depends on the type of materials [66,72,81,82], specimen thickness [81], and the loading parameters, such as the ratio of overload amplitude over minor cycle amplitude [66,81,82], the stress intensity factor range of minor cycles [81] and the number of minor cycles between two neighboring overloads [82]. The effect of the ratio of overload amplitude over minor cycle amplitude has been extensively studied: the higher the ratio, the higher the magnitude of the retardation effect will be.

The retardation effect caused by applied overload has been observed and applied in industries. An aircraft that occasionally traveled through high gust winds in bad weather possessed a longer service time than a plane with a more steady flight weather history

[83]. For the application, the service life of bridge components can be extended by applying overload [82].

The hydrostatic tests are often applied to buried pipelines to check whether the pipelines contain the critical dimension cracks. The pipelines are pressurized up to 110% Specific Minimum Yield Strength (SMYS) or even higher using water. In case the pipeline failure occurs, water has limited influence on environment. In fact, the hydrostatic test is of overload loading. Overload can cause an active crack to grow at a reduced rate or to become dormant [1,84]. However, a hydrostatic test has its own drawback. If the monotonic loading rate during the hydrostatic test is not properly controlled, significant crack advancement can be caused by the hydrostatic test itself [85] through the mechanism of hydrogen embrittlement as stated in Section 1.3.1.4 [86]. In addition, the investigation of plastic zones near SCC tips in a pipeline showed that SCC continued to propagate during pipeline routine operations after hydrostatic testing [87].

To perform a hydrostatic test, the pipeline has to be shut down twice: for pumping water into and out of the pipeline. This involves the process of depressurization in addition to the overload cycle. The process of depressurization itself is a large amplitude underload cycle from the point view of fatigue, which could lead to an enhancement in crack growth during subsequent cyclic loading [27]. Fig. 1.13(b) shows the waveform formed by combining an underload cycle with minor pressure fluctuations, which is also seen during routine operation of pipelines in Fig. 1.7. Contrary to the retardation effect caused by overload, acceleration in crack growth is induced by underload, which will be illustrated

in the following section. On the other hand, if the underload is applied right before or after an overload, the magnitude of the retardation effect introduced by overload can be reduced [66,67]. Hydrostatic testing is a typical case of overloading followed by unloading. This type of waveform would limit the benefit of the retardation effect associated with the overloading. It was reported that the retardation effect vanished within four months of the introduction of a hydrostatic test [27].

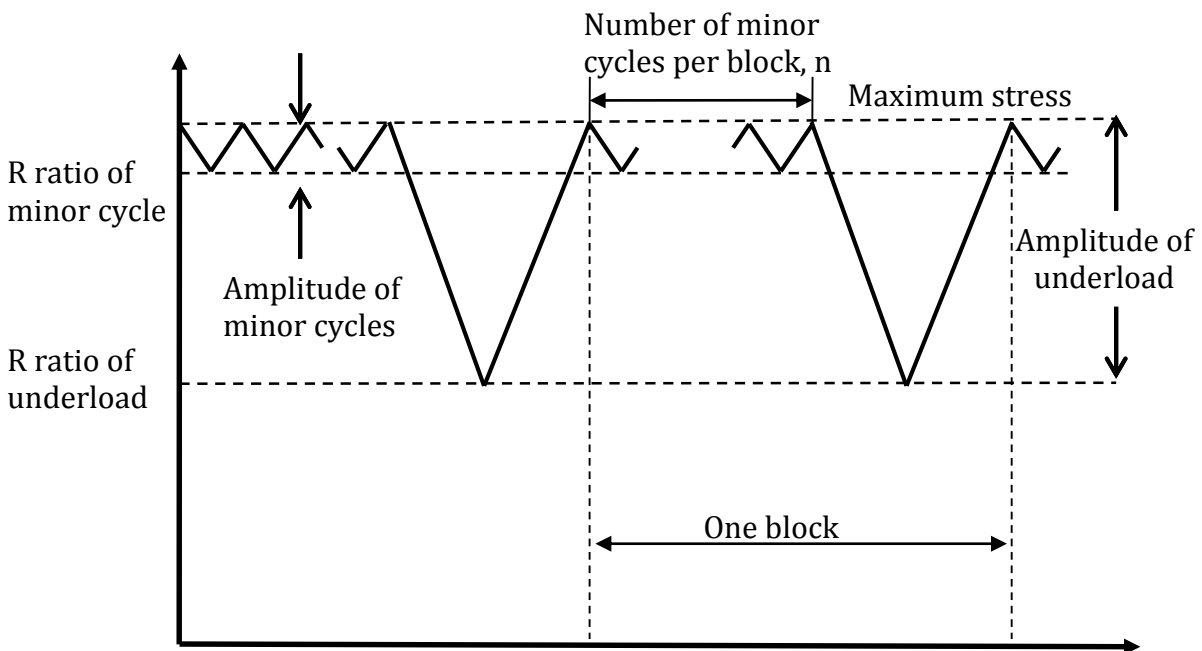


**Figure 1.15 Variables in underload waveform**

### **1.4.2 Underload cyclic loadings – acceleration effect**

Although there are comparatively fewer publications on the effects of underload than on those of overload [66,67], the acceleration of crack growth associated with the underload plays an important role in predicting the remaining lifetime of engineering structures. As stated previously, the combination of depressurization (due to shut-down or routine operations) and re-loading back to normal pressure is actually an underload-type variable amplitude fatigue, as schematically show in Fig. 1.15. The underload cycle could not only cause crack advancement by itself [27], but also accelerate the crack growth rate of the subsequent minor cycles [66,67,75]. A factor termed as acceleration factor,  $\gamma$ , is often used to determine the magnitude of the crack growth rate enhancement, which is defined as the ratio of measured growth rate per block over the predicted growth rate per block by a linear summation of the constant amplitude crack growth response [75], that is,

$$\gamma = \frac{\text{measured growth rate per block}}{\text{predicted growth rate per block by a linear summation of the constant amplitude crack growth response}} \quad (1-6)$$

The predicted growth rate can be expressed by Equation (1-5). The acceleration factor is affected by several variables, as shown in Fig. 1.15, such as the number of minor cycles per block, maximum stress, amplitudes of minor and underload cycles, and environments. The effects of these variables on crack growth are further reviewed in the sections below.

#### **1.4.2.1 Number of minor cycles**

From Fig. 1.16, it can be seen that the acceleration factor increases with the number of minor cycles per block,  $n$ , until  $n = 10$  for different materials (other conditions may vary).

When  $n$  exceeds 10 cycles,  $\gamma$  usually decreases. The maximum value of the acceleration factor depends on the type of materials. As can be seen in Fig. 1.16, it can be up to eight for Al 8090, while only about two for steel. The dependence of the acceleration factor on the type of materials suggests the necessity of studying the crack growth behavior of pipeline steels under variable amplitude cyclic loading, which has not been addressed so far.

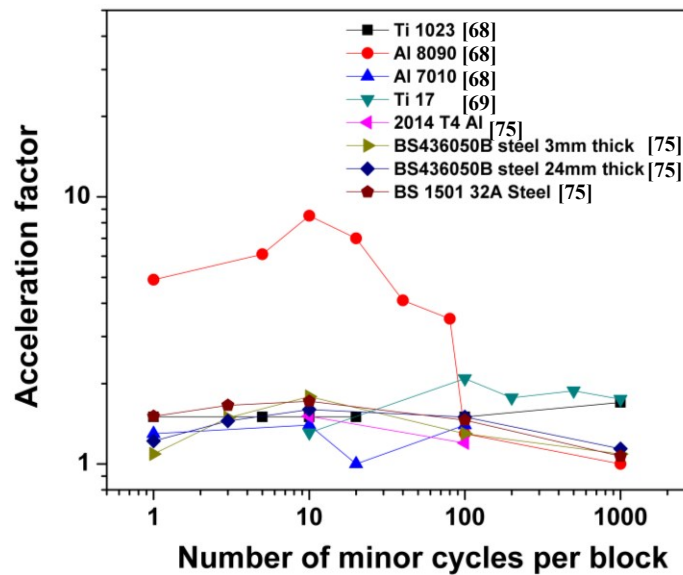


**Figure 1.16** Effect of the number of minor cycles per block on the acceleration factor (other conditions may vary)

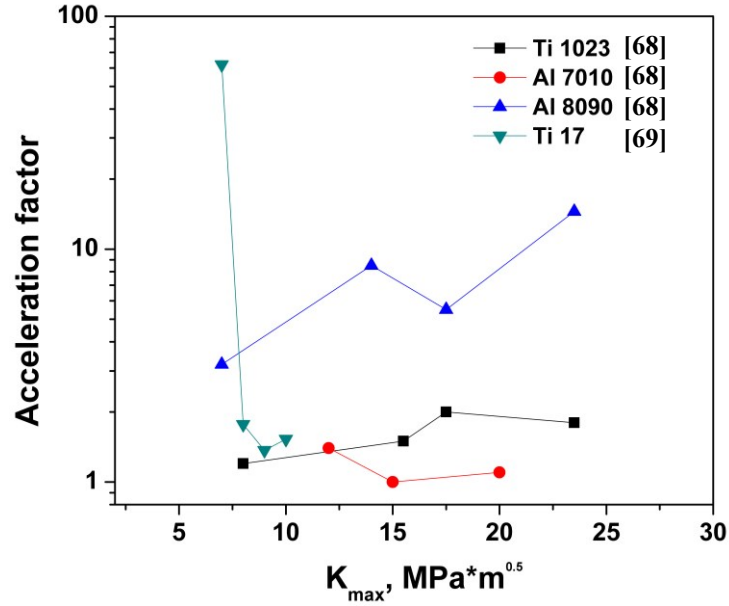
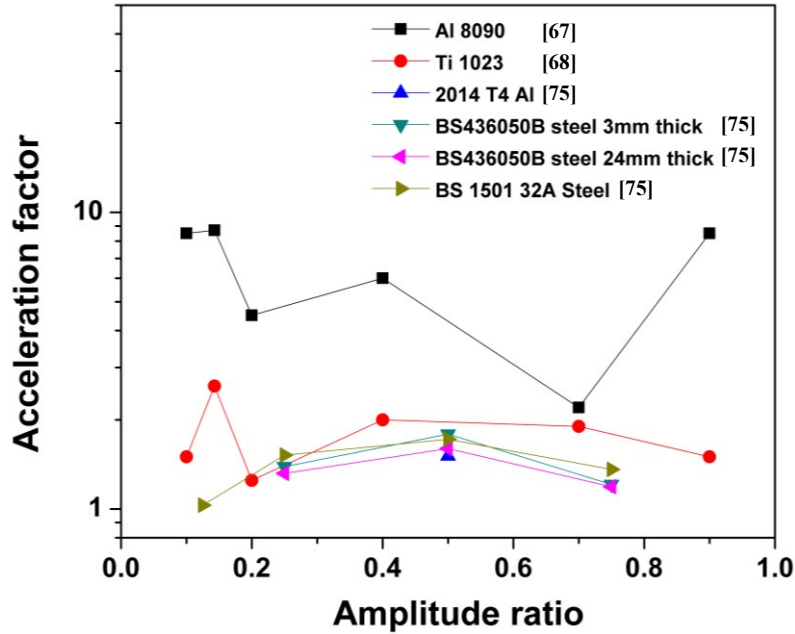


Figure 1.17 Effect of maximum stress on acceleration factor (other conditions may vary)

#### 1.4.2.2 Maximum stress

The effect of the maximum stress intensity factor on the acceleration factor is shown in Fig. 1.17 for different materials (other conditions may vary). It can be seen that the acceleration factor is also affected by the maximum stress intensity factor. A general trend for the effect of the maximum stress intensity factor in different materials does not seem to exist.



**Figure 1.18 Effect of amplitude ratio on the acceleration factor (other conditions may vary)**

### 1.4.2.3 Amplitudes of large (underload) and minor cycles

It is believed that it is the ratio of minor cycle amplitude over underload amplitude that affects the acceleration factor [75]. Thus, the amplitude effects were converted into the amplitude ratio (other conditions may vary), as shown in Fig. 1.18. It can be seen that the acceleration factor generally increases with the amplitude ratio up to 0.5, after which it decreases. But it is rather complicated for Ti 1023 and Al 8090. It can be seen that the value of the acceleration factor is also affected by materials.

The results shown in Figs. 1.16 to 1.18 were obtained from tests conducted when the stress intensity factor range of the minor cycles was above the constant amplitude

threshold. Would the minor cycles cause the crack to grow if the stress intensity factor range of the minor cycles was below the constant amplitude threshold determined in the presence of underload? The answer is yes. A significant acceleration of crack growth was observed, and the acceleration factor was reported to a value up to 100 [88]. Therefore, it can be seen that even small fluctuations with high R ratios can still significantly influence the fatigue life of engineering components.

#### **1.4.2.4 Environments**

All of the tests of underload-type variable amplitude fatigue shown in Figs. 1.16 to 1.18 were performed in air. Few tests were performed in corrosive environments [79,88]. As shown in Fig. 1.19 [88], the acceleration factor in a vacuum is smaller than that in other environments, and the acceleration factor in moist air is obviously lower than that in dry air and nitrogen, which indicates that environments do play an important role in load interactions and can not be ignored.

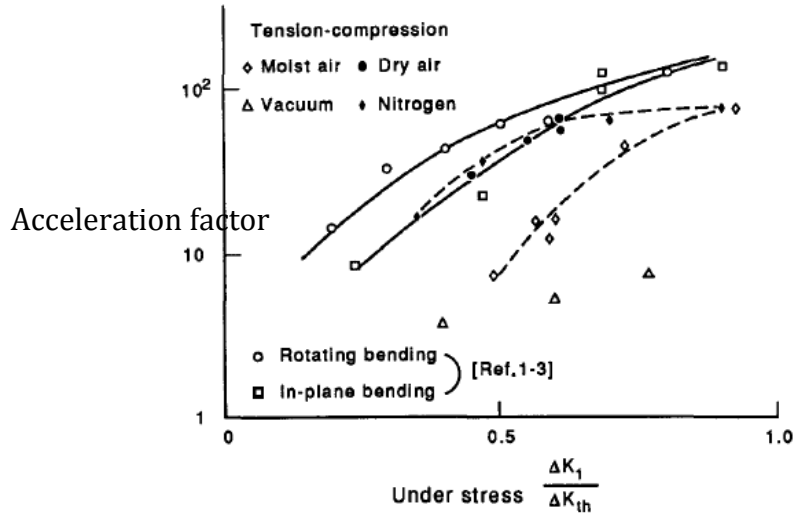
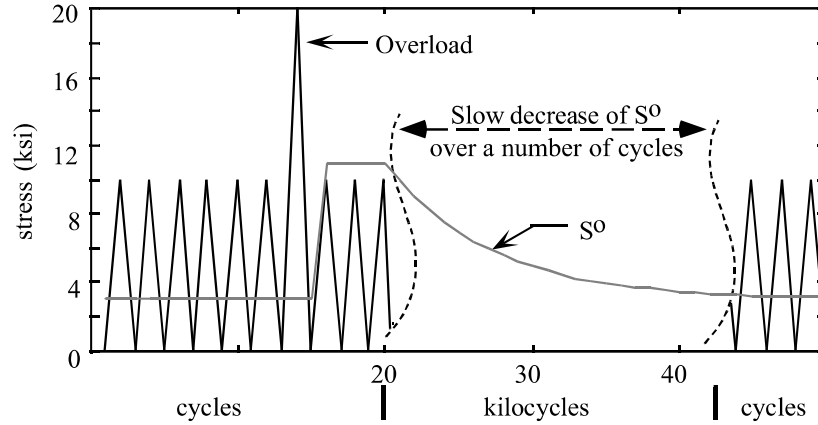


Figure 1.19 Effects of environments on acceleration factor [88]

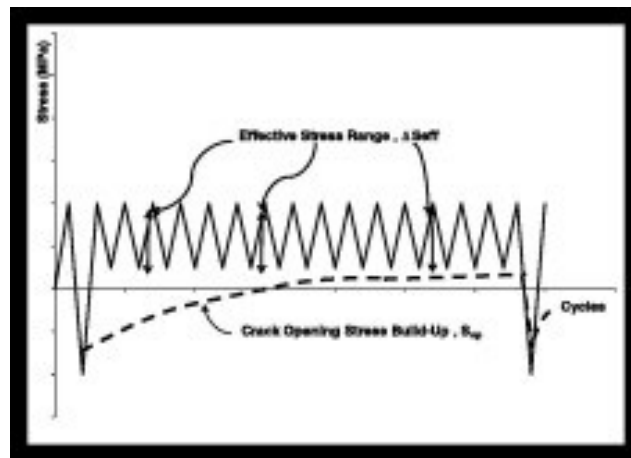
## 1.5 Mechanisms of Load Interactions

Many mechanisms [67,75] have been proposed to explain the observed phenomena of load interactions. Some, including crack closure, residual stress, dislocation substructure changes and strain hardening/softening, will be introduced in the sections below.

### 1.5.1 Crack closure



(a)



(b)

**Figure 1.20 Changes in crack opening stress level after a) overload [91]; and b) underload [77]**

The crack closure model assumes that the portion during unloading in one cycle may lead to a direct contact of the fractured surfaces behind the crack tip (crack closure), and therefore that portion does not contribute to fatigue crack growth because of the reduction of the effective stress intensity factor range or crack tip strain during cyclic loading [89].

The stress intensity factor at which the crack surfaces start to contact each other during

unloading or the crack surfaces become separated during loading is termed as the opening stress intensity factor,  $K_{op}$ . The effective stress intensity factor range,  $\Delta K_{eff} = K_{max} - K_{op}$ , which contributes to fatigue damage, is lower than the applied  $\Delta K$ . The crack closure model is often applied to explain acceleration and retardation effects induced by underloads and overloads, respectively, through the change of  $K_{op}$  [66-69,76,77,87,90,91]. As shown in Fig. 1.20, the opening stress is increased after overload, and thus the effective stress intensity factor range is decreased, resulting in the crack growth retardation effect, while underload can decrease the opening stress of minor cycles, leading to crack growth acceleration.

### **1.5.2 Residual stress**

After overload, a plastic zone, one that is larger than the one generated by previous minor cycles, forms [92]. During the subsequent minor cyclic loadings, the surrounding elastic material forces the material at the crack tip to conform to its original shape. This results in compressive residual stresses in the plastic zone. The stress at the crack tip is the result of the applied tensile stress subtracting residual compressive stress. Thus, retardation in crack growth occurs. Opposite to this, tensile residual stress can be formed ahead of the crack tip upon the application of compressive underload (negative R ratio) [92]. The residual compressive stress caused by overload and residual tensile stress caused by underload were observed and measured in [93]. However, it is still questionable whether the above explanation can be applied to the situation of a tensile underload (positive R ratio) [68].

### **1.5.3 Strain hardening/softening**

Strain hardening of the material at the crack tip was believed to be one of the mechanisms of the load interactions, as fatigue crack growth can be accelerated by pre-straining [75,94]. Although it is generally accepted that overload can lead to strain hardening, the strain hardening occurring upon underload is inexplicable, as the maximum stress is kept constant. Opposite to the strain hardening, the strain softening could be a reason for the acceleration caused by underload. In fact, the strain increment during the minor cyclic loading (R ratio 0.7) after underload (R ratio 0.1) was predicted by a finite element analysis in a Ti alloy [69]. However, experimental validation was not provided.

### **1.5.4 Dislocation substructure changes**

It is well established that the material damage due to fatigue fundamentally results from the localized irreversibility of a dislocation slip through various mechanisms as summarized in [95]. These mechanisms include a cross slip of screw dislocations, and different paths for the forward and reverse gliding during one complete fatigue cycle. Therefore, it is believed that the retarded and accelerated fatigue growth rate caused by overload and underload, respectively, could be associated with the change of dislocation structures. The development of a radial dislocation structure near the crack tip after

overloads was indeed observed [96]. However, there has been very limited work on the dislocation substructure changes caused by underload.

## **1.6 Challenges in Crack Growth Study of Pipeline Steels**

### **Exposed to NNpH Environments**

Although NNpHSCC has been studied for more than two decades since it was identified in the 1980s, the majority of work was performed by applying constant stress loading, or by slow strain rate testing, or under constant amplitude cyclic loadings. However, all of these loading conditions could not represent the variable amplitude loading conditions in the field. Until now, the obtained results and conclusions from available publications could not fully answer the following questions:

- 1). Why do more than 70% of all in-service and hydrostatic-test failures attributed to SCC often occur in the discharge section (downstream of the pump station), but much less in the suction part even though there are more pressure fluctuations in the suction part [1,62]?
- 2). More than 70% of failures are located within 30 km downstream of a pump station. Why does such a correlation exist [1,2,11]?
- 3). What is the crack growth behavior under the variable amplitude loading conditions seen in the field?
- 4). Is the shutdown or the depressurization of a pipeline harmless?

5). How can the pressure fluctuations be controlled to minimize crack growth?

Questions 1 and 2 are often answered by considering the factors such as temperature [1], CO<sub>2</sub> level [1], mean stress level [1], coating disbondment [97], and loading rate [98]. We believe that the above considerations are contradictory and are not the root causes of the dilemma.

The correlation between temperature and the number of SCC colonies was not observed [1]. The fluid temperatures are often controlled and fall to soil temperature within 5 km of the pump station. Thus temperature may not be a critical attribute of NNpHSCC. The CO<sub>2</sub> level in the ground may vary with temperature, the type of soils and seasonal conditions, but should bear little connection to the distance from a pump station while the pipe failures do. The mean stress indeed decreases with the distance from the pump station, but its effect is secondary compared with the effect of fatigue amplitude, as discussed in Section 1.3.1. Coating disbondment was proposed and attributed to higher temperature, more stress fluctuations, and higher stress levels [97]. As described above, the temperature and stress level are not the critical issues. In terms of stress fluctuations, there are more large fluctuations close to the suction sites than there are close to discharge sites; however, the least number of failures are reported at the suction sites [62]. The loading rate is similar from the discharge part of the pump station down to the next suctions. These suggest that the existing explanations are very speculative.

One important factor that has been ignored is the effect of load interactions. As shown in Fig. 1.21, the discharge site shows underload-type variable amplitude fatigue, while the suction site exhibits overload-type variable amplitude fatigue. It is anticipated that systematically studying crack growth behavior under variable amplitude cyclic loadings will provide answers to the questions raised above. However, to date, few tests have been conducted under variable amplitude cyclic loadings for pipeline steels exposed to near-neutral pH environments. Although the acceleration effect caused by underloads in pipeline steels was indeed observed in near-neutral pH environments in [99], the R ratios of underload and minor cycles were too low, 0.1 and 0.5, respectively. These are not typical of the pressure fluctuations seen in the field, as shown in Fig. 1.7 as an example; and the growth rates determined were scattered nearly one order of magnitude.

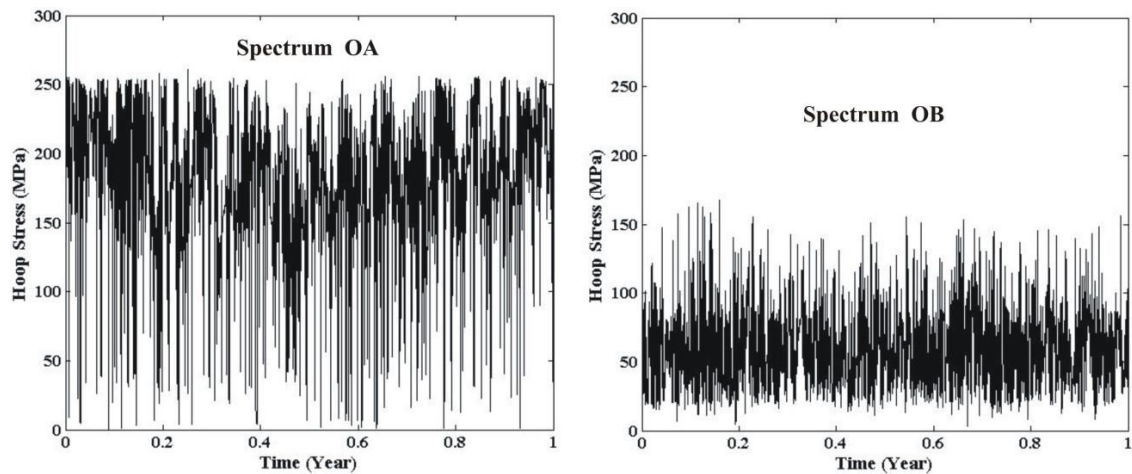


**Figure 1.21 Spectra of an oil pipeline: OA discharge part; and OB suction part**

## 1.7 Research Objectives and Thesis Structure

The objective of this thesis study is to investigate and understand the crack propagation behavior of pipeline steels under underload-type variable amplitude cyclic loadings. The tests will be performed both in air and in near-neutral pH environments to determine the key environmental factors responsible for the crack growth behavior. In this regard, specific goals, as outlined below, are to study and determine:

- The effect of different loading waveforms on the crack growth rate, especially to determine the acceleration effect caused by underload in a near-neutral pH environment
- The effects of loading frequency and maximum stress intensity factor of underload on the crack growth rate of a pipeline steel both in air and in a near-neutral pH solution
- The effects of the number of minor cycles between two neighboring underloads on crack growth rate of a pipeline steel both in air and in near-neutral pH solution
- The effects of amplitudes of underload and minor cycles on the crack growth rate of a pipeline steel both in air and in near-neutral pH solution
- The role of hydrogen in crack growth

The structure of this dissertation, which is meant to cover the mentioned objectives, is as follows:

- Chapter 2 will report the depressurization-induced crack growth enhancement for a pipeline steel exposed to a near-neutral pH environment. This chapter will provide new insights about the role of minor cycles with high R ratios in crack growth in the presence of large cycles.
- Chapter 3 will investigate the accelerated crack propagation of a pipeline steel exposed to a near-neutral pH solution in underload testing, specifically the effect of loading frequency and  $K_{max}$ .
- Chapter 4 will look into the accelerated crack propagation of a pipeline steel exposed to a near-neutral pH solution in underload testing, specifically the effect of number of minor cycles.
- Chapter 5 will study the acceleration of crack propagation of a pipeline steel exposed to a near-neutral pH solution in underload testing, specifically the effect of amplitudes of underload and minor cycles.
- Chapter 6 will investigate the role of hydrogen in crack propagation of a pipeline steel exposed to a near-neutral pH solution.

## References

- [1] B. S. Delanty, J. O'Beirne. Major Field Study Compares Pipeline SCC with Coatings. Oil & Gas Journal 15 (1992) 39-44.
- [2] Parkins RN. A review of stress corrosion cracking of high pressure gas pipelines proceedings of corrosion 2000. Paper 00363. Houston, Texas: NACE International; 2000.

- [3] J. A. Beavers and C. E. Jaske. Near-neutral pH SCC in Pipelines: Effects of Pressure Fluctuations on Crack Propagation. Corrosion: 1999, NACE International, Paper No.: 98257.
- [4] Weixing Chen and Robert L. Sutherby. Crack Growth Behavior of Pipeline Steel in Near-Neutral pH Soil Environments. Metallurgical and Materials Transactions A 2007; 38A; pp.1260-1268.
- [5] W. Chen, Richard Kania, Robert Worthingham, Gregory Van Boven. Transgranular crack growth in the pipeline steel exposed to near-neutral pH soil aqueous solutions: The role of hydrogen. Acta Materialia 57 (2009) 6200-6214.
- [6] Alberta Energy Regulator. Report 2013-B: Pipeline Performance in Alberta, 1990-2012.
- [7] National Energy Board (NEB), Focus on Safety and Environment a Comparative Analysis of Pipeline Performance 2000-2007, July 2009.
- [8] R.L. Wenk. Field Investigations of Stress Corrosion Cracking, 5<sup>th</sup> Symposium on Line Pipe Research, American Gas Association, 1974.
- [9] K. Sieradzki and R.C. Newman. Stress-Corrosion Cracking, J. Physics and Chemistry of Solids, Vol. 48, No.11, pp. 1101-1113, 1987.
- [10] National Energy Board (NEB), Report of the Inquiry-Stress Corrosion Cracking on Canadian Oil and Gas Pipelines, 1996.
- [11] C. Manfredi, and J.L. Otegui. Failures by SCC in buried pipelines. Engineering Failure Analysis 9 (2002) 495-509.

- [12] John A. Beavers, and Brent A. Harle. *Journal of Offshore Mechanics and Arctic Engineering*. 123 (2001). pp.147-151.
- [13] Jones DA. *Principles and prevention of corrosion*. 2<sup>nd</sup> ed. Upper Saddle River (NJ): Prentice Hall; 1996. pp.291.
- [14] W. Chen, F. King, and E. Vokes. Characteristics of Near-Neutral pH Stress Corrosion Cracks in an X-65 Pipeline. *Corrosion* 2002, Vol. 58, No. 3, pp. 267-275.
- [15] W. Bouaeshi, S. Ironside, and R. Eadie. Research and Cracking Implications from an Assessment of Two Variants of Near-Neutral pH Crack Colonies in Liquid Pipelines. *Corrosion*: July 2007, Vol. 63, No. 7, pp. 648-660.
- [16] Karina Chevil, Abdoulmajid Eslami, Weixing Chen, Reg Eadie, Richard Kania, Robert Worthingham, and Greg Van Boven. Developing Cathodic Protection Based on Disbondment Geometry. *Proceedings of 2012 9<sup>th</sup> International Pipeline Conference*, Calgary, Alberta, Canada, Sept. 24-28, 2012. Vol. 2, paper No. IPC2012-90675, pp. 583-590.
- [17] Eslami, A., B. Fang, R. Kania, B. Worthingham, J. Been, R. Eadie, and W. Chen. Stress corrosion cracking initiation under the disbonded coating of pipeline steel in near-neutral pH environment. *Corrosion Science*, Vol. 52, Issue 11, November 2010. pp.3750-3756.
- [18] Karina Chevil, Weixing Chen, Reg Eadie, Richard Kania, Greg Van Boven, and Jenny Been. Correlating Corrosion Field Data with Experimental Findings for the Development of Pipeline Mitigation Strategies. *Proceedings of IPC2014*, 10<sup>th</sup>

International Pipeline conference, Calgary, Alberta, Canada, Sept. 29- Oct. 3, 2014.  
Paper No. IPC2014-33678.

[19] Abdoulmajid Eslami, Trevor Place, Shamus McDonnell, Chijikoe Ukiwe and Qin You. Landscape Investigation on External Corrosion and SCC of a Tape Coated Enbridge Pipeline. Proceedings of the 2012 9<sup>th</sup> International Pipeline Conference, IPC2012, Sept. 24-28, 2012, Calgary, Alberta, Canada. Paper No. IPC2012-90598.

[20] F. King, Tom Jack, Miroslav Kolar and Robert Worthingham. A Permeable Coating Model for Predicting the Environment at the Pipe Surface under CP-Compatible Coatings. Corrosion 2004, New Orleans, USA, 2004, Paper No. 04158.

[21] X. Chen, X.G. Li, C.W. Du, and Y.F. Cheng. Effect of cathodic protection on corrosion of pipeline steel under disbonded coating. Corrosion Science, Vol. 51, Issue 9, Sept. 2009, pp. 2242-2245.

[22] Barlo T.J. and Berry W.E.. An assessment of the current criteria for cathodic protection of buried steel pipelines. Materials Performance. Vol. 23:9, 1984,

[23] F. Gan, Z.-W. Sun, G. Sabde, and D.-T. Chin. Cathodic Protection to Mitigate External Corrosion of Underground Steel Pipe Beneath Disbonded Coating. Corrosion: October 1994, Vol. 50, No. 10, pp. 804-816.

[24] R. R. Fessler, A. J. Markworth, and R. N. Parkins. Cathodic Protection Levels under Disbonded Coatings. Corrosion: January 1983, Vol. 39, No.1, pp. 20-25.

[25] Robert G. Wakelin, Robert A. Gummow, and Sorin Marius Segall. AC Corrosion – Case Histories, Test Procedures, & Mitigation. Corrosion 1998, 22-27 March, San Diego, California. Paper No. NACE-98565.

- [26] Canadian Gas Association OCC-1 Task Force. Recommended Practice OCC-1-2013, Control of External Corrosion on Buried or Submerged Metallic Piping Systems, June 2013.
- [27] O. Vosikovskiy, and R.J. Coole. An Analysis of Crack Extension by Corrosion Fatigue in a Crude Oil Pipeline. *International Journal of Pressure Vessels and Piping*, Vol. 6, Issue 2, March 1978, pp. 113-129.
- [28] T.M. Ahmed, S. B. Sutherby, and A. Plumtree. Cyclic Crack Growth rates of X-60 Pipeline Steel in a Neutral Dilute Solution. *Corrosion*: July 1997, Vol. 53, No. 7, pp.581-590.
- [29] Baotong Lu, Jingli Luo and Brian McCrady. Near-Neutral pH SCC Initiation and Early Propagation of X70 Pipeline Steel. *Proceedings of IPC2002, 4<sup>th</sup> International Pipeline Conference*, Sept. 29-Oct. 3, 2002, Calgary, Alberta, Canada. Paper No. IPC2002-27234.
- [30] Weimin Zhao, Yongxing Wang, Timing Zhang, and Tong Wang. Study on the mechanism of high-cycle corrosion fatigue crack initiation in X80 steel. *Corrosion Science* 57 (2012) 99-103.
- [31] A. Mustapha, E.A. Charles, and D. Hardie. Evaluation of environment-assisted cracking susceptibility of a grade X100 pipeline steel. *Corrosion Science* 54 (2012) 5-9.
- [32] Frand Cheng. *Stress Corrosion Cracking of Pipelines*. A John Wiley & Sons, Inc., Publication, New Jersey, 2013, pp. 73-111.
- [33] Abdoulmajid Eslami. PhD thesis, Near-neutral pH Stress Corrosion Crack Initiation under Simulated Coating Disbondment. University of Alberta, Fall 2012.

- [34] Syed J. Haider, Steven Textor, Aaron Sutton and Yvan Hubert. Managing a New Pressure Cycling Reality in Liquid Pipelines. Proceedings of IPC2014, 10<sup>th</sup> International Pipeline Conference, Sept. 29-Oct. 3, 2014, Calgary, Alberta, Canada. Paper No. IPC2014-33485.
- [35] O. Vosikovsky, and R. J. Cooke. An analysis of crack extension by corrosion fatigue in a crude oil pipeline. International Journal of Pressure Vessels and Piping, Vol. 6, Issue 2, March 1978, pp. 113-129.
- [36] R. N. Parkins and B. S. Greenwell. The interface between corrosion fatigue and stress-corrosion cracking. Metal Science, Vol. 11, Issue 8-9 (01 August 1977), pp. 405-413.
- [37] Richard W. Hertzber. Deformation and Fracture Mechanics of Engineering Materials, Fourth Edition, John Wiley and Sons, Inc., New York, NY, 1989, pp. 591-604.
- [38] P. C. Paris, and F. Erdogan. A Critical Analysis of Crack Propagation Laws. Journal of Basic Engineering, Vol. 85, 1960, pp. 528-534.
- [39] J. Been, R. Eadie, and R. Sutherby. Prediction of Environmentally Assisted Cracking on Gas and Liquid Pipelines. Proceedings of IPC2006, 6<sup>th</sup> International Pipeline Conference, Sept. 25-29, 2006, Calgary, Alberta, Canada. Paper No. IPC2006-10345.
- [40] J.A. Beavers, and C.E. Jaske. Effects of Pressure Fluctuations on SCC Propagation". PRCI Report on Contract PR-186-9706, Arlington, Virginia 2004.
- [41] R. L. Eadie, K.E. Szklarz, and R. L. Suthery. Corrosion Fatigue and Near-Neutral pH Stress Corrosion Cracking of Pipeline Steel and the Effect of Hydrogen Sulfide. Corrosion: February 2005, Vol. 61, No. 2, pp.167-173.

- [42] Afolabi Egbewande, Weixing Chen, Reg Eadie, Richard Kania, Greg Van Boven, Robert Worthingham and Jenny Been. Transgranular crack growth in the pipeline steel exposed to near-neutral pH soil aqueous solutions: Discontinuous crack growth mechanism. *Corrosion Science*, Vol. 83, June 2014, pp. 343-354.
- [43] P.S. Pao and R.A. Bayles. Effect of Ripple Loads on Stress-Corrosion Cracking in Structural Steel. Technical Report, Report No. NRL ser 6310/003, May 30, 1995.
- [44] T.L. Anderson. *Fracture Mechanics, Fundamentals and Applications*, Third Edition. Taylor & Francis Group, 2005. pp: 464-473.
- [45] S. Srivatsan, and T.S. Sudarshan. Mechanisms of fatigue crack initiation in metals: role of aqueous environments. *Journal of Materials Science*, May 1988, Vol. 23, Issue 5, pp. 1521-1533.
- [46] Weixing Chen, and Robert Sutherby. Laboratory Simulation of Hydrostatic Test in Near-Neutral pH Soil Environments. Proceedings of IPC2006, 6<sup>th</sup> International Pipeline Conference, Sept. 25- 29, 2006, Calgary, Alberta, Canada. Paper No. IPC2006-10477.
- [47] T.L. Anderson. *Fracture Mechanics, Fundamentals and Applications*, Third Edition. Taylor & Francis Group, 2005. pp: 529-537.
- [48] R. E. Ricker, and D. J. Duquette. The role of hydrogen in corrosion fatigue of high purity Al-Zn-Mg exposed to water vapor. *Metallurgical Transactions A*, Vol. 19A, July 1988, pp. 1775-1783.
- [49] Roy Johnsen, Bård Nyhus and Stig Wästberg. Hydrogen Induced Stress Cracking (HISC) of Stainless Steel under Cathodic Protection in Seawater: Presentation of a New

Test Method. Proceedings of the ASME 2009 28<sup>th</sup> International Conference on Ocean, Offshore and Arctic Engineering, OMAE2009, May 31- June 5, 2009, Honolulu, Hawaii, USA.

[50] N. Nanninga, A. Slifka, Y. Levy, and C. White. A Review of Fatigue Crack Growth for Pipeline Steel Exposed to Hydrogen. Journal of Research of the National Institute of Standards and Technology, Vol. 115, No. 6, Nov. - Dec. 2010, pp. 437-452.

[51] Arnaud Macadre, Maxim Artamonov, Saburo Matsuoka, and Jader Furtado. Effects of hydrogen pressure and test frequency on fatigue crack growth properties of Ni-Cr-Mo steel candidate for a storage cylinder of a 70 MPa hydrogen filling station. Engineering Fracture Mechanics 78 (2011) 3196-3211.

[52] Z. Sun, C. Moriconi, G. Benoit, D. Halm, and G. Henaff. Fatigue Crack Growth under High Pressure of Gaseous Hydrogen in a 15-5PH Martensitic Stainless Steel: Influence of Pressure and Loading Frequency. Metallurgical and Materials Transactions A, March 2013, Vol. 44, No. 3, pp. 1320-1330.

[53] D. X. He, W.X. Chen, and J.L. Luo. Effect of cathodic potential on hydrogen content in a pipeline steel exposed to NS4 near-neutral pH soil solution. Corrosion 2004;60(8):778-786.

[54] W. Chen, S.-H Wang, F. King, T. R. Jack, M. J. Wilmott. Hydrogen Permeation Behavior of X-70 Pipeline Steel in a Near-Neutral pH Soil Environment. Proceedings of IPC2000, 3<sup>rd</sup> International Pipeline Conference, Vol. 2, New York, NY: ASME International, 2000, pp. 953-960.

- [55] D.X. He, W. Chen, and J.L. Luo. Effect of Cathodic Potential on Hydrogen Content in a Pipeline Steel Exposed to NS4 Near-Neutral pH Soil Solution. *Corrosion* 2004;60(8):778-786.
- [56] Y.F. Cheng. Fundamentals of hydrogen evolution reaction and its implications on near-neutral pH stress corrosion cracking of pipeline. *Electrochimica Acta* 52 (2007) 2661-2667.
- [57] Z.Y. Liu, X.G. Li, Y.F. Cheng. Mechanistic aspect of near-neutral pH stress corrosion cracking of pipelines under cathodic polarization. *Corrosion Science* 55 (2012) 54-60.
- [58] Lisa M. Young, Peter L. Andresen, and Thomas M. Angeliu. Crack tip Strain Rate: Estimates Based on Continuum Theory and Experimental Measurement. *Corrosion* 2001, March 11-16, 2001, NACE, Houston, TX, 2001, paper No. 01131.
- [59] R.N. Parkins and J.A. Beavers. Some Effects of Strain Rate on the Transgranular Stress Corrosion Cracking of Ferritic Steel in Dilute Near-Neutral pH Solutions. *Corrosion*: March 2003, Vol. 59, No. 3, pp. 258-273.
- [60] T. L. Anderson. *Fracture Mechanics, Fundamentals and Applications*, Third Edition. Taylor & Francis Group, 2005. pp: 538-545.
- [61] Shyyuan-Fang Chen, Robert P Wei. Environmentally assisted crack growth in a Ni-18Cr-18Fe ternary alloy at elevated temperatures. *Materials Science and Engineering A*, Vol. 256, Issue 1-2, 1998, pp. 197-207.
- [62] G. Van Boven, R. Sutherby, and F. King. Characterizing Pressure Fluctuations on Buried Pipelines in Terms Relevant to Stress Corrosion Cracking. *Proceedings of*

IPC2002, 4<sup>th</sup> International Pipeline Conference, Sept. 29- Oct. 3, 2002, Calgary, Alberta, Canada. Paper No. IPC2002-27149.

[63] Jenny Been, Raymond R. Fessler, Sean Keane, and Walter Kresic. History of Pressure Fluctuations Related to Severity of Near-Neutral pH SCC. Proceedings of IPC2006, 6<sup>th</sup> International Pipeline Conference, Sept. 25- 29, 2006, Calgary, Alberta, Canada. Paper No. IPC2006-10412.

[64] ASTM E1049 – 85 (reapproved 2011)<sup>E1</sup>. Standard Practices for Cycle Counting in Fatigue Analysis. American Society for Testing and Materials, West Conshohocken, PA, 2011.

[65] G. Van Boven, R. Sutherby, and F. King. Characterizing Pressure Fluctuations on Buried Pipelines in Terms Relevant to Stress Corrosion Cracking. Proceedings of IPC2002, 4<sup>th</sup> International Pipeline Conference, Sept. 29- Oct. 3, 2002, Calgary, Alberta, Canada. Paper No. IPC2002-27149.

[66] M. Skorupa. Load Interaction Effects During Fatigue Crack Growth under Variable Amplitude loading- a Literature Review. Part I: Empirical Trends. Fatigue & Fracture of Engineering Materials & Structures 1998; 21: 987-1006.

[67] M. Skorupa. Load Interaction Effects During Fatigue Crack Growth under Variable Amplitude loading- a Literature Review. Part II: Qualitative explanation. Fatigue & Fracture of Engineering Materials & Structures 1999; 22: 905-926.

[68] Vasilios Zitounis. Fatigue Crack Growth Rates under Variable Amplitude Load Spectra Containing Tensile Underloads. PhD thesis, Cranfield University, 28 October 2003.

- [69] Stephan M. Russ. Effect of Underloads on Fatigue Crack Growth of Ti-17. PhD thesis, Georgia Institute of Technology, October 2003.
- [70] Fowler, K.R. and Watanabe, R.T.. Development of Jet Transport Airframe Fatigue Test Spectra, Development of Fatigue Loading Spectra, ASTM STP 1006, J. M. Potter and R. T. Watanabe, Eds., American Society for Testing and Materials, Philadelphia, 1989, pp. 36-64.
- [71] Sunder, R. Contribution of Individual Load Cycles to Crack Growth under Aircraft Spectrum Loading, Advances in Fatigue Lifetime Predictive Techniques, ASTM STP 1122, M. R. Mitchell and R. W. Landgraf, Eds., American Society for Testing and Materials, Philadelphia, 1992, pp. 176-190.
- [72] T. L. Anderson. Fracture Mechanics, Fundamentals and Applications, Third Edition. Taylors & Francis Group, 2005. pp: 473-488.
- [73] Henning Agerskov. The Fatigue Behavior of Steel Structures under Random Loading. Key Engineering Materials, Vols. 378-379 (2008) pp.3-16.
- [74] Yan-Hui Zhang, and S.J. Maddox. Investigation of fatigue damage to welded joints under variable amplitude loading spectra. International Journal of Fatigue 31 (2009) 138-152.
- [75] N.A. Fleck. Fatigue Crack Growth due to Periodic Underloads and Overloads. Acta Metallurgica, Vol. 33, No. 7, July 1985, pp. 1339-1354.
- [76] Colin MacDougall, and T.H. Topper. The influence of variable amplitude loading on crack closure and notch fatigue behavior. International Journal of Fatigue, Vol. 19, No. 5, pp. 389-400, 1997.

- [77] M. El-Zeghayar, T.H. Topper, F.A. Conle, and J.J. F. Bonnen. Modeling crack closure and damage in variable amplitude fatigue using smooth specimen fatigue test data. *International Journal of Fatigue*, Vol. 33, No. 2, Feb. 2011, pp. 223-231.
- [78] J. C. Newman, Jr. and E.P. Phillips. Prediction of Crack Growth Under Variable-Amplitude and Spectrum Loading in a Titanium Alloy. *Fatigue Testing and Analysis under Variable Amplitude Loading Conditions*, ASTM STP 1439, Peter C. McKeighan, and Narayanaswami Ranganathan, American Society for Testing and Materials, Philadelphia, 2005, pp. 232-250.
- [79] N. Ohrloff, A. Gysler and G. Lütjering. *Journal DE Physique*, Colloque C3, supplement au n°9, Tome 48, Sept. 1987, C3-801.
- [80] M. Krkoska, S.A. Barter, R.C. Alderliesten, P. White, R. Benedictus. Fatigue crack paths in AA2024-T3 when loaded with constant amplitude and simple underload spectra. *Engineering Fracture Mechanics*, Vol. 77, No. 11, July 2010, pp. 1857-1865.
- [81] Richard W. Hertzberg. *Deformation and Fracture Mechanics of Engineering Materials*, Fourth Edition, John Wiley & Sons, Inc., 1996, pp. 634-641.
- [82] Kentaro Yamada, Qiuliang Cao, Yuji Okuhara and Xiaohua Cheng. Fatigue Crack Growth Behavior of Various Structural Steel after Single and Periodic Overloads. *Structural Eng./Earthquake Eng., JSCE*, Vol. 15, No. 2, 191s-200s, 1998 July. pp. 37-46.
- [83] J. Schijve, F. A. Jacobs, and P. J. Tromp. Crack propagation in 2024-T3Al cald under flight-simulation loading effect of truncating high gust loads. National Aerospace Laboratory, NLR, The Netherlands, NLR TR-69050-U, June 1969.

- [84] Raymond R. Fessler and Steve Rapp. Method for Establishing Hydrostatic Re-Test Intervals for Pipelines with Stress-Corrosion Cracking. Proceedings of IPC2006, 6<sup>th</sup> International Pipeline Conference, Sept. 25- 29, 2006, Calgary, Alberta, Canada. Paper No. IPC2006-10163, pp. 259-263.
- [85] Weixing Chen, Yongwang Kang, Reg Eadie, Richard Kania, Greg Van Boven, and Robert Worthingham. Proceedings of the 2012 9<sup>th</sup> International Pipeline Conference, IPC2012, Sept. 24- 28, 2012, Calgary, Alberta, Canada. Paper No. IPC2012-90635.
- [86] Yongwang Kang, Weixing Chen, Richard Kania, Gregory Van Boven, Robert Worthingham. Simulation of crack growth during hydrostatic testing of pipeline steel in near-neutral pH environment. Corrosion Science 53 (2011) 968-975.
- [87] Jian Li, M. Elboujdaini, M. Gao, R. W. Revie. Investigation of plastic zones near SCC tips in a pipeline after hydrostatic testing. Materials Science and Engineering A 486 (2008) 496-502.
- [88] Ryoichi Koterazawa, and Takayoshi Noshio. Acceleration of Crack Growth under Intermittent Overstressing in Different Environments. Fatigue & Fracture of Engineering Materials & Structures. Vol. 15, No. 1, pp. 103-113, 1992.
- [89] T. L. Anderson. Fracture Mechanics, Fundamentals and Applications, Third Edition. Taylors & Francis Group, 2005. pp: 457-464.
- [90] Eric F. J. von Euw. Effect of Overload Cycle(s) on Subsequent Fatigue Crack Propagation in 2024-T3 Aluminum Alloy. PhD Dissertation, Lehigh University, 1971.

- [91] Asok Ray, and Ravindra Patankar. Fatigue crack growth under variable-amplitude loading: Part I – Model formulation in state-space setting. *Applied Mathematical Modelling* 25 (2001) 979-994.
- [92] T. L. Anderson. *Fracture Mechanics, Fundamentals and Applications*, Third Edition. Taylors & Francis Group, 2005. pp: 473-488.
- [93] Soo Yeol Lee. *Effects of Overload and Underload on Internal Strains/Stresses and Crack Closure during Fatigue-Crack Propagation*. Doctoral Dissertations, University of Tennessee - Knoxville, December, 2009.
- [94] J. Schijve. The Effect of Pre-strain on Fatigue Crack Growth and Crack Closure. *Engineering Fracture Mechanics*, 1976, Vol. 8, pp. 575-581.
- [95] S. Suresh. *Fatigue of Materials*. Cambridge University Press, Cambridge, New York Port Chester, Melbourne Sydney, 1991, pp:113.
- [96] K. Katagiri, R. Koterazawa, T. Yamada, and T. Tsuboi. Changes in dislocation structures adjacent to fatigue crack tips induced by intermittent overstressing. *Metal Science*, Vol. 17, November 1983, pp:556-562.
- [97] Canadian Energy Pipeline Association (CEPA). *Stress Corrosion Cracking Recommended Practices*, 2<sup>nd</sup> Edition, An industry leading document detailing the management of transgranular SCC, December 2007, pp.5-5.
- [98] TransCanada Pipeline (1996) Response to National Energy Board Information Request 2 of Proceeding MH-2-5, TCP, Calgary, Alberta, Canada, pp.3.

[99] B. W. Williams, S. B. Lamber, R. Sutherby, A. Plumtree. Environmental Crack Growth under Variable Amplitude Loading of Pipeline Steel. Corrosion: January 2004, Vol. 60, No.1, pp. 95-103.

# **Chapter 2      Depressurization-Induced Crack Growth Enhancement for Pipeline Steel Exposed to a Near- Neutral pH Environment<sup>1</sup>**

## **2.1. Introduction**

Although near-neutral pH stress corrosion cracking (NNpHSCC) has been studied since 1985, it is still not fully understood [1-3]. Crack propagation in near-neutral pH environments has never been observed under static tensile loading conditions, by the definition of SCC, except for the initiation of a crack where galvanic corrosion may be predominant [1]. Also, it has been determined that crack growth in near-neutral pH SCC is driven by mechanisms consistent with corrosion fatigue [1,4,5].

Based on long-term and extensive laboratory crack growth simulations, under constant amplitude cyclic loading in near-neutral pH environments, it was found that the crack growth rate could be correlated to a combined factor that incorporated both the mechanical and the environmental driving forces [6] as:

---

<sup>1</sup> A version of this chapter has been published: M. Yu, W. Chen, R. Kania, G. V. Boven, J. Been. In: *proceedings of the 10<sup>th</sup> International Pipeline Conference 2014, IPC2014*, Sept. 29 – Oct. 3, 2014, Calgary, Alberta, Canada. Paper No.: IPC2014-33282.

$$\frac{da}{dN} = a \left( \frac{\Delta K^\alpha K_{max}^\beta}{f^\gamma} \right)^n + b \quad (2 - 1)$$

where  $a$ ,  $n$ ,  $\alpha$ ,  $\beta$ , and  $\gamma$  are all constants,  $\alpha + \beta = 1$ , and  $b$  is the contribution of stress corrosion cracking, which was found to be about one order of magnitude lower than the first term in Stage II crack growth and can be ignored.  $(\Delta K^\alpha K_{max}^\beta)/f^\gamma$  is termed as the combined factor,  $\Delta K$  is the change in stress intensity at the crack tip due to cyclic loading,  $K_{max}$  is the maximum stress intensity at the crack tip, and  $\gamma$  is a factor representing the influence of the corrosion environment on the crack growth rate which is found to be around 0.1.  $\Delta K$  and  $K_{max}$  are strongly dependent on the geometry of the specimen, while  $\gamma$  is dependent on the corrosiveness of environment. A threshold value of  $(\Delta K^\alpha K_{max}^\beta)/f^\gamma$  is also determined, below which crack will cease to grow.

However, there are two main unsolved issues with this model: first, this empirical correlation is based on the laboratory tests done in a frequency range of  $1 \times 10^{-1}$  to  $1.25 \times 10^{-3}$  Hz, which is above the actual frequencies of pressure fluctuations in the field, especially during the operation of high-pressure gas transmission pipelines where loading frequencies are about  $1 \times 10^{-5}$  Hz (one cycle per day) [7]. Although the crack growth at such a low frequency has been studied in near-neutral pH environments [8,9], it cannot be concluded that the crack growth would increase with lowering frequency due to insufficient data [8,10]. Thus, crack growth at frequencies lower than  $1 \times 10^{-3}$  Hz remains to be studied.

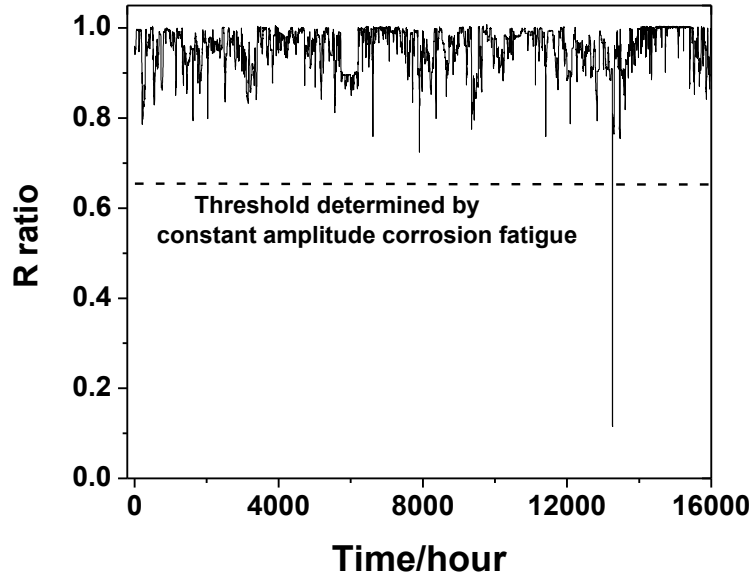


**Figure 2.1 Pressure fluctuations recorded for a high-pressure gas transmission pipeline**

The second issue is that when examining the combined factor values calculated based on the actual pressure fluctuations in the field, as shown in Fig. 2.1 [11] - a typical example of pressure fluctuation recorded in high-pressure gas transmission line where NNpHSCC was found - there are only a limited number of pressure fluctuations with combined factors exceeding the threshold value determined by Eq. (2-1) (represented by the dashed line in Fig. 2.1, assuming that  $K_{\max}=33 \text{ MPa}\cdot\text{m}^{0.5}$ ). And to propagate a crack to the critical dimension at which instant failure would occur should need hundreds of years. This contradicts the fact that failure of pipelines by cracking in the field when exposed to near-neutral pH environments could occur as soon as a few years after the surface of pipeline steel is in direct contact with near-neutral pH environments.

As shown in Fig. 2.1, pressure fluctuates randomly during operation, a typical situation of cyclic loading with varied stress amplitudes. Crack growth behaviour under variable amplitude cyclic loadings has been found to be very different from that under constant amplitude loading. Underloads and overloads, as schematically shown in Fig. 2.2, could accelerate and retard the crack growth rate of the subsequent minor cycles through load interactions, respectively [12,13]; and even the minor cycles whose crack propagation driving force is well below the determined constant amplitude threshold could cause significant crack growth [14]. As a result, the measured crack growth rate may be higher or lower than that calculated using a linear summation of crack growth determined from tests under constant amplitude cyclic loading.

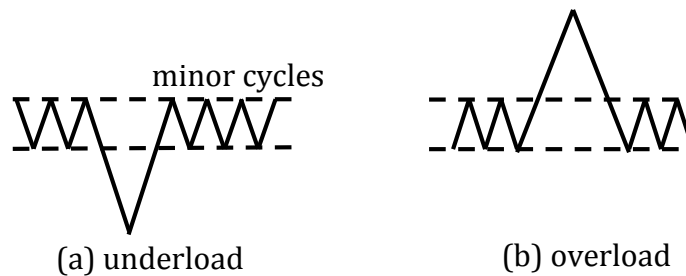


**Figure 2.2 Basic loading waveforms in variable amplitude fatigue test**

Many materials have been extensively studied under variable amplitude fatigue tests, including steel [15,16,17], titanium [18], and especially aluminum alloys for aircraft applications [12,13,15,19-21]. In such studies, an increase of crack growth by a factor varying from 1 up to 20 has been found under underload waveforms [12,15,18], while the crack growth rate after overload can be reduced by several orders of magnitude [12].

The accelerated crack growth of the minor cycles with R ratio 0.5 caused by underload with R ratio of 0.1 was observed in pipeline steel exposed to near-neutral pH environments [22]. However, the minor cycles in the study had very low R ratios and could cause direct crack growth as predicted by the constant amplitude crack growth model and therefore were not typical of pressure fluctuations seen in the field. This investigation was initiated to consider the effect of minor cycles with R-ratios typically seen in the field.

## **2.2 Experimental**

### **2.2.1 Specimen and near-neutral pH solution**

The X60 pipeline steel used in this study was received from Spectra Energy Transmission after being in service for 19 years, with a thickness of 10.4 mm and outer diameter of 913 mm. The chemical composition (wt.%) of the steel is as follows: C: 0.15, Mn: 1.27, P: 0.019, S: 0.005, Si: 0.37, Ni: 0.045, Cr: 0.2, Cu: 0.27, Al: 0.023, Fe: Balance. The microstructures (ferrite and pearlite) of the steel are shown in Fig. 2.3; the grain size was approximately 7  $\mu\text{m}$ . Compact tension (CT) specimens machined from the pipeline steel were used in this study, the dimension of which was shown in Fig. 2.4. The machined notch was perpendicular to the pipe hoop direction. Pre-fatigue cracking was conducted to initiate a sharp crack tip from the machined notch according to the procedures

described in ASTM E647-08 after the surface of the specimen was polished to 600-grit paper. The sharp crack initiated from the machined notch was controlled to be between 2 and 3 mm long with a difference of less than 0.2 mm on the two sides of one sample, measured by an optical microscope.

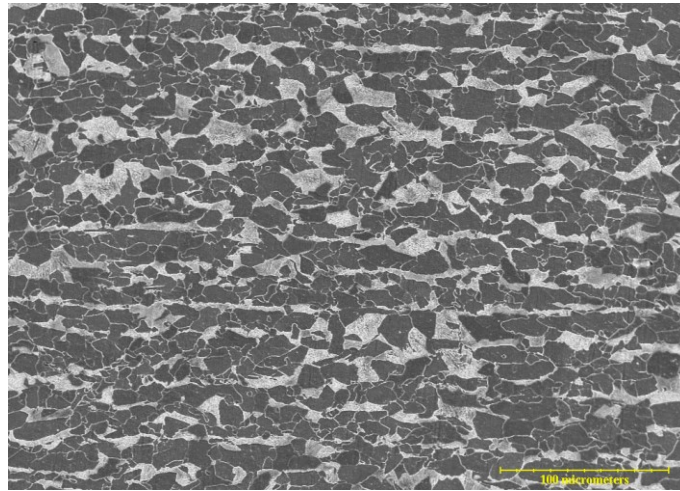


**Figure 2.3 SEM image (secondary electron SE) of pipeline steel microstructures in the transverse section**

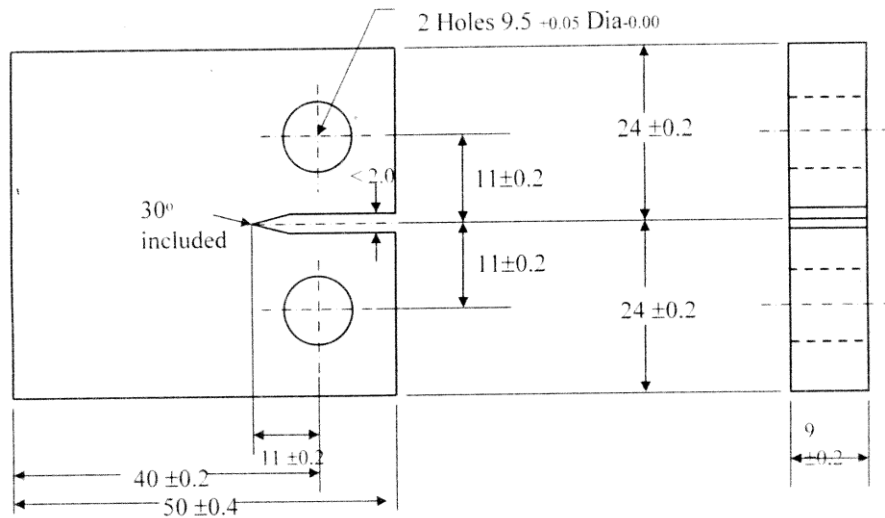


**Figure 2.4 Dimension of compact tension (CT) specimen used in the testing**

**Table 2.1 Summary of tests performed with constant and variable amplitude loading**

Description	Frequency of large cycle (Hz)	Frequency of minor cycles (Hz)	No. of cycles at R=0.5 (per block)	No. of cycles at R=0.9 (per block)	No. of blocks	Duration (days)
Constant amplitude	$1.04 \times 10^{-3}$	-	801	0	-	9
	$2.78 \times 10^{-4}$	-	280	0	-	25
	$3.97 \times 10^{-5}$	-	140	0	-	41
	$2.78 \times 10^{-5}$	-	140	0	-	59
Variable amplitude	$5 \times 10^{-2}$	$5.38 \times 10^{-3}$	1	697	24	38
	$1.04 \times 10^{-3}$	$5.38 \times 10^{-3}$	1	697	24	38
	$2.78 \times 10^{-4}$	$5.38 \times 10^{-3}$	1	697	24	39
	$3.97 \times 10^{-5}$	$5.38 \times 10^{-3}$	1	697	24	45
	$2.78 \times 10^{-5}$	$5.38 \times 10^{-3}$	1	697	24	48
	$2.31 \times 10^{-5}$	$5.38 \times 10^{-3}$	1	697	24	50

One near-neutral pH solution, namely C2 solution (0.0035 KCl, 0.0195 NaHCO<sub>3</sub>, 0.0255 CaCl<sub>2</sub>, 0.0274 MgSO<sub>4</sub>.7H<sub>2</sub>O, 0.0606 CaCO<sub>3</sub> g/l) was used as the aqueous near-neutral pH environment. Gas mixture of 5% CO<sub>2</sub> balanced with nitrogen was purged into the C2 solution (at least 24 hours) before and during the test to achieve a stable near-neutral pH value of 6.29 [6]. The CT specimens were pin-hole loaded and sealed in test cells filled with C2 solution. The temperature of the solution and environment during tests is controlled at 30±0.1°C (above room temperature to be easily controlled). The cyclic loadings were conducted on a horizontal pneumatic loading machine, which was controlled by a computer.

## 2.2.2 Loading conditions

### 2.2.2.1 Constant amplitude cyclic loading.

As shown in Table. 2.1, the CT specimen was loaded to reach a maximum stress intensity factor ( $K_{\max}$ ) of  $33 \text{ MPa}\sqrt{\text{m}}$ . This level of  $K_{\max}$  can be achieved in field pipes, when a long but shallow crack (typical field SCC cracks) with depth of about 20-30% of wall thickness and with a crack length to depth ratio of 10 is loaded to 75% SMYS (specified minimum yield strength). The R ratio was controlled to be 0.5, and the frequency varied from  $1.04 \times 10^{-3} \text{ Hz}$  to  $2.78 \times 10^{-5} \text{ Hz}$ . The test duration varied significantly with frequency. When tested at high frequencies, for example,  $1.04 \times 10^{-3} \text{ Hz}$ , a total of 801 cycles was conducted which lasted 9 days, while only 140 cycles were performed for the test with a frequency at  $2.78 \times 10^{-5} \text{ Hz}$ , which lasted 58 days. The crack growth rate in the frequency range of  $5 \times 10^{-2} \text{ Hz}$  to  $1.04 \times 10^{-3} \text{ Hz}$  was determined based on Eq. (2-1) [6].

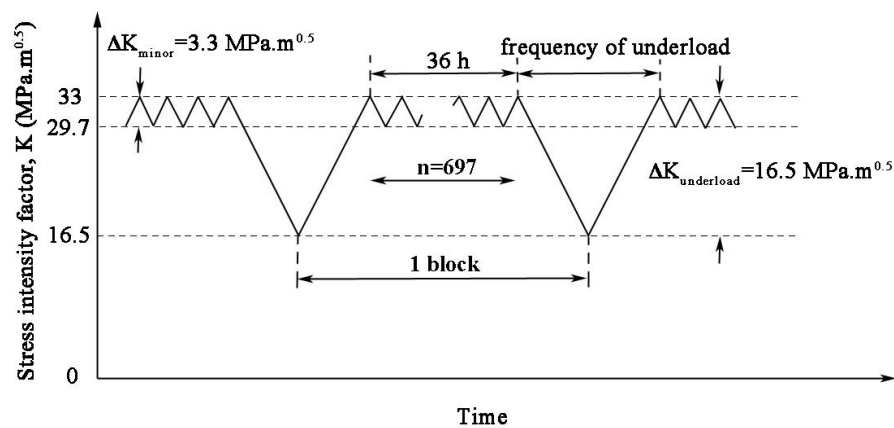


**Figure 2.5** Loading waveform applied in the variable amplitude cyclic loading in C2 solution

### **2.2.2.2 Variable amplitude cyclic loading.**

The waveform shown in Table. 2.1 and Fig. 2.5 was designed to simulate the actual spectrum of pressure fluctuations of pipelines. The  $K_{\max}$  was also kept at 33 MPa $\sqrt{m}$ . The R ratios of minor cycles and underload were 0.9 and 0.5, respectively. The frequency of underload varied from  $5 \times 10^{-2}$  Hz (20 s/cycle) to  $1 \times 10^{-5}$  Hz (27.8 hours/cycle), while that of minor cycles in the waveform was kept constant at  $5.38 \times 10^{-3}$  Hz. The number of minor cycles per block (as defined in the waveform, Fig. 2.5) was set at 697, which lasted 36 hours. 24 blocks (24 underloads) as seen in Fig. 2.5 were applied; the first and last event in the waveform were the minor cycles so that all the load interactions could be included. To further confirm the role of minor cycles with R ratio as high as 0.9 in crack propagation, static hold was applied to replace the minor cycles in the waveform shown in Fig. 2.5. The static hold period was exactly the same as that of minor cycles, 36 hours. The other conditions were the same.

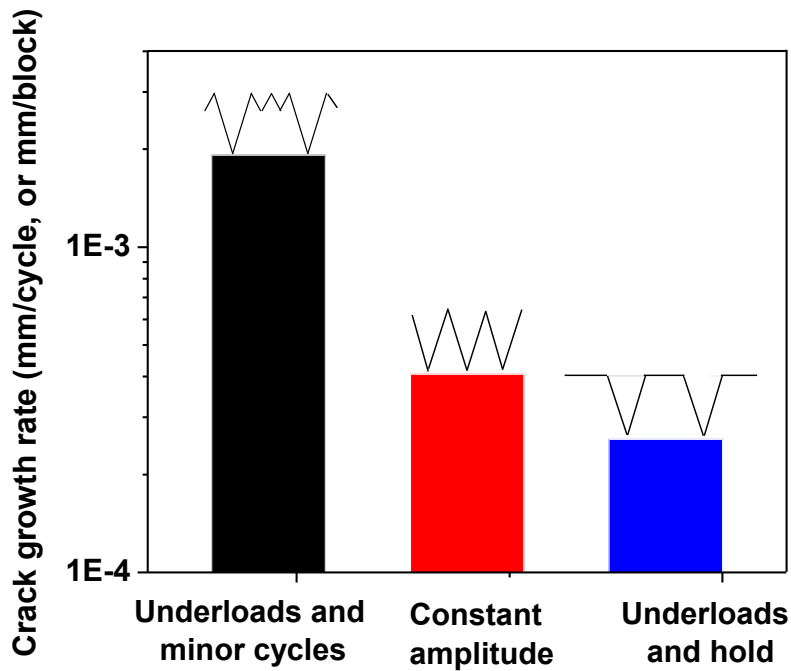


**Figure 2.6 Crack propagation response under different loading waveforms in C2 solution**

Crack growth was determined by measuring the crack length before and after tests on a scanning electron microscope (SEM), Zeiss EVO MA 15, while the fractured surfaces were observed on field emission JEOL 6301F. The crack growth rate, expressed as millimeter per block and millimeter per cycle, was calculated by dividing the measured crack growth length over the number of blocks and cycles applied for variable amplitude cyclic loadings and constant amplitude cyclic loadings, respectively. The specimen after testing was fracture opened in liquid nitrogen and examined on SEM.

## **2.3 Results and Discussion**

### **2.3.1 The role of minor cycles**

A comparison of the crack growth rate under three different kinds of waveforms in C2 solution is shown in Fig. 2.6. The frequency of large cycles in the three loading waveforms was the same,  $1.04 \times 10^{-3}$  Hz. The growth rate of constant amplitude test is  $4.07 \times 10^{-4}$  mm/cycle, while that of underload plus minor cycles is  $1.92 \times 10^{-3}$  mm/block, 4.7 times higher because of the introduction of minor cycles. The minor cycles in this test have a combined factor calculated using Eq. (2-1) well below the crack growth threshold determined from constant amplitude loading.

### **2.3.2 Fracture surface examination**

The specimens tested in C2 solution were fracture opened in liquid nitrogen to observe the striations, which are direct physical evidence of crack growth by fatigue. Only large striations were observed on the fracture surface of the specimen tested under constant amplitude loading, as shown in Fig. 2.7 (a), while mini-striations were also found on the fractured surface in the variable amplitude test, as shown in the inserted image in Fig. 2.7 (b). The striation spacing of constant amplitude test was measured to be about  $1.29 \times 10^{-3}$  mm on average, much higher than that of obtained surface crack growth rate of  $4.07 \times 10^{-4}$  mm/cycle. Similarly from Fig. 2.7 (b), the large striation spacing of the variable

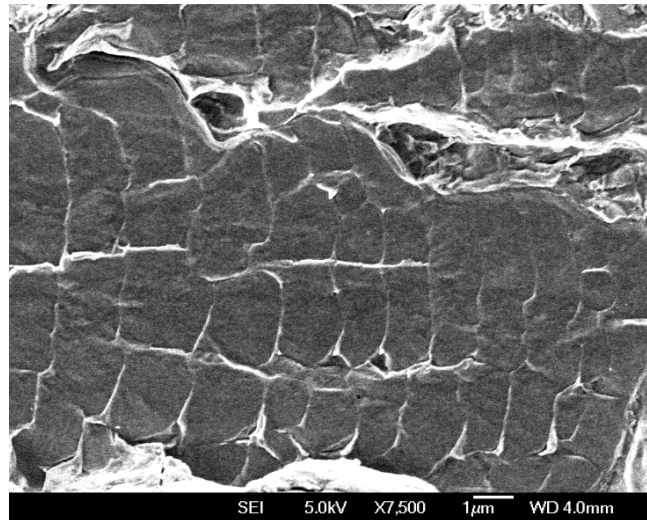
amplitude test was measured to be  $5.92 \times 10^{-4}$  mm, which is higher than the constant amplitude growth rate of underload,  $4.07 \times 10^{-4}$  mm/cycle; and that of the mini-striations was  $1.13 \times 10^{-4}$  mm. All of these suggest that one striation needs multiple loading cycles [23], especially for the minor cycles since they are below constant amplitude threshold; and that the dormant-active discontinuous crack growth may be predominant in the variable amplitude cyclic loadings. The fractographic examination confirms that crack growth of pipeline steel can be caused by the minor cycles in the presence of underloads, even though the minor cycles have a mechanical driving force well below the constant amplitude threshold.

To further confirm the importance of minor cycles in crack growth, static hold was applied to replace the minor cycles while other conditions were kept the same. It is found that the growth rate under the waveform of underload and minor cycles was 7.2 times higher than that under the combination of underload and static hold as shown in Fig. 2.6.

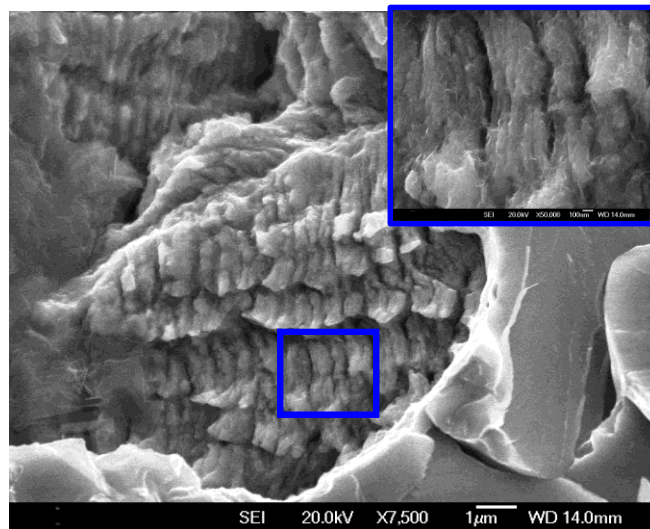
Therefore, the evidence presented strongly suggests that the minor cycles do in fact contribute to the crack propagation of pipelines in near-neutral pH environments through load interaction.

In addition, the growth rate of underload and static hold was only 60% of that obtained from testing under constant amplitude fatigue, which indicates that static hold could actually retard the crack propagation caused by underload. This echoes the conclusion that crack propagation in near-neutral pH environments has never been observed under

static tensile loading conditions except for the initiation of a crack where galvanic corrosion may be predominant [5,6].



(a) LARGE STRIATIONS



(b) LARGE AND MINI- STRIATIONS

**Figure 2.7 SEM images (SE) of fractured surface of specimens in C2 solution, crack propagating from left to right: a) constant amplitude test; and b) variable amplitude test**

These findings contradict a number of general beliefs on crack growth in near-neutral pH environments. First, reducing the maximum pressure to a very low value (one large underload generated) would not produce any benefit to crack growth since the pipeline would be in a lower stress state, as generally believed. Second, one unload cycle would yield crack growth far larger than that predicted by models based on tests under constant amplitude cycles, which has not been adequately considered. Third, the small fluctuations with R ratios as high as 0.9 - which are often considered to be near static and therefore negligible in terms of crack growth - can actually play a role in crack growth. These findings should be implemented into guidelines for daily operation for the purpose of minimizing crack growth.

### **2.3.3 Crack growth behavior at different frequencies**

All the tests at different frequencies were conducted at the same maximum stress intensity factor and R ratio of the underload cycles of the comparative tests shown in Fig. 2.6. Only the frequencies of the large cycles varied for both the constant and variable amplitude fatigue in C2 solution. The test results are shown in Fig. 2.8 for both constant and variable amplitude cyclic loadings.

#### **2.3.3.1 Constant amplitude cyclic loading**

The frequencies of operation pipelines can be often well below  $1 \times 10^{-3}$  Hz, and around  $1 \times 10^{-5}$  Hz (one cycle per day) for gas pipelines [7]. However, laboratory tests were usually done at frequencies higher than  $1 \times 10^{-3}$  Hz.

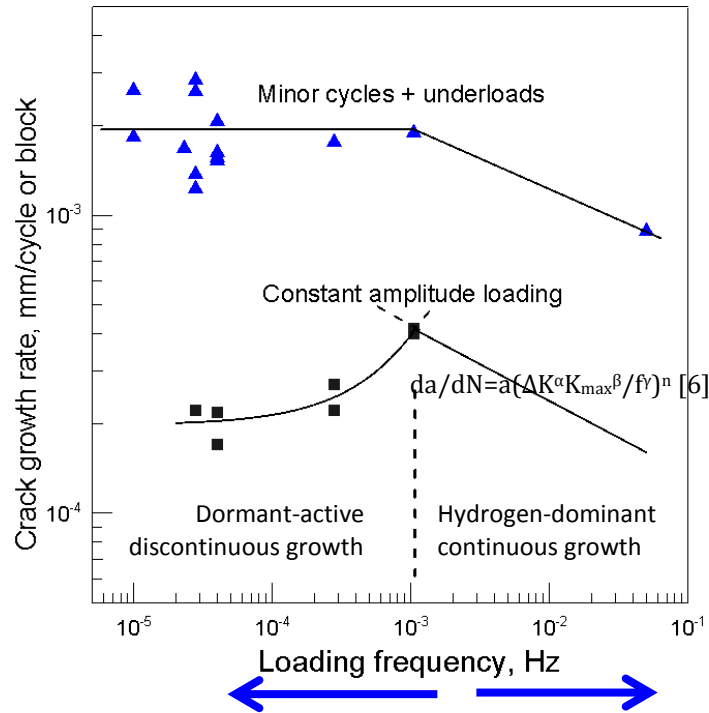


**Figure 2.8 Crack growth behavior at different frequency for both constant and variable amplitude cyclic loadings in C2 solution**

In the high frequency range of  $5 \times 10^{-2}$  Hz to  $1 \times 10^{-3}$  Hz, the crack growth rate has been well studied and can be expressed by Eq. (2-1) [6]. Under the circumstances, crack growth rates are seen to increase with decreasing frequency, as generally found for corrosion fatigue. The crack growth rate at  $1 \times 10^{-3}$  Hz was predicted to be  $4.3 \times 10^{-4}$  mm/cycle by Eq. (2-1), which is consistent with the growth rate experimentally determined in this investigation, which was about  $4.07 \times 10^{-4}$  mm/cycle (average of two experimental points in Fig. 2.8).

However, the crack growth rates were found to decrease with decreasing frequency and to reach a steady value when the frequency is lower than  $1 \times 10^{-3}$  Hz. This positive relationship between the growth rate and the loading frequency can be expressed as:

$$\frac{da}{dN} = 1.94 \times 10^{-4} + 0.204f \quad (2 - 2)$$

In the regime with frequencies higher than  $1 \times 10^{-3}$  Hz, where the crack growth rate is governed by Eq. (2-1), the diffusion of hydrogen - which is a by-product of corrosion - to the triaxial zone ahead of the crack tip is a controlling step of crack growth. A lower frequency allows more time for hydrogen to be diffused to the triaxial zone and thus accelerates crack growth through the mechanisms of hydrogen embrittlement, which has been well studied [5]. On the other hand, in the low frequency regime, for example, below  $10^{-3}$  Hz, the continuous corrosion of crack tip and walls can also contribute to crack tip blunting in near-neutral pH environments [5], reducing the mechanical driving force for crack growth.

### **2.3.3.2 Variable amplitude cyclic loading**

By introducing the minor cycles with a R ratio of 0.9, as shown in Fig. 2.5, the crack growth rate is enhanced by a factor of 6 in the frequency range of  $5 \times 10^{-2}$  Hz to  $1 \times 10^{-3}$  Hz, as compared with constant amplitude test results shown in Fig. 2.8. This further confirms the importance of minor cycles in crack propagation. In this high frequency

regime, the crack growth rate-frequency dependence is found to be similar to that under constant amplitude cyclic loadings; that is, increasing frequency leads to a lower crack growth rate. The crack growth rate was enhanced by a factor of 2.13 with decreasing frequency from  $5 \times 10^{-2}$  Hz to  $1 \times 10^{-3}$  Hz. It is believed that the crack growth under the current variable loading condition was also governed by the hydrogen-dominant crack growth mechanisms.

With further decreases of the frequency of underload to  $1 \times 10^{-5}$  Hz (27.8 hours per cycle): the crack growth rate neither increases with decreasing frequency, as generally believed in corrosion fatigue, nor decreases with decreasing frequency, as observed in the constant amplitude tests; however, it instead approaches a steady value of about  $2 \times 10^{-3}$  mm/block. Several tests were repeated in this low frequency range to confirm the trend. It can be seen that the crack growth rate is increased 10 times of that of constant amplitude fatigue in C2 solution at the frequency  $1 \times 10^{-5}$  Hz. This enhanced crack growth rate in variable amplitude tests results from the load interaction of variable amplitude loading [12-15]. When accelerated crack growth due to load interaction is considered, the remaining life of high-pressure gas transmission pipelines with SCC can be predicted to yield a value consistent with the field experiences.

The crack tip morphology on the middle plane in the thickness direction is shown in Fig. 2.9 - note that a single specimen was etched to show that the etchant may affect the crack tip sharpness. The arrow marks the position of pre-cracking tip before corrosion fatigue tests. It can be seen that the crack tip after tests in the high frequency range of  $5 \times 10^{-2}$  Hz

to  $1 \times 10^{-3}$  Hz remains sharp. However, with further lowering frequency, the crack tip becomes blunter. It is believed that the near constant crack growth rate at frequencies lower than  $1 \times 10^{-3}$  Hz is a result of competition between increased mechanical driving force induced by the interaction between the underload and the minor cycles, and the crack tip blunting resulting from corrosion. Further research is needed to elucidate the physical process of crack tip blunting and re-sharpening for the discontinuous growth.

The variable loading spectrum shown in Fig. 2.5 is much closer to the pressure fluctuations of pipelines in daily operation than the constant amplitude loading scenarios. The remaining life prediction made based on crack growth rate of variable loading is also consistent with the field experiences [24].

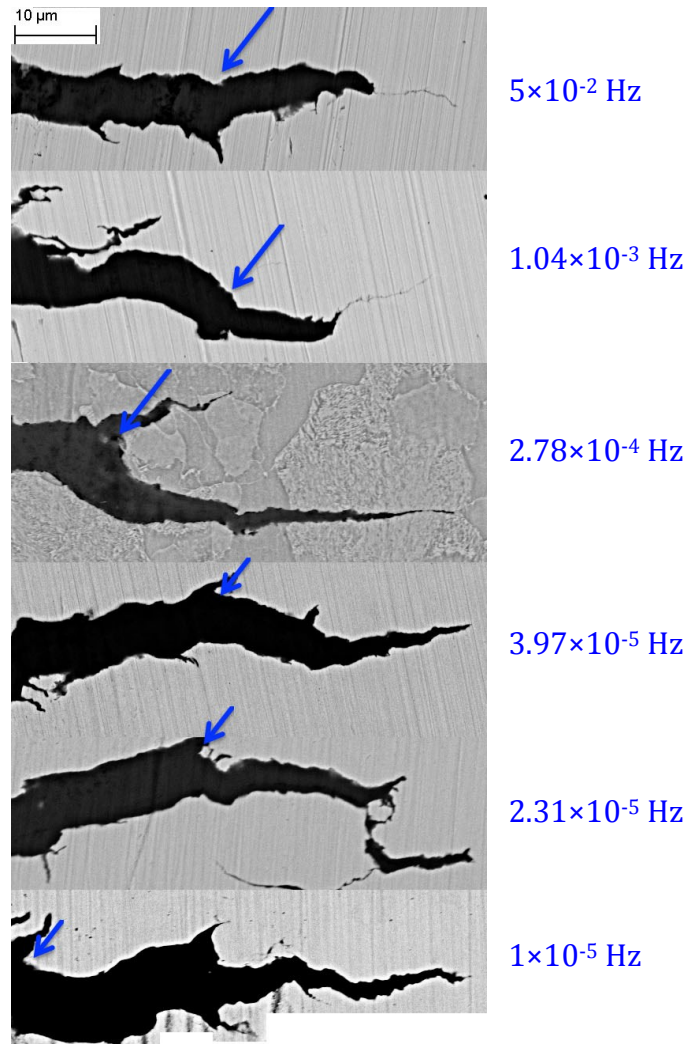


**Figure 2.9** The crack tip morphology (backscatter electron detector BSD) on the middle plane in the thickness direction on the samples of variable amplitude tests at different frequencies. The arrow marks the position of the pre-cracking tip before test (by comparing with the images taken before test).

## 2.4 Practical Strategies for Avoiding Enhanced Crack Growth

Several pipeline operation strategies able to avoid enhanced crack growth are available based on the outcome of this investigation.

- 1) The minimum normal operation pressure should be controlled to as high as possible to reduce the amplitude of large cycle (reducing acceleration effect).
- 2) It is recommended that the pipeline be operated with a control of mean pressure, rather than the current maximum pressure. This would allow for a certain level of overloading, which on one hand could minimize the enhanced crack growth by underload, and on the other hand achieve retarded growth by overloading.
- 3) If underloads, for example, due to shutdown or hydrotests, are not avoidable, a static hold for a period of at least 24 hours following each underload is recommended to achieve crack tip blunting and thus to reduce load interaction for an enhanced crack growth in the subsequent load cycles. A similar recommendation has been proposed [25,26], which was made based on the results of hydrostatic simulations.
- 4) If possible, an overloading could be applied following each underload or after a period of operation.

## **2.5 Conclusions**

A comparative study has been made of X60 pipeline steel to investigate the crack propagation in near-neutral pH solution under both constant and variable amplitude loadings in a wide frequency range of  $5 \times 10^{-2}$  Hz to  $1 \times 10^{-5}$  Hz. Variable amplitude cyclic loading was designed to consist of an underload with a relatively low R ratio of 0.5 and minor cycles having a R ratio of 0.9. This loading spectrum simulates pressure

fluctuations experienced by high-pressure gas transmission pipelines. It has been found from this investigation that:

- (1) The minor cycles with very high R-ratios that have been previously considered to be non-propagating based on constant amplitude crack growth model can cause significant crack advance in the presence of underload. Its growth rate is about 5 times of that of constant amplitude testing, and 7 times of that of static hold and underload.
- (2) Two different crack growth rate-frequency dependences were observed. When the loading frequency is above  $1 \times 10^{-3}$  Hz, crack growth rate was found to increase with decreasing frequency, which confirms the findings reported previously. In the loading frequency lower than  $1 \times 10^{-3}$  Hz, the crack growth rate was found to decrease with decreasing loading frequency and then to reach a constant at around  $1 \times 10^{-4}$  Hz, which has not been reported before.
- (3) Crack growth rate under the loading spectrum consisting of underloads and minor cycles was found to increase by a factor of up to 10 when compared with constant amplitude underloading without the inclusion of minor cycles in the low frequency range.
- (4) Four pipeline operation recommendations were made based on the outcomes of this investigation, which could substantially avoid the impact of underloads and the load interactions during pipeline operation.

## References

- [1] Parkins RN. Paper 00363. Houston, Texas: NACE International; 2000.
- [2] W. Chen, F. King, and E. Vokes. Corrosion 2002, Vol. 58, No. 3, pp.267-275.
- [3] W. Bouaeshi, S. Ironside, and R. Eadie. Corrosion 2007, Vol. 63, No. 7, pp.648-660.
- [4] J. A. Beavers and C. E. Jaske. NACE International, ISBN: 98257 1998 CP.
- [5] W. Chen, Richard Kania, Robert Worthingham, Gregory Van Boven. Acta Materialia 57 (2009) 6200-6214.
- [6] Weixing Chen and Robert L. Sutherby. Metallurgical and Materials Transactions A, Vol. 38A, June 2007, pp.1260-1268.
- [7] G. Van Boven, R. Sutherby, F. King. Proceedings of IPC 2002, 4<sup>th</sup> International Pipeline conference, Sept. 29-Oct. 3, 2002, Calgary, Alberta, Canada. Paper No.: IPC2002-27149, pp: 1-12.
- [8] T.M. Ahmed, et al. Corrosion, Vol. 53, No.7, 1997, pp.581-590.
- [9] J. A. Beavers, C. J. Maier, and C. E. Jaske. NACE International, Corrosion 2007 Conference & Expo, Paper No. 07128.
- [10] Weixing Chen, and Robert Sutherby. IPC06-10477, Sept. 25-29, 2006, Calgary, Alberta, Canada.
- [11] Brett Conrad, et al. Proceedings of IPC 2012, 9<sup>th</sup> International Pipeline conference, Sept. 24-28, 2012, Calgary, Alberta, Canada. Paper No.: IPC2012-90629, pp: 559-567
- [12] M. Skorupa. Fatigue & Fracture of Engineering Materials & Structures, 1998, 21, pp. 987-1006.

- [13] M. Skorupa. *Fatigue & Fracture of Engineering Materials & Structures*, 1999, 22, pp. 905-926.
- [14] Ryoichi Koterazawa, and Takayoshi Nosho. *Fatigue & Fracture of Engineering Materials & Structures*, Vol. 15, No.1, pp.103-113, 1992.
- [15] N. A. Fleck. *Acta metall.* Vol. 33, No.7, pp. 1339-1354, 1985.
- [16] Colin MacDougall and T.H. Topper. *International Journal of Fatigue*, Vol. 19, No. 5, pp.387-400, 1997.
- [17] M. El-Zeghayer, T.H. Topper, F.A. Conle, J.J.F. Bonnen. *International Journal of Fatigue* 33 (2011) 223-231.
- [18] Stephan M. Russ. *Effect of Underloads on Fatigue crack Growth of Ti-17*. PhD thesis, Georgia Institute of Technology, October 2003.
- [19] N. Ohrloff, A. Gysler and G. Lütjering. *Journal DE Physique*, Colloque C3, supplément au n°9, Tome 48, Septembre 1987. C3-801-C3-807.
- [20] V. Zitounis and P. E. Irving. *International Journal of Fatigue* 29 (2007) 108-118.
- [21] M. Krkoska, et al. *Engineering Fracture Mechanics* 77 (2010) 1857-1865.
- [22] B.W. Williams, et al. *Corrosion*, Vol. 60, No. 1, Jan. 2004. pp. 95-103.
- [23] D. L. Davidson and J. Lankford. *International Materials Reviews*. Vol. 37, No. 2, 1992, pp. 45-74.
- [24] Jiayi Zhao, et al. Full paper submitted to the 10<sup>th</sup> International Pipeline Conference (IPC 2014), Sept. 29- Oct. 3, 2014, Calgary, Alberta, Canada. Paper No. IPC2014-33325.

[25] Weixing Chen, Achieving Maximum Crack Remediation Effect from Optimized Hydrotesting, Final Report Prepared for US Department of Transportation PHMSA, Client Contract Number: DTPH56-08-T-000008-WP#355, June 15, 2011, total pages: 93.

[26] Chen, W., et al. Proceedings of IPC2012, the 9th International Pipeline Conference, Sept. 24-28, 2012, Calgary, Alberta, Canada. Paper No.: IPC2012-90635, pp: 267-276.

# **Chapter 3      Crack Growth Behavior of Pipeline Steel**

## **Exposed to a Near-Neutral pH Environment under**

### **Variable Pressure Fluctuations: Effects of Loading**

#### **Frequency<sup>1</sup>**

### **3.1 Introduction**

This investigation gives an explanation for the various corrosion fatigue (SCC) failure scenarios found during pipeline operations. In particular, it will focus on the crack growth behavior over a wide range of loading frequency found in service considering both gas and liquids pipelines. The corrosion fatigue failure of pipeline steel in near-neutral pH environments was described as stress corrosion cracking when first reported in 1985 [1]. Although three decades have passed, the models governing the crack growth still cannot predict failure time accurately, and pipeline failures caused by corrosion fatigue continue imposing a significant threat to the safety of the operation of the pipeline network [2, 3].

---

<sup>1</sup> A version of this chapter has been submitted to *Acta Materialia* for publication after first revision.

Corrosion fatigue is often classified into three categories: cyclic dependent, time dependent, and time and cycle dependent [4]. Crack growth in the first category of corrosion fatigue is not loading frequency dependent, while the latter two are frequency dependent. The frequency-dependent growth in essence is attributed to time-dependent processes that contribute either directly or indirectly to the crack growth, which may include:

- i. The time-dependent process of surface passivation or oxide film formation, which usually yields an inverse dependence of crack growth rate on loading frequency [4, 5]. But this is not the case for the near-neutral pH corrosion system as no passivation or oxide films are observed in near-neutral pH environments [1].
- ii. The time-dependent process of corrosion where lower loading frequencies give rise to a higher crack growth rate per cycle.
- iii. Both time- and cycle-dependent processes, for example, may correspond to a maximum segregation of hydrogen to the crack tip that is both time and stress dependent [6, 7, 8].
- iv. Time-dependent mechanical property attributes, such as room temperature creep [9-11] and high temperature creep [12], both of which could lead to crack tip blunting and mechanical damage to the crack tip materials. Although blunting can be beneficial as it reduces stress enhancement at the crack tip, it can cause

mechanical damage such as void formation (either the ductile dimples or the creep voids), which accelerates crack growth.

- v. Many other specific conditions that could enhance or reduce the time-dependent crack growth, such as temperature [12], chemistry of materials and electrolytes [6, 13], mechanical characteristics [3, 6, 14], and electrolyte dynamics [6].

Corrosion fatigue of pipeline steel in near-neutral pH environments is very complicated because it involves 4 (that is, ii-v) of the 5 aspects of time-dependent processes defined above. For the physical mechanisms of crack growth, it is generally believed that crack growth proceeds by either or all of the following processes: 1) by dissolution at the crack tip only, which is primarily a process of major influence in the earliest stage of crack growth when the crack is shallow, for example, up to 1 mm in depth, and during the growth of these small cracks on the pipe surface; 2) by direct cracking of the crack tip through hydrogen embrittlement mechanisms, which is primarily the mechanism of crack growth following the dissolution mechanism in the initial stage; 3) by direct cracking caused by cyclic loading which results from the pressure fluctuations during normal pipeline operation.

In addition to the above considerations, the complexity of corrosion fatigue of pipeline steel in near-neutral pH environments also arises from the following unique situations:

- a) The range of loading frequency is very large, typically in the range from  $10^{-1}$  to  $10^{-6}$  Hz [15]. Crack growth behavior in the low range (lower than  $10^{-3}$  Hz) of loading frequencies has not been well studied [6,16].
- b) The pressure fluctuations are dictated by unpredictable supply and consumption of fluid media and the location relative to the pumps or pumps which are used to transport the fluids. This variability of loading and the cycle interactions can lead to large variations in crack growth as will be shown. However existing life prediction models of either fatigue or corrosion fatigue [6, 16, 17] do not adequately account for these effects.

Both of the above two unique conditions will be dealt with in this investigation. The crack growth rate in the frequency range higher than  $10^{-3}$  Hz under constant amplitude fatigue loading has been well studied. It is generally believed that the fatigue crack growth rate increases with lowering frequency, because of the increased time either for the interaction of corrosive chemicals with the metal or for hydrogen diffusion [6, 7]. However, such a conclusion could not be extended to the frequency range lower than  $10^{-3}$  Hz, within which there is always sufficient time for hydrogen to diffuse to the weakest link in the material ahead of the crack tip, in accordance with the change of stress. For these lower frequencies, the effect of room temperature creep may also become significant. However, only a few investigations have been reported for the corrosion fatigue crack growth at loading frequencies lower than  $10^{-3}$  Hz [16,18].

Pipelines are operated under variable pressure fluctuations. All existing crack growth models were developed based on results obtained from tests either under constant load for the case of SCC or under constant stress amplitude loading for the case of fatigue or corrosion fatigue. These models generally yield a prediction that fails to accurately predict real crack growth because they fail to consider the effect of both the stress-dependent and the time-dependent load interactions on crack growth during variable pressure fluctuations. Such predictions may under predict or over predict depending on the loading. These load interaction situations are essential to the nature of stress-cracking of pipeline steel in near-neutral pH environments and may be summarized as follows:

- 1) Scenario 1: A previous cyclic loading with an R-ratio different from the current cyclic loading may condition the crack tip mechanically to either increase or decrease the crack growth rate of the current cycle and/or the future cycles, which is the so-called stress-dependent load interaction [19, 20].
- 2) Scenario 2: The rate of pressure fluctuations, often referred as loading frequency, produces variable pressure fluctuations, which may yield different time-dependent contributions to the crack growth. These time-dependent contributions may include: the rate of corrosion, the rate of hydrogen segregation by diffusion to the crack tip [7], and the degree of crack tip blunting caused by room temperature creep [7, 9-11] and hydrogen facilitated local plasticity (HELP) [21, 22].
- 3) Scenarios 1) and 2) can also mutually interact, for example, crack tip blunting caused by the situations described in Scenario 2 which may lead to different stress states at the crack tip and therefore yield different stress-dependent load

interactions considered in Scenario 1.

The pressure fluctuations in the field could be roughly categorized into the following three types: Type I - underload pressure fluctuations, Type II – load fluctuations above and below the mean, and Type III - overload fluctuations. Type I is typically seen within 30 km downstream of a pump station and is the harshest pressure fluctuations in terms of crack growth rate because the maximum pressure of the variable pressure fluctuations is generally highest and often controlled to be at or close to the design limit. It, however, is reduced as the fluids move away from the discharge site of a pump station because of the friction between the fluids inside the pipeline and the pipeline internal surface. Type III exits at the suction section of a pipeline and is usually associated with a reduced potential of crack growth. Type II is very typical for pipeline sections located between Type I and Type III sections and has a moderate potential for inducing crack growth.

This investigation was initiated to address crack growth behavior corresponding to Type I pressure fluctuations because these may be life-limiting for the pipeline. A typical example of Type I pressure fluctuations is illustrated in Fig. 3.1, which is featured with a combination of occasional underloads with the majority of time periods with stress cycles with R-ratios (minimum stress/maximum stress) above 0.9. The high R ratio cycles are often considered to be near-static and non-propagating. In a recent preliminary investigation, it was found that the minor cycles with an R ratio as high as 0.9 could cause significant crack propagation in the presence of an underload cycle with lower R-ratios [23, 24]. This study will focus on the effect of loading frequencies on corrosion

fatigue crack growth in near-neutral pH environments, especially when the loading frequencies are lower than  $10^{-3}$  Hz and the loading waveforms consisting of occasional underloads with many minor cycles with high R ratios.

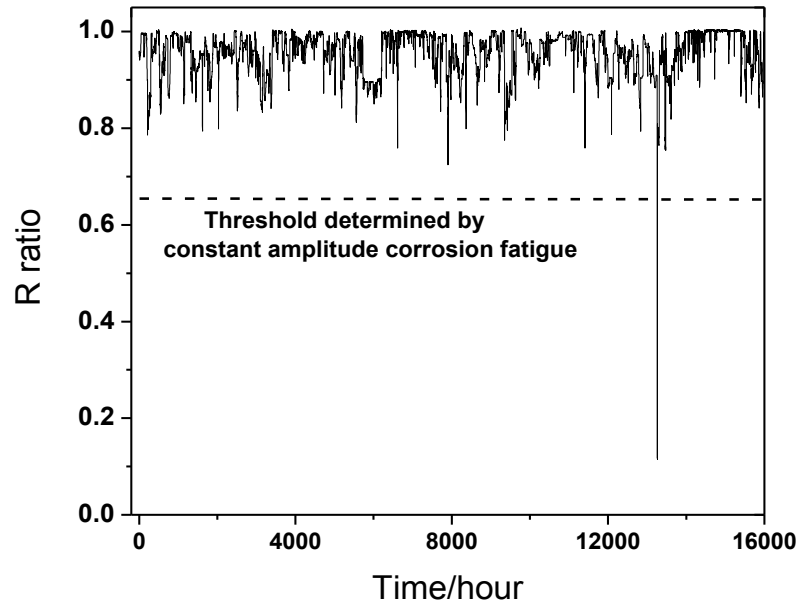


**Figure 3.1** Pressure fluctuations recorded for a high-pressure gas transmission pipeline (SCADA data)

## **3.2 Experimental**

### **3.2.1 Materials and environment**

An X60 pipeline steel with a wall thickness of 10.4 mm and outer diameter of 913 mm was used in this study, which was received from Spectra Energy Transmission. Near-neutral pH corrosion fatigue (NNpHCF) was found in the pipeline, which had 19 years of operation. Pipeline sections that were cut from the joint where cracking had been found were used in this investigation. Compact tension (CT) specimens with a thickness of  $9 \pm 0.2$  mm were machined from the pipeline regions that were free of crack colonies. The chemical composition (wt.%) of the steel studied was as follows: C: 0.15, Mn: 1.27, P: 0.019, S: 0.005, Si: 0.37, Ni: 0.045, Cr: 0.2, Cu: 0.27, Al: 0.023, Fe: Balance. The notch in the CT specimens was orientated in a direction parallel to the pipe longitudinal direction so that the path of crack growth in the specimen is the same as that of the longitudinal cracks found in the field. The CT specimens were polished to 600 grit finish and then pre-cracked by fatigue in air to produce a sharp crack tip from the machined notch according to ASTM E647-08. The sharp crack initiated from the machined notch was controlled to be between 2 and 3 mm long and the difference in crack length on either side of the specimen was less than 0.2 mm.

The corrosion fatigue tests were performed in a near-neutral pH solution, namely C2 solution (0.0035 KCl, 0.0195 NaHCO<sub>3</sub>, 0.0255 CaCl<sub>2</sub>, 0.0274 MgSO<sub>4</sub>·7H<sub>2</sub>O, 0.0606 CaCO<sub>3</sub> g/l). A gas mixture of 5% CO<sub>2</sub> balanced with nitrogen was purged through the C2 solution before and during the test to achieve a stable pH value in the solution of 6.29 [6].

### **3.2.2 Mechanical loading conditions**

### 3.2.2.1 Effect of loading frequency

The CT specimens were sealed in test cells filled with C2 solution and pin loaded on a horizontal pneumatic loading machine with computer load control [7]. The waveform shown in Fig. 3.2 was designed to simulate the field pressure fluctuations shown in Fig. 3.1. The starting  $K_{\max}$  applied was  $33 \text{ MPa}\sqrt{\text{m}}$ . This level of  $K_{\max}$  can be achieved in field pipes, when a long but shallow crack (typical field SCC cracks) with depth of about 20-30% of wall thickness and with a crack length to depth ratio of 10 is loaded to 75% specified minimum yield strength (SMYS). The R ratio of underload and minor cycles was 0.5 and 0.9, respectively. The number of minor cycles per block (between two neighbouring large cycles) was 697 cycles, at which the acceleration effect was found to be close to the saturation state [24].

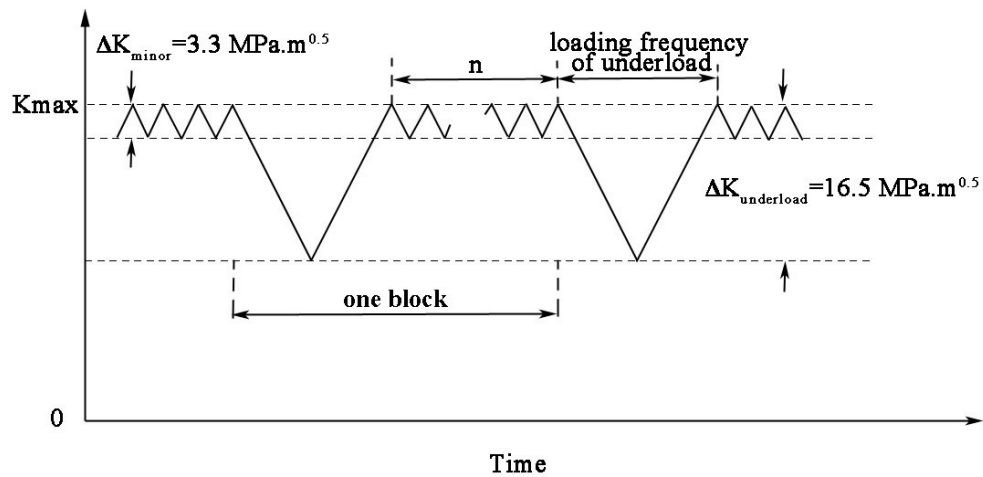


**Figure 3.2** Variable amplitude fatigue waveform designed to simulate the pressure fluctuations in Figure 3.1

The number 697 was found in the following way. The average time interval between two neighboring cycles with R-ratios lower than 0.9 in the spectra shown in Fig. 3.1 was found to be 36 hours. The loading frequency of minor cycles was set to be at  $5.0 \times 10^{-3}$  Hz, which is often used in laboratory simulations [6, 7, 16]. The loading frequency actually measured during testing on a pneumatic loading frame was  $5.4 \times 10^{-3}$  Hz due to some execution errors in the test system, which yielded a total of 697 cycles for a 36-hour loading interval of the minor cycles.

The loading frequency range of underload cycle was varied from  $1.0 \times 10^{-5}$  Hz (27.8 h/cycle) to  $5.0 \times 10^{-1}$  Hz (2 s/cycle) in C2 solution. This frequency range was selected based on the statistics of a total of 18 pressure spectra (14 gas pipelines and 4 oil pipelines), which were originated from discharge sections of pipeline segments. The statistical analysis was performed by one self-developed computer program that was built by the in-house code utilizing MATLAB software. It was found that the statistical distribution of the loading frequency was within the range of  $10^{-5}$  to  $10^{-6}$  Hz and  $10^{-2}$  to  $10^{-5}$  Hz, respectively, for the gas pipeline and the oil pipeline. The detailed analyses of pressure spectra are to be published [25].

To understand the effect of environment, fatigue tests with a similar range of loading frequency were also performed in air. The tests in air were conducted on a closed loop hydraulic Instron machine (8516) at room temperature, around 22°C. The waveform shown in Fig. 3.2 was also executed using computer control with Instron Wavemaker- Runtime software [11]. The loading frequency of underload varied from  $2.8 \times 10^{-4}$  Hz (1

s/cycle) to  $5.0 \times 10^{-1}$  Hz (2 s/cycle), while the other loading conditions were the same as those used for the tests in C2 solution.

### **3.2.2.2 Effect of maximum stress**

The maximum stress intensity factor of the waveform shown in Fig. 3.2 was selected at 27, 33 and  $43 \text{ MPa}\sqrt{\text{m}}$ , while the amplitude of underload and minor cycles was kept the same as for the loading frequency tests, which was  $16.5$  and  $3.3 \text{ MPa}\sqrt{\text{m}}$  respectively. Correspondingly, the R ratios of underload and minor cycles would be different. The loading frequency of underload and minor cycles was  $1.0 \times 10^{-3}$  Hz and  $5.4 \times 10^{-3}$  Hz, respectively. The number of minor cycles,  $n$ , was 300 cycles (more blocks could be performed compared with  $n=697$  in the same period). 61 blocks were applied for the three tests in solution, the duration of which was 41 days. For comparison, tests with the same test conditions were also performed in air on the Instron machine at room temperature. The net crack growth length for loading frequency and maximum stress tests was less than 0.5 mm and can be considered as under K control.

### **3.2.3 Determination of crack growth rate**

Crack growth was determined by measuring the crack length before and after tests on scanning electron microscopy (SEM) on the fracture surface. The crack growth rate, expressed in millimeter per block, was calculated by dividing the measured crack growth length by the number of cyclic blocks applied. For this investigation, the crack

propagation caused by underload cycles could not be separated from that caused by the minor cycles.

### **3.3 Results**

To observe the acceleration effect caused by variable amplitude fatigue through load interaction, constant amplitude crack growth rate was either determined in this investigation or obtained from publications [6, 24] for tests in air and in C2 solution. Using these cracking rates, the predicted crack growth rate of variable amplitude fatigue could be calculated through linear summation (*i.e.* ignoring the effects of load interaction). All the experimental results obtained are listed in Table 3.1.

#### **3.3.1 Frequency dependence of crack growth rate under constant amplitude cyclic loading**

The constant amplitude crack growth rate at different frequencies tested in air and in near-neutral pH solution (C2) is shown Fig. 3.3. It can be seen that the fatigue crack growth rate in air was insensitive to the change of loading frequencies in the range of  $10^{-3}$  to  $10^{-1}$  Hz under  $\Delta K = 15.3 \text{ MPa}\cdot\text{m}^{0.5}$  (using the same material and maximum stress). And thus the fatigue crack growth rate in air was also believed insensitive to loading frequency under  $\Delta K = 16.5 \text{ MPa}\cdot\text{m}^{0.5}$ , which was determined to be  $4.2 \times 10^{-5}$  mm/cycle. For tests in C2 solution, the crack propagation at frequencies higher than  $10^{-3}$  Hz has

been well studied and can be expressed as a function of the combined factor of maximum stress intensity factor  $K_{max}$ , stress intensity factor range  $\Delta K$  and frequency  $f$  (for details, refer to Ref. [6]). The representative crack growth rate data (open diamond) were shown in Fig. 3.3. In such a frequency range, the crack growth rate increases with lowering frequency until  $10^{-3}$  Hz. However, crack growth rate decreases with further decreasing loading frequency [23], rather than increases as generally believed [6, 7, 26]. ]. A linear relationship can be obtained between the growth rate,  $da/dN$ , and the loading frequency,  $f$ , through curve fitting [23]:

$$\frac{da}{dN} (mm/cycle) = 1.94 \times 10^{-4} + 0.204f \quad (3 - 1)$$

The standard error in Eq. (3-1) was  $1.3 \times 10^{-5}$  mm/cycle. Although crack growth rate decreases linearly with lowering  $f$ , the reduction of crack growth rate at very low frequencies (the small absolute value of frequency) is so small that crack growth rate appeared constant in logarithm scale shown in Fig. 3.3, about  $1.9 \times 10^{-4}$  mm/cycle, which is about one order of magnitude higher than the standard error.

**Table 3.1 Crack growth rate obtained at different frequencies and maximum stress in this investigation**

	Frequency, Hz	$K_{max}$ , $MPa \cdot m^{0.5}$	Crack growth rate in solution, mm/cycle or mm/block	Crack growth rate in air, mm/cycle or mm/block
Constant amplitude loading	$1.0 \times 10^{-3}$	33	$4.0 \times 10^{-4}$	$4.2 \times 10^{-5}$
	$1.0 \times 10^{-3}$		$4.1 \times 10^{-4}$	
	$2.8 \times 10^{-4}$		$2.7 \times 10^{-4}$	
	$2.8 \times 10^{-4}$		$2.2 \times 10^{-4}$	
	$4.0 \times 10^{-5}$		$1.7 \times 10^{-4}$	
	$4.0 \times 10^{-5}$		$2.2 \times 10^{-4}$	
Variable amplitude loading	$2.8 \times 10^{-5}$	33	$2.2 \times 10^{-4}$	$6.7 \times 10^{-4}$
	$5.0 \times 10^{-1}$			
	$5.0 \times 10^{-2}$		$9.0 \times 10^{-4}$	
	$1.0 \times 10^{-3}$		$1.9 \times 10^{-3}$	
	$2.8 \times 10^{-4}$		$1.8 \times 10^{-3}$	
	$4.0 \times 10^{-5}$		$1.6 \times 10^{-3}$	
	$4.0 \times 10^{-5}$		$2.1 \times 10^{-3}$	
	$4.0 \times 10^{-5}$		$1.6 \times 10^{-3}$	
	$4.0 \times 10^{-5}$		$1.7 \times 10^{-3}$	
	$4.0 \times 10^{-5}$		$1.4 \times 10^{-3}$	
	$2.8 \times 10^{-5}$		$1.2 \times 10^{-3}$	
	$2.8 \times 10^{-5}$		$2.9 \times 10^{-3}$	
	$2.8 \times 10^{-5}$		$2.6 \times 10^{-3}$	
	$2.3 \times 10^{-5}$		$1.7 \times 10^{-3}$	
$1.0 \times 10^{-5}$	$1.9 \times 10^{-3}$			
Variable amplitude loading	$1.0 \times 10^{-5}$	27	$7.2 \times 10^{-4}$	$4.1 \times 10^{-4}$
		33	$1.2 \times 10^{-3}$	$3.5 \times 10^{-4}$
		33	$1.4 \times 10^{-3}$	
		43	$1.8 \times 10^{-3}$	$3.7 \times 10^{-4}$
		43	$1.8 \times 10^{-3}$	

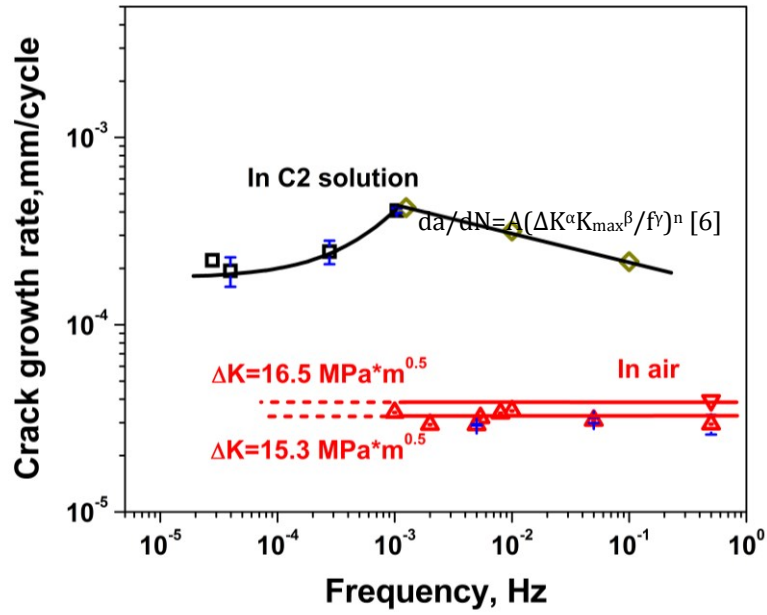


Figure 3.3 Frequency dependence of constant amplitude crack growth rate in C2 solution and in air

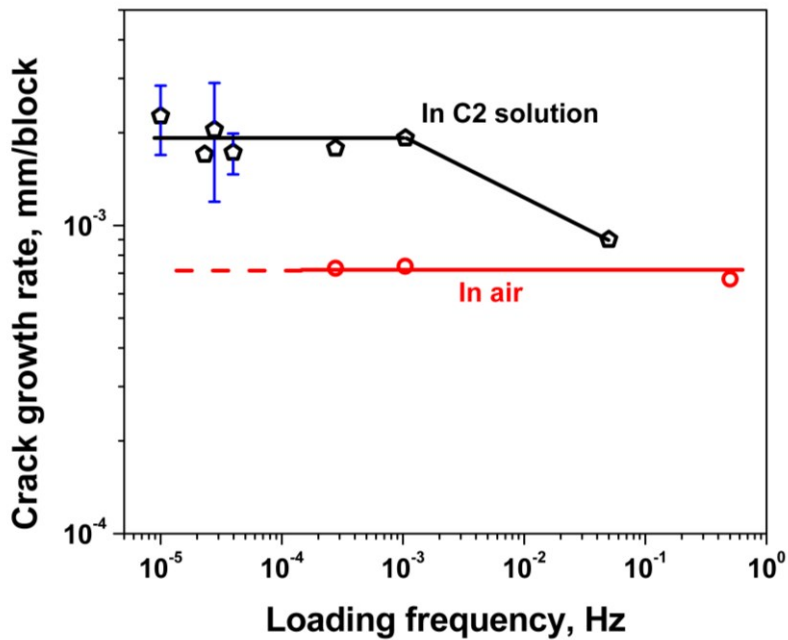


Figure 3.4 Frequency dependence of variable amplitude crack growth rate in C2 solution and in air

### **3.3.2 Frequency dependence of crack growth rate under variable amplitude cyclic loading**

As shown in Fig. 3.4, the crack growth rate measured from tests in air was also found to be insensitive to loading frequencies, about  $7.1 \times 10^{-4}$  mm/block in the frequency range of  $5.0 \times 10^{-1}$  to  $2.8 \times 10^{-4}$  Hz. Therefore the repeated tests were not performed.

For tests with frequencies higher than  $10^{-3}$  Hz, the variable amplitude growth rate in C2 solution exhibited the same trend as that under constant amplitude fatigue, i.e., increasing with lowering frequency from  $9.0 \times 10^{-4}$  mm/block at  $5.0 \times 10^{-2}$  Hz to  $1.9 \times 10^{-3}$  mm/block at  $10^{-3}$  Hz. Numerous corrosion fatigue tests either reported in literature [3, 4, 16], or from our investigations using the same grade of pipeline steel [6, 7] have been performed in the frequency range above  $10^{-3}$  Hz, and the conclusion that corrosion fatigue crack growth rate increases with lowering frequency is well accepted. As a result, extensive crack growth tests in this higher frequency range were not performed. However, when the frequency was lower than  $10^{-3}$  Hz, the crack growth rate neither increased with decreasing frequency, as generally believed in the case of corrosion fatigue, nor decreased as observed during tests under the constant amplitude loading, but maintained constant at about  $2.0 \times 10^{-3}$  mm/block, which is about 3 times more than the rate in air.

Because of time-consuming of each test, the tests at selected frequencies in the very low frequency range were repeated, the growth rates at which are critical to understand the

crack propagation in the high pressure gas transmission pipelines. Relatively larger data scatters appeared in the low frequency regime. This may reflect on one hand the heterogeneity of steel microstructures. On the other hand, the number of loading blocks applied in the low frequency regime was limited by the test duration. This yielded smaller total crack advancement and might have caused slightly larger scatters of experimental data, despite the fact that each test lasted over a period of 2 months.

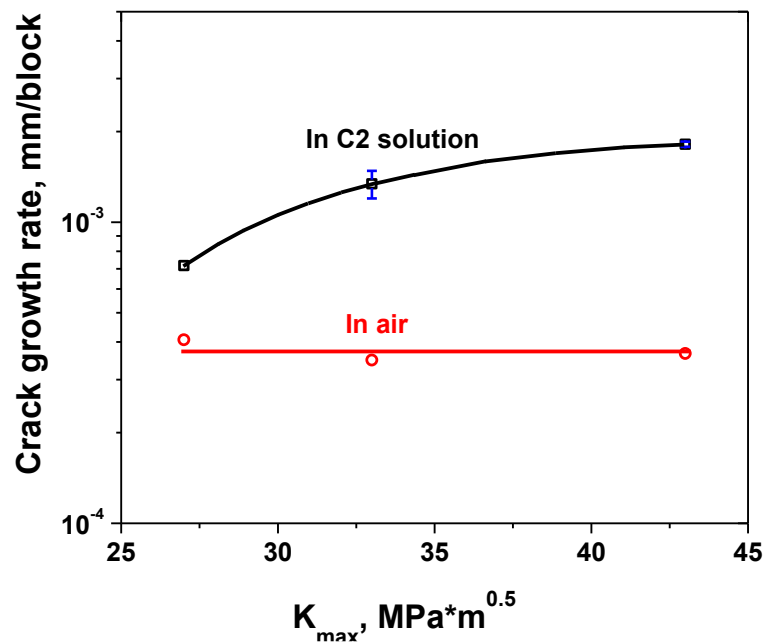


Figure 3.5  $K_{max}$  dependence of variable amplitude crack growth rate in C2 solution and in air

### 3.3.3 $K_{max}$ dependence of crack growth rate

As shown in Fig. 3.5, the measured crack growth rate under variable amplitude cyclic loading in air was not sensitive to the variation of  $K_{\max}$  and was at about  $3.8 \times 10^{-4}$  mm/block in the  $K_{\max}$  range of 27 to 43  $MPa\sqrt{m}$ . However, the measured growth rate in C2 solution increased with  $K_{\max}$ , from  $7.2 \times 10^{-4}$  mm/block at 27  $MPa\sqrt{m}$  to about  $1.8 \times 10^{-3}$  mm/block at 43  $MPa\sqrt{m}$  (average of the two values). The crack growth rates in C2 solution were different from those in air by a factor up to about 5.

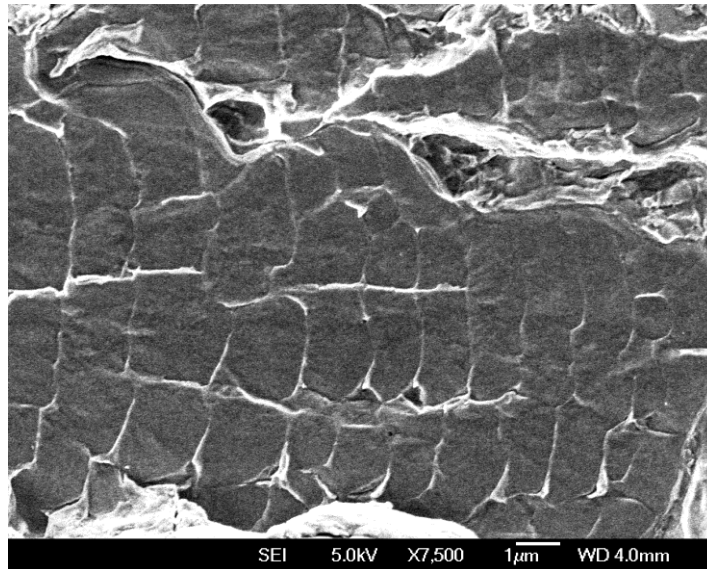
## **3.4 Discussion**

### **3.4.1 Acceleration effect caused by underload**

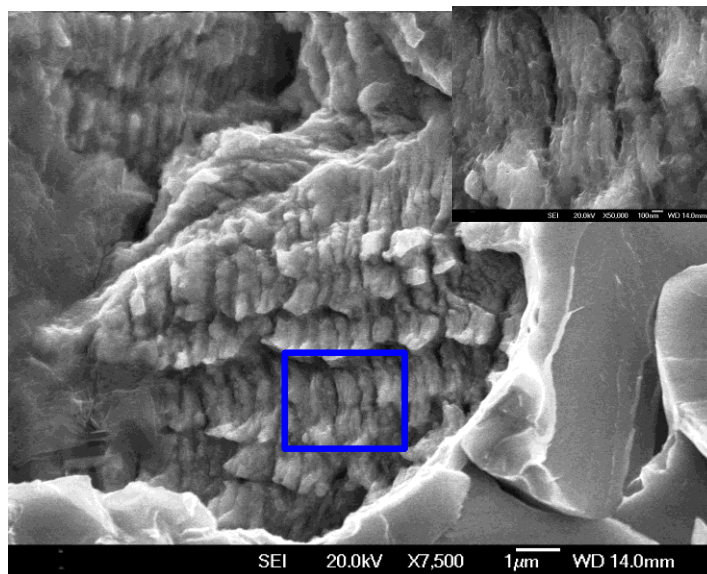
It has been well demonstrated that the crack growth rate can be significantly accelerated by the minor cycles with high R ratios in the presence of underloads through load interaction [23, 24]. Such crack growth caused by minor cycles was verified by examining the fracture surface after the tests. Fig. 3.6 [23] is a comparison of the fracture surface of the specimens tested in C2 solution under the constant amplitude loading and the variable amplitude loading. As shown in Fig. 3.6, large regularly spaced striations were observed on the specimen of the constant amplitude test, while mini-striations were additionally observed, which were generally located between two large regular striations for the variable amplitude cyclic tests with 300 minor cycles per block. The observation of mini-striations is direct evidence of crack propagation caused by the applied minor

cycles. The mini-striations have been found to depend on the number of minor cycles, which has been reported in detail in Ref. [24].

Based on the results shown in Figs. 3.3 – 3.5, Figs. 3.7 and 3.8 were plotted to better visualize the difference in crack growth behavior between the constant amplitude loading and the variable amplitude loading. It can be seen that the crack growth rate under variable amplitude fatigue is higher than that of constant amplitude fatigue both in air and in near-neutral pH solution over a wide range of loading frequencies and at different maximum stress intensity factors. For loading frequency tests shown in Fig. 3.7, a factor up to 2 and 10 was observed in accelerating crack growth rate in air and in C2 solution, respectively; for maximum stress test shown in Fig. 3.8, a factor up to 2 and 3 could be seen for tests in air and in C2 solution, respectively. These observations further confirm the importance of acceleration effects caused by underload in understanding crack propagation of pipeline steel in the field.



(a)



(b)

**Figure 3.6 SEM images showing the striations observed on the specimens after testing in C2 solution: a) under constant amplitude loading; and b) under variable amplitude loading with 300 minor cycles (crack propagation from left to right) [23]**

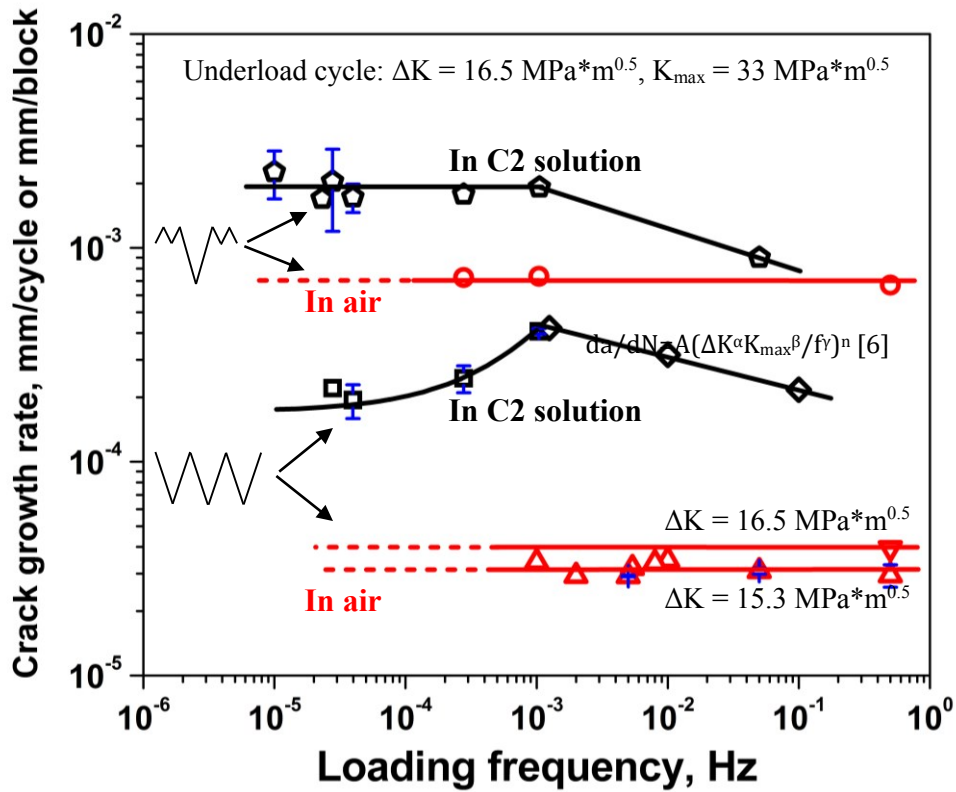
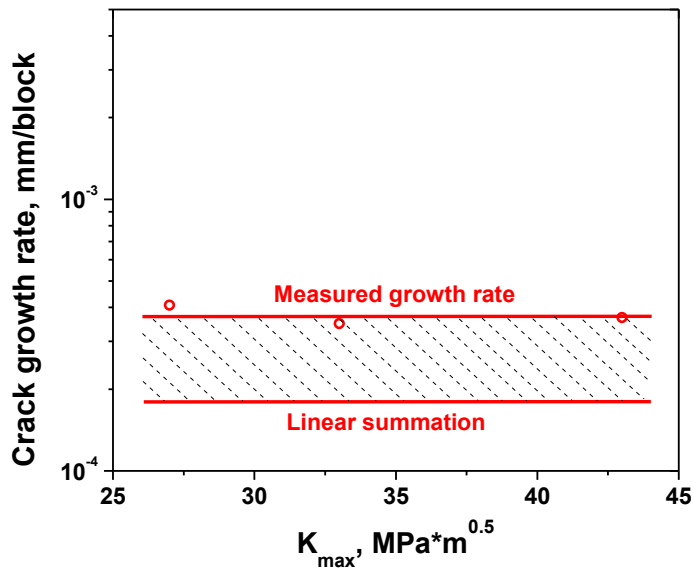
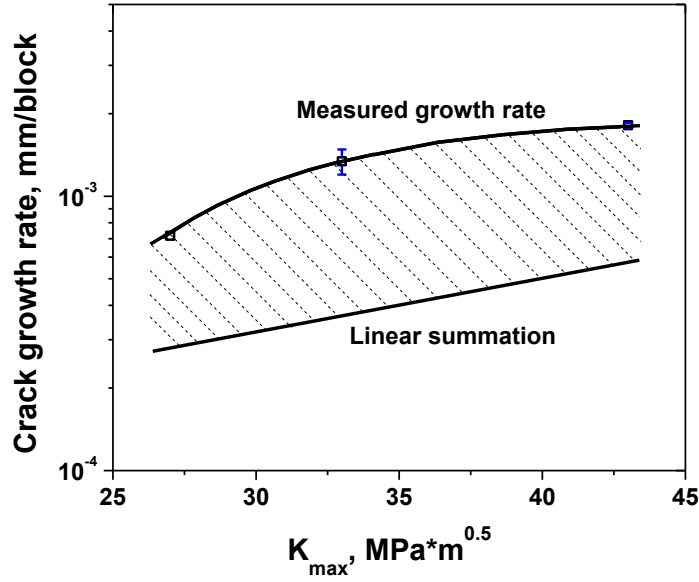


Figure 3.7 Crack growth rate under different loading frequency of underload: a) in air; and b) in C2 solution



(a)



(b)

**Figure 3.8 Crack growth rate under different  $K_{max}$ : a) in air; and b) in C2 solution**

### 3.4.2 Role of corrosive near-neutral pH environments

The environmental contribution to crack propagation of pipeline steel can be clearly seen from a comparison of the crack growth behavior in air and in near-neutral pH solution, as shown in Figs. 3.3 – 3.5, because the crack growth in air (inert environment) is driven by mechanical driving forces only. An enhancement in crack growth rate by a factor between 3 and 5 was determined because of environmental effects for the loading frequencies and the  $K_{max}$  tests (in Sections 3.2 and 3.3), respectively. But why is the crack growth rate not affected by loading frequency and  $K_{max}$  in air but influenced in corrosive near-neutral pH solution?

It has been determined in many previous studies that the crack growth rate in near-neutral pH environments cannot be correlated to the rate of dissolution of the material at the crack tip through corrosion [3, 6, 7]. The latter is negligible as compared with the rate of crack growth. This is also true in the current investigation. The crack growth rate in C2 solution was about one order of magnitude higher than the crack growth rate calculated based on the corrosion rate, typically about  $1.6 \times 10^{-9}$  mm/s ( $5.0 \times 10^{-2}$  mm/year) [27]. For example, for the test conducted at  $27 \text{ MPa}\sqrt{m}$ , the crack advancement due to corrosion within the time for one block was calculated to be about  $9.0 \times 10^{-5}$  mm, which is one order of magnitude lower than the corresponding crack growth rate,  $7.2 \times 10^{-4}$  mm/block.

The much higher crack growth rate in near-neutral pH environments, as compared with the rate of corrosion, has been rationalized through the effects of hydrogen embrittlement. The effects of loading frequency and  $K_{\max}$  on the crack growth in near-neutral pH environments are also elucidated below based on hydrogen embrittlement mechanisms.

#### **3.4.2.1 Observation of critical frequency**

As shown in Figs. 3.3, 3.4 and 3.7, the dependence of crack growth on loading frequency in C2 solution can be divided into the following two frequency regimes:

- 1) The high frequency (HF) regime, typically with a loading frequency higher than  $10^{-3}$  Hz, where the crack growth rate increases as loading frequency decreases.

- 2) The low frequency (LF) regime where the loading frequency is lower than  $10^{-3}$  Hz and the crack growth rate is insensitive to the loading frequency under variable amplitude fatigue; whereas, there is a slight decrease of crack growth rate down to a plateau at lower loading frequencies under constant amplitude fatigue loading.

Although the corrosion of the metal at the crack tip makes negligible contribution to the crack growth, as indicated previously, the influence of the corrosion environment on crack growth is primarily achieved through hydrogen embrittlement mechanisms with hydrogen being generated by the corrosion in near-neutral pH solution [6, 7]. Therefore, the transition of crack growth behavior from the HF regime to the LF regime is believed to be related to the saturation of hydrogen segregation in the crack processing zone/plastic zone ahead of the crack tip at the peak stress of cyclic loading. Interestingly, such transition with frequency has also been observed in an aluminum alloy charged with hydrogen, but happened at a higher critical frequency due to the higher diffusivity of hydrogen in aluminum [28].

However, the level of hydrogen generated in near-neutral pH aqueous-steel system has been characterized to be less than 0.1 ppm at the steel surface, of which only a small fraction of hydrogen atoms being generated can diffuse into the lattice of steel [29]. It has been further determined that the minimum level of hydrogen at the surface to produce hydrogen induced cracking is 0.4 ppm or above [29]. Therefore, an elevation of hydrogen concentration is necessary to produce crack growth through a hydrogen embrittlement

mechanism. This is possible in the plastic zone ahead of crack tip where hydrogen content would be elevated by hydrostatic stress.

To lower the chemical potential, it is generally believed that hydrogen segregates to the hydrostatic zone ahead of the crack tip as stress increases, which is determined as [30]:

$$c_{eq} = c_0 \exp\left(\frac{\sigma^{hyd}\Omega}{k_B T}\right) \quad (3 - 2)$$

where  $c_0$  is the lattice concentration of hydrogen in the absence of stress,  $c_{eq}$  is the steady-state lattice concentration of hydrogen under hydrostatic stress,  $\Omega$  is the partial molar volume of hydrogen atom,  $\sigma^{hyd}$  is the hydrostatic stress,  $k_B$  is the Boltzmann constant, and  $T$  is the absolute temperature of the system. The temperature was controlled at 30°C for all the tests in near-neutral pH solution in this investigation.

Once equilibrium of hydrogen concentration in the plastic zone is achieved with peak loading, the hydrogen embrittlement effect would be at its maximum. To further confirm this discussion, theoretical calculations are made in the following section.

#### **3.4.2.2 Theoretical prediction of critical frequency for hydrogen embrittlement<sup>2</sup>**

---

<sup>2</sup> This section was performed by Xiao Xing and Dr. Hao Zhang.

**Assumptions.** To simplify calculations, the irregular plastic zone shape (*i.e.*, plane strain condition) is assumed to be a circular region with radius  $r_p$ , as shown in Fig. 3.9, which is a reasonable geometric approximation because if the hydrogen concentration within the circular region with radius  $r_p$  reaches equilibrium, the hydrogen concentration in the plastic zone will be saturated too. The hydrogen concentration outside of the plastic zone is estimated to be  $c_0$ . To reach the equilibrium of hydrogen concentration in the plastic zone during cyclic loading, an annulus region with the inner radius  $r_p$  and the outer radius  $R_{eq}$  is needed to supply hydrogen atoms. The time,  $t_{critical}$ , for hydrogen diffusion into/out of the peak hydrogen region during cyclic loading is related to critical frequency through  $f_{critical} = 1/2t_{critical}$ .

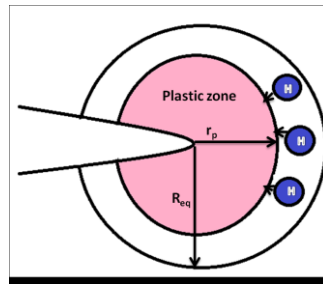


**Figure 3.9** A schematic showing hydrogen diffusion from the annulus region with an outer radius  $R_{eq}$  to a circular region with the radius  $r_p$  ( $r_p$  is the plastic zone size)

**Determination of critical frequency.** By introducing  $\sigma^{hyd}$  [31] into Eq. (3-2) the equation of  $c_{eq}$  can be expressed as:

$$c_{eq} = c_0 \exp\left(\frac{2(1 + \nu)K_I\Omega}{3k_B T\sqrt{2\pi r}} \cos\frac{\theta}{2}\right) \quad (3 - 3)$$

where  $K_I$  is the stress intensity near crack tip,  $r$  is the distance to crack tip,  $\nu$  is the Poisson's ratio, and  $\theta$  is the angle between the crack front and the line from specific position to the crack tip. The number of hydrogen atoms in an infinitesimal region within plastic zone is expressed as:

$$dN = \frac{c_{eq} 2\pi r l_z}{a_0^3/2} dr \quad (3-4)$$

where  $a_0$  is lattice parameter,  $l_z$  is the thickness of specimens. Substitute Eq. (3-3) into Eq. (3-4) and integrate over distance:

$$N(K_I) = \int_0^{r_p} \frac{c_0 \exp\left(\frac{4(1+\nu)K_I \Omega}{3\pi k_B T \sqrt{2\pi r}}\right) 2\pi r l_z}{a_0^3/2} dr \quad (3-5)$$

It is found that  $N$  is only function of stress intensity factor  $K_I$ .  $r_p$  can be calculated as follows:

$$r_p = \frac{1}{6\pi} \left( \frac{K_{max}}{\sigma_{ys}} \right)^2 \quad (3-6)$$

where  $K_{max}$  is the maximum stress intensity in one cycle and  $\sigma_{ys}$  is the yield strength. Substituting Eq. (3-6) into Eq. (3-5), the number of hydrogen atoms needed to saturate a circular region as the  $K$  varies from  $K_{min}$  to  $K_{max}$  is:

$$N(K_{max}) - N(K_{min}) = \frac{2\pi c_0 l_z}{a_0^3} (R_{eq} - r_p)^2 \quad (3 - 7)$$

Details of the calculations can be found in the Appendix A. The term  $(R_{eq}-r_p)$  is the hydrogen atom diffusion distance. The minimum time,  $t_{critical}$ , needed to achieve equilibrium hydrogen concentration can be approximated with diffusion distance divided by H velocity, which is related to H diffusivity and driving force (see Appendix A for details):

$$t_{critical} = \frac{R_{eq} - r_p}{\bar{V}_r} \quad (3 - 8)$$

Finally, the critical frequency can be obtained by substituting the test conditions in the current investigation (please refer to Appendix A) into these equations.  $R_{eq}$  and  $r_p$  were determined to be about 0.47 mm and 0.34 mm, respectively; and thus hydrogen atom diffusion distance  $(R_{eq}-r_p)$  was determined to be about 0.13 mm, which covers multiple grains of the pipeline steel with a ferrite plus pearlite structure (grain size about 0.01 mm [23]). The predicted critical frequency is found in a range of  $9.2 \times 10^{-4}$  to  $1.2 \times 10^{-3}$  Hz (the range is from the variation of H diffusivity [32]). The result agrees well with the experimental critical frequency in Fig. 3.7,  $1.04 \times 10^{-3}$  Hz, which further confirms the importance of HE in crack propagation in corrosive near-neutral pH environments.

Despite the fact that the model only accounted for the input and boundary conditions for constant amplitude fatigue, the output results are still quite consistent with the test

observations. The reason that the model did not consider the detailed mechanisms of crack propagation under the synergistic interactions of hydrogen and fatigue, such as the role of accumulated cycles (that is, one cycle may not generate one striation shown in Fig. 3.6) is due to the debatable observations and theories [33, 34, 35]. The model could be further modified once the role of hydrogen in NNP<sub>H</sub> corrosion fatigue is determined in detail, such as the interactions between hydrogen and fatigue, and thus material damage, which is currently under investigation.

#### **3.4.2.3 Understanding the effect of frequency on crack growth behavior**

Based on this critical frequency, further discussion of the effect of frequency on crack growth behavior is made based on the type of cyclic loading used in the current investigation.

**Under constant amplitude cyclic loading.** Under constant amplitude cyclic loading,  $c_{eq}$  would be largest when the applied cyclic stress reaches the peak value. The actual level of  $c_{eq}$  at the peak stress is dependent on the loading frequency because of the diffusion of hydrogen as demonstrated in the former sections.

In the HF range, the crack growth rate under constant amplitude fatigue loading in C2 solution can be rationalized by the following equation [6]:

$$\frac{da}{dN} = a \left( \frac{\Delta K^\alpha K_{max}^\beta}{f^\gamma} \right)^n + b \quad (3 - 9)$$

where  $a$ ,  $n$ ,  $\alpha$ ,  $\beta$  and  $\gamma$  are all constants,  $\alpha+\beta=1$ , and  $b$  is the contribution of stress corrosion cracking, which is found to be about one order of magnitude lower than the first term in Stage II crack growth and can be ignored.  $(\Delta K^\alpha K_{max}^\beta / f^\gamma)$  is called the combined factor. The value of  $\gamma$  is found to be around  $3.3 \times 10^{-2}$ , which is a factor representing the influence of the corrosion environment on the crack growth rate. Although the corrosion of the material at the crack tip makes a negligible contribution to the crack growth, as indicated previously, the influence of corrosive environment on crack growth is primarily achieved through hydrogen embrittlement with hydrogen being generated by the corrosion in near-neutral pH solution.

In the LF range, crack growth rate is seen to decrease slightly before reaching a steady value, as shown in Figs. 3.3 and 3.7. This reduction could be caused by the two time-dependent processes at the crack tip outlined below:

- a) Time-dependent corrosion: Lower loading frequency allows more time for corrosion at the crack tip. Although the corrosion rate is very low as stated previously and is insignificant in terms of its contribution to crack advancement, dissolution at the crack tip could reduce crack tip sharpness and therefore the stress intensity factor, lowering crack growth [23, 36].

- b) Time-dependent room temperature creep. Lower loading frequency allows more time to produce room-temperature creep deformation that can also blunt the crack tip, leading to a reduced crack growth [7, 9, 11]. The fact that the crack growth rate in air is insensitive to loading frequency suggests that crack tip blunting caused by room temperature creep could be insignificant. However, this cannot rule out the possible effect of room temperature creep in C2 solution. The segregation of hydrogen to the crack tip could facilitate the plastic deformation through HELP (hydrogen enhanced localized plasticity) [21, 22].

Both the above factors would yield the same effect, that is, to blunt the crack tip, therefore leading to a lower crack growth rate in the LF regime. It is not clear, however, from this investigation which of the above factors is predominant. Investigations are underway to delineate clearly their relative contribution to crack growth.

A steady state crack growth rate at very low loading frequency was observed. This reflects the fact that crack tip blunting could reduce the stress intensity factor at the crack tip but could not eliminate the risk of hydrogen embrittlement. As the crack tip becomes blunter, the region with the highest hydrogen segregation may move with the hydrostatic zone gradually away from the crack tip. This would allow more volume of materials at the crack tip to be sampled by hydrogen segregation. Hydrogen embrittlement would occur at the weakest links where micro-cracking could be initiated due to the reduced cohesion strength of materials caused by hydrogen segregation.

**Underload plus static hold loading.** As compared with constant amplitude loading, the static hold could further enhance crack tip blunting caused by the two time-dependent factors discussed above, and, therefore, a lower crack growth rate can be expected as compared with the constant amplitude loading [23]. This argument seems consistent with the experimental observations. It further confirms that crack growth would not have occurred during static hold although the hold could maximize the segregation of hydrogen.

**Under the combination of underload and minor cyclic loading.** When the static hold in the loading is replaced by minor cycles, the following similarities between the two loading scenarios can be identified:

- a) Crack tip morphology or degree of the crack tip blunting should be similar because the R-ratio of minor cycles is very high (near-static) [23].
- b) Hydrogen segregation and the location of maximum hydrogen segregation should be similar since the minor cycles have little effect.
- c) The mechanical conditioning to the crack tip caused by the underload should be similar.

Therefore, the enhanced crack growth should be attributed first to the fatigue nature of the minor cycles. Regardless of whether hydrogen segregation at the crack tip is present or not, that is, whether in C2 solution or in air, crack growth enhancement is realized

through cyclic loading even at very high ratios (the minor cycles), as shown in Figs. 7 and 8.

The above discussion provides some insights of the loading interactions between the underload and the minor cyclic loading. It is clear that the underload is a prerequisite for the crack growth enhancement as the minor cycles alone are non-propagating without the underload, while the minor cycles are the necessary condition as a static hold is also non-propagating. The presence of hydrogen could yield the following effects: a) making the prerequisite condition sufficient, and b) making the necessary condition less critical.

#### **3.4.2.4 Understanding the effect of maximum stress on crack growth behavior**

As shown in Fig. 3.5, the crack growth rate increased with  $K_{\max}$  in C2 solution while it remained constant in air could be explained by considering Eq. (3-3). The hydrogen concentration in the plastic zone ahead of crack tip increases with the hydrostatic stress, resulting in a higher magnitude of hydrogen embrittlement and higher crack growth rate. On the other hand, the increase of crack growth rate with increasing  $K_{\max}$  becomes weaker at higher  $K_{\max}$ . This could be attributed either to the time-dependent effects on crack tip blunting discussed in Section 4.2.3.3 or to the transition of the linear elastic behavior to the elastic-plastic behavior of the materials at the crack tip at higher  $K_{\max}$ .

#### **3.4.3 Study results applied to real cracking in the field**

Field experience has shown that more than 70% of all-service and hydrostatic-test failures attribute to CF have occurred within 30 km downstream (pressure discharge) of a pump station [1]. This finding is consistent with the experimental results obtained in this investigation.

The maximum pressure of the variable pressure scheme is highest (at the design limit) at the discharge site of a pump station but decreases with distance from the pump station due to the friction between the fluid media inside of the pipeline and the pipeline internal surface. As demonstrated in Fig. 3.5, the measured crack growth rate decreases with lower maximum stress. Therefore, there is a higher risk of pipeline failure within 30 km downstream of a pump station. Near the suction inlet (upstream from the pump), the overload-type of variable amplitude fatigue prevails, which reduces the fatigue crack growth rate through the well-established concept of overload induced retardation effect [19, 20]. This makes the relative risk of failure at the discharge section of a pipeline higher, although more and larger amplitude of pressure fluctuations may occur in suction sections [17].

Even though much higher maximum pressure exists at the discharge section, the pressure fluctuations, especially for gas pipelines, are not sufficient to cause pipeline steel to fail by a fatigue mechanism without a consideration of the load interaction effects identified in this investigation. For example, a rainflow counting method usually predicts an operating life of the pipeline of several hundred years, inconsistent with an operating life of less than 50 years found in pipelines with CF cracking. Many other attempts have also

been made unsuccessfully to rationalize the premature failures, including pipeline temperature, CO<sub>2</sub> level, mean stress level, coating disbondment, operating stress, and loading rate [1, 3, 14, 37-39].

The findings in the current investigation could be applied to both gas and liquid pipelines, as they have similar underload-type of loading conditions at the discharge sections, which has been discussed in [24]. Because of the different compressibility of liquids and gases, gas pipelines often experience much lower loading frequency and smaller amplitude pressure fluctuations than oil pipelines [15, 17].

For the convenience of life prediction, the crack growth per cycle in C2 solution, as shown in Fig. 3.7, was converted to crack growth per unit time, as shown in Fig. 3.10. The typical range of loading frequency and the number of minor cycles are also shown in Fig. 3.10 for both the gas pipelines and oil pipelines. The crack growth behavior under constant amplitude loading is also included in the figure. Several key conclusions can be drawn:

- a) The constant amplitude growth behavior would over-estimate the crack growth of oil pipeline in the high frequency range but significantly under-estimate the crack growth of gas pipelines typically operated in a low loading frequency regime.
- b) Crack growth rate in oil pipeline is generally higher than in gas pipelines because of larger amplitude and more frequent of pressure fluctuations in oil pipelines.

c) When prediction is made using the actual data of pressure fluctuation, the constant amplitude prediction equation would significantly under-estimate the crack propagation in both oil and gas pipelines as constant amplitude prediction models do not consider crack growth acceleration caused by load interaction [15].

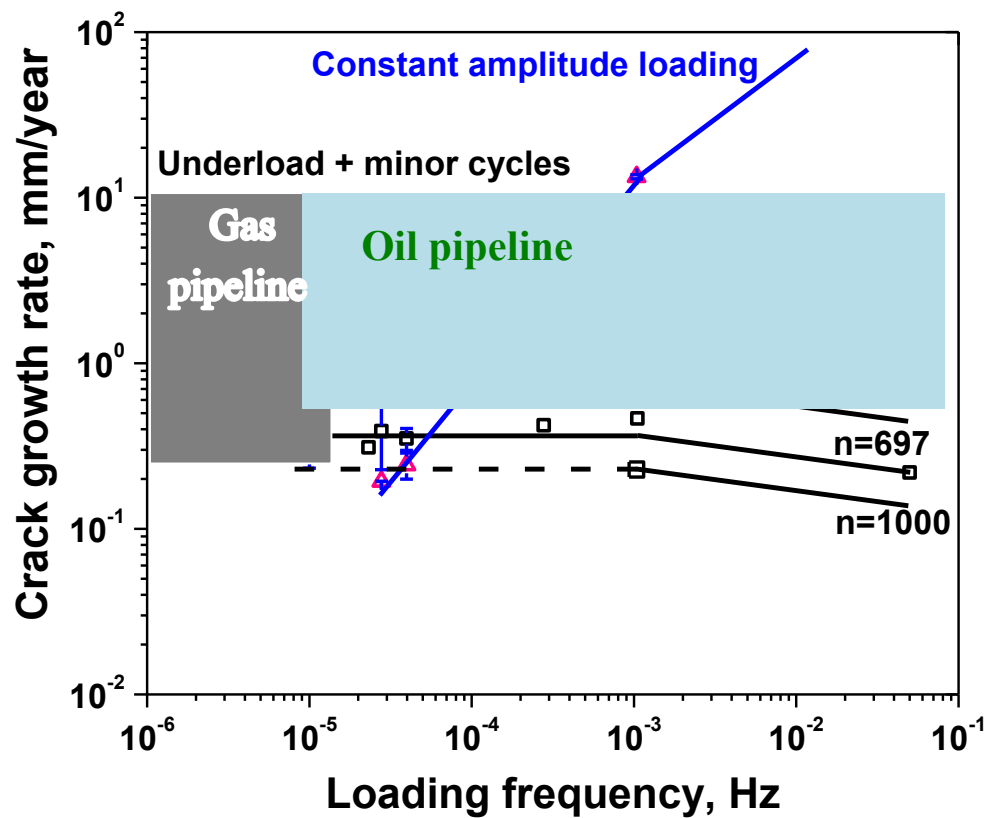


Figure 3.10 Understanding crack growth behavior of gas and oil pipelines exposed to near-neutral pH environments. n is the number of minor cycles per block.

### 3.5 Conclusions

The underload-type variable amplitude cyclic loading schemes represent the most risky pressure fluctuations during pipeline operations. In this study underload type scenarios were designed and used for crack growth measurements in pipeline steel in a near-neutral pH environment over a wide loading frequency range, from  $5.0 \times 10^{-1}$  Hz to  $10^{-5}$  Hz, and at different  $K_{\max}$ . Comparative tests were also performed under constant amplitude cyclic loading and in air to elucidate the crack growth mechanisms. Major findings are as follows:

- 1) Crack growth enhancement by a factor of up to 10 was found with the underload-type variable amplitude cyclic loading, as compared with the constant amplitude cyclic loading.
- 2) Crack growth rates measured in air were found to be insensitive to the variation of loading frequency and  $K_{\max}$ , while these two parameters significantly affected crack growth rate in near-neutral pH solution.
- 3) There exist two distinct regimes of crack growth behavior over the range of loading frequency studied. Crack growth rate was found to increase with decreasing loading frequency until  $10^{-3}$  Hz, while it either remained constant for the underload-type variable amplitude cyclic loadings, or decreased slightly for the constant amplitude loading when the loading frequency was lower than  $10^{-3}$  Hz. The transition of crack

growth behavior at about  $10^{-3}$  Hz was successfully predicted by a mechanistic model established based on the hydrogen assisted crack growth mechanisms identified.

- 4) The results obtained from this investigation agree well with various failure scenarios found in the field, including the high frequency of failure at the discharge sections of pipelines and different crack growth characteristics between oil pipelines and gas pipelines.

## References

- [1] Delanty BS, Beirne JO. Major Field Study Compares Pipeline SCC with Coatings. Oil & Gas Journal 1992;15;39.
- [2] National Energy Board (NEB), Focus on Safety and Environment a Comparative Analysis of Pipeline Performance 2000-2007, July 2009.
- [3] Parkins RN. A review of stress corrosion cracking of high pressure gas pipelines In: Proceedings of corrosion 2000. In: Proceedings of corrosion 2000. Houston, Texas: NACE International; 2000. Paper No. 00363.
- [4] Anderson TL. Fracture Mechanics, Fundamentals and Applications, 3rd ed. Boca Raton (FL): CRC Press; 2005. p. 538.
- [5] Staehle RW, Staehle RW, et al., editors. Stress corrosion cracking and hydrogen embrittlement of iron base alloys, NACE-5. Houston (TX): NACE; 1977. p. 193.
- [6] Chen W, Sutherby RL. Met Mater Trans A 2007; 38A:1260.
- [7] Chen W, Kania R, Worthingham R, Boven GV. Acta Mater 2009;57:6200-6214.
- [8] Srivatsan TS, Sudarshan TS. J Mater Sci 1988;23:1521-1533.

- [9] Wang S, Chen W. Mater Sci Eng 2002;A325:144.
- [10] Wang S, Zhang YG, Chen W. J Mater Sci 2001;36:1931(8).
- [11] Wang S, Chen W. Mater Sci Eng A 2001;A301:147.
- [12] Makhlof K, Jones JW. Int J Fatigue 1993;15(3):163-171.
- [13] Chen W, King F, Jack TR, Wilmott MJ. Met Mater Trans A 2002;33(5):1429-1436.
- [14] Lambert SB, Beavers JA, Delanty B, Sutherby R, Plumtree A. Mechanical factors affecting stress corrosion cracking growth rates in buried pipelines. In: Proceedings of 3rd International Pipeline Conference; 2000, Calgary. p.961-965.
- [15] Zhao J, Chen W, Boven GV, Keane S, Been J. Development and Validation of Load-Interaction Based Models for Crack Growth Prediction. In: Proceedings of 10th International Pipeline Conference; 2014, Calgary. Paper No.: IPC2014-33325.
- [16] Been J, Eadie R, Sutherby R. Prediction of Environmentally Assisted Cracking on Gas and Liquid Pipelines. In: Proceedings of 6th International Pipeline Conference; 2006, Calgary. Paper No. IPC2006-10345.
- [17] Boven GV, Sutherby R, King F. Characterizing Pressure Fluctuations on Buried Pipelines in Terms Relevant to Stress Corrosion Cracking. In: Proceedings of 4th International Pipeline Conference; 2002, Calgary. Paper No. IPC2002-27149.
- [18] Ahmed TM, Lambert SB, Sutherby R, Plumtree A. Corrosion 1997;53(7):581-590.
- [19] Skorupa M. Fatigue Fract Eng Mater Struct 1998(21):987-1006.
- [20] Skorupa M. Fatigue Fract Eng Mater Struct 1999(22):905-926.

- [21] Beachem CD. *Met Trans* 1972;3(2):437-451.
- [22] Ferreira PJ, Robertson IM, Birnbaum HK. *Acta Mater* 1999;47(10):2991-2998.
- [23] Yu M, Chen W, Kania R, Boven GV, Been J. Depressurization-Induced Crack Growth Enhancement for Pipeline Steel Exposed to Near-Neutral pH Environments. In: *Proceedings of 10th International Pipeline conference*; 2014, Calgary. Paper No. IPC2014-33282.
- [24] Yu M, Chen W, Kania R, Boven GV, Been J. *Fatigue Fract Eng Mater Struct* (DOI: 10.1111/ffe.12274)
- [25] Zhao J *et al.* Statistical analysis on pipeline spectra, in preparation.
- [26] Davidson DL, Lankford J. *Int Mater Reviews* 1992;37(2):45-74.
- [27] Chevillat K, Chen W, Eadie R, Kania R, Boven GV, Been J. Correlating Corrosion Field Data with Experimental Findings for the Development of Pipeline Mitigation Strategies. In: *Proceedings of 10th International Pipeline Conference*; 2014, Calgary. Paper No. IPC2014-33678.
- [28] Zuhair Mattoug Gasem. Frequency dependent environmental fatigue crack propagation in the 7XXX alloy/aqueous chloride system. PhD thesis, University of Virginia, May 1999.
- [29] Chen W, King F, Jack TR, Wilmott MJ. Hydrogen Permeation Behavior of X-70 Pipeline Steel in a Near-neutral pH Soil Environment. In: *Proceedings of International Pipeline Conference*; 2000, Calgary. ASME, New York. p. 953-960
- [30] Matsumoto R, Taketomi S, Matsumoto S, Miyazaki N. *Int J Hydrogen Energy* 2009;34(23):9576–9584.

- [31] Anderson TL. Fracture Mechanics, Fundamentals and Applications, 3rd ed. Boca Raton (FL): CRC Press; 2005. p.44-45.
- [32] Liu X, Xie W, Chen W, Zhang H. J Mater Res 2011;26(21):2735–2743.
- [33] Troiano A. Trans ASM 52 (1960) 147-157.
- [34] Birnbaum H, Sofronis P. Mater Sci Eng A 176 (1994) 191–202.
- [35] Doshida T, Nakamura M, Saito H, Sawada T, Takai K. Acta Mater 61 (2013) 7755-7766.
- [36] Egbewande A, Chen W, Eadie R, Kania R, Boven GV, Worthingham R, Been J. Corrosion Science 2014;83:343-354.
- [37] Manfredi C, Otegui JL. Eng Failure Analysis 2002;9:495-509.
- [38] Canadian Energy Pipeline Association (CEPA). Stress Corrosion Cracking Recommended Practices, 2nd Edition, An industry leading document detailing the management of transgranular SCC, December 2007, p.5.
- [39] TransCanada Pipeline (1996) Response to National Energy Board Information Request 2 of Proceeding MH-2-5, TCP, Calgary, Alberta, Canada, p.3.

# **Chapter 4      Crack Growth Behavior of Pipeline Steel Exposed to a Near-Neutral pH Environment under Variable Pressure Fluctuations: Effects of Number of Minor Cycles<sup>1</sup>**

## **4.1 Introduction**

Engineering components are often operated under variable amplitude cyclic loadings. Underload and overload are two common features of variable amplitude cyclic loading, which could accelerate and retard subsequent fatigue crack growth, respectively [1,2]. These effects are seen when compared with the crack growth predicted by a linear summation of damage of constant amplitude cyclic loading, with magnitudes equal to the variable amplitude load history.

Many materials have been extensively studied to determine their crack growth behavior under variable amplitude fatigue tests, including: steel [3-5], titanium alloys [6], and especially Al alloys [1,3-10] that are widely used in aircraft industry. In such studies, an increase of crack growth rate by a factor ranging from 1 to 20 has been found during

---

<sup>1</sup> A version of this chapter has been published. M. Yu, W. Chen, R. Kania, G. Van Boven and J. Been. *Fatigue & Fracture of Engineering Materials & Structures*. Vol. 38, Issue 6, June 2015, pp. 681-692.

variable amplitude loading with underload cycles included [1,3,6,9], while the crack growth rate of subsequent minor cycles was reduced by several orders of magnitude [1]. It has also been observed that when the minor cycles are well below the constant amplitude threshold, significant crack propagation may occur in the presence of overstress, by a factor of 100 in crack growth rate [11]. It has been found that the magnitude of the acceleration effect in crack growth under underload-type variable amplitude fatigue follows a parabolic relationship with the number of minor cycles ( $n$ ), reaching a maximum value at  $n = 10$  for several materials; the maximum magnitude of acceleration was also found to be material dependent, ranging from 1.4 to 8.5 being reported for materials, such as steel, and Ti and Al alloys [3,6,9].

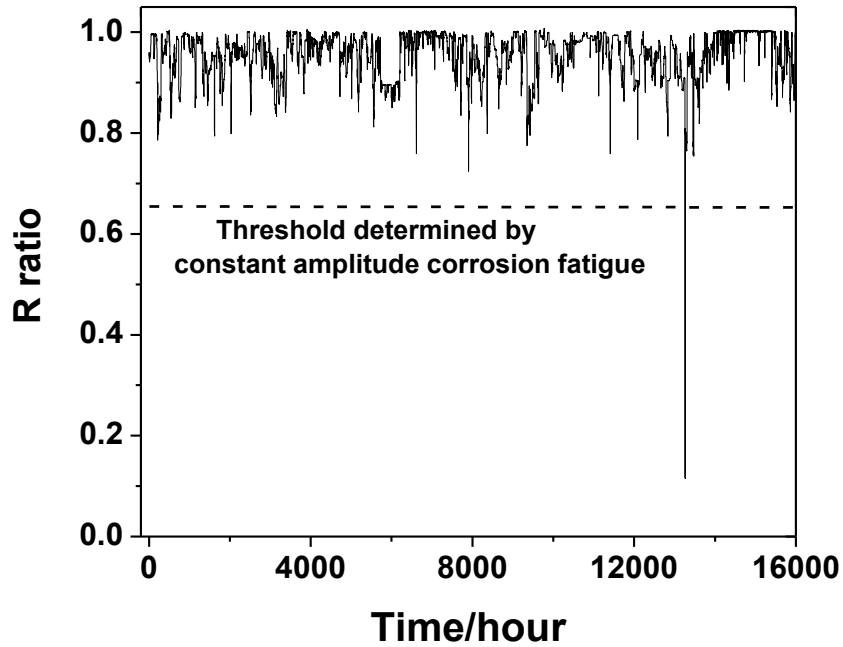
Laboratory studies on crack growth behavior of pipeline steel in near-neutral pH environments have been primarily conducted under constant amplitude cyclic loading since the discovery of near-neutral pH stress corrosion cracking (NNpHSCC) in 1985 [12], although the variable pressure fluctuations have been recognized as a crack propagation driving force [13-15]. Despite decades of research, the exact mechanisms of NNpHSCC are still not fully understood and NNpHSCC continuously remains as a major threat to pipeline integrity [16]. One of the dilemmas is that constant amplitude cyclic loadings are applied in laboratory tests, while random pressure fluctuations occur in the field.

The acceleration of crack growth by applying underloads with an R ratio of 0 was observed for pipeline steel in near-neutral pH solution [17]. In the study, however, the

minor cycles had an R ratio of 0.5 and could cause crack propagation in the absence of underloads. Such a loading scheme is not typical of pressure spectra recorded during pipeline operation. Occasional underload cycles and overwhelming periods of minor cycles at very high R-ratios are main features of the pressure fluctuations experienced by steel pipelines for high-pressure gas transmission as shown in Fig. 4.1(a). The crack growth behavior of pipeline steel under realistic loading spectra is still not determined. The minor cycles typically observed in the field usually have R-ratios at which the corresponding mechanical driving forces are well below the threshold determined by tests under constant amplitude loading.

The present investigators have recently demonstrated that the minor cycles, even with an R-ratio as high as 0.9, could contribute to crack growth following an underload cycle in a preliminary investigation, as shown in Fig. 4.2 [18]. The mechanical driving force corresponding to such minor cycles was well below the determined threshold based on constant amplitude tests [19]. In addition, previous studies of the crack growth behavior under similar loading spectra in other materials were performed either in air or moist air, which is irrelevant to the crack growth of pipeline steel exposed to near-neutral pH environments, where both corrosion and hydrogen embrittlement [15] should be considered simultaneously. This investigation was initiated in order to understand the role of minor cycles in the crack propagation of pipeline steel. In particular, attention will be given to the dependence of crack growth rate on the number of minor cycles in between two neighboring underload cycles. Comparatively tests were performed in air and near-

neutral pH solution to demarcate the contribution of corrosion, mechanical driving force and their synergistic interactions to crack growth rate.



(a)

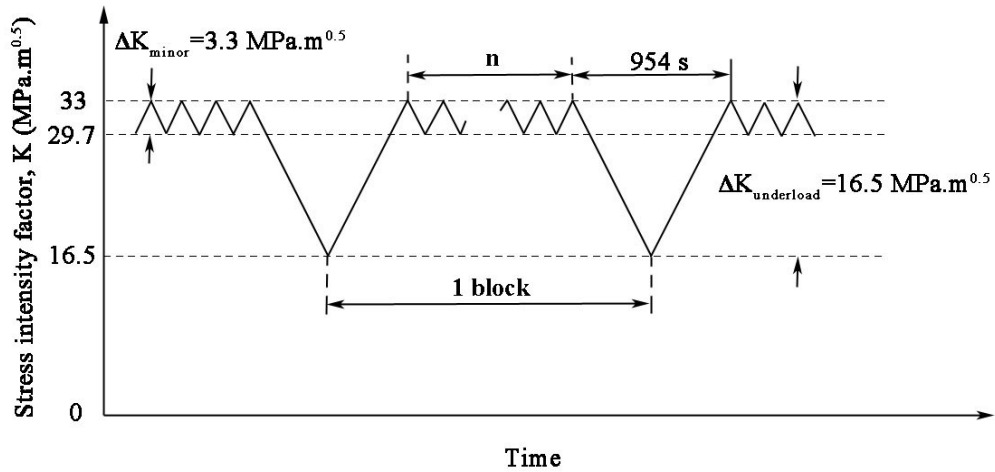
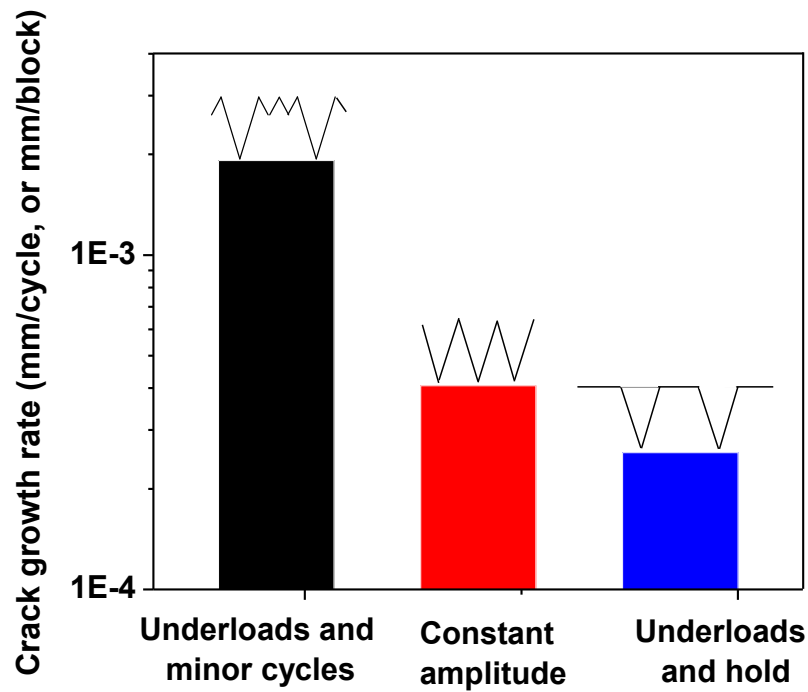


Figure 4.1 (a) Pressure fluctuations recorded for a high-pressure gas transmission pipeline; (b) designed test waveform



**Figure 4.2 Comparison of crack growth rate under different waveforms to demonstrate the importance of minor cycles in the crack growth in C2 solution [18]**

## **4.2 Experimental**

### **4.2.1 Materials and preparation of specimen**

An X60 pipeline steel with a thickness of 10.4 mm and outer diameter of 913 mm was used in this study, which was received from Spectra Energy Transmission. The chemical composition (wt.%) of the steel is as follows: C: 0.15, Mn: 1.27, P: 0.019, S: 0.005, Si: 0.37, Ni: 0.045, Cr: 0.2, Cu: 0.27, Al: 0.023, Fe: Balance. NNpHSCC was found in the

pipeline after being in field service for 19 years. Pipeline sections cut from the location where SCC was found were used in current investigation. Compact tension (CT) specimens with a thickness of  $9\pm 0.2$  mm were machined from the pipeline sections free of SCC colonies, which were inspected in the field prior to the shipping. The notch in the CT specimens was orientated in a direction parallel to the pipe longitudinal direction so that the path of crack growth in the specimen is the same as that of the longitudinal cracks found in the field. The CT specimens were ground to a 600 grit paper finish and then pre-cracked by fatigue to produce a sharp crack tip from the machined notch according to ASTM E647-08. The sharp crack initiated from the machined notch was controlled to be between 2 and 3 mm long and the difference in crack length on both sides of the specimen was less than 0.2 mm.

#### **4.2.2 Tests in near-neutral pH solution**

The corrosion fatigue tests were performed in a near-neutral pH solution, namely C2 solution, and its composition is listed in Table 4.1. A gas mixture of 5% CO<sub>2</sub> balanced with nitrogen was purged through C2 solution prior to- and during the test to achieve a stable pH value of 6.29 [19]. These tests were conducted on a horizontal pneumatic loading frame and the CT specimens were pin-hole loaded and sealed in test cells filled with the C2 solution. The temperature of the solution and the environment during tests was controlled at  $30\pm 0.1$ °C (above room temperature to achieve a better control of temperature).

**Table 4.1 Chemical compositions of C2 solution**

<b>Chemical composition</b>	<b>Concentration</b>
MgSO <sub>4</sub>	274 mg/L
CaCl <sub>2</sub>	255 mg/L
CaCO <sub>3</sub>	606 mg/L
NaHCO <sub>3</sub>	195 mg/L
KCl	35 mg/L

Periodic underload tests: The waveform shown in Fig. 4.1(b) to simulate the field pressure fluctuations shown in Fig. 4.1 (a) was conducted on CT specimens in C2 solution. The starting  $K_{max}$  applied was  $33 \text{ MPa}\sqrt{m}$ . This level of  $K_{max}$  can be achieved in field pipes, when a long but shallow crack (typical field SCC cracks) with depth of about 20-30% of wall thickness and with a crack length to depth ratio of 10 is loaded to 75% SMYS (specified minimum yield strength). The frequency (loading rate) of the underload and minor cycles were 0.00104 Hz and 0.0054 Hz, respectively [18]. The R ratio of underload and minor cycles was at 0.5 and 0.9, respectively.

The maximum acceleration effect was observed when the number of minor cycles, was around 10 cycles for several materials [3,6,9]. It seems, however, that the presence of a peak value of acceleration at a critical number of minor cycles is material and environment dependent [3,6,9,11]. For the current pipeline steel and environment system, the critical number of minor cycles at which the maximum acceleration effect is achieved has never been studied. Thus, the number of minor cycles,  $n$ , varied from 1 to 697.

The maximum value for the number of minor cycles, 697, was determined in the following way: The average time intervals between two neighboring cycles with R-ratios lower than 0.9 in the spectra shown in Fig. 4.1a) was found to be 36 hours. The loading frequency of minor cycles was set to be at  $5 \times 10^{-3}$  Hz, which is often used in laboratory simulations [15,19- 21 ] and is consistent with the loading frequency of pressure fluctuations during field operation. The loading frequency actually measured during testing on a pneumatic loading frame was  $5.38 \times 10^{-3}$  Hz due to some execution errors in the test system, which yielded a total of 697 cycles for a 36-hour loading interval of the minor cycles.

To ensure that the maximum acceleration effect was achieved at 697, the number of minor cycles was further increased to 1000 for tests in C2 solution. The test duration in solution varied from 12 to 57 days depending on the number of blocks applied. A limited number of blocks were carried out in each test to avoid significant increment of stress intensity factor due to crack growth. It was 920 blocks for the loading waveform with  $n = 1$ , corresponding to a test duration of 12 days, and only 24 blocks for the test with  $n = 1000$ , which lasted over 57 days.

All the tests in this investigation were performed under a constant maximum load or maximum stress intensity factor to simulate the pressure fluctuations at the discharge sites where the maximum pressure is strictly controlled. Therefore, the plastic zone size produced by previous underload cycle was always equal or slightly smaller than that

produced by the subsequent underload cycle. The plastic zone size at  $K_{\max} = 33 \text{ MPa}\sqrt{m}$  was estimated to be about 1 mm and 0.33 mm in plane stress and plane strain, respectively. It is impossible to grow the crack by increasing the number of minor cycles to a length longer than the above calculated plastic zone size because minor cycles do not contribute to crack growth after a critical number is reached (acceleration effect disappeared).

Following the tests in C2 solution, the specimens were cut along the middle plane in the thickness direction. Then, one segment was polished to observe the crack tip morphology (in the middle plane) via scanning electron microscopy (SEM), while the other half was sectioned in liquid nitrogen for fractographic examination.

### 4.2.3 Tests in air

Constant amplitude tests: The CT specimen was pin-hole loaded on a closed loop hydraulic Instron 8516 loading frame at about 22°C, in laboratory air. The initial  $K_{\max}$  was also  $33 \text{ MPa}\sqrt{m}$ . A loading frequency of 0.5 Hz was used all tests conducted in air. It has been determined that the crack growth rate of the current steel is insensitive to the loading frequency when testing in air within the frequency range of 0.5 to  $10^{-4}$  Hz. The R ratio – the only variable for the constant amplitude tests in air – was varied from 0.1 to 0.9. Each test was conducted for a period to achieve a crack growth less than 0.4 mm, which only yields an increase of  $K_{\max}$  for about  $0.9 \text{ MPa}\sqrt{m}$  in current investigation.

Periodic underload tests: For comparison with tests in solution, the waveform shown in Fig. 4.1(b) was also executed using a computer running Instron's Wavemaker-Runtime software. Here, the initial  $K_{max}$  was also  $33 \text{ MPa}\sqrt{m}$ . The R ratio of underloads and minor cycles was at 0.5 and 0.9, respectively, corresponding to a  $\Delta K$  value of 16.5 and  $3.3 \text{ MPa}\sqrt{m}$ . The frequency (loading rate) of underloads and minor cycles were 0.00105 Hz (954 s/cycle) and 0.5 Hz, respectively. The number of minor cycles per block, n, was ranged from 1 to 697 cycles. The first and last event of the variable amplitude waveform was the minor cyclic loading.

#### **4.2.4 Determination of crack growth rate and acceleration factor**

Crack growth was determined by measuring the crack length before and after tests via SEM. The crack growth rate, expressed as millimeter per block, was calculated by dividing the measured crack growth length by the total number of cyclic blocks applied. In the current investigation, the crack propagation correlated to the individual underload and minor cycles could not be differentiated from each other, and thereby the explicit contribution of underloads to the total crack growth could not be defined. After testing in solution, the specimen was fractured open along the notch direction in liquid nitrogen and examined on SEM.

A variable  $\gamma$ , termed as the acceleration factor, is often used to determine the degree of crack growth acceleration, which is defined as the ratio of measured growth rate per

block to the predicted growth rate per block by a linear summation of the constant amplitude crack growth response [3], that is,

$$\gamma = \frac{\text{measured growth rate per block}}{\text{predicted growth rate per block by a linear summation of the constant amplitude crack growth response}} \quad (4 - 1)$$

The predicted growth rate per block can be expressed by the following equation:

$$\left(\frac{da}{dN}\right)_{\text{block}} = N_1 \left(\frac{da}{dN}\right)_{\text{underload}} + N_2 \left(\frac{da}{dN}\right)_{\text{minor cycle}} \quad (4 - 2)$$

where,  $(da/dN)_{\text{underload}}$  is the constant amplitude crack growth rate at the same loading conditions of underload (large cycle) during variable amplitude fatigue, and  $N_1$  is the number of underload cycles in one block – for the current study,  $N_1 = 1$ .  $(da/dN)_{\text{minor cycle}}$  is the constant amplitude crack growth rate at the same loading conditions of minor cycles during variable amplitude fatigue, and  $N_2$  is the number of minor cycles in one block, which is  $N_2 = n$  for current study.

## 4.3 Results

### 4.3.1 Tests in air

#### 4.3.1.1 Constant amplitude test

Paris' Law, as expressed below, is often used to correlate the crack growth data with the stress intensity factor range for fatigue crack growth under constant amplitude loading.

$$\frac{da}{dN} = C\Delta K^m \quad (4 - 3)$$

Where  $\Delta K$  is the stress intensity factor range, and  $C$  and  $m$  are constants.

Since the maximum stress intensity factor  $K_{max}$  at the beginning of each test was kept the same, at  $33 \text{ MPa}\sqrt{m}$ , and the growth of the crack was limited to about 0.3 mm, the value of  $K_{max}$  can be considered to be constant during the tests. Since  $\Delta K = K_{max}(1 - R)$ , the Paris' Law can be re-expressed as a function of R ratio,

$$\frac{da}{dN} = CK_{max}^m(1 - R)^m \quad (4 - 4)$$

The crack growth rates obtained from the tests under constant amplitude load with different R-ratios are presented in Fig. 4.3. The results obtained were fitted using Eq. (4-4), which yields the following relation between  $da/dN$  and  $R$ .

$$\left(\frac{da}{dN}\right) = 2.93E - 4 * (1 - R)^{2.79} \quad (4 - 5)$$

where  $(da/dN)$  is the crack growth rate in terms of millimeter per cycle. As illustrated in Fig. 4.3, the curve generated using Eq. (4-5) depicts a trend line that is in close agreement with the shape of the plotted experimental results.

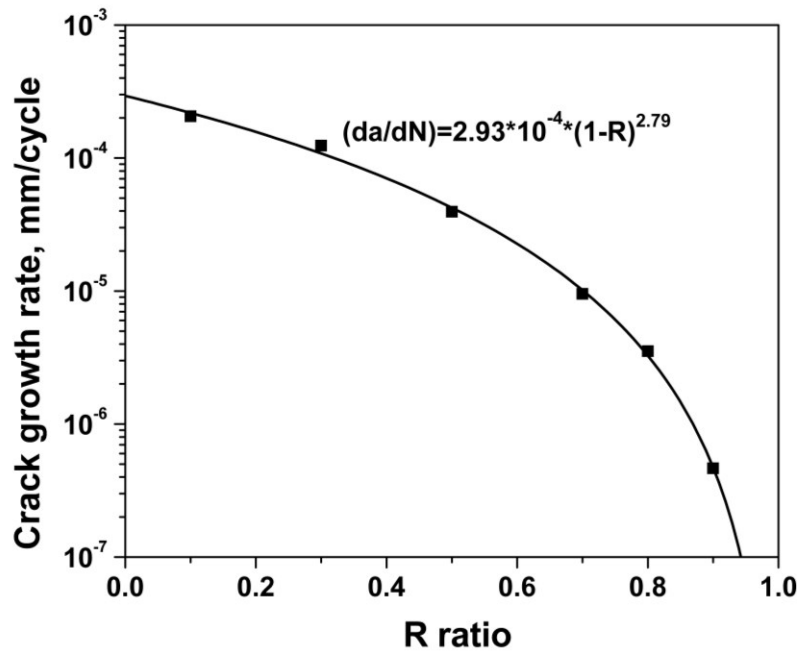


**Figure 4.3** Variation of crack growth rate with variable R ratios in air. The tests were performed at  $K_{max} = 33 \text{ MPa}\sqrt{m}$  and frequency = 0.5 Hz

The method of linear summation, as defined in Eq. (4-2), was used to calculate the crack growth per block of the variable amplitude waveforms; through such calculations, the enhanced crack growth caused by load interactions was ignored. The crack growth rate under constant amplitude loading at different R-ratios was experimentally determined and is mathematically expressed by Eq. (4-5). To demonstrate, take the loading waveform in air shown in Fig. 4.1(b) with  $n$ , the number of minor cycles per block, equal to 100, as an example. The R ratio of underload and minor cycles is 0.5 and 0.9, respectively, and the

corresponding crack growth rate is calculated using Eq. (4-5) to be  $4.23\text{E-}05$  and  $4.72\text{E-}07$  mm/cycle, respectively. The block growth rate by linear summation is then calculated as  $4.72\text{E-}07 \times 100 + 4.23\text{E-}05 = 8.95 \text{E-}05$  mm/block. As illustrated by the calculation, despite the low constant amplitude growth rate of minor cycles, its contribution to crack growth rate per block becomes comparable to that of one underload cycle when the number of minor cyclic loading is large. The linear summation method is often used for assessing fatigue damage of engineering structures in service.

#### **4.3.1.2 Periodic underload test**

The effect of the number of minor cycles per block,  $n$ , of the waveform in Fig. 4.1 (b) was experimentally determined. As shown in Table 4.2 and Fig. 4.4 (a), the measured crack growth rate increases with  $n$ , from  $7.20\text{E-}05$  mm/block at  $n = 1$  to  $9.49\text{E-}04$  mm/block at  $n = 697$ , about 1200% increase. This rate of crack growth enhancement appears to diminish with increases in  $n$ . The experimentally determined growth rate is larger than the calculated growth rate made based on the method of linear summation (Eqs. 3 and 6) at all levels of  $n$ . The growth rate data at  $n < 80$  is enlarged in the insert in Figure 4(a). It can be seen that the measured crack growth rate increases sharply from  $n = 0$  (constant amplitude) to  $n = 1$  (variable amplitude), and then increases at a lower rate up to  $n = 20$ . This is followed by a quicker increase with  $n$ ; while the growth rate calculated based on the linear summation using Eqs. (4-3) and (4-4) increases linearly with  $n$ , reflecting the increased contribution of the minor cycles to the crack growth.

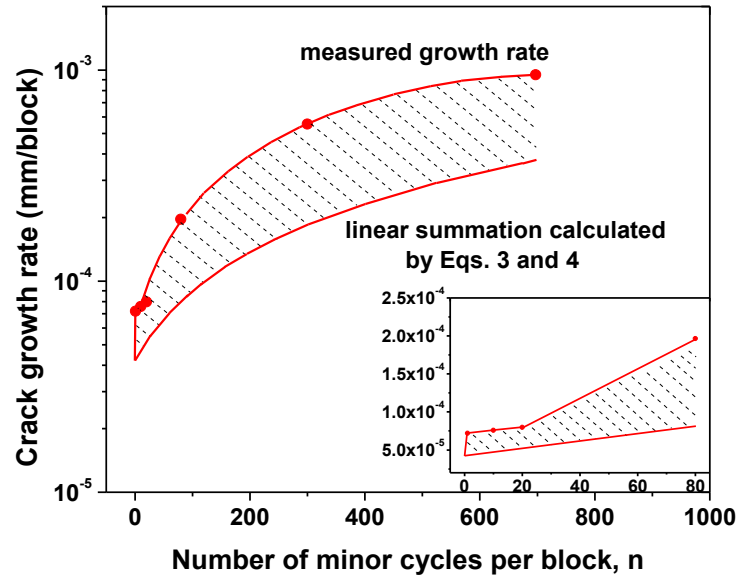
**Table 4.2 Results of periodic underload tests in air**

Number of minor cycles per block, n	Measured crack growth rate (mm/block)	Predicted crack growth rate* (mm/block)	Acceleration factor, $\gamma$
1	7.20E-05	4.28E-05	1.68
10	7.58E-05	4.70E-05	1.61
20	7.98E-05	5.17E-05	1.54
80	1.97E-04	8.01E-05	2.46
300	5.54E-04	1.84E-04	3.02
697	9.49E-04	3.71E-04	2.56

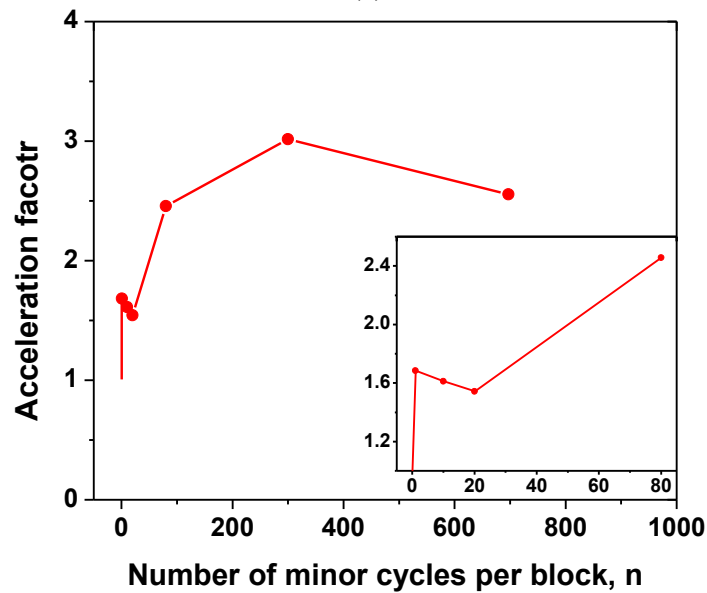
\*Predicted crack growth rate in air was calculated by linear summation of crack growth due to minor cycles and underloads, that is,  $4.72E-07 \times n + 4.23E-05$ , in terms of mm/block.

The deviation between the measured growth rate and the values calculated using Eqs. (4-3) and (4-4), illustrated by the shaded area in Fig 4.5(a), is attributed to the acceleration effect caused by the underloads and can be quantified by the acceleration factor,  $\gamma$ , defined in Eq. (4-1). As shown in Fig. 4.4 (b),  $\gamma$  increases sharply from 1 (constant amplitude at  $n = 0$ ) to 1.7 ( $n = 1$ ) then decreases with increasing  $n$  until  $n = 20$  cycles, as shown by the inserted close-up of the plot from  $n = 0$  to  $n = 20$  in Fig. 4.4 (b) (the trend of which was confirmed by the fractured surface observations in the following section). Beyond  $n = 20$ ,  $\gamma$  increases with  $n$  up to 300 cycles, achieving a peak value of  $\gamma = 3$ . Further increases in  $n$  to a value exceeding 300 result in a reduction in the acceleration factor. This varied dependence of the acceleration factor with  $n$  was also observed during

the tests in C2 solution introduced in the proceeding section and therefore, can be excluded from the possibility of experimental errors.



(a)



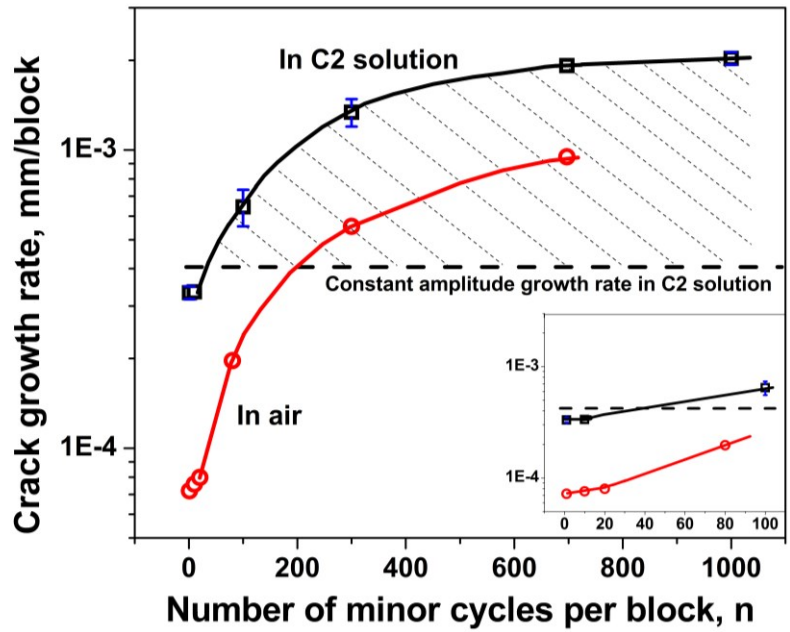
(b)

**Figure 4.4 Results of periodic underload tests in air: (a) measured and predicted crack growth rates; and (b) variation of acceleration factor with the number of minor cycles per block**

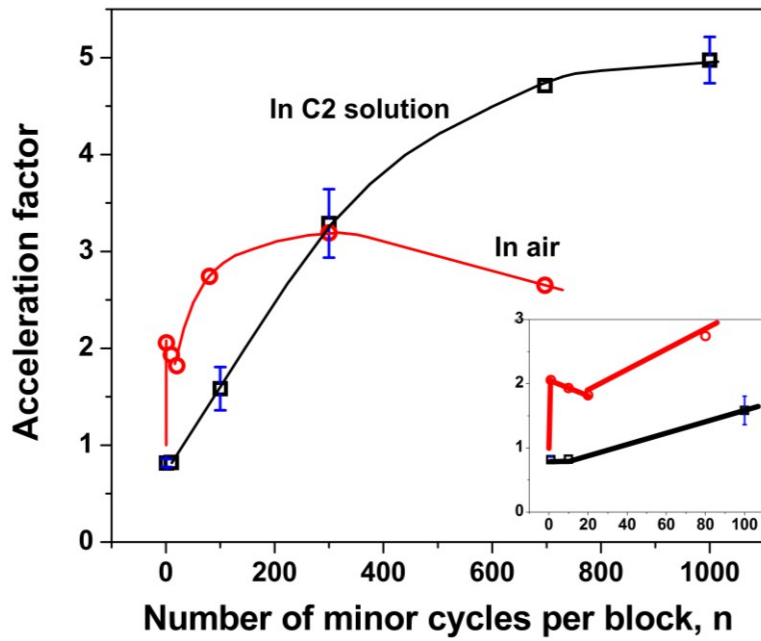
### 4.3.2 Periodic underload test in C2 solution

The crack propagation driving force of the minor cycles in the current waveform are well below the determined threshold in C2 solution as far as the constant amplitude corrosion fatigue model is considered [19]. Therefore, the predicted growth rate per block of the variable amplitude waveform in Fig. 4.1(b) is actually the constant amplitude growth rate of large underload cycles in the waveform ( $4.07\text{E-}04$  mm/cycle, in C2 solution) and is represented by the horizontal line in Fig. 4.5 (a).

Crack growth behavior: As shown in Table 4.3 and Fig. 4.5 (a), the general trend of the measured crack growth rate in C2 solution is similar to that found in air, that is, increasing crack growth rate with  $n$  until a maximum is reached. The measured crack growth rate in C2 solution was approximately  $3.32\text{E-}04$  mm/block at  $n = 1$  and  $2\text{E-}03$  mm/block at  $n = 1000$ , or about 500% increase, which is significantly less than the increase observed in air (1200% increase). It is surprising that the measured growth rate is seen to remain constant with a value below the constant amplitude growth rate from  $n = 0$  (constant amplitude) to 10; however, for  $n > 10$ , an increase of crack growth rate occurs, as shown in the insert in Fig. 4.5(a). This varied dependence of crack growth rate enhancement with increasing  $n$  is quite similar to that found in air.



(a)



(b)

**Figure 4.5 Results of periodic underload tests in C2 solution: (a) measured and predicted crack growth rates; and (b) variation of acceleration factor with the number of minor cycles per block**

**Table 4.3 Results of periodic underload tests in C2 solution**

Number of minor cycles per block, n	Measured crack growth rate (mm/block)	Predicted crack growth rate* (mm/block)	Acceleration factor, $\gamma$
1	3.44E-04		0.84
1	3.20E-04		0.79
10	3.35E-04		0.82
100	7.09E-04		1.74
100	5.81E-04	4.07E-04	1.43
300	1.24E-03		3.04
300	1.44E-03		3.54
697	1.92E-03		4.71
1000	2.10E-03		5.14
1000	1.96E-03		4.81

\*Because the minor cycles are below constant amplitude threshold, the predicted crack growth rate is actually the underload growth rate obtained in constant amplitude cyclic loading in C2 solution.

The difference between the measured crack growth rate and that predicted by the constant amplitude test (horizontal line), marked by the shaded area in Fig. 4.5(a), is due to the acceleration effect caused by underloads. The acceleration factor ( $\gamma$ ) was calculated via Eq. (4-1) and is shown in Fig. 4.5(b). It can be seen that  $\gamma$  generally increases with n, and can be up to 5 times higher at n = 1000, beyond which it remains constant, while  $\gamma$  in air peaks out at n = 300 and then decreases with further increases in n. The acceleration factor in C2 solution is less than that in air when n is less than 300, but higher when n is larger than 300. The acceleration factor in C2 solution maintained a constant value that was less than 1 in the first few minor cycles, as shown in the insert in Fig. 4.5(b), while the decreasing trend was also found from tests in air.

Fracture surface observation: The fracture surface of the specimens tested in C2 solution at different number of minor cycles was examined via SEM after the tests. As shown in Fig. 4.6, large regularly spaced striations are observed on the specimen of constant amplitude test ( $n = 0$ ). For the variable amplitude cyclic tests, striations with a interspacing similar to those seen at  $n = 0$  were also found for tests with  $n = 1$  and 10. However, when  $n \geq 100$  cycles, the mini-striations were also observed, which are generally located between two large regular striations. The observation of mini-striations is believed to be a direct evidence of crack propagation caused by the applied minor cycles. The mini-striations at  $n = 1000$  seemingly appear to be blurred, which was likely due to long-term corrosion exposure.

The striation interspacing was measured using an intercept method and the average value was compared with the measured surface crack growth rate. For the specimen of constant amplitude fatigue testing ( $n = 0$ ), the large regular striation interspacing was about  $1.42\text{E-}3$  mm, which is much higher than the measured surface crack growth rate  $4.07\text{E-}4$  mm/cycle [18]. For  $n = 1$  and 10 of the variable amplitude fatigue tests, the striation interspacing was  $1.56\text{E-}3$  and  $1.44\text{E-}3$  mm, respectively, which are close to that of constant amplitude testing,  $1.42\text{E-}3$  mm, but were also much larger than the measured surface growth rate,  $3.32\text{E-}4$  (average value in Table 4.2) and  $3.35\text{E-}4$  mm, respectively. This echoes the previous observation that the acceleration due to the introduction of minor cycles was small when  $n$  is small. However, when  $n$  was increased past 10, for example, at  $n = 300$ , both the large and mini- striations were observed. It is found that the

large striation interspacing induced by the underload cycles was  $5.92\text{E-}4$  mm. This is higher than the constant amplitude growth rate of underloads,  $4.07\text{E-}4$  mm/cycle. The spacing of the mini-striations was measured to be  $1.13\text{E-}4$  mm at  $n = 300$ , which is about two orders of magnitude greater than the calculated growth rate of minor cycles shown in the next section, the discrepancy of which is often observed [22].

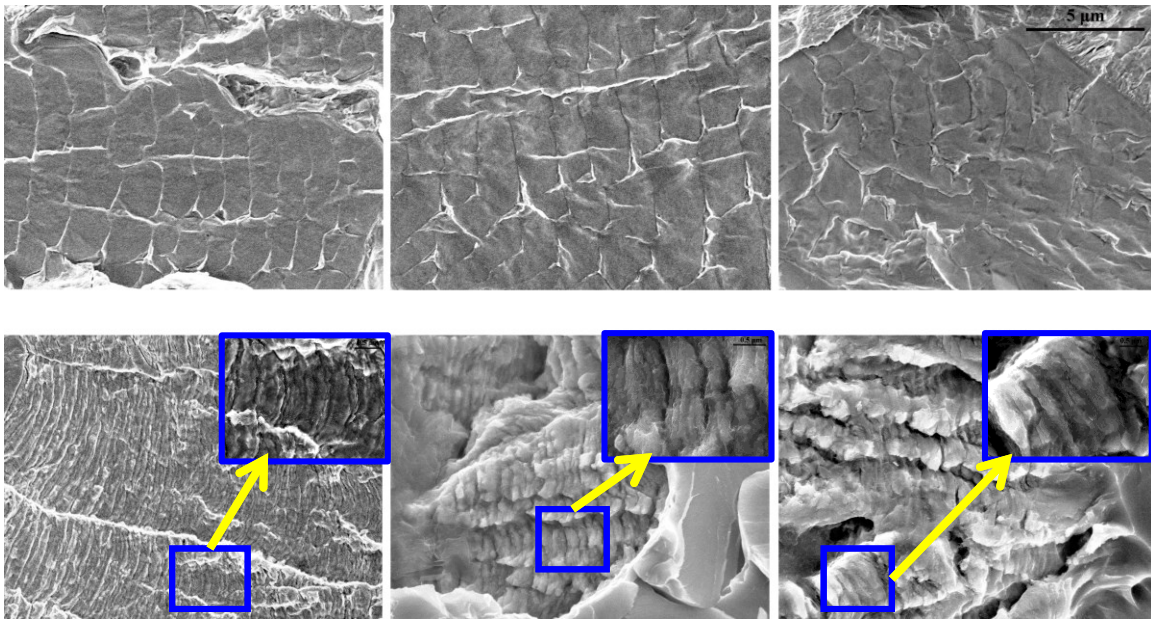


**Figure 4.6 SEM images (SE) showing the striations observed on the fractured surface of the specimens tested under different numbers of minor cycles per block in solution (crack propagated from left to right)**

Crack tip morphology: The specimens tested in C2 solution were cut along the middle plane in the thickness direction. After polishing, the crack tip morphology on this plane was observed via SEM and shown in Fig. 4.7. It can be seen that the crack tips are sharp

when  $n < 1000$  cycles, but become blunt at  $n = 1000$ . A wedge-shaped crack crevice behind the crack tip was observed.

## 4.4 Discussion

Variable amplitude cyclic loading waveforms were designed to simulate the actual pressure fluctuations during pipeline routine operations. It has been demonstrated that the minor cycles even with a very high R ratio could make a significant contribution to the crack growth in the presence of underloads with a relatively lower R ratio as shown in Fig. 4.2 [18]. This type of pressure fluctuations is very typical for high pressure gas pipelines, especially at the discharge sections of the pump station, where more than 70% of in-service and hydrostatic-test failures in connection to SCC have been found [12].

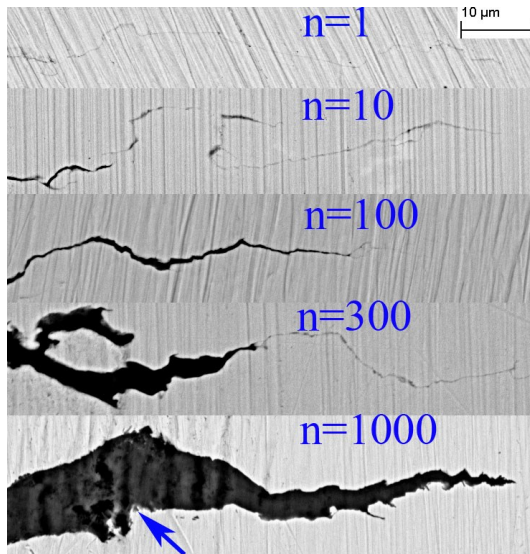


**Figure 4.7** Crack tip morphology on the middle plane in the thickness direction for specimens tested at a different number of minor cycles per block ( $n$ ) in C2 solution

#### 4.4.1 The role of minor cycles in fatigue crack propagation

It can be seen from Fig. 4.4 and 4.5 that the measured crack growth rate in air and in C2 solution increases with  $n$  and is generally higher than that obtained from linear summation. This implies that the fatigue damage is enhanced by variable amplitude cyclic loadings.

The contribution of minor cycles to crack growth can be quantified by the method introduced in [3]. The crack growth increment for a loading block consisting of one underload and  $n$  number of minor cycles is registered as  $\Delta a_n$ . The average crack growth rate between the 2<sup>nd</sup> and the 10<sup>th</sup> minor cycle is calculated as  $(\Delta a_{10} - \Delta a_1)/(10-1)$ , while the mid-point of the 1<sup>st</sup> and the 10<sup>th</sup> minor cycles, i.e.,  $(1+10)/2$ , is taken as the value for x-axis corresponding to the average crack growth rate. Fig. 4.8 shows the variation of average crack growth rate with the average minor cycles as determined using the above method.

As seen in Fig. 4.8, the crack growth during minor cycle loading after the introduction of an underload cycle can be divided into three stages.

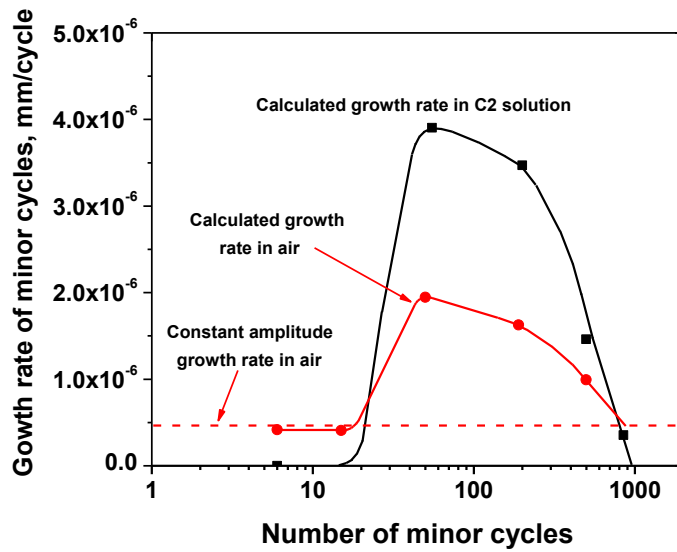


**Figure 4.8 Growth rate of minor cycles in C2 solution and in air**

- 1) The initial incubation stage up to 15 cycles where acceleration of crack growth was not observed. The growth rate of the minor cycles in C2 solution is zero because the driving force of the minor cycles was well below the determined constant amplitude threshold. This is consistent with the fracture surface morphology shown in Fig. 4.6 where either the morphology or the interspacing of the striations at  $n = 1$  and 10 were similar to that of constant amplitude test ( $n = 0$ ). For the tests in air, the calculated growth rate at  $n \leq 15$ , at about  $4.1E-7$  mm/cycle, is very close to the constant amplitude growth rate at  $4.72E-7$  mm/cycle. The  $n$ -insensitive stage observed in this investigation is also reported in the test on a 3 mm-thick BS 4360 50B steel in air [3], although its loading conditions were different. However, it is generally believed that the first several minor cycles following the underload would have the highest crack propagation driving force and should yield the highest growth rate [1,2]. The presence

of a period of incubation prior to the onset of acceleration effects is further discussed in Section 4.4 on the mechanisms of acceleration by underloads.

- 2) The subsequent stage up to 55 cycles, where the crack growth rate increases by increasing  $n$ , The mini-striations observed in current pipeline steel were a direct evidence of crack propagation caused by the minor cycles, as shown in Fig. 4.6. This local acceleration behavior, however, was not reported in [10] and [3].
- 3) The final stage up to 960 cycles depending on the test environments, where crack growth rate decreases as  $n$  increases to a level at which crack growth enhancement due to underload effects disappears.

#### **4.4.2 The role of environments in fatigue crack propagation**

Crack growth behavior: The effect of environments could be assessed by comparing the results obtained from tests in C2 solution and in air. Fig. 4.9 shows the ratio of growth rate in C2 solution to that in air. Linear interpolation was applied if there was not a corresponding point in air. It can be seen in Fig. 4.9 that the ratio of the measured growth rate of underload-minor cyclic loadings decreases sharply when  $n$  is increased from 1 to 100 cycles, but slowly there afterwards. The ratio of growth rate of the minor cycles is less sensitive to  $n$  when  $n < 600$ , beyond which it decreases quickly. This suggests that

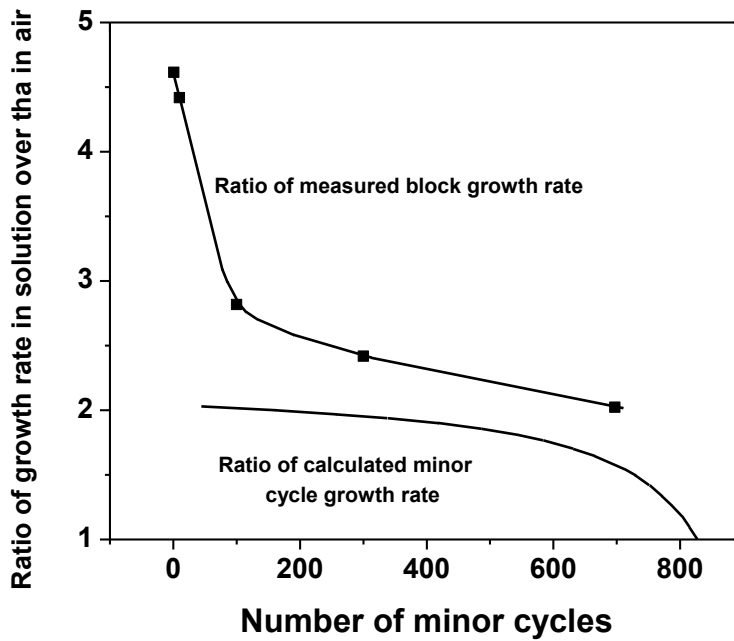


**Figure 4.9 Ratio of data in C2 solution over that in air for measured growth rate and calculated minor cycle growth rate**

the contribution of corrosion factor to the crack growth was larger when crack growth rate was lower, which is consistent with the mechanism of corrosion fatigue [19].

The enhancement in crack growth rate as a result of underload-minor cycle interactions is smaller in the near-neutral pH environment than in air. The measured crack growth rate was enhanced by maximum 12 times in air, while only a maximum of 5 times in C2 solution, as shown in Fig. 4.5. The number of minor cycles at which acceleration is negligible is similar in C2 solution and in air, although the peak growth rate in the former is about twice of that in the latter. This makes the reduction of growth rate of the minor cycles in C2 solution at a higher rate after the peak growth rate. In addition, the

acceleration factor in air was higher than that in C2 solution when  $n$  is below 300 cycles, as shown in Fig. 4.5 (b). The lower acceleration factor had also been observed for low carbon steel in moist air compared with that in dry air [11].

The above comparison has clearly demonstrated the different growth behavior of the minor cycles in air and in the near-neutral pH environment. The environmentally enhanced crack growth rate is attributed to the effect of hydrogen embrittlement [15], while a quick diminishment of the acceleration effect in C2 solution could be caused either by a faster crack growth in C2 solution or by blunting of the crack tip due to corrosion as indicated in Fig. 4.7 [15]. In the former consideration, a faster crack growth rate would need fewer minor cycles to achieve a given length of crack growth within which the underload effect is present; in the latter case, the mechanical driving force would decrease as crack tip becomes blunter.

#### **4.4.3 Mechanisms of acceleration effect induced by underloads**

A number of mechanisms that account for the acceleration effect induced by underloads have been proposed and discussed in [3], which include crack closure, residual stress, strain hardening, and change in dislocation structures. These proposed mechanisms are re-examined based on the experimental findings from this investigation, especially the results from tests in the near-neutral pH environment. However, all the existing mechanisms cannot be directly applied to NNpHSCC because they were all proposed based on the results of tests in air.

Crack closure: The crack closure model assumes that a portion of one cyclic cycle that is after the fractured surface behind the crack tip contact each other (crack closure) does not contribute to fatigue crack growth because there is no change in crack-tip strain during cyclic loading of a closed crack [23]. The crack closure model is often applied to explain the acceleration and retardation induced by underloads and overloads, respectively [2]. The acceleration effect caused by compressive underloads (loading with an R ratio below zero) was modeled and explained through crack closure [5]. The crack closure, however, is usually observed during cyclic loading with small R ratios, for example, lower than 0.5~0.6 for steel. In addition, the crack closure model is unable to explain the accelerated crack growth by the minor cycles with an R ratio as high as 0.9 in air. Furthermore, the crack closure model would predict the fastest crack growth in the very first minor cycle following the underload, which is contrary to the current experimental results obtained from tests in air and in C2 solution, as shown in Fig. 4.8. Similar observations were also made during the crack growth of BS 4360 50B steel [3]. Thus, crack closure model could not explain the current acceleration effect caused by underloads.

Residual tensile stress ahead of crack tip: Residual tensile stress was proposed to explain the crack growth acceleration after compressive underloads [24]. Residual tensile stress would be generated ahead of the crack tip by the plastic deformation of the fractured surfaces during the compressive loading, adding to the applied tensile stress, resulting in acceleration in crack growth. Since tension-tension cyclic loading was applied, the residual tensile stress mechanism might not be applicable to this study. In addition,

similar to the dilemma of the crack closure model, the residual tensile stress could not explain why the fastest growth rate did not occur during the initial cycles of minor cycle loading following the underload.

Strain hardening: Strain hardening of the material at the crack tip [3] was believed to be one of the mechanisms of the load interactions, including acceleration and retardation caused by underloads and overloads, respectively, because fatigue crack growth could be accelerated by pre-straining. Although it is generally accepted that overload could lead to strain hardening, the strain hardening occurring upon an underload cycle is not justified because the maximum stress was kept constant in the current investigation. Opposite to strain hardening, strain softening could be a reason for the acceleration. The strain increment during the minor cyclic loading (R ratio 0.7) after underload (R ratio 0.1) was predicted by finite element analysis in Ti alloy [6], although experimental validation was not provided.

Change in dislocation structure: It is well established that the material damage due to fatigue fundamentally results from the localized irreversibility of dislocation slip through various mechanisms as summarized in [25], such as cross slip of screw dislocations and different paths for their forward and reverse gliding during the complete fatigue cycle. Therefore, it is believed that the accelerated and retarded fatigue growth rate caused by underload and overload, respectively, could be associated with the change of dislocation structures. The development of a radial dislocation structure near the crack tip was observed due to the overloads [26], which could be a result of strain hardening caused by

overloads. There has been very limited work, however, on the dislocation substructure changes caused by underloads and the mechanisms for the delayed acceleration remain to be determined.

Room temperature creep: It is also suspected that room temperature creep, which is time-dependent plastic deformation, could play a role in crack propagation of pipeline steel [15]. The effect of room temperature creep at the crack tip on crack growth could be determined if the loading frequency is varied. Although it is beyond the scope of the current investigation, the effect of loading frequency is currently under investigation.

#### **4.4.4 Understanding the field crack behaviors in NNpHSCC**

The high-pressure gas transmission pipelines are operated with limited number of large cycles (underloads with R ratio less than 0.5), fewer than 10 in one year [27]. For the majority time in operation the pipelines are under minor pressure fluctuations, which are insufficient to drive a crack to grow under fatigue or corrosion-fatigue if underload effects are not considered. The crack tip is usually at a blunt state because of corrosion of steel in non-passivating environments (near-neutral pH environments) and the hydrogen facilitated plastic deformation [28]. In the case of a pressure cycle with lower R-ratios, the blunt crack tip may not necessarily be reactivated for growth on the basis of fatigue or corrosion fatigue mechanisms without considering the load interactions.

The current investigation that is focused on the load interaction between the underload and the minor cycles can rationalize the field observation that 70% of all-service and hydrostatic-test failures attributed to SCC have occurred within 30 km downstream (pressure discharge) of a pumping station [12]. At these sections, the maximum pressure is controlled to be the design limit, which allows the occurrence of underload cycles but, consequently, prevents overload cycles, and the minor cycles are predominant, as shown in Fig. 4.1a). This creates a perfect underload-plus-minor-cycle-scenario and substantial enhancement to crack growth rate can be achieved, especially by those minor cycles that are often considered to be non-propagating.

In comparison, the downstream sections beyond the first 30 km are featured with a much lower operation pressure, resulting in a reduced mechanical driving force. At the same time the overloading cycles become possible, which could further retard the crack growth.

For liquid transmission pipelines, the pressure fluctuates more rapidly and over larger amplitudes due to the incompressibility of the liquid fluids. More than 2500 large cycles with R ratio lower than 0.5 could occur per year [27]. The overall crack growth rate of oil pipelines could be larger due to the substantially increased contribution of large (underload) cycles. The number of minor cycles between two neighboring large cycles is limited and thus, the contribution of minor cycles to crack growth, as shown in Fig. 4.5(a). This would also rationalize the observations of sharp crack morphology [29] and a shorter life span [27] in the discharge section of the pump station of oil pipelines.

## 4.5 Conclusions

Variable amplitude cyclic loading waveforms were applied to X60 pipeline steel to observe the crack growth response both in air and in a near-neutral pH environment. The underloads with an R ratio of 0.5 were periodically introduced into the minor cycles with an R ratio of 0.9. Such waveforms were designed to simulate the pressure fluctuations during pipeline operation, particularly the high-pressure gas transmission pipelines that are normally operated with a near-static pressure condition, except for occasional underloads. This investigation focused primarily on the effect of minor cycles, with special attention paid to the number of minor cycles after an underload, on crack growth.

- (1) The introduction of an underload cycle could lead to a substantial level of crack growth during the subsequent minor cycle loadings even with very high R-ratios. These minor cycles are well below the threshold of growth under constant amplitude loading. The crack growth of the underload-minor cycle loading combination could be increased by a factor of 3 and 5, respectively, in air and in C2 solution, when compared to that of constant amplitude underload cycles alone.
- (2) The crack growth during minor cycle loading after the introduction of an underload cycle can be divided into three stages: 1) The initial incubation stage up to 15 cycles where acceleration of crack growth was not observed; 2) the subsequent stage up to 55 cycles, where crack growth rate increases by increasing the number of minor cycles; and 3) the final stage up to 960 cycles depending on the test environments,

where crack growth rate decreases with increasing number of minor cycles to a level at which underload effects disappear.

- (3) Crack growth produced by minor cycles after an underload was illustrated by a direct observation of well-defined mini-striations different from those produced by underloads.
- (4) Under the same underload-minor cycle loading conditions, the crack growth rate of pipeline steel in near-neutral pH environments was about 4 times higher than that in air.
- (5) The enhanced crack growth as a result of underload-minor cycle interaction could rationalize the premature failure of high pressure gas transmission pipelines that are operated most of time under a near-static loading condition but only occasionally experience relatively larger pressure fluctuations (underloads).

## References

- [1] M. Skorupa (1998). *Fatigue Fract. Engng. Mater. Struct.* 21, 987-1006.
- [2] M. Skorupa (1999). *Fatigue Fract. Engng. Mater. Struct.* 22, 905-926.
- [3] N. A. Fleck (1985). *Acta Metall.* 33, 1339-1354.
- [4] Colin MacDougall and T.H. Topper (1997). *Int. J. Fatigue* 19, 387-400.
- [5] M. El-Zeghayar, T.H. Topper, F.A. Conle, and J.J.F. Bonnen (2011). *Int. J. Fatigue* 33, 223-231.
- [6] Stephan M. Russ (2003). Effect of Underloads on Fatigue Crack Growth of Ti-17. PhD Thesis, Georgia Institute of Technology.

- [7] M. Baker Jr. (2004), Stress Corrosion Cracking Studies, Integrity Management Program DTRS56-02-D-70036, Department of Transportation, Office and Pipeline Safety.
- [8] N. Ohrloff, A. Gysler and G. Lütjering (1987). *Journal DE Physique*, Colloque C3, supplément au n°9, Tome 48, C3-801-C3-807.
- [9] V. Zitounis (2004). Fatigue Crack Growth Rates Under Variable Amplitude Load Spectrum Contaminating Tensile Underloads. PhD Thesis, Cranfield University.
- [10] M. Krkoska, S.A. Barter, R.C. Alderliesten, P. White, and R. Benedictus (2010). *Engng. Fract. Mech.* 77, 1857-1865.
- [11] Ryoichi Koterazawa and Takayoshi Nosho (1992). *Fatigue Fract. Engng. Mater. Struct.* 15, 103-113.
- [12] B. S. Delanty, J. O’Beirne (1992). Major Field Study Compares Pipeline SCC with Coatings. *Oil & Gas Journal*, 15, 39-44.
- [13] Parkins RN (2000). In: *Proceedings of Corrosion 2000*. Houston, Texas: NACE 2000, Paper 00363.
- [14] J. A. Beavers and C. E. Jaske (1998). In: *Proceedings of Corrosion 1998*. Houston, Texas: NACE 1998, Paper 98257.
- [15] W. Chen, Richard Kania, Robert Worthingham, and Gregory Van Boven (2009). *Acta Mater.* 57, 6200-6214.
- [16] National Energy Board (NEB) (1996). Report of the Inquiry – Stress Corrosion Cracking on Canadian Oil and Gas Pipelines.

- [17] B. W. Williams, S. B. Lambert, R. Sutherby, and A. Plumtree (2004). *Corrosion*, 60, 95-103.
- [18] Mengshan Yu, Weixing Chen, Richard Kania, Greg Van Boven, and Jenny Been (2014). In: *Proceedings of IPC 2014, 10<sup>th</sup> International Pipeline conference*, Sept. 29-Oct. 3, Calgary, Alberta, Canada. Paper No.: IPC2014-33282.
- [19] Weixing Chen and Robert L. Sutherby (2007). *Metall. and Mater. Trans. A*, 38A, 1260-1268.
- [20] Weixing Chen and Robert Sutherby (2004). In: *Proceedings of IPC 2004, 5<sup>th</sup> International Pipeline Conference*, Oct. 4-8, 2004, Calgary, Alberta, Canada. Paper No.: IPC2004-449.
- [21] J. Been, R. Eadie and R. Sutherby (2006). In: *Proceedings of IPC 2006, 6<sup>th</sup> International Pipeline Conference*, Sept. 25-29, 2006, Calgary, Alberta, Canada. Paper No.: IPC2006-10345.
- [22] D. L. Davidson and J. Lankford (1992). *Int. Mater. Reviews*, 37, 45-74.
- [23] T.L. Anderson (2005). *Fracture Mechanics, Fundamentals and Applications*, Third Edition. Taylors & Francis Group, 457-464.
- [24] T.L. Anderson (2005). *Fracture Mechanics, Fundamentals and Applications*, Third Edition. Taylors & Francis Group, 482.
- [25] S. Suresh (1991). *Fatigue of Materials*. Cambridge University Press, Cambridge, New York Port Chester, Melbourne Sydney, 113.

- [26] R. Koterazawa (1981). In: *Proc. Fatigue '81, SEE Fatigue Group Conf.* Warwick Univ. England (edited by F. Sherratt and J. B. Sturgeon), 318-327. Westbury House, Guildford, England.
- [27] G. Van Boven, R. Sutherby, and F. King (2002). In: *Proceedings of IPC 2002, 4th International Pipeline Conference*, Sept. 29-Oct. 3, Calgary, Alberta, Canada. Paper No.: IPC2002-27149.
- [28] W. Chen, F. King, and E. D. Vokes (2002). *Corrosion*, 58, 267-275.
- [29] W. Bouaeshi, S. Ironside, R. Eadie (2007). *Corrosion*, 63, 648-660.

# **Chapter 5     Crack Growth Behavior of a Pipeline Steel Exposed to a Near-Neutral pH Environment under Variable Pressure Fluctuations: Effects of Amplitudes<sup>1</sup>**

## **5.1 Introduction**

Although fatigue has been studied for more than 100 years [1], the mechanisms of structure failures caused by fatigue are still not fully understood, especially when other failure mechanisms, such as corrosion [2], erosion [3], and high temperature [4], are present simultaneously. Fatigue failures can occur through a three-stage process: crack initiation (Stage I), propagation (Stage II) and final rupture (Stage III). This investigation is aimed at understanding the crack growth behavior of pipeline steels exposed to corrosive near-neutral pH environments, within the scenario of corrosion fatigue.

It has been well studied that the corrosion fatigue crack growth rate in Stage II is affected by the following four factors:

---

<sup>1</sup> A version of this chapter has been submitted to *International Journal of Fatigue* for publication (under review)

- 1) Stress intensity factor range  $\Delta K$ , the primary driving force for crack growth, which is exponentially correlated to the crack growth rate [5].
- 2) Maximum stress intensity factor,  $K_{\max}$ , which usually yields a higher crack growth rate at higher  $K_{\max}$  [2,6].
- 3) Loading frequency,  $f$ , which is an environmentally sensitive factor. Crack growth rate is often found to be insensitive to  $f$  in inert environments [7], but increases with decreasing  $f$  in corrosive environments because of time-dependent processes, such as corrosion [2], hydrogen embrittlement [8] and creep [9].
- 4) Environments, which synergistically interact with mechanical driving forces and thus enhance crack growth in a way that is sensitive to the loading frequency [2].

Based on the understanding of the crack growth behavior affected by these four factors, several models have been proposed in an attempt to rationalize fatigue crack growth rates. These include the Paris Law [5], superposition model [2], crack closure model [10], two-driving force model [11] and combined factor model [12].

The above models usually yield a predicted service life very different from that obtained by field observations. For example, oil and gas pipelines have been estimated to possess a service life over several hundred years when predictive methods developed from the Paris Law [13] are used, while pipelines experiencing corrosion fatigue often fail after being in service for 20 – 30 years [14].

We believe that the above inconsistency is largely caused by the randomness of pressure fluctuations in the field. The random pressure fluctuations are the typical case of variable amplitude cyclic loadings. Such variable amplitude loadings create strong load interactions: that is, fatigue crack growth rate depends on not only the current loading conditions but also the loading history. It has been well demonstrated that underload-type variable amplitude fatigue accelerates the crack growth rate of subsequent cycles, while overload-type variable amplitude fatigue retards crack growth [15,16,17].

The random pressure fluctuations of pipeline steel can be categorized into three types, based on the analysis of pressure spectra from more than 20 oil and gas pipelines. Type I - underload pressure fluctuations, are typically seen downstream of pump or pump stations. The maximum pressure of Type I spectra is often controlled to be at or close to the design limit, only allowing pressure to fluctuate to a level lower than the design limit. Fig. 5.1 is one typical Type I spectrum normalized by R ratio (minimum stress/maximum stress), which consists of the underload cycles (the large fluctuation cycles) and the minor cycles (also called ripple loads). Type II – mean load pressure fluctuations, are usually observed further down from the pump station. The pressure fluctuates higher or lower than the average. Such a spectrum is the combination of Type I and Type III. Type III – overload pressure fluctuations, are typically observed at or close to the suction segment of pump stations. Such a spectrum suggests that the pressure is controlled at the minimum for most of the time period, while there are many pressure spikes (overloads) that are obviously above the average.

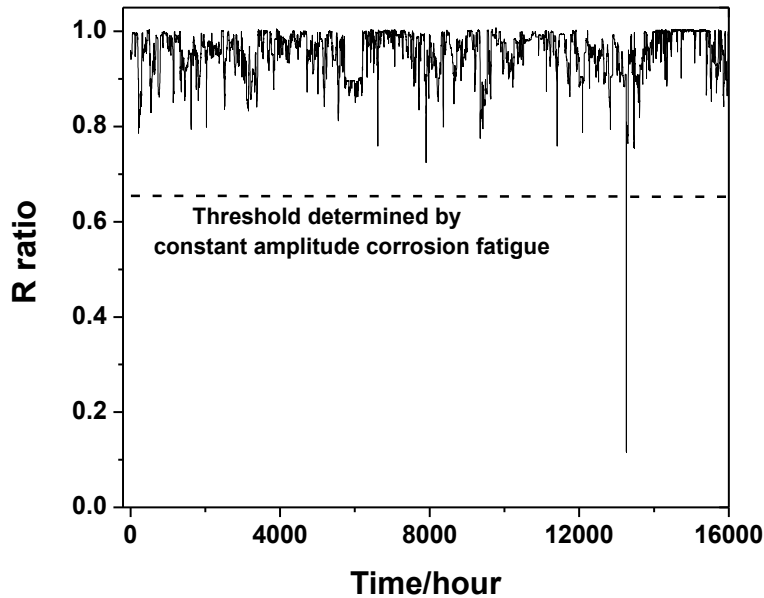


**Figure 5.1 Normalized pressure fluctuations recorded for a high-pressure gas transmission pipeline (SCADA data)**

The Type I pressure fluctuation spectrum has been identified to be the harshest in terms of crack growth. It has been well studied that the fatigue crack growth rate is accelerated by underload in various engineering components or structures, such as turbine blades [18,19], aircraft [20,21] and bridges [22]. It was reported that the magnitude of the acceleration effect could be by a factor up to 100 [16,17, 23]. Our previous studies have determined that the crack growth rate is also accelerated under Type I pressure fluctuations, as evidenced in Fig. 5.2 [24]. Additional investigations have been further conducted to understand the effects of loading frequency [25], maximum stress [25], and number of minor cycles [26] on crack growth. The results obtained from these studies could well rationalize the field observation that more than 70% of pipeline failures

attributed to stress corrosion cracking (SCC) occur within 30 km downstream of a pump station [25,27], where Type-I pressure fluctuations are dominant.

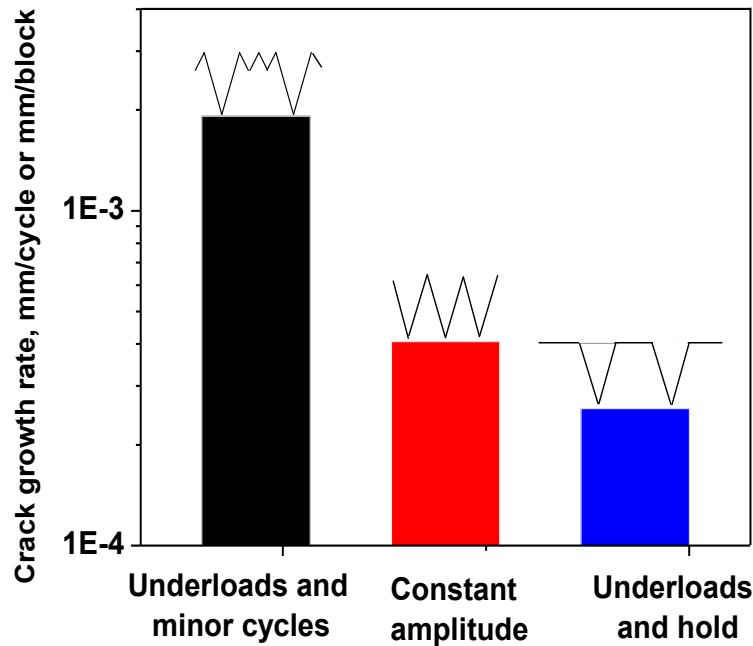


**Figure 5.2 Crack propagation response under different loading waveforms in C2 solution [24]**

This investigation was initiated to address the effect of stress amplitude in Type I pressure fluctuations on acceleration effects in crack growth, which has not been studied so far, although it is important to the development of a predictive model with high accuracy. A term called amplitude ratio was defined for the convenience of quantifying the effects of amplitude of underload cycles and minor cycles. Amplitude ratio is defined as the ratio of minor cycle amplitude divided by underload amplitude [15,16]. It has been seen that the degree of acceleration effect induced by underload reached the maximum when the amplitude ratio was about 0.5 for several materials [15,28]. The presence of

such a peak value has also been found to be material- [15,28] and environment- [23] dependent.

The environment involved in the current investigation is a near-neutral pH aqueous soil solution. The corrosion cracking associated with this environment was initially termed near-neutral pH stress corrosion cracking (NNpHSCC). It was first reported in 1985 [27], but remains a major threat to pipeline integrity worldwide today [29] as its mechanisms are still open to debate. It has been demonstrated that its mechanism is consistent with corrosion fatigue, rather than SCC, as no crack growth could be detected under static loading (by definition of SCC), even if the stress intensity factor was high [6,30,31]. The corrosion fatigue crack growth behavior of the pipeline steel exposed to near-neutral pH environments under Type I pressure fluctuations forms the topic of this study, the results of which could shed light on understanding its mechanism.

## **5.2 Experimental**

### **5.2.1 Materials and environment**

An X60 pipeline steel with a wall thickness of 10.4 mm and outer diameter of 913 mm was used in this study. The steel came from Spectra Energy Transmission. The pipeline steel had been in operation for 19 years, and showed near-neutral pH stress corrosion cracking. Pipeline sections that were cut from locations where cracking had been found

were used in this investigation. The chemical composition (wt.%) of the steel studied was as follows: C: 0.15, Mn: 1.27, P: 0.019, S: 0.005, Si: 0.37, Ni: 0.045, Cr: 0.2, Cu: 0.27, Al: 0.023, Fe: Balance. Compact tension (CT) specimens with a thickness of  $9 \pm 0.2$  mm were machined from pipeline sections that were free of crack colonies. The notch in the CT specimens was orientated in a direction parallel to the pipe longitudinal direction so that the path of crack growth in the specimen was the same as that of the longitudinal cracks found in the field. The CT specimens were polished to a 600 grit finish and then pre-cracked by fatigue in air to produce a sharp crack tip from the machined notch, according to ASTM E647-08. The sharp crack initiated from the machined notch was controlled to be between two and three mm long, and the difference in crack length on either side of the specimen was less than 0.2 mm.

The corrosion fatigue tests were performed in a near-neutral pH solution, namely C2 solution (0.0035 KCl, 0.0195 NaHCO<sub>3</sub>, 0.0255 CaCl<sub>2</sub>, 0.0274 MgSO<sub>4</sub>.7H<sub>2</sub>O, 0.0606 CaCO<sub>3</sub> g/l). A gas mixture of 5% CO<sub>2</sub> balanced with nitrogen was purged through the C2 solution before and during the test to achieve a stable pH value of 6.29 [6]. The CT specimens were sealed in test cells filled with the C2 solution and pin-hole loaded on a horizontal pneumatic loading frame with computer load control [30]. The temperature of the solution and the environment during the tests was controlled at  $30 \pm 0.1^\circ\text{C}$  so that a better control could be achieved when the temperature was above room temperature, as heating is required to maintain the temperature.

## 5.2.2 Determination of crack growth rate and acceleration factor

Crack growth was determined by using scanning electron microscopy (SEM) to measure the crack length before and after tests. The crack growth rate, expressed as millimeter per block, was calculated by dividing the measured crack growth length by the number of cyclic blocks applied. The crack advancement in each test was less than 0.5 mm, which only yields an increase of  $K_{\max}$  for about  $1 \text{ MPa}\sqrt{m}$  in current investigations. Thus, the tests can be considered under K control. As the maximum stress intensity factor can be considered constant, the amplitudes will be expressed as R ratio in the following sections.

A factor,  $\gamma$ , termed as the acceleration factor, is often used to describe the degree of crack growth acceleration, which is defined as the ratio of measured growth rate per block over the predicted growth rate per block by a linear summation of the constant amplitude crack growth response [15], that is,

$$\gamma = \frac{\text{measured growth rate per block}}{\text{predicted growth rate per block by a linear summation of the constant amplitude crack growth response}} \quad (5 - 1)$$

The linear summation (predicted growth rate) can be expressed by the following equation:

$$\left(\frac{da}{dN}\right)_{\text{block}} = N_1 \left(\frac{da}{dN}\right)_{\text{underload}} + N_2 \left(\frac{da}{dN}\right)_{\text{minor cycles}} \quad (5 - 2)$$

where  $(da/dN)_{\text{underload}}$  is the constant amplitude crack growth rate at the same loading conditions of underload (large cycle) during variable amplitude fatigue, and  $N_1$  is the number of underload cycles in one block, which is  $N_1=1$  for the current study;  $(da/dN)_{\text{minor cycles}}$  is the constant amplitude crack growth rate at the same loading conditions of minor cycles during variable amplitude fatigue, and  $N_2$  is the number of minor cycles in the block, which is  $N_2=n=300$  (as indicated in the following section) for the current study. The constant amplitude crack growth rates in the current investigation can be obtained from Ref. [12,24,25,26].

### 5.2.3 Mechanical loading conditions

Effect of R ratio of underload cycles: The variable amplitude cyclic loading waveform shown in Fig. 5.3 was designed to simulate the field pressure fluctuations shown in Fig. 5.1. The starting  $K_{\text{max}}$  applied was at  $33 \text{ MPa}\sqrt{m}$ . This level of  $K_{\text{max}}$  can be achieved in field pipes, when a long but shallow crack (typical field SCC cracks) with depth of about 20-30% of wall thickness and with a crack length to depth ratio of 10 is loaded to 75% SMYS (specified minimum yield strength). The R ratio of minor cycles was kept at 0.9, corresponding to  $3.3 \text{ MPa}\sqrt{m}$ , while that of underload cycles varied from 0.1, 0.3, 0.5, 0.7 until 0.8. The loading rate of the underload cycles was kept the same, while the loading frequency of underload cycles varied with R ratios (amplitude) of the underload cycle accordingly, ranging from  $5.79 \times 10^{-4}$  to  $2.6 \times 10^{-3}$  Hz. The frequency of minor cycles was selected at  $5.38 \times 10^{-3}$  Hz, and the number of minor cycles per block (between two neighboring underload cycles),  $n$ , was at 300 cycles [26]. The first and last event of the

variable amplitude waveform in Fig. 5.3 was the minor cyclic loading. To obtain a certain amount of crack advancement, 92 blocks were performed for R ratio 0.8, while 61 blocks were performed for other R ratios.

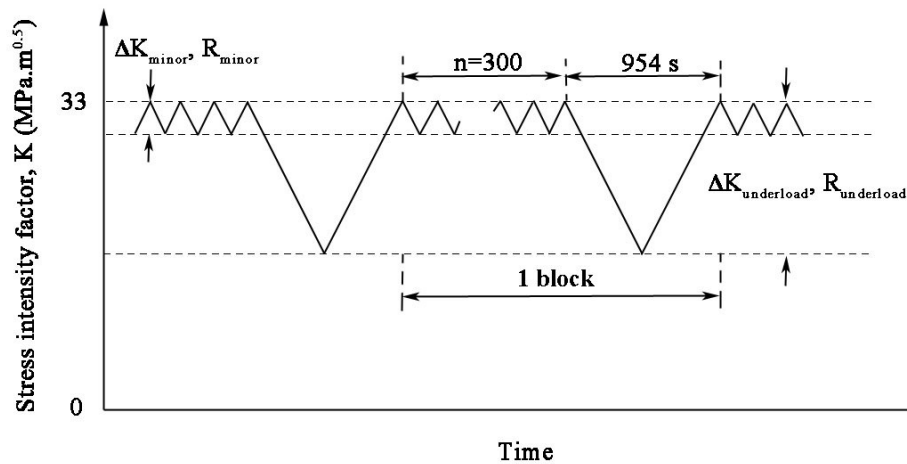


**Figure 5.3 Variable amplitude fatigue waveform designed to simulate the pressure fluctuations in Figure 1**

For comparison, the same waveform was also performed on a closed loop hydraulic Instron machine (8516) in air at room temperature, around 22°C, which was executed by a computer with Instron Wavemaker-Runtime software. The tests in air were performed at a higher loading frequency with 0.5 Hz for the minor cycles, as it is found that the fatigue crack growth rate of the current pipeline steel was insensitive to the loading frequency in air [25]; and a greater number of blocks was applied for the tests in air because the crack growth rate in air is lower than that in the C2 solution. All the other loading conditions for the tests in air were kept the same as in the C2 solution.

Effect of R ratio of minor cycles: The same  $K_{\max}$ ,  $33 \text{ MPa}\sqrt{m}$ , was also applied. The R ratio of minor cycles was varied from 0.8, 0.9, 0.95 to 1 (static hold), while the frequency of minor cycles was kept the same,  $5.38 \times 10^{-3}$  Hz. The number of minor cycles per block and the number of blocks applied were 300 cycles and 61 blocks, respectively. The static hold duration at  $R = 1$  was the same as the duration of minor cycles in each loading block: 15.5 hours.

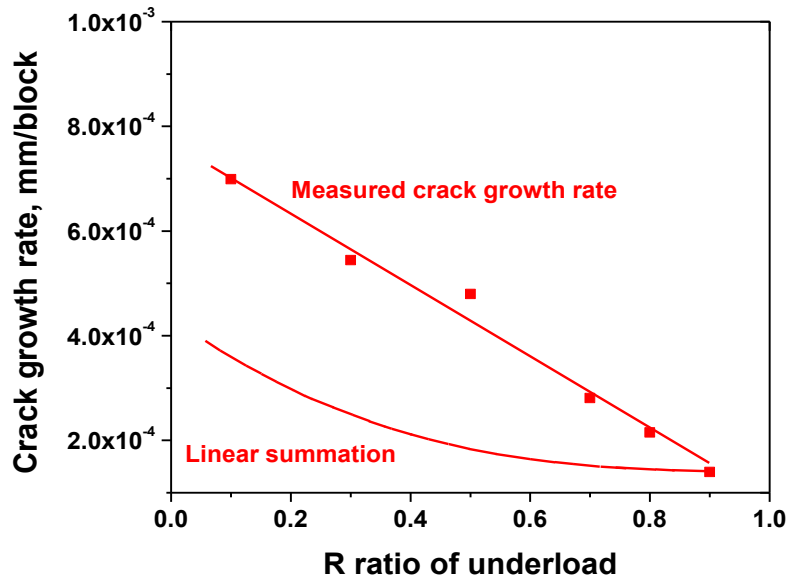
For comparison, similar tests were also conducted in air. The only difference in loading conditions from those in solution was that the number of blocks was in a range of 30 for R ratio 0.7, to 1500 for R ratio 1 to achieve a certain amount of crack advancement; and that the R ratio of minor cycles was selected to be at 0.7, 0.8, 0.9, 0.94, 0.97 and 1.

## **5.3 Results**

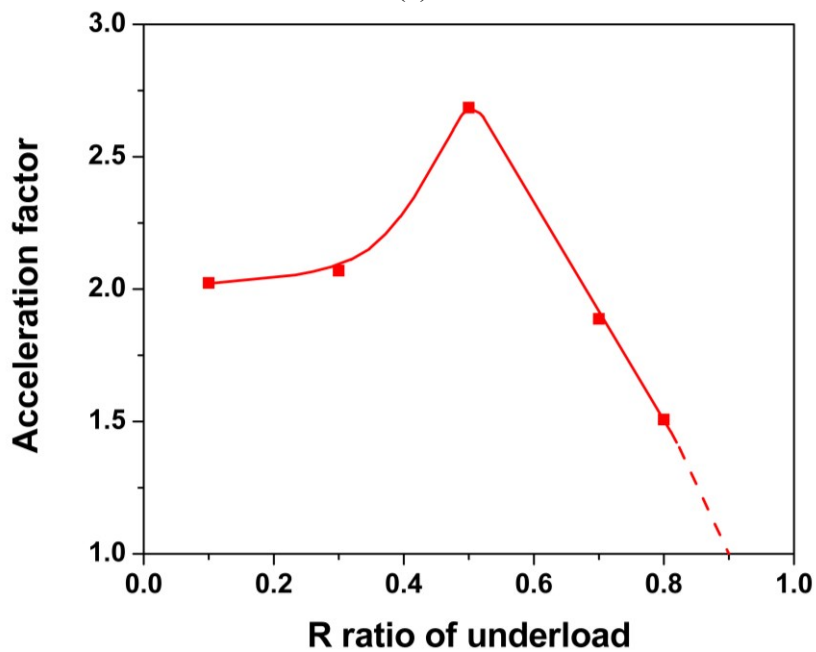
### **5.3.1 Dependence of crack growth rate on R ratio of underload**

Tests in air: As shown in Fig. 5.4(a), both the crack growth rate measured and the linear summation values calculated by Eq. (5-2) decrease with the R ratio of underload, and the measured crack growth rates were higher than the linear summation values at all R ratios. The measured crack growth rate varied from  $6.99 \times 10^{-4}$  mm/block at underload  $R = 0.1$  to  $1.40 \times 10^{-4}$  mm/block at underload  $R = 0.9$ . At the later condition, the variable amplitude

fatigue waveform becomes the constant amplitude fatigue, and thus the measured variable amplitude crack growth rate is merged with the value of linear summation.



(a)



(b)

**Figure 5.4** Crack growth behaviors of test of R ratio of underload in air: a) crack growth rate; and b) acceleration factor

The effect of the underload R ratio on the acceleration factor is shown in Fig. 5.4(b). It can be seen that the acceleration factor increased from about 2.0 at underload  $R = 0.1$  to a maximum value of 2.7 at  $R = 0.5$ , and it then dropped to 1.5 at  $R = 0.8$ .

Tests in C2 solution: Similar to the results obtained from tests in air, both linear summation and the measured crack growth rate in the C2 solution decreased with increasing underload R ratios, as seen in Fig. 5.5(a). However, the linear summation curve intercepted the variable amplitude curve at around  $R = 0.2$ , below which the linear summation value was higher than the variable amplitude crack growth rates. Unlike the case in air, the two curves did not approach to a merging point at higher R-ratios in C2 solution.

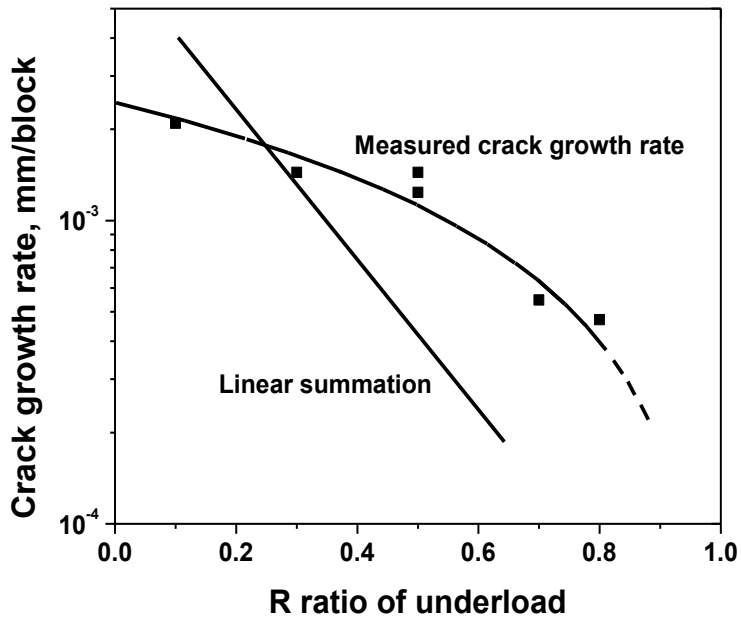
The acceleration factor in C2 solution is shown in Fig. 5.5(b). It can be seen that the acceleration factor increased with the underload R ratio, from 0.52 (deceleration) at  $R = 0.1$  to 3.29 at  $R = 0.5$ . When R is about 0.6, the mechanical driving forces for constant amplitude fatigue are reduced to the threshold in the C2 solution [6], and thus the acceleration factor increased sharply with increasing R ratios (dash line).

### **5.3.2 Dependence of crack growth rate on R ratio of minor cycles**

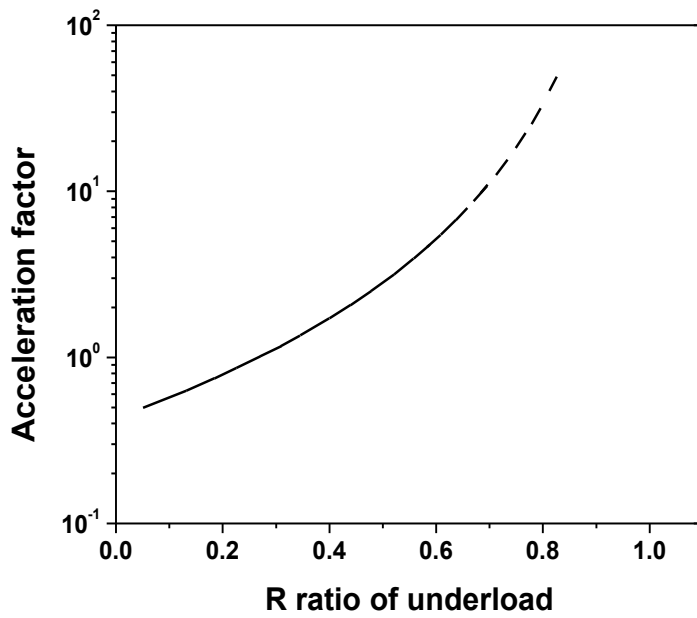
Tests in air: As seen in Fig. 5.6(a), both the measured crack growth rate and the linear summation decreased with the R ratio of minor cycles. The measured variable amplitude crack growth rate varied from  $3.43 \times 10^{-3}$  mm/block at R ratio 0.7 to  $3.56 \times 10^{-5}$  mm/block

at R ratio 1 (static hold). At  $R = 1$ , the variable amplitude fatigue waveform becomes underload + static hold. At R ratio 1, the difference in crack growth rate between the measured and the linear summation is small, about 16%, and the measured value appears lower than the calculated value. This difference, on one hand, could be attributed to experimental scatters. On the other hand, the difference could be related to the effect of hold, a non-cyclic condition, which is further discussed later.

The acceleration factor is shown in Fig. 5.6(b). It can be seen that the acceleration factor reaches a maximum value, about 2, at the R ratio of minor cycles 0.9.

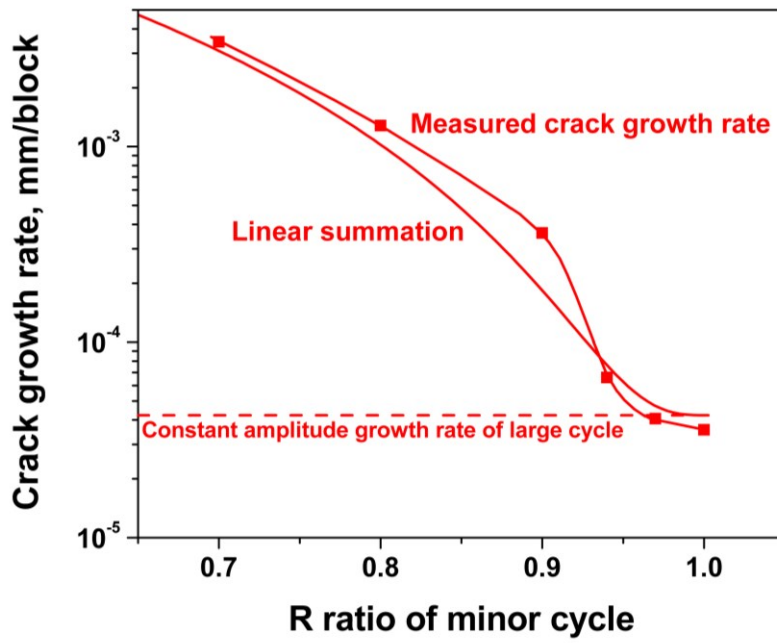


(a)

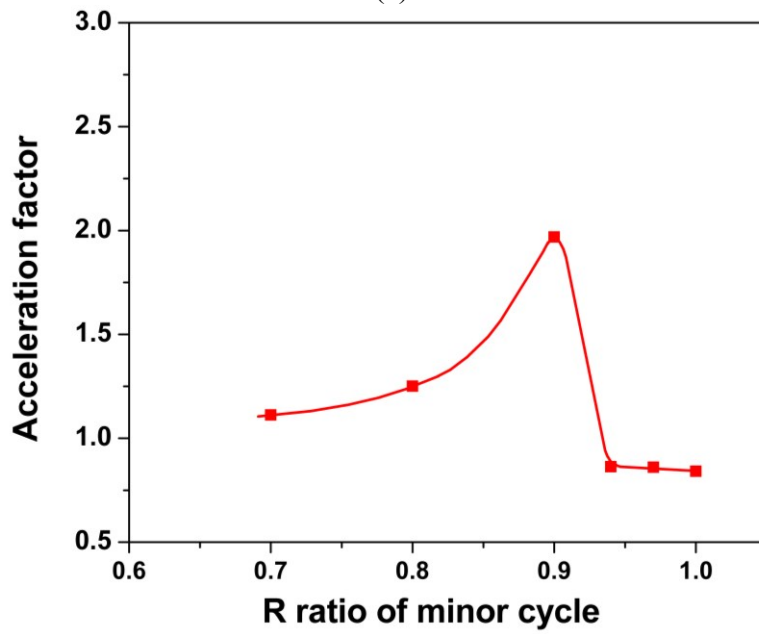


(b)

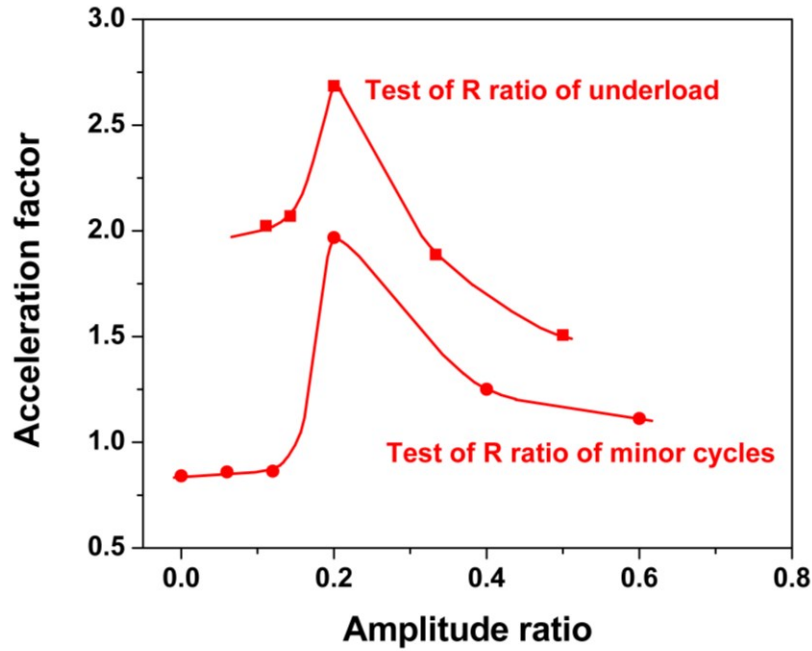
**Figure 5.5 Crack growth behaviors of test of R ratio of underload in C2 solution:  
a) crack growth rate; and b) acceleration factor**



(a)



(b)



(c)

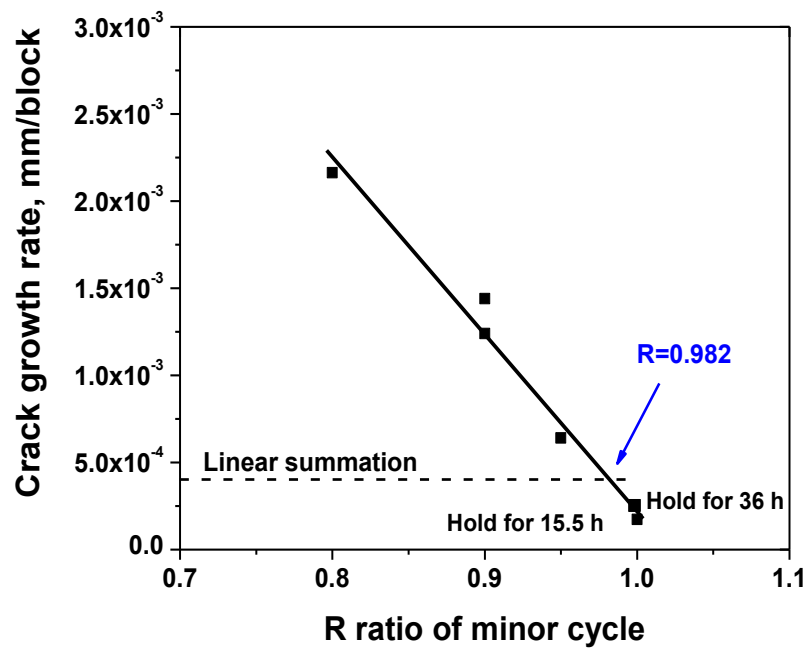
**Figure 5.6 Crack growth behaviors of test of R ratio of minor cycles in air: a) crack growth rate; and b) acceleration factor - R ratio of minor cycles; and c) acceleration factor – amplitude ratio**

Tests in solution: As the minor cycles are well below the determined constant amplitude threshold [6], the linear summation is a horizontal line,  $4.07 \times 10^{-4}$  mm/block, shown in Fig. 5.7(a). The measured crack growth rate decreased with the R ratio of minor cycles, from  $2.16 \times 10^{-3}$  mm/block at R ratio 0.8 to  $1.72 \times 10^{-4}$  mm/block at R ratio 1 (static hold). The growth rate at R ratio 1 was 58% lower than the constant amplitude growth rate ( $4.07 \times 10^{-4}$  mm/block), which can not be attributed to experimental scatters. In addition, this data coincides with the previous crack growth rate of static hold for 36 hours (all the other loading conditions were consistent),  $2.56 \times 10^{-4}$  mm/block, as shown in Fig. 5.6(a).

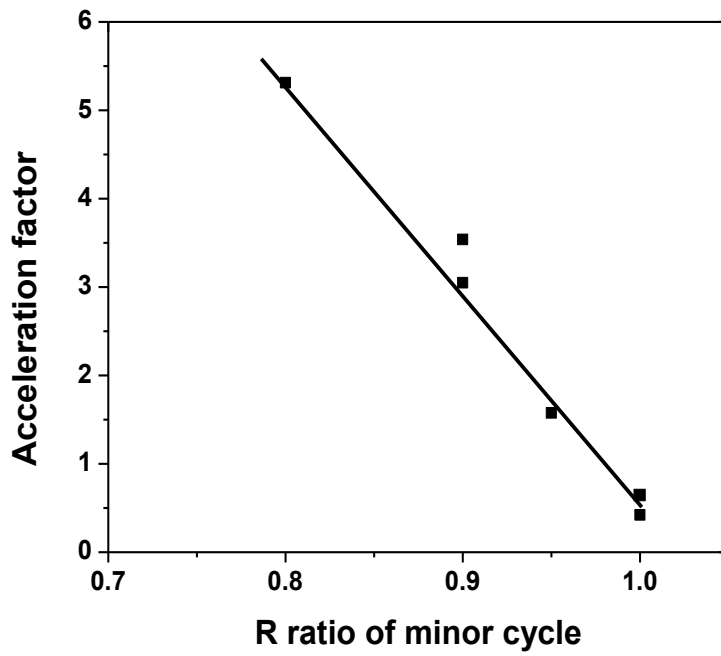
The acceleration factor, as can be seen in Fig. 5.7(b), had the same trend as the measured crack growth rate, decreasing with the R ratio of minor cycles, from 5.3 at R ratio 0.8 to 0.42 (retardation in fact) at R ratio 1.

### **5.3.3 Dependence of acceleration factor on amplitude ratio**

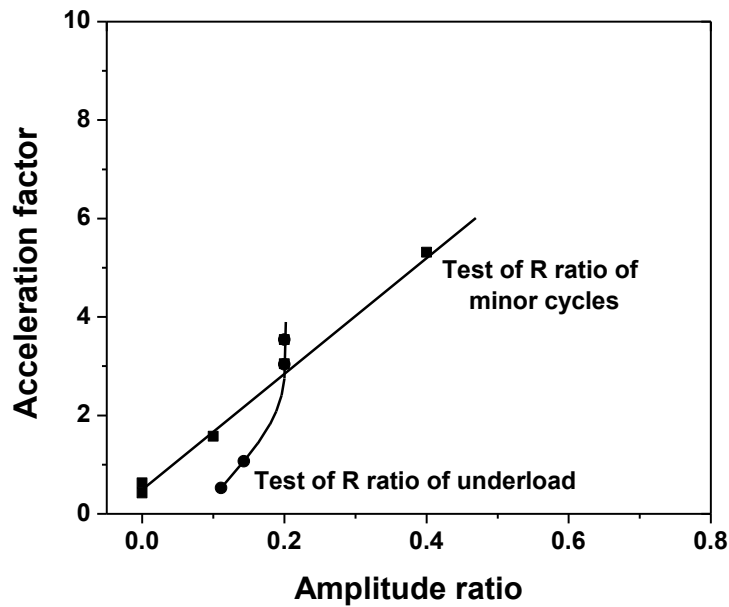
The amplitude ratio, as defined as the ratio of minor cycle amplitude over underload amplitude, is used to rationalize the acceleration factor. The amplitude ratio was calculated for amplitude tests of underload and minor cycles, as shown in Figs. 5.6(c) and 5.7(c). For tests in air in Fig. 5.6(c), it can be seen that the acceleration factor reached a peak value at amplitude ratio 0.2 for both underload and minor cycle amplitude tests, instead of at amplitude ratio 0.5 found in other materials in Ref. [15,16,28]. For tests in the near-neutral pH solution, the acceleration factor increased with the amplitude ratio, and no peak value appeared, as shown in Fig. 5.7(c).



(a)



(b)



(c)

**Figure 5.7 Crack growth behaviors of test of R ratio of minor cycles in C2 solution: a) crack growth rate; and b) acceleration factor – R ratio of minor cycles; and c) acceleration factor – amplitude ratio**

## 5.4 Discussion

### 5.4.1 Enhanced crack growth rate by underload

As shown in Fig. 5.2, it has been well demonstrated that the minor cycles, even with an R ratio as high as 0.9, can still contribute to crack propagation for pipeline steel exposed to near-neutral pH environments in the presence of larger pressure fluctuations (underload) through load interactions [13,24,25,26]. In addition to the studies of loading frequency

[25], maximum stress [25] and number of minor cycles [26] on crack growth rate, the amplitude effects in the current investigation have also confirmed the accelerated crack growth effects both in air and in the near-neutral pH environments, as shown in Figs. 4-7. It can be seen that the established models based on constant amplitude fatigue, such as the Paris Law [5], superposition model [2], crack closure [10], two driving force [11] and combined factor [6], significantly underestimate the crack growth of pipeline steel under random pressure fluctuations. The observations of load interaction could well bridge the large discrepancy between predicted service life and field observations [13,24,25].

This investigation has also found some unique crack growth behavior characteristics of pipeline steels under the underload-type variable amplitude fatigue. The acceleration factor reached the maximum at amplitude ratio 0.2 in air, and no peak value was observed for tests in the near-neutral pH environments, while a peak value of the acceleration factor was reported at amplitude ratio 0.5 for several other materials [15,16,28]. This further confirms that the crack growth acceleration under variable loading is both material- and environment-sensitive [15,23,28].

The mechanisms of the acceleration effect induced by underloads, such as crack closure, residual stress, strain hardening and change in dislocation structures, have been discussed in Ref. [26]. Although strain softening and the change in dislocation structures were suspected to be the mechanisms, further research should be conducted.

## 5.4.2 Reduced corrosion fatigue threshold by underload

As shown in Fig. 5.7(a), when the minor cycles were replaced by static hold while keeping other conditions constant, the block crack growth rate was reduced by 58%. Thus the static hold could actually retard crack propagation caused by underload. A similar result was also found when the period of static hold was increased to 36 hours, while the other conditions were kept the same as those in the current investigations [24]. This observation echoes the conclusion made in many previous studies that crack growth in near-neutral pH environments does not occur under static tensile stress (a condition of SCC), with an exception of crack formation in the stage of initiation, where a crack forms through galvanic corrosion [3,30].

Based on the above observations, it is possible to define the critical R ratio of minor cycles below which minor cycles make a contribution to crack growth through load interaction. The relationship between the growth rate,  $(da/dN)_{block}$  in terms of millimeter per block, and the R ratio of minor cycles (including static hold for 15.5 hours) can be expressed as:

$$\left(\frac{da}{dN}\right)_{block} = 0.010 - 0.010 \times R_{minor} \quad (5 - 3)$$

The critical R ratio of minor cycles is the intercept between the linear relation defined in Eq. (5-3) with a horizontal line, that is, 0.982, as shown in Fig. 5.7(a). It corresponds to a stress intensity factor range of  $0.594 \text{ MPa}\sqrt{m}$ .

The determination of the critical R ratio of minor cycles makes it possible to clearly demarcate the true boundary between SCC and corrosion fatigue. This boundary is usually defined based on the constant amplitude fatigue threshold, which is about  $10 \text{ MPa}\sqrt{m}$  for pipeline steel in NNpHSCC [6] and about  $3 \text{ MPa}\sqrt{m}$  for most engineering materials in air [32]. These defined boundaries are obviously much higher than the critical amplitude of minor cycles determined with a consideration of load interactions, which is found to be as low as  $0.594 \text{ MPa}\sqrt{m}$  in the current investigation.

Another application of this critical R ratio is to filter the raw data of stress fluctuations. To analyze the loading history data of structures in service, a data filter is usually set to remove the intermediate points and small stress cycles that are thought to be too small to cause any fatigue damage [17]. However, such filters are often set arbitrarily. Based on the current investigation, this filter could be as low as  $0.594 \text{ MPa}\sqrt{m}$ .

The effect of load interactions should also be incorporated into fatigue design for engineering structures or components with routine stress fluctuations and/or frequent shutdown-restart cycles. Traditionally, engineering structures are designed either based on the stress-number of cycles to failure (S-N) curve [33] or fracture mechanics criteria [32]. However, based on Ref. [34] and the current investigation, the traditional fatigue design approaches would significantly underestimate the fatigue damage, even if the safety factor is selected at 10 [24].

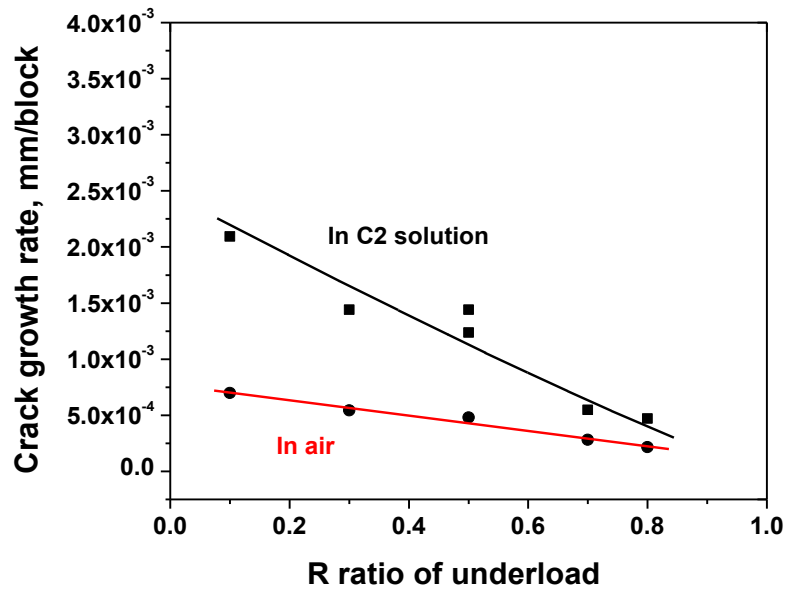
### 5.4.3 Effects of environments on crack growth behaviors

The role of environments in the crack propagation of pipeline steels can be determined by comparing the crack growth rates in the near-neutral pH solution with those in air under the same loading conditions. This is shown in Fig. 5.8. It can be seen that the crack growth rate in C2 solution is higher than that in air.

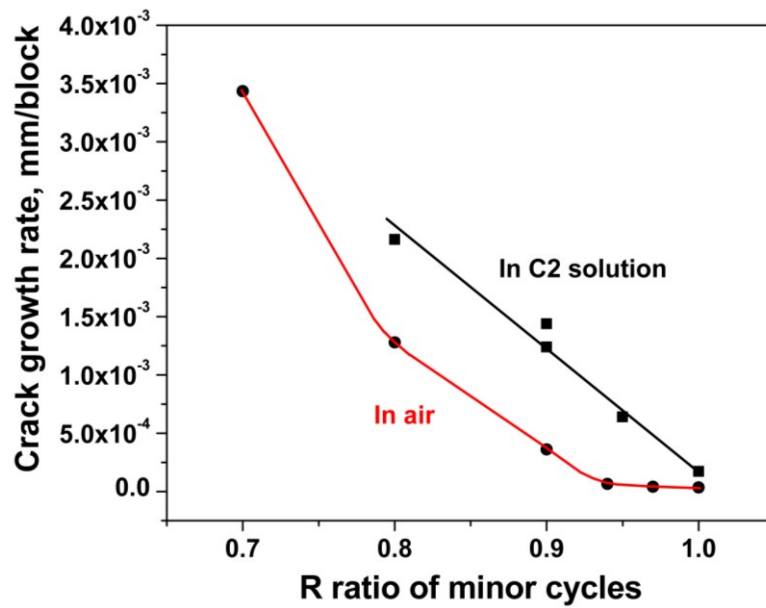
An environmental factor is used to determine the role of environments on crack growth. The environmental factor is defined as the ratio of crack growth rate in solution divided by that in air. As seen in Fig. 5.9, the environmental factor decreased with the R ratio of underload, from three at underload  $R = 0.1$  to about two at underload  $R = 0.8$ , while it increased to a peak value of 10.7 at the R ratio of minor cycles 0.95, and then decreased to 4.8 at the R ratio of minor cycles 1 (static hold). (As no test was performed at the R ratio of minor cycles 0.95 in air, the crack growth rate at R ratio 0.95 was obtained from linear interception.)

As well documented in previous studies, the contribution of near-neutral pH environments to crack propagation was attributed to hydrogen embrittlement (HE) [12,25]. However, HE alone was not sufficient to rationalize the observed crack growth behavior [25]. The synergistic interaction between HE and the underload cycles must be considered. Based on the current investigation and those reported previously [1,6,13,17,24,25,26,27,30], crack propagation behavior in the current corrosion fatigue system is believed to be governed by the following four factors:

- i. Although a crack advance by a direct dissolution of the material at the crack tip was found to be very limited (typically as low as  $1.6 \times 10^{-9}$  mm/s or 0.05 mm/year) [35], the fact that the dissolution could occur at the crack tip and the crack wall because of the non-passivating nature of the environment makes the crack blunt. This reduces stress intensity at the crack tip, and thus the crack growth rate [24,36].
- ii. Hydrogen could be generated as a byproduct of corrosion of steel in near-neutral environments, or by cathodic potential imposed on the outer surface [37] or at the inner surface due to internal corrosion [38]. Regardless of its sources, it could diffuse to the crack tip and build up to higher concentrations in the plastic zone ahead of the crack tip because of the presence of high hydrostatic stresses and high density of dislocations (effective H traps), leading to the potential occurrence of HE and increased crack growth rate [30].
- iii. Pressure fluctuations cause direct crack propagation through the mechanisms of fatigue even in inert environments [39], and enhance fatigue crack growth rate in the presence of corrosive environments through various mechanisms of corrosion fatigue, as seen in Figs. 9 and 10.
- iv. The variable amplitude pressure fluctuations create various synergistic interactions, for example, between the current load cycle and previous ones, between time dependent driving forces such as corrosion and diffusion of hydrogen and the mechanical driving forces, as found in our current and previous studies [24,25,26,30].

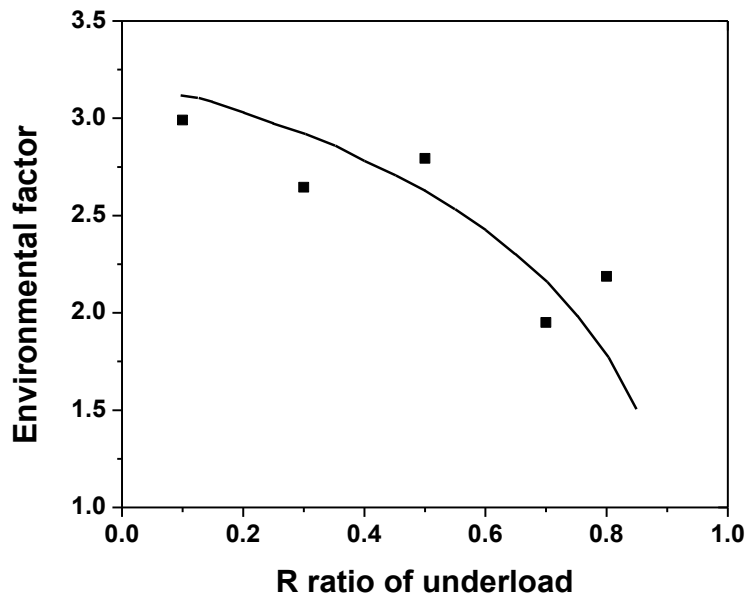


(a)

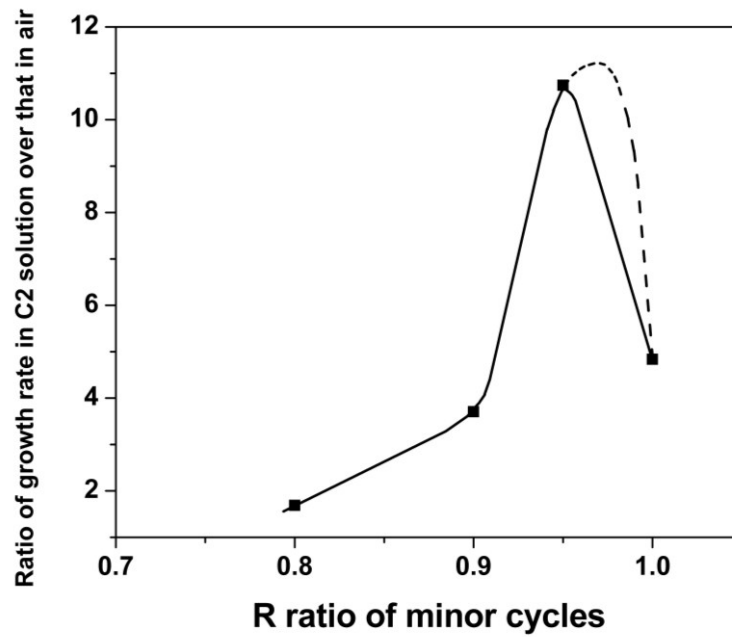


(b)

Figure 5.8 Comparison of crack growth in solution and in air: a) R ratio of underload; and b) R ratio of minor cycles



(a)



(b)

**Figure 5.9** Ratio of crack growth rate in C2 solution over that in air: a) R ratio of underload; and b) R ratio of minor cycles

The results shown in Figs. 5.8 and 5.9 are a good reflection of the above four factors. With the increasing R ratio of the underload cycle, the fact that both the crack growth rate and the environmental factor decrease indicates that the underload component (and thus the acceleration effect) is dominant in crack propagation in the current corrosion fatigue system, which echoes the importance of fatigue (pressure fluctuations) in NNpHSCC [3-30].

With the increasing R ratio of minor cycles, the environmental factor increases to a peak value and hereafter drops, as can be seen in Fig. 5.9(b). This is believed to be the result of from the following two opposite effects of the R of minor cycles on crack growth:

- Higher R ratios of minor cycles favor hydrogen segregation to the crack tip that drives crack growth through HE mechanisms,
- Higher R ratios of minor cycles lower the mechanical driving force for fatigue crack growth, and favor crack tip blunting through corrosion [36].

When these two opposite effects reach balance, a peak value of the environmental factor is obtained, which should correlate to the critical R ratio of minor cycles in Section 4.2 where the minor cycles do not contribute to crack growth. Although the peak value in Fig. 5.9 (b) is shown at 0.95, it is supposed to be the critical R ratio of minor cycles, 0.982 (dash line), because no actual test was performed at the R ratio of minor cycles 0.95 in air and the crack growth rate at R ratio 0.95 was obtained from linear interception.

### 5.4.4 Understanding NNpHSCC crack growth

A schematic diagram shown in Fig. 5.10 was drawn to elucidate the complex processes of crack growth of pipeline steel exposed to near-neutral pH environments under variable amplitude pressure fluctuations. It was made based on the original diagram reported in Ref. [30]. The material factors were not included, as pipeline steel of all grades are found to be susceptible to cracking in near-neutral pH environments [40]. Fig. 5.10 reflects how a crack propagates through the synergistic interactions among the variables of pressure fluctuation, corrosive environments, and cathodic protection.

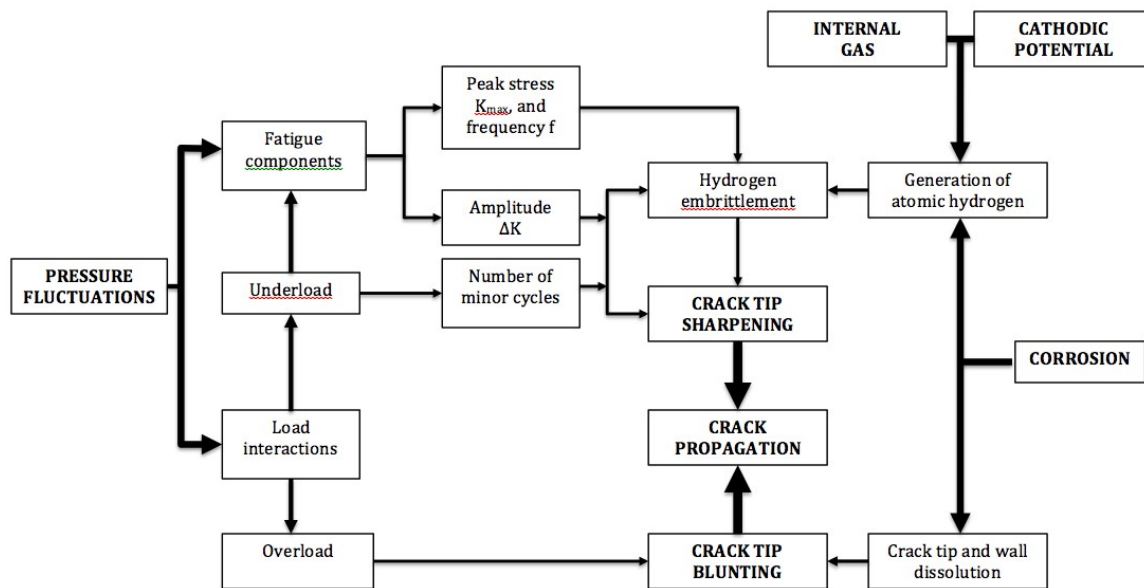


**Figure 5.10** A schematic showing the mechanism of crack propagation in pipeline steels exposed to near-neutral pH environments under pressure fluctuations

## 5.5 Conclusions

A comparative study of X60 pipeline steel was performed in air and in a near-neutral pH environments under variable amplitude fatigue. The underload waveform was designed based on the pressure fluctuations during pipeline routine operations. The effects of amplitudes (R ratios) of underload and minor cycles have been investigated. It has been found from this investigation that:

- 1) The crack growth rate was enhanced significantly through load interaction of the variable amplitude fatigue. The acceleration factor could be up to 2.7 and 5.3 for tests in air and in the near-neutral pH solution, respectively.
- 2) The crack growth rate decreased with R ratios of underload and minor cycles for tests for both in air and in the C2 solution.
- 3) The corrosive C2 solution could contribute to crack propagation by a factor up to 11 by comparing the crack growth rate in C2 solution and in air, which was attributed to the synergistic interaction of mechanical loading and hydrogen embrittlement.
- 4) The critical R ratio of minor cycles at which the minor cycles do not contribute to crack propagation through load interaction was determined to be as high as 0.982, corresponding to  $0.594 \text{ MPa}\sqrt{m}$  of the stress intensity factor range, which is much lower than the threshold determined by constant amplitude fatigue. This critical R ratio could be utilized to demarcate stress corrosion cracking and corrosion fatigue, and should be incorporated as one of the design principles for components/structures subjected to variable amplitude cyclic loading.

## References

- [1] S. Suresh. *Fatigue of Materials*, Second Edition, Cambridge University Press, Cambridge, UK, 1998 (Chapter 1).
- [2] T. L. Anderson. *Fracture Mechanics, Fundamentals and Applications*, Third Edition. Taylors & Francis Group, 2005. pp. 538-547.
- [3] V. M. Pleskach and P. A. Averchenko. Effect of gaseous erosion on a decrease of the fatigue strength of specimens of titanium alloy VT8. *Plenum Publishing Corporation*, 1976, No. 8, pp.118-119.
- [4] H-J Christ, A Jung, H J Maier and R Teteruk. *Sādhanā*, Vol. 28, Parts 1 & 2, February/April 2003, pp. 147–165.
- [5] P. C. Paris. *Fatigue—An Interdisciplinary Approach*, Proceedings, 10th Sagamore Conference, Syracuse University Press, Syracuse, NY, 1964, pp. 107.
- [6] B.L. Boyce and R.O. Ritchie. *Engineering Fracture Mechanics* 68 (2001) 129-147.
- [7] M. O. Speidel, S. Stanzl and E. Tschegg: *Z. Werkstofftech.*, 1980, 11, 305-308.
- [8] Arnaud Macadre, Maxim Artamonov, Saburo Matsuoka, Jader Furtado. *Engineering Fracture Mechanics* 78 (2011) 3196-3211.
- [9] Kamel Makhoul and J.W. Jones. *International Journal of Fatigue*. Vol. 15, No. 3, pp.163-171.
- [10] Elber, Wolf. *Engineering Fracture Mechanics*, Vol. 2, No. 1, 1970, pp.37-44.
- [11] A.K. Vasudevan, K. Sadananda, G. Glinka. Vol. 23, 2001, pp. 39-53.

- [12] Weixing Chen and Robert L. Sutherby. Metallurgical and Materials Transactions A 2007; 38A; pp. 1260-1268.
- [13] Jiayi Zhao, Weixing Chen, Richard Kania, Sean Keane, and Jenny Been. Proceedings of IPC 2014, 10th International Pipeline conference, Sept. 29-Oct. 3, 2014, Calgary, Alberta, Canada. Paper No. IPC2014-33325.
- [14] C. Manfredi and J.L. Otegui. Engineering Failure Analysis, Vol. 9, 2002, pp. 495-509.
- [15] N. A. Fleck. Acta Metall. Vol. 33, No. 7, pp. 1339-1354, 1985.
- [16] M. Skorupa. Fatigue & Fracture of Engineering Materials & Structures, 1998, 21: 987-1006.
- [17] M. Skorupa. Fatigue & Fracture of Engineering Materials & Structures, 1999, 22: 905-926.
- [18] Vasilios Zitounis. Fatigue Crack Growth Rates under Variable Amplitude Load Spectra Containing Tensile Underloads. PhD thesis, Cranfield University, 28 October 2003.
- [19] Stephan M. Russ. Effect of Underloads on Fatigue Crack Growth of Ti-17. PhD thesis, Georgia Institute of Technology, October 2003.
- [20] Fowler, K.R. and Watanabe, R.T.. Development of Jet Transport Airframe Fatigue Test Spectra, Development of Fatigue Loading Spectra, ASTM STP 1006, J. M. Potter and R. T. Watanabe, Eds., American Society for Testing and Materials, Philadelphia, 1989, pp. 36-64.

- [21] Sunder, R. Contribution of Individual Load Cycles to Crack Growth under Aircraft Spectrum Loading, *Advances in Fatigue Lifetime Predictive Techniques*, ASTM STP 1122, M. R. Mitchell and R. W. Landgraf, Eds., American Society for Testing and Materials, Philadelphia, 1992, pp. 176-190.
- [22] T. L. Anderson. *Fracture Mechanics, Fundamentals and Applications*, Third Edition. Taylors & Francis Group, 2005. pp: 473-488.
- [23] Ryoichi Koterazawa and Takayoshi Nosho. *Fatigue & Fracture of Engineering Materials & Structures*, Vol. 15, No. 1, pp. 103-113, 1992.
- [24] Mengshan Yu, Weixing Chen, Richard Kania, Greg Van Boven, and Jenny Been. *Proceedings of IPC 2014, 10th International Pipeline conference*, Sept. 29-Oct. 3, 2014, Calgary, Alberta, Canada. Paper No. IPC2014-33282.
- [25] Mengshan Yu, Xiao Xing, Hao Zhang, Jiayi Zhao, Reg Eadie, Weixing Chen, Jenny Been, Greg Van Boven, Richard Kania. Corrosion fatigue crack growth of pipeline steel under underload-type variable amplitude loading schemes. Submitted to *Acta Materialia* (under review).
- [26] Mengshan Yu, Weixing Chen, Richard Kania, Greg Van Boven, and Jenny Been. Full paper submitted to *Fatigue & Fracture of Engineering Materials & Structures* (In press, DOI: 10.1111/ffe.12274.).
- [27] B. S. Delanty, J. O'Beirne. Major Field Study Compares Pipeline SCC with Coatings. *Oil & Gas Journal* 15 (1992) 39-44.

- [28] Vasilios Zitounis. Fatigue Crack Growth Rates under Variable Amplitude Load Spectra Containing Tensile Underloads. PhD thesis, Cranfield University, 28 October 2003.
- [29] National Energy Board (NEB), Focus on Safety and Environment a Comparative Analysis of Pipeline Performance 2000-2007, July 2009.
- [30] W. Chen, Richard Kania, Robert Worthingham, and Gregory Van Boven. *Acta Materialia* 57 (2009) 6200-6214.
- [31] Parkins RN. A review of stress corrosion cracking of high pressure gas pipelines proceedings of corrosion 2000. Paper 00363. Houston, Texas: NACE International; 2000.
- [32] T.L. Anderson. *Fracture Mechanics, Fundamentals and Applications*, Third Edition. Taylors & Francis Group, 2005. pp: 451-500.
- [33] Richard W. Hertzber. *Deformation and Fracture Mechanics of Engineering Materials*, Fourth Edition, John Wiley and Sons, Inc., New York, NY, 1989, pp. 521-586.
- [34] Yan-Hui Zhang, and S.J. Maddox. *International Journal of Fatigue* 31 (2009) 138-152.
- [35] Karina Chevill, Weixing Chen, Reg Eadie, Richard Kania, Greg Van Boven, and Jenny Been. Proceedings of IPC 2014, 10th International Pipeline conference, Sept. 29-Oct. 3, 2014, Calgary, Alberta, Canada. Paper No. IPC2014-33678.
- [36] Afolabi Egbewande, Weixing Chen, Reg Eadie, Richard Kania, Greg Van Boven, Robert Worthingham, Jenny Been. *Corrosion Science*, Vol. 83, June 2014: 343-354.
- [37] C.F. Dong, Z.Y. Liu, X.G. Li and Y.F. Cheng. *International Journal of Hydrogen Energy* 34 (2009) 9879-9884.

[38] R.L. Eadie, K.E. Szklarz and R.L. Sutherby. *Corrosion*, Vol. 61, No. 2, 2005, pp. 167-173

[39] R. Sunder, W. J. Porter and N. E. Ashbaugh. *Fatigue Fract. Engng. Mater. Struct.*, Vol. 26, Issue 1, Jan. 2003: 1-16.

[40] National Energy Board (NEB), *Report of the Inquiry-Stress Corrosion Cracking on Canadian Oil and Gas Pipelines*, 1996.

# **Chapter 6      Crack Growth Behavior of a Pipeline Steel Exposed to a Near-Neutral pH Environment under Variable Pressure Fluctuations: the Role of Hydrogen**

## **6.1 Introduction**

Premature failures of many engineering components in the presence of hydrogen have been extensively studied [1]. Understanding the role of hydrogen in these failures could yield benefits to many industries, like material production [1], electroplating [2], oil/gas transmission [3,4] and hydrogen energy [5]. However, the related mechanisms, especially in steel, are still not fully understood, despite extensive researches for more than 100 years [6,7,8,9,10].

The shortened service lifetime or failures caused by hydrogen-assisted cracking have been macroscopically attributed to the degradation of mechanical properties, such as decreased ductility and fracture toughness (commonly known as hydrogen embrittlement, or HE). The occurrence of HE could be affected by many factors, including material factors such as chemical composition [11,12], phases [13], grain size [14], inclusions [15] and surface conditions [16]; mechanical loading conditions such as loading rate [17], pre-strain [17,18], and fatigue [11,19]; aggressive environments such as gaseous hydrogen

environments [11, 20 ], corrosive electrolytes [ 21 ], and cathodic potentials [ 22 ]. Contradictory results are often obtained by using different materials, or even using the same material but under different testing conditions. These contradictory observations result in debatable theories or micro-mechanisms.

Except for cracking caused by hydride formation [23], many micro-mechanisms have been proposed [24], and each is supported by some experimental observations. But none of the micro-mechanisms can explain all the experiment results [9]. Despite this, two of them seem widely accepted: the hydrogen enhanced decohesion (HEDE) micro-mechanism and the hydrogen enhanced localized plasticity (HELP) micro-mechanism.

The HEDE mechanism [25] assumes that lattice hydrogen reduces the bond strength of host atoms and may cause brittle fracture through the cleavage of crystallographic planes, especially at locations with high hydrogen concentrations. According to the micro-mechanism of HELP [26], the macroscopic observation of HE is a result of the highly localized deformation through ductile processes since the flow stress is reduced by the high concentration of hydrogen in the plastic zone ahead of the crack tip [27,28]. The enhanced dislocation mobility in the presence of hydrogen was supported by the in situ TEM (transmission electron microscope) examinations [9,29,30].

Understanding the micro-mechanisms of hydrogen in the cracking of pipeline steel externally exposed to near-neutral pH environments could yield benefits to the oil/gas transmission industry [4,22,31,32,33,34,35 36,37]. Atomic hydrogen is generated on a

pipe surface as a by-product of corrosion or as a result of cathodic reactions. Only a small fraction of the generated atomic hydrogen can enter into the lattice steel [35]. Once entered, the hydrogen may first get trapped in a variety of locations, such as dislocations, phase interfaces, grain boundaries, and stress raisers including corrosion pits and cracks. The other hydrogen atoms which remain in the lattice and are diffusible are often proposed to be responsible for the increased crack growth rate [1].

However, a clear physical process of HE in enhancing the crack growth of pipeline steels exposed to near-neutral pH environments remains to be determined. It is challenging to achieve a clear understanding of the process because of

- 1) The concurrent occurrence of corrosion and HE. Corrosion generates the hydrogen required for HE to occur; however, corrosion also destroys or covers up the evidence of HE on the fractured surface.
- 2) The uncertainty of the exact mechanism governing the HE between HELP and HEDE. HELP is related to the enhanced plasticity, which can yield two different effects: increased crack tip blunting caused by the enhanced plasticity and facilitated formation of microvoids, which can cause micro-failures through the ductile failure mechanism at the crack tip [38] or a quasi-cleavage process based on hydrogen-dislocation interaction. On the other hand, HEDE is related to the occurrence of micro-cleavage in the plastic zone, which is affected by 1) the level of hydrostatic stress (in case of plane strain) and 2) the level of hydrogen segregation at the weakest links located in the plastic zone, such as inclusions, grain boundaries, and phase

interfaces. Both of these two factors can also be explained by HELP micro-mechanism.

- 3) The influence of the stress state, that is, plane stress vs. plane strain. The direct evidence of HELP was identified in an in-situ transmission electron microscope (TEM) examination using extremely thin film samples with a plane stress state, while cracks in the bulk materials are primarily loaded in a plane strain state. The plane strain condition was found to be the most severe micromechanical condition for HE by studying single crystal materials [39]. But HE is microstructure sensitive [13,14,15].
- 4) The effect of loading conditions. The above mechanisms are usually established based on the experimental observations under static loading. In contrast, the cyclic loadings, typically variable amplitude cyclic loadings, are often encountered for structures in service. When cyclic loading (fatigue) is applied, which is itself a failure mechanism, micro-mechanisms governing HE become even more complicated. A lowered fatigue limit and enhanced fatigue crack growth rate have been observed in many steel that are either serviced in gaseous hydrogen environments or are in contact with aqueous electrolytes where atomic hydrogen is generated [11,19]. They have been explained on the basis of HELP, as morphological features of the fracture surface or dislocation slip bands on the surface are often altered in the presence of atomic hydrogen [26]. However, the correlation of such changes with enhanced fatigue crack growth or shortened fatigue life is often ambiguous.

Through an innovative experimental setup, this investigation was initiated to address all of the above challenges. Compact tension specimens were utilized and comparatively loaded in air and in corrosive near-neutral pH environments. For the latter environment, the specimen was pre-immersed in the environment for sufficient periods of time, allowing hydrogen equilibrium to be reached throughout the specimen with or without a direct exposure of the cracks to the test environments, so that the effects of hydrogen could be separated from those of corrosion. Variable amplitude cyclic loadings were applied to simulate the stress states of pipelines in service. It is believed that understanding the role of hydrogen in the cracking behavior in the current investigation will shed light on other materials suffering hydrogen effects.

## **6.2 Experimental**

### **6.2.1 Environment**

Samples were charged with hydrogen (open circuit potential) in a near-neutral pH solution, namely the C2 solution (0.0035 KCl, 0.0195 NaHCO<sub>3</sub>, 0.0255 CaCl<sub>2</sub>, 0.0274 MgSO<sub>4</sub>·7H<sub>2</sub>O, 0.0606 CaCO<sub>3</sub> g/l), to simulate one type of the electrolytes trapped within the coating disbondment on pipelines in the field, where stress cracking is observed. A gas mixture of 5% CO<sub>2</sub> balanced with nitrogen was purged through the C2 solution before and during the test to achieve a stable pH value of 6.29 [31]. The temperature of the solution and the environment during tests was controlled at a constant 30 ± 0.1°C

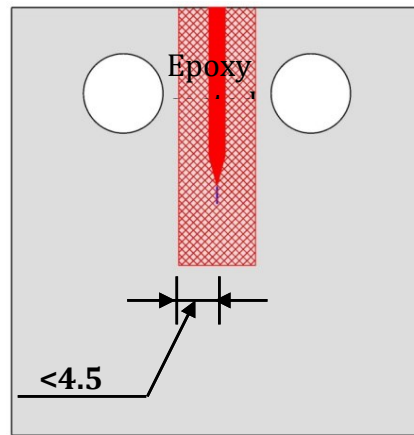
because the temperature could be controlled more accurately if it was above room temperature.

### **6.2.2 Specimen**

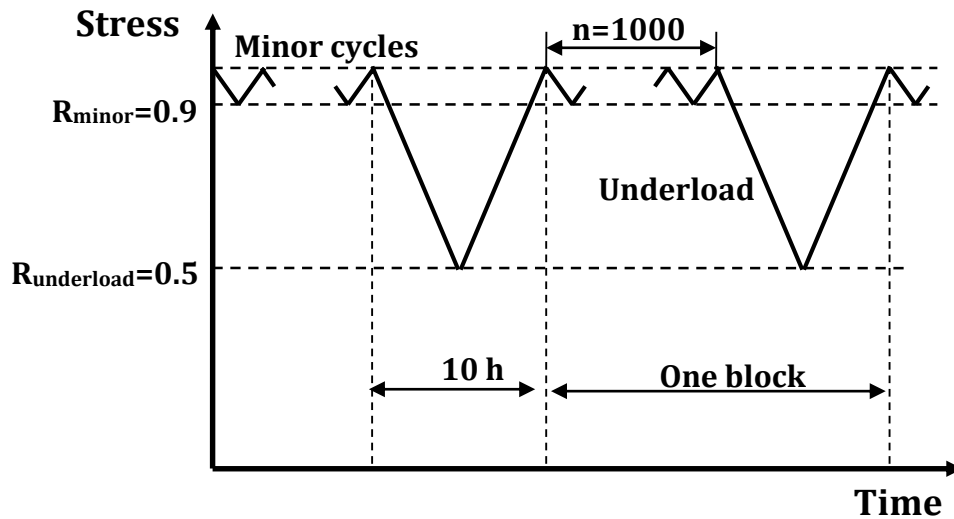
An X65 pipeline steel with a wall thickness of 12 mm was used in this study. Its chemical composition (wt.%) is as follows: C: 0.06, Mn: 1.43, P: 0.011, Si: 0.31, Ni: 0.063, Cr: 0.066, Mo: 0.020, Cu: 0.21, V: 0.034, Nb: 0.070, Ti: 0.014, Al: 0.025, Fe: Balance. Compact tension (CT) specimens with a thickness of  $9 \pm 0.2$  mm were machined. The notch in the CT specimens was orientated in a direction parallel to the pipe's longitudinal direction so that the path of crack growth was in the same direction as that of the longitudinal cracks found in the field. The CT specimens were ground to a 600 grit finish and then pre-cracked by fatigue in air to produce a sharp crack tip from the machined notch according to ASTM E647-08. The sharp crack was controlled to be between two and three mm long and the difference in crack length on either side of the specimen was less than 0.2 mm.

The specimen surface was partially coated according to the method introduced in Ref. [33]: the notch and crack region of the specimen surface were coated in such a way, as shown in Fig. 6.1(a), that only the hydrogen generated on the specimen surface by corrosion could diffuse into the crack tip through the steel lattice. This prevented a direct contact between the aqueous electrolyte and the crack. The distance between the edge of the coating strip and the center of the specimen was less than half of the thickness

(4.5 mm) of the specimen. These specimens were sealed in test cells and pre-exposed to C2 solution under a very low load (0.5 kN) for about 300 h, the time during which hydrogen equilibrium is believed to be achieved throughout the specimen (hydrogen diffusivity in steel of  $2 \times 10^{-7} \text{ cm}^2/\text{s}$  [40]).



(a)



(b)

**Figure 6.1** Experimental (a) surface treated compact tension specimen; and (b) variable amplitude waveform:  $K_{\text{max}} = 33 \text{ MPa}\sqrt{\text{m}}$ , R ratio of minor cycles = 0.9, R ratio of underload = 0.5, frequency of minor cycles = 0.00538 Hz, frequency of underload = 0.0000278 Hz (10 h/cycle), number of minor cycles per block  $n = 1000$

### 6.2.3 Mechanical loading conditions

An underload-type variable amplitude cyclic loading waveform, as shown in Fig. 6.1(b), was designed to simulate the actual pressure fluctuations during pipeline routine operations. It has been demonstrated that the fatigue crack growth rate under this loading scheme is higher than that under the corresponding constant amplitude fatigue loading [12,41,42]. The starting mechanical loading conditions are as follows: the maximum stress intensity factor,  $K_{\max} = 33 \text{ MPa}\sqrt{\text{m}}$  [34], R ratio (minimum stress/maximum stress) of minor cycles = 0.9, R ratio of underload = 0.5, frequency of minor cycles = 0.00538 Hz, frequency of underload = 0.0000278 Hz (10 h/cycle) [34], and number of minor cycles per block  $n = 1000$  [42]. Each test lasted 46 days (for a total of two months including the pre-exposure time of 300 h), during which 17 blocks were applied. This waveform was performed on a horizontal pneumatic loading machine with CT specimens pin-hole loaded.

After exposure to the C2 solution for about 300 h, one of the two surface-coated specimens was taken out of the test cell and immediately cleaned with acetone and ethanol. Its surface coating was removed and the bare sample was re-sealed into the test cell filled with a newly prepared C2 solution. The whole process was finished within 20 minutes to minimize the effusion of hydrogen. This procedure was adopted to ensure that the same crack tip conditions existed when the specimens were loaded. A bare specimen was also tested in air for the purpose of comparison.

Another surface-coated specimen was also prepared but with the number of minor cycles increased to 2000 cycles and a total of 11 blocks were executed. This later test was performed to validate the test conducted with the number of minor cycles set at 1000, and also to determine the effect of increasing the number of minor cycles.

#### **6.2.4 Observation of crack growth, widening and fracture surface**

Crack growth was determined using SEM to measure the crack length on the specimen surface before and after tests. The crack growth rate, expressed in millimeters per block, was calculated by dividing the measured crack growth length (the average of the two surfaces of one CT specimen) by the number of blocks applied. The bare specimen in solution was slightly polished before the measurement to remove the rough surface caused by the dissolution in the C2 solution.

The crack width was also measured at about 70  $\mu\text{m}$  behind the precrack tip. At least five spots on each surface were measured, and the average of the two surfaces was taken as the crack width of the sample.

Each specimen was sectioned along the middle plane in the thickness direction. One half was ground and polished to observe the crack morphologies in the middle plane on SEM using backscatter electron detector (BSD) (which can sharply show the cracks with high

contrast). The other half was fracture-opened in liquid nitrogen and the fracture surfaces were examined on SEM.

## **6.3 Results and Discussion**

### **6.3.1 Determination of crack growth rate**

The crack morphologies on the surface and in the middle plane of each specimen are shown in Fig. 6.2 (the bare sample tested in the C2 solution was lightly polished to produce a better view of the crack morphologies). The arrows in the image mark the position of pre-cracking tip.

As shown in Fig. 6.2(a), the crack growth was measured and the corresponding crack growth rate, in terms of millimeters per block, was calculated by dividing the net crack advance by the total number of blocks applied, as shown in Fig. 6.3(a). It can be seen that the crack growth rate for the coated specimen at  $n = 1000$  tested in the C2 solution was about twice that of the bare specimen in air, but it was almost the same as that of the bare specimen in the C2 solution (the coating was removed after pre-exposure).

The crack growth rate at  $n = 2000$  was found to be higher than that at  $n = 1000$ . This increase is found to be caused by the increase of minor cycles. Fig. 6.3(b) shows the dependence of the crack growth rate on the number of minor cycles. The data points with

solid black dots have been reported in Ref. [42], and were obtained from testing bare specimens in C2 solutions. The growth data of the partially coated specimens (the green data points) from this investigation fall into the same regression curve as those of bare specimens with increasing number of minor cycles. So did the bare specimen (the blue point). This further confirms the conclusion that it is the hydrogen, rather than the direct dissolution of the crack tip, that dictates the crack growth of pipeline steel in the corrosive near-neutral pH environments [32,41,42].

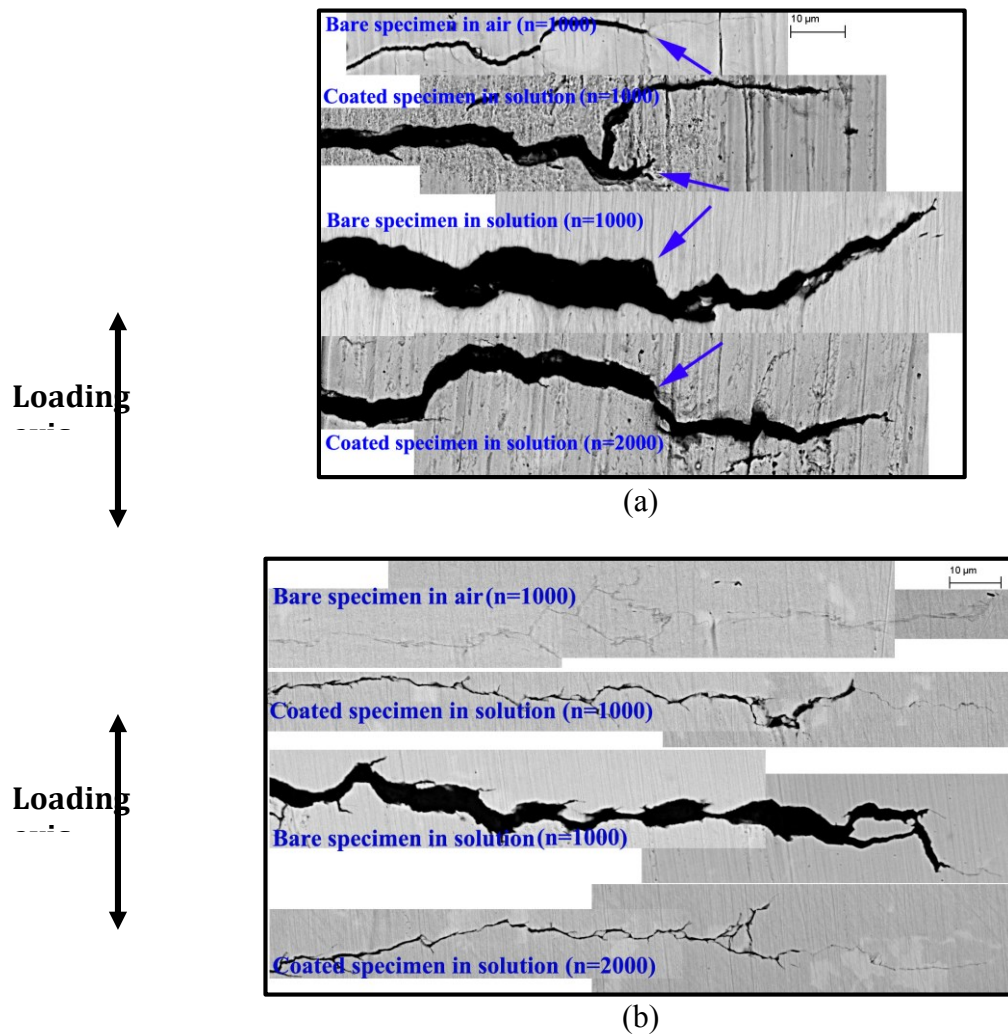
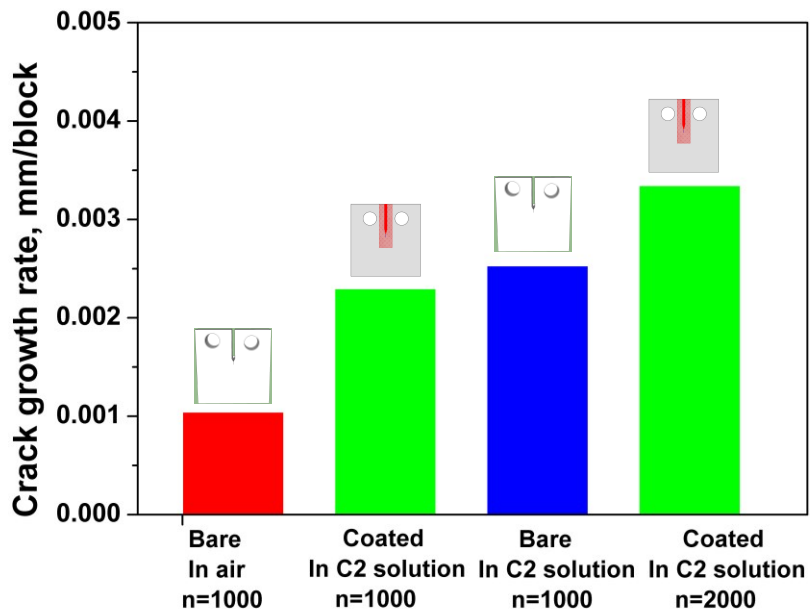
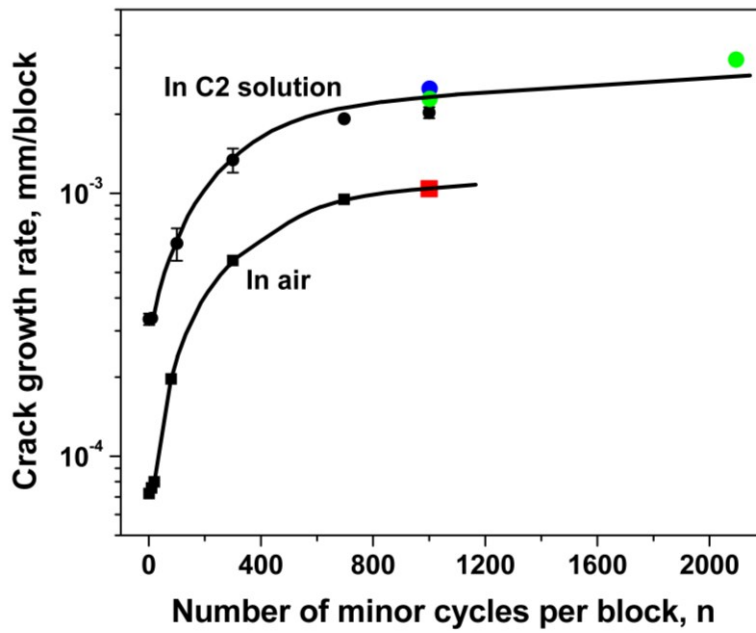


**Figure 6.2 SEM images (BSD) of crack morphologies of specimens after tests (crack propagation from left to right): a) on surface (the arrow marks the pre-cracking tip before loading); and b) in the middle**

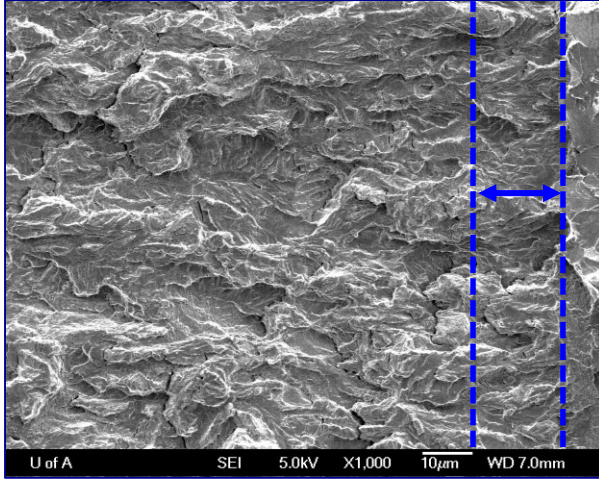


(a)

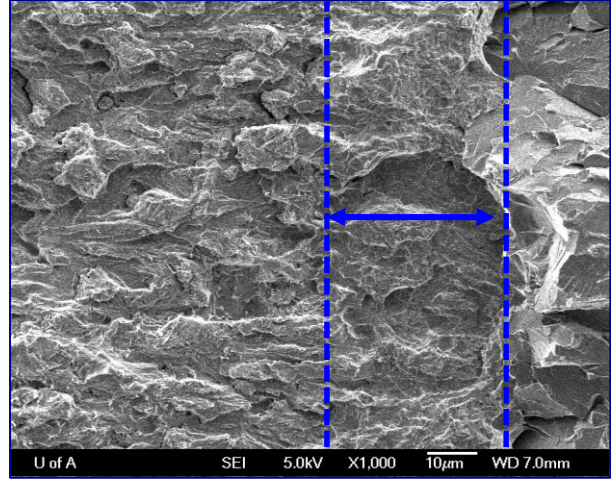


(b)

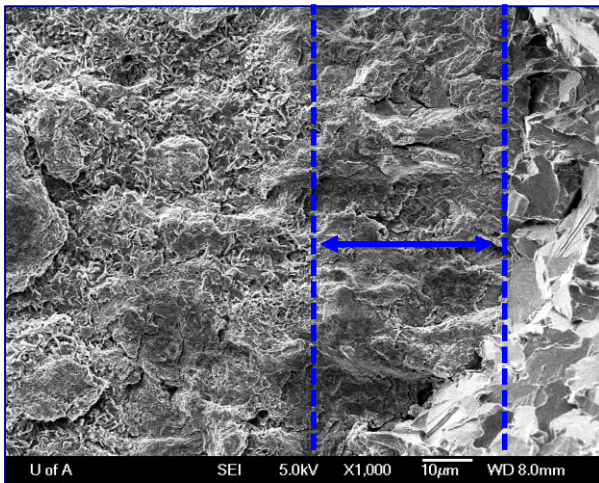
Figure 6.3 (a) Measured crack growth rate; and (b) effects of number of minor cycles on crack growth rate in C2 solution and in air [42]. The data in the current investigation were shown as colored dots.



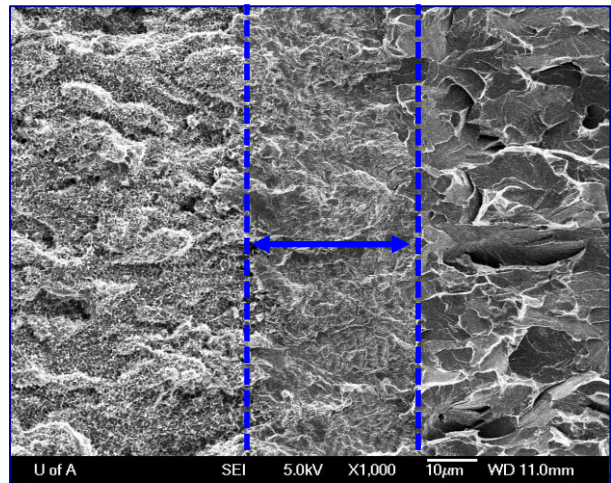
(a) Bare specimen in air, n=1000



(b) Coated specimen in solution, n=1000



(c) Bare specimen in solution, n=1000



(d) Coated specimen in solution, n=2000

**Figure 6.4 Fracture surface images (SE) in the middle (crack propagation). The marked zone is the crack growth (from left to right) during the test. Eleven blocks were applied to the coated specimen in solution at n = 2000, while 17 blocks were performed for others.**

Since the position of the pre-cracking tip in the middle plane of the specimen is unknown in Fig. 6.2(b), the crack growth rate in the middle plane was determined based on the

morphologies on the fractured surface opened in liquid nitrogen. As shown in Fig. 6.4, the crack advancement (the marked zone) was found to be consistent with that measured from the surface, which suggests that the crack growth was not affected by the stress state: that is, plane stress on the surface and plane strain in the middle. This seems inconsistent with the conclusion drawn in Ref. [39] on the study of a Fe-Si single crystal.

It should be noted that the surface surrounding the pre-cracking tip of the partially coated specimen tested at the  $n = 1000$  cycle was slightly corroded as shown in Fig. 6.2(a). However, no corrosion was observed on the surface for the partially coated specimen tested at  $n = 2000$  cycles. Corrosion products were observed on the fracture surface for the partially coated specimens as shown in Fig. 6.4. These products were probably caused by moistures trapped in the crack crevice. However, the fact that there is a much narrower crack crevice in the middle plane in Fig. 6.2(b) suggests the negligible influence of the corrosion. The implication of different crack crevices observed is further discussed in the following section.

### **6.3.2 Characterization of crack width**

Significant variations in the width of the crack crevice are found, as shown in Fig. 6.2.

Major observations are summarized as follows:

- 1) The bare specimen exposed in the C2 solution shows the largest crack crevice compared with that of other specimens. The crack crevice in the middle plane is much narrower than the corresponding surface crack width.
- 2) It is surprising that the crack crevice at the surface of the partially coated specimens in solution is wider than that in air. It is even more surprising that the crack crevice in the middle plane of these two specimens is very narrow, although it is slightly wider than that of specimen tested in air. The possible reason, due to corrosion, has been excluded, as stated above.
- 3) The specimen tested in air has a much narrower crack crevice at the surface than other specimens, but its crevice on surface is slightly wider than that in its own middle plane.

To further understand the mechanisms governing the widening of the crack crevice, the crack width at the position about 70  $\mu\text{m}$  behind the pre-cracking tip was measured and compared in Fig. 6.5. It is obvious that the width of the crack crevice can be related to the following factors:

- 1) Direct corrosion: This explains the wider crack crevice of the bare specimen tested in solution, as compared with the partially coated specimens. The crack crevice in the middle plane, which is narrower than that on the surface, is related to the reduced corrosion rate inside the crack crevice, which is a unique phenomenon for the corrosion of pipeline steel in near-neutral pH environments [43] and is also

responsible for the occurrence of crack dormancy in crack depth direction commonly found in crack colonies in the field [37].

- 2) Stress state (plane stress vs. plane strain)-dependent mechanical blunting: It is well accepted that the crack tip at the surface is in plane stress, while that in the middle plane is in plane strain. This can explain why a slightly wider crack crevice is found at the surface than that in the middle for the specimen tested in air (without hydrogen or corrosion). However, as shown in Fig. 6.2, the very narrow crack crevice tested in air, compared with that tested in solution, indicates that blunting due to mechanical loading alone is very limited.
- 3) Crack closure [44]: It might occur and contribute to crack widening in the presence of corrosion products within the crack crevice. However, it is usually observed during cyclic loading with small R ratios, for example, lower than 0.5-0.6 for steel. In the current investigation, the overwhelming periods of time are minor cycles with an R ratio of 0.9. In addition, the crack closure model could not explain some cracking behaviors observed in Ref. [42]. Even if crack closure occurs, its extent should be larger than that tested in air, resulting in the lower effective stress intensity factor range and thus lower crack growth rate, which contradicts to the observations in Fig. 6.3 (a).
- 4) The effect of hydrogen: Because of the lack of corrosion and the same stress intensity factor applied as in air, the above attributing factors cannot explain the wider crack crevice at the surface in the partially coated specimens. Therefore, the wider crack crevice on the surface of the partially coated specimens can only be attributed to the

higher plastic deformation in the plastic zone. Naturally, the micro-mechanism of HELP is considered.

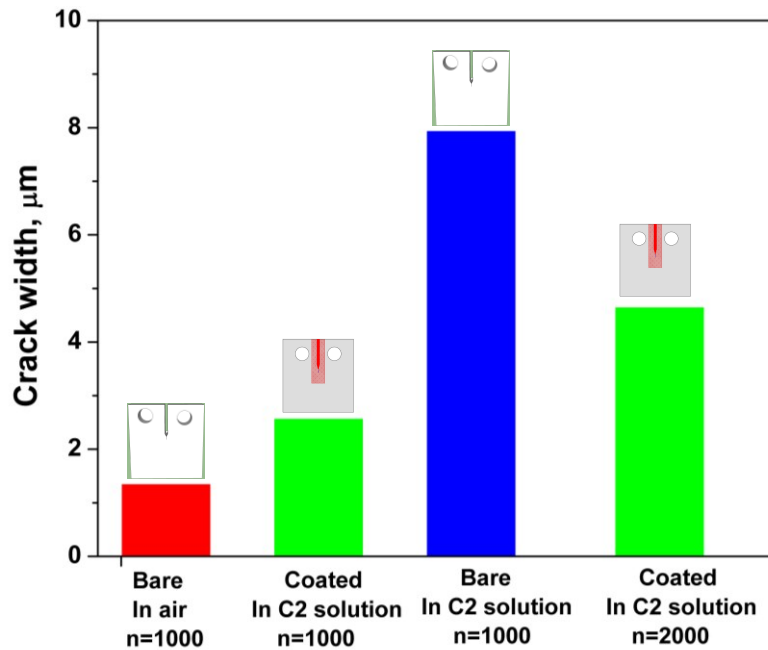


**Figure 6.5 Measured crack width behind pre-cracking tip**

The degree of crack tip blunting can be increased if the steel has lower resistance to plastic deformation, which can be manifested in three ways: lower yield strength, lower strain hardening rate, and lower strain to the tensile strength or necking. Fig. 6.6 compares the stress–strain curves of an X70 pipeline steel with and without hydrogen charging [45]. The three manifestations can be clearly seen in the presence of hydrogen.

It may be argued that the decrease of yield strength caused by the presence of hydrogen is limited as shown in Fig. 6.6. However, the increase in plastic deformation caused by the

presence of hydrogen could be very large at high stress in the work-hardening state, especially close to tensile strength. Such high stress could be achieved in the plastic zone ahead of the crack tip. Moreover, the hydrogen concentration ahead of the crack tip could be much higher than the bulk concentration because of the high plastic deformation and high hydrostatic stress, and thus the dislocation mobility could be significantly enhanced [46]. These result in the higher plastic deformation in the plastic zone, and thus a wider crack crevice.

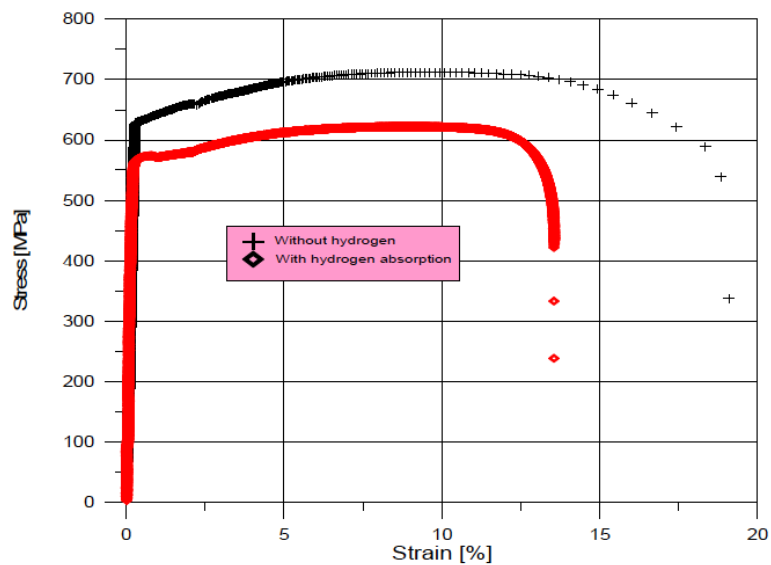


**Figure 6.6 Comparison of stress-strain curves of an X70 pipeline steel with and without hydrogen charging [45]**

Although plane stress facilitates plastic deformation while plane strain restricts in fracture mechanics, the observation that the crack crevice in the middle was not widened at all suggests that HELP prevails in plane stress conditions, rather than in plane strain

conditions. This is also consistent with many other HELP observations, especially observations made regarding the in-situ TEM film sample [29].

This could also explain the wider crack crevice at  $n = 2000$  than at  $n = 1000$ : the higher concentration of hydrogen could segregate in the plastic zone at  $n = 2000$ , and thus cause the higher magnitude of plastic deformation and the wider crack crevice.

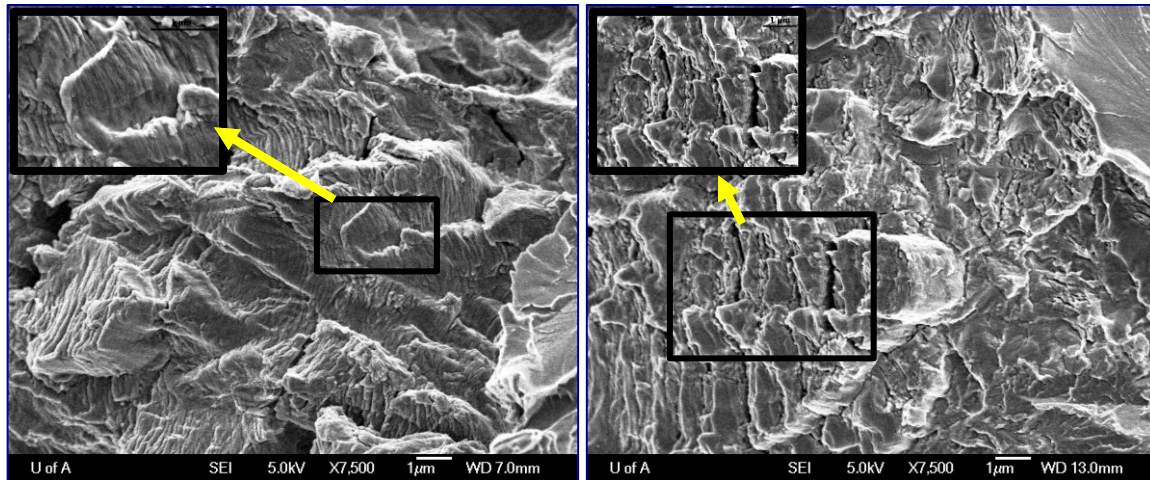
On the other hand, the observation that the crack was widened by the presence of hydrogen does not support HEDE mechanism since the reduced bond strength can not be related to the larger plastic deformation in the presence of hydrogen. But from point view of crack propagation, both mechanisms can be explained, however, from the point of view of crack propagation, as will be discussed in the next section.

### **6.3.3 Fracture surface observation**

The fractured surface in the middle section of specimens shown in Fig. 6.4 was further examined and is shown in Fig. 6.7. It can be seen that striations were observed on the entire surface for the bare specimen tested in air as shown in Fig. 6.7(a), which confirms that the crack advancement is caused by the mechanism of fatigue alone. On the other hand, the fractured surface of the partially coated specimen exhibits a combination of quasi-cleavage (flat parts) and striations that are alternatively arranged. This progressive advancement is seen on both the partially coated specimens tested at  $n = 1000$  and  $n = 2000$ , respectively, as shown in Fig. 6.7(b) and 6.7(d). For the bare specimen in solution,

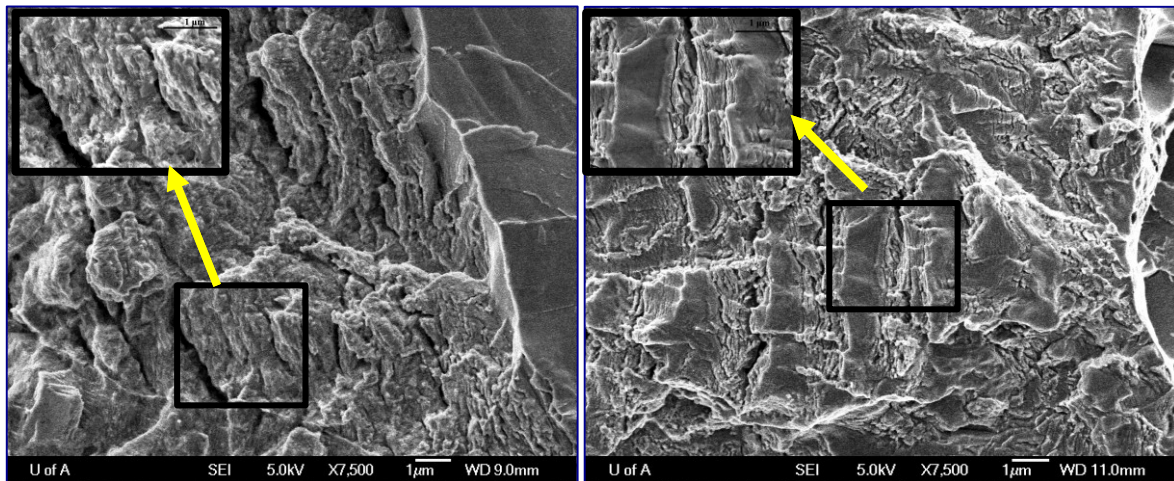
the morphology on the fracture surface appears similar, but could not be viewed clearly because of corrosion, as shown in Fig. 6.7(c).

To understand the process of crack propagation, the topography of the fractured surface of the coated specimen at  $n=2000$  was further examined. As shown in Fig. 6.8, the fractured surface was tilted or rotated to different angles. The area in the blue frame shows the same feature after rotation or tilting. It can be seen that the flat feature is about one micron wide and is separated by regions with striations, indicating the sequential occurrence of striations and flat feature, which is further illustrated in Fig. 6.9. The formed topography looks like the “fish ladder” in a dam. The ladder in Fig. 6.9 is drawn in an upward position to reflect the localized Zigzag path of propagation, although the fatigue crack propagates macroscopically in a direction perpendicular to the loading axis.



(a) Bare specimen in air,

(b) Coated specimen in solution,



(c) Bare specimen in solution,

(d) Coated specimen in solution,

**Figure 6.7** Fracture surface images near the crack tip after tests (crack propagation from left to right). The insert is a magnified view of the fracture surface. Quasi-cleavage can be seen in the coated specimens.

One may ask, when was the quasi-cleavage formed, during underload or during minor cycles of the waveform in Fig. 6.1(b)? And by what mechanism did such a “fish ladder” form?

For the first question, it has been demonstrated that underload could not only cause crack propagation by itself, but it could also accelerate/initiate the crack growth of the following minor cycles. Increasing the number of minor cycles,  $n$ , caused the crack growth rate to increase and the crack advanced through the synergistic interactions of hydrogen and fatigue; with further increasing  $n$ , the crack growth rate reached a saturation state as shown in Fig. 6.3(b), and the corresponding growth rate of minor cycles decreased to close to zero [42]. On the other hand, hydrogen could continuously segregate in the plastic zone ahead of the crack tip under such high R ratio cyclic loadings. This suggests that a limited crack growth rate and continuous hydrogen segregation favor the occurrence of quasi-cleavage during the minor cyclic loadings. This could also explain why the quasi-cleavage for  $n = 2000$  is wider than that for  $n = 1000$ : the more cycles, the more time for hydrogen segregation.

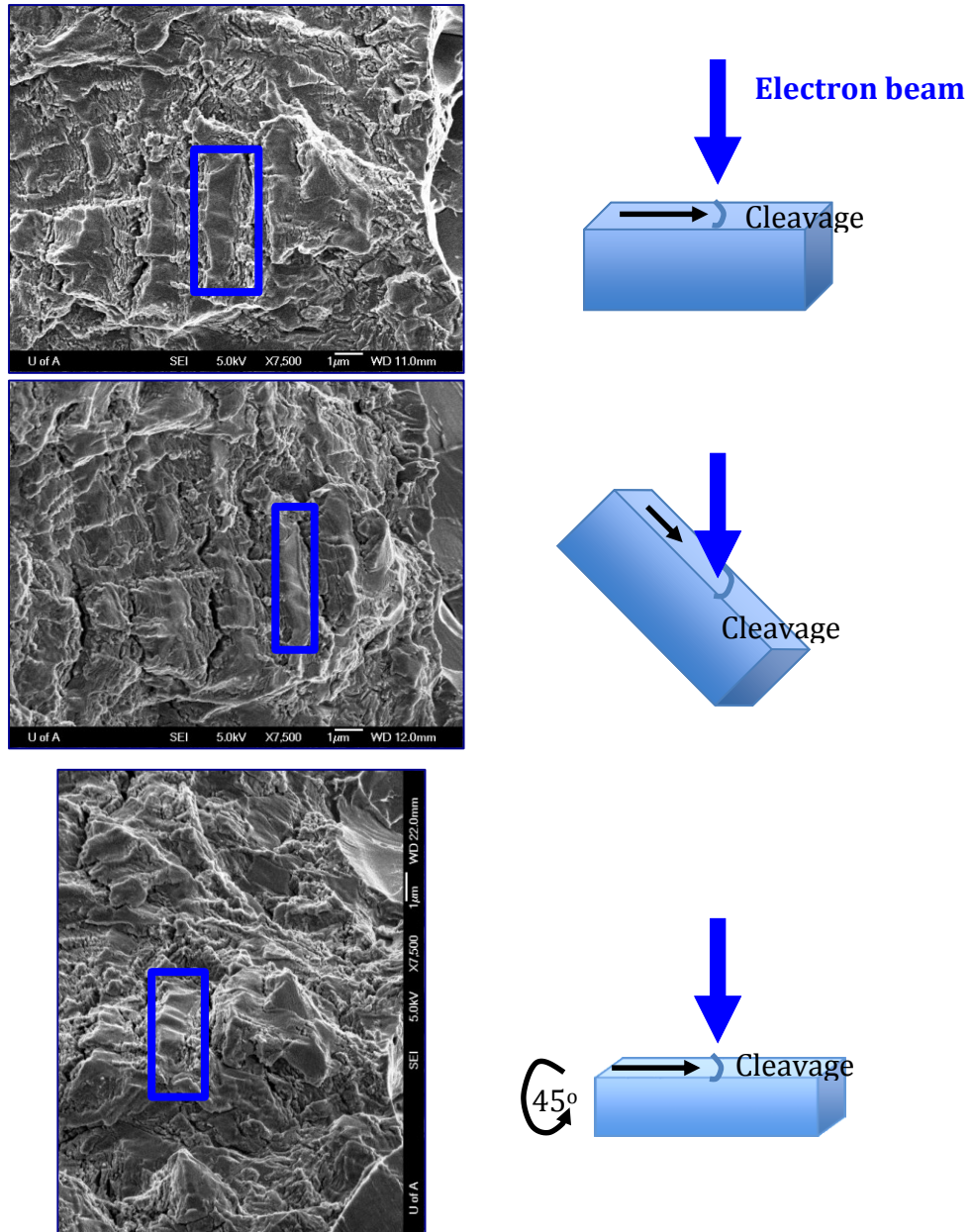


**Figure 6.8** Observation of fractured surface in Figure 6 (d) at different orientations (SE) The blue square is the reference (the same area) at difference orientations.

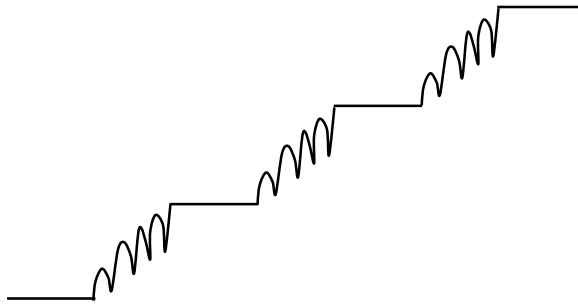


**Figure 6.9** Illustration showing the “fish ladder” formation during crack propagation (from left to right)

For the micro-mechanisms, both HELP and HEDE could explain this. For HEDE, the decreased growth rate and the atomic bond strength favor the hydrogen sampling process during minor cyclic loadings, resulting in the occurrence of quasi-cleavage at the weakest links when the applied stress exceeds the cohesive stress. For HELP, in the regions of high hydrogen concentration, the resistance to dislocation motion and thus flow stress is decreased and dislocation moves at stresses well below those that are required for plastic deformation. Because of the localized slip, the crack propagates along the slip plane [26].

HEDE and HELP cannot be differentiated by the presence of quasi-cleavage. However, as discussed in the previous section, HELP is supported by the widened crack crevice, because the crack is the same for either crack growth or crack widening. For this reason, HELP is believed to be the micro-mechanism governing the cracking behavior in near-neutral pH environments.

In addition, HELP also echoes the synergistic interactions of hydrogen and cyclic loadings [11,19,34]. As has been well demonstrated, fatigue fundamentally results from the localized dislocation irreversible slip [47]. The enhanced dislocation mobility and/or lowered flow stress caused by the presence of hydrogen (HELP) can facilitate the dislocation irreversible slips during cyclic loadings, resulting in more point defects [17] and thus an enhanced fatigue crack growth rate.

#### **6.3.4 Process of crack propagation in near-neutral pH environments**

Based on the understanding of the role of hydrogen on the cracking behaviors under cyclic loading, the crack propagation process can be schematically illustrated by Fig. 6.10.

- 1) The sharp crack tip generated from the pre-cracking can be blunted due to the plastic deformation in the plastic zone ahead of the crack tip by applying mechanical loads. This plastic deformation might be further increased due to room temperature creep [32]. But the blunting extent was not high, as shown in Figs. 6.2 and 6.5. And the crack tip sharpness in the middle of the specimen under plane strain condition is not affected at all, as shown in Fig. 6.2. In addition, the fact that the crack growth rate is not affected by the stress states also indicates that the mechanical loads alone have a limited effect on blunting.
- 2) The hydrogen generated on the pipe surface would enter the steel lattice and diffuse into the high stress zone ahead of the crack tip to lower the chemical potential. Because of HELP, the localized flow stress is reduced and dislocation

- mobility is enhanced by the presence of hydrogen, resulting in more plastic deformation in the plastic zone, which contributes to blunting the crack tip.
- 3) Once the crack walls are opened by mechanical loading and/or HELP, the crack walls and tip will be exposed to the corrosive near-neutral pH solution, as no passive film is formed [36]. Dissolution to crack tip and crack walls further blunts the crack tip.
  - 4) When the tip is blunted, the location of highest hydrostatic stress is lowered and shifted away from the crack tip, which favors the hydrogen sampling process. Through HELP, a micro-crack may be formed ahead of the main crack tip.
  - 5) Once the micro-crack joints back to the main crack, a crack propagates. The newly formed sharp crack tip will repeat the whole process again. The stress ahead of the sharp crack tip is enhanced.
  - 6) The crack propagation rate is the same under plane stress and plane strain conditions as the crack advancement (the marked zone) in Fig. 6.4 was found to be consistent with that measured from the surface.

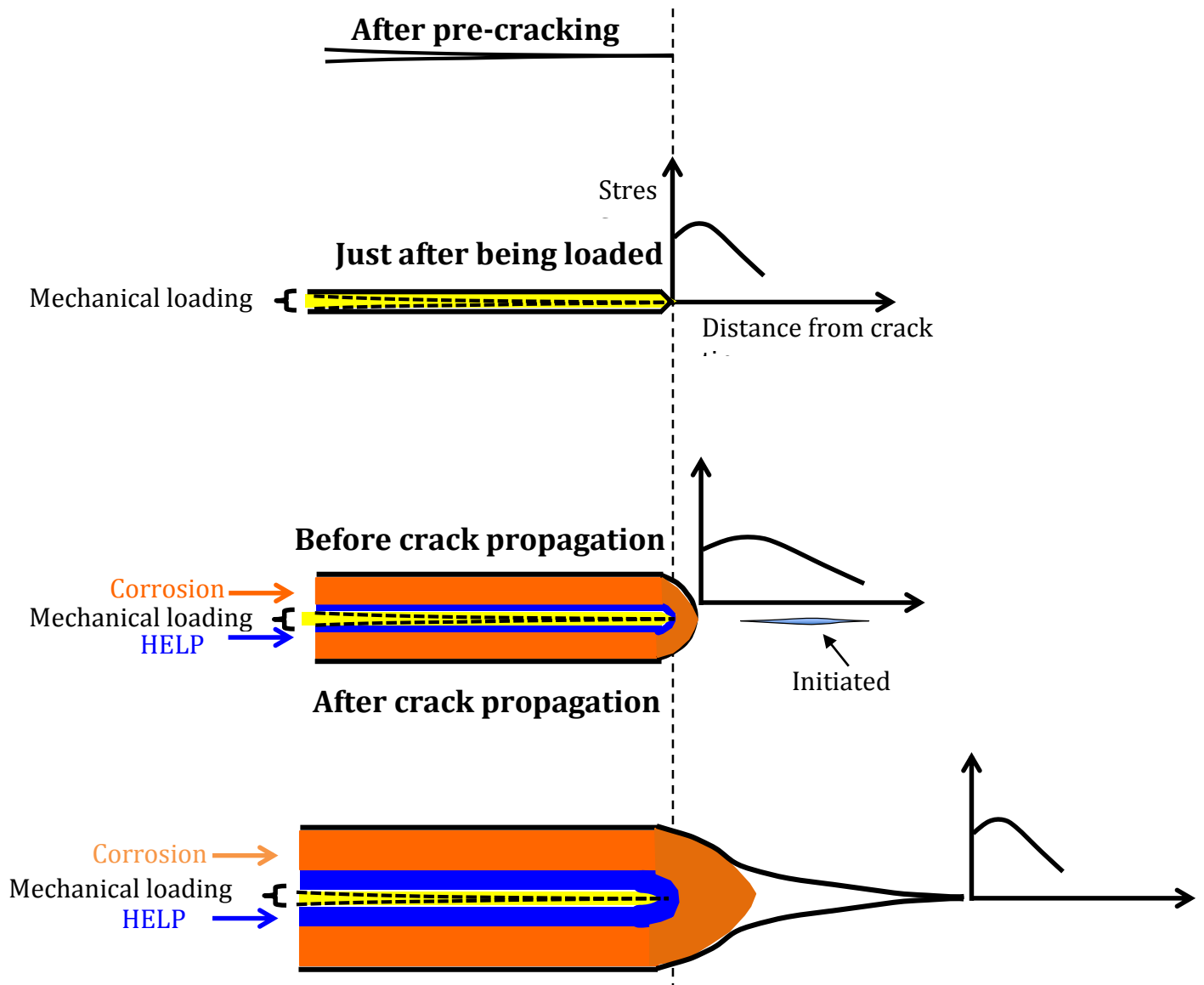


**Figure 6.10** Illustration showing the crack widening behind the pre-cracking tip due to mechanical loading, HELP and corrosion during the corrosion fatigue test

Based on this, the corrosion rate can be calculated by measuring the crack width, which can be expressed as:

$$\text{Corrosion rate} = \frac{1}{2} \times \frac{\text{crack width in solution} - \text{crack width in air} - \text{HELP}}{\text{test duration}} \quad (6 - 1)$$

The subtraction is intended to remove the crack widening by mechanical loading and HELP. Since both sides of the crack walls were corroded simultaneously, a factor of 1/2 was applied to Eq. (6-1). This calculation should give the accurate corrosion rate inside of crack crevice. However, because the magnitude of the HELP effect and the corresponding crack width in air are not known for many previous tests, it is still possible to estimate the corrosion rate from the crack width in the middle, which is caused only by dissolution, as demonstrated in Fig. 6.2:

$$\text{Corrosion rate} = \frac{1}{2} \times \frac{\text{crack width in solution}}{\text{test duration}} \quad (6 - 2)$$

From previous related tests with periods longer than 30 days [34,41,42], the corrosion rate was shown in Fig. 6.11. It can be seen that the corrosion rate is much lower than the field crack growth rate data [48], which also confirms that in near-neutral pH environments, it is the hydrogen effect, rather than corrosion, that contributes to crack growth.

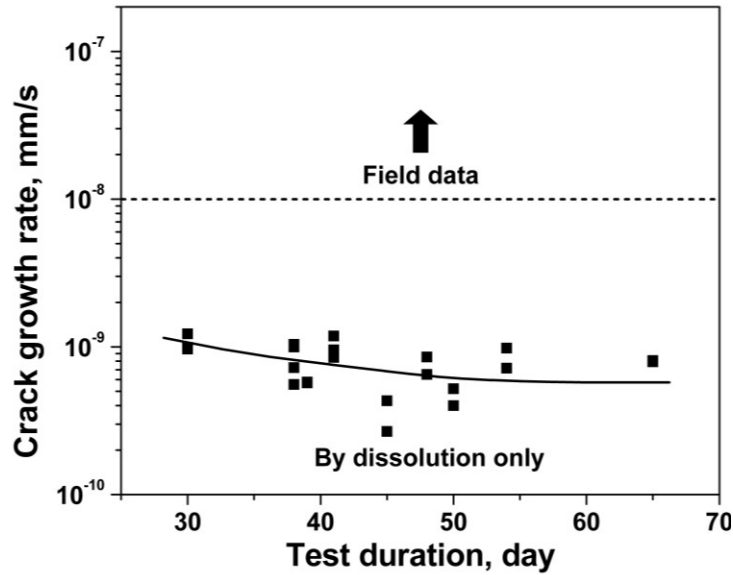


**Figure 6.11 Comparison of the crack growth rate and corrosion rate in near-neutral pH solutions under variety of loading conditions**

## 6.4 Conclusions

A comparative study was performed on X65 pipeline steel under variable amplitude fatigue in different environments. Surface coating was applied to the notch and crack regions of the CT specimen to prevent corrosion but allow hydrogen to diffuse into the bulk material. Major findings are as follows:

- 1) The crack growth rate for the coated and bare specimens in a near-neutral pH solution was the same, but higher than that in air. These findings echo the conclusion that in near-neutral pH environments, it is the hydrogen that

- contributes to crack growth, rather than the direct dissolution of the crack tip. This is further confirmed by the calculated corrosion rate.
- 2) The fractured surface was featured with striations and the quasi-cleavage fracture alternatively arranged, and the crack growth rate was not affected by stress states, which could be explained by both HELP and HEDE.
  - 3) The crack width on the surface was found to be widened by the presence of hydrogen, which can only be explained by HELP. Thus it is believed that HELP governs the cracking behavior of pipeline steels in near-neutral pH environments. The fact that the crack width was not widened under the plane strain state suggests that HELP prevails in the plane stress state.
  - 4) Based on the understanding of the micro-mechanisms of hydrogen in cracking behavior, the process of crack propagation in near-neutral pH environments was illustrated.

## References

- [1] L. Raymond. Hydrogen Embrittlement: Prevention and Control, ASTM STP 962, L. Raymond, Ed., American Society for Testing and Materials, Philadelphia, 1988, pp. 10-16.
- [2] M.A.V. Devanathan, Z. Stachurski, W. J. Beck. Electrochem. Soc. 1963 Vol. 110, Issue 8, 886-890.
- [3] D. Hardie, E.A. Charles, A.H. Lopez. Corrosion Sci. 48 (2006) 4378-4385.
- [4] R. L. Eadie, K.E. Szklarz, R. L. Suthery. Corrosion 61 (2) (2005) 167-173.

- [5] J.L. Gillette, R.L. Kolpa. ANL/EVS/TM/08-2, November 2007.
- [6] W.H. Johnson. Proc. R. Soc. London. 23 (1875) 168–179.
- [7] R.P. Gangloff, R.P. Wei. Met. Trans. A 8 (1977) 1043-1053.
- [8] R. A. Oriani. Ann. Rev. Mater. Sci. 1978.8:327-357.
- [9] J.P. Hirth, R.F. Mehl Medalist. Met. Trans. A 11A (1980) 861-890.
- [10] A. Nagao, C.D. Smith, M. Dadfarnia, P. Sofronis, I.M. Robertson. Acta Mater. 60 (2012) 5182-5189.
- [11] S. Ohmiya, H. Fujii. ISIJ Int. 52 (2) (2012) 247-254.
- [12] J. Zhao, Z. Jiang, C.S. Lee. Corrosion Sci. 82 (2014) 380-391.
- [13] V. Venegas, F. Caleyo, T. Baudin, J.H. Espina-Hernández, J.M. Hallen. Corrosion Sci. 53 (2011) 4204-4212.
- [14] S. Chen, M. Zhao, L. Rong. Mater. Sci. Eng. A 594 (2014) 98-102.
- [15] O.M.I. Todoshchenko, Y. Yagodzinsky, T. Saukkonen, H. Hänninen. Metall. Mater. Trans. A 45 (11) (2014) 4742-4747.
- [16] O. Takakuwa, T. Ohmi, M. Nishikawa, A. Toshimitsu Yokobori Jr. and H. Soyama. Strength, Fract. Complexity 7 (2011) 79-85.
- [17] T. Doshida, M. Nakamura, H. Saito, T. Sawada, K. Takai. Acta Mater. 61 (2013) 7755-7766.
- [18] K. Takai, H. Shoda, H. Suzuki, M. Nagumo. Acta Mater. 56 (2008) 5158-5167.
- [19] Y. Murakami. Advances in Fracture Research. 2006, p.167-195.
- [20] Z. Sun, C. Moriconi, G. Benoit, D. Halm, G. Henaff. Metall. Mater. Trans. A 44(3)(2013) 1320-1330.

- [21] J.J. DeLuccia. Hydrogen Embrittlement: Prevention and Control, ASTM STP 962, L. Raymond, Ed., American Society for Testing and Materials, Philadelphia, 1988, pp. 17-34.
- [22] C. Dong, Z. Liu, X. Li, Y. Cheng. *Int. J. Hydrogen Energy* 34 (2009) 9879-9884.
- [23] H.D. Fleming, R. G. Ide. *Analytica Chimica Acta*. 83 (1976) 67-82.
- [24] M.R. Louthan Jr. *J. Fail. Anal. And Preven.* (2008) 8:289-307.
- [25] A. Troiano, *Trans. ASM* 52 (1960) 147-157.
- [26] H. Birnbaum, P. Sofronis. *Mater. Sci. Eng. A* 176 (1994) 191–202.
- [27] R.A. Vennett, G.S. Ansell. *Trans. Am. Soc. Met.* 60 (1967) 242-251.
- [28] Z.T. Liu, X.G. Li, Y.F. Cheng. *Corrosion Science* 55 (2012) 54-60.
- [29] I.M. Robertson, H.K. Birnbaum, P. Sofronis. *Dislocations in Solids*, J.P. Hirth and L. Kubin Ed. 15 (2009) 249–293.
- [30] S. Wang, M.L. Martin, P. Sofronis, S. Ohnuki, N. Hashimoto, I.M. Robertson. *Acta Mater.* 69 (2014) 275-282.
- [31] W. Chen, R.L. Sutherby. *Met. Mater. Trans. A* 38A(2007) 1260-1268.
- [32] W. Chen, R. Kania, R. Worthingham, G. Boven. *Acta Mater.* 57 (2009) 6200-6214.
- [33] Y. Kang, W. Chen, R. Kania, G. Boven, R. Worthingham. *Corrosion Sci.* 53 (3) (2011) 968-975.
- [34] M. Yu, X. Xing, H. Zhang, J. Zhao, R. Eadie, W. Chen, J. Been, G.V. Boven, R. Kania. *Acta Materialia* (under review).
- [35] W. Chen, F. King, T.R. Jack, M.J. Wilmott. Hydrogen permeation behavior of X-

70 pipeline steel in a near-neutral pH soil environment. In: Proc. of the International Pipeline Conference, pp. 953-960. 2000.

[36] B.S. Delanty, J.O. Beirne. Major Field Study Compares Pipeline SCC with Coatings. Oil & Gas Journal 1992;15;39.

[37] W. Chen, F. King, and E. Vokes. Corrosion 2002;58(3):267-275 .

[38] T. Neeraj, R. Srinivasan, Ju Li. Acta Materialia 60 (2012) 5160–5171.

[39] X. Chen, T. Foecke, M. Lii, Y. Katz, W.W. Gerberich. Engineering Fracture Mechanics. Vol. 35, No. 6, pp. 997-1017, 1990.

[40] E. Hörnlund, J.K.T. Fossen, S. Hauger, C. Haugen, T. Havn, T. Hemmingsen. Int. J. Electrochem. Sci. 2 (1) (2007) 82-92.

[41] M. Yu, W. Chen, R. Kania, G.V. Boven, J. Been. In: Proc. of the 10th International Pipeline Conference (IPC2014), Sept. 29- Oct. 3, 2014, Calgary, Canada. Paper No. IPC2014-33282.

[42] M. Yu, W. Chen, R. Kania, G.V. Boven, J. Been. Fatigue. Fract. Eng. Mater. Struct.; in press. DOI: 10.1111/ffe.12274.

[43] K. Chevill, W. Chen, G.V. Boven, R. Kania, J. Been. In: proceedings of IPC 2014, 10th International Pipeline conference, Sept. 29 – Oct. 3, 2014, Calgary, Alberta, Canada. Paper No.: IPC2014-33678.

[44] W. Elber. ASTM STP-486, ASTM, PA, 1970, p.230.

[45] T. Bellahcene, J. Capelle, M. Aberkane, Z. Azari. Effect of hydrogen on mechanical properties of pipeline API 5L X70 steel. Applied Mechanics and Materials, Vol. 146 (2012) pp. 213-225.

- [46] Afolabi Taiwo Egbewande. Growth behaviour of surface cracks in pipeline steel exposed to near-neutral pH environments. PhD thesis, Fall 2013, University of Alberta. Chapter 6.
- [47] S. Suresh. Fatigue of Materials. Cambridge University Press: Cambridge, New York Port Chester, Melbourne Sydney, 1991; 113.
- [48] K. Chevil, et al. In: proceedings of IPC 2012, 9th International Pipeline conference, Sept. 24-28, 2012, Calgary, Alberta, Canada. Paper No.: IPC2012-90675, pp: 583-590.

# **Chapter 7      Conclusions, research impact and recommendations**

## **7.1 Conclusions**

The objective of this thesis was to shed light on understanding the crack propagation of pipeline steels exposed to a near-neutral pH environments under pressure fluctuations. In this regard, a novel waveform, the underload-type variable amplitude cyclic loadings, was designed to simulate the actual pressure fluctuations during routine pipeline operations. By comparatively performing this waveform both in air and in the near-neutral pH environment, different aspects of near-neutral pH crack propagation were investigated. The acceleration effect caused by this variable amplitude waveform was first demonstrated in Chapter 2, by comparing the crack growth rate under different kinds of waveforms. Based on the results, several parameters of this waveform were studied systematically both in air and in near-neutral pH environments, including the effect of the number of minor cycles, loading frequency, the maximum stress and amplitudes, which were covered in Chapters 3-5. It is found that the contribution of near-neutral pH environments to crack growth was mainly through the hydrogen effect. Therefore, the effects of hydrogen on the cracking behavior were investigated in detail in Chapter 6. The main conclusions obtained from these studies are summarized below.

### **7.1.1 Observation of acceleration effect**

The minor cycles with a very high R-ratio of 0.9, which have previously been considered to be non-propagating based on a constant amplitude crack growth model, can cause a significant crack advance in the presence of an underload with an R-ratio of 0.5 in a near-neutral pH solution. Such variable amplitude growth rate in terms of millimeters per block is about five times higher of that of the corresponding constant amplitude testing, and seven times of that of the static hold and underload. The mini-striations observed on the fractured surface are the direct evidence of the crack growth induced by the minor cycles.

### **7.1.2 Effects of number of minor cycles on crack growth**

1. Compared to the crack growth rate at constant amplitude, the crack growth rate at the variable amplitude waveform can be increased by a factor of three and five, respectively, in air and in the C2 solution.
2. Under the same loading conditions, the crack growth rate in the C2 solution was up to four times higher than that in air.
3. The crack growth during minor cycles loading after the introduction of an underload cycle can be divided into three stages: (1) the initial incubation stage up to 15 cycles, where acceleration of crack growth is not observed; (2) the subsequent stage up to 55 cycles, where the crack growth rate increases by increasing the number of minor cycles; and (3) the final stage up to 960 cycles

depending on the test environments, where crack growth rate of minor cycles decreases with further increasing number of minor cycles to a level at which acceleration effects disappear.

### **7.1.3 Effects of frequency and maximum stress on crack growth**

1. Compared with the crack growth rate under constant amplitude cyclic loading, the underload-type variable amplitude cyclic loading accelerates the crack growth rate by a factor of up to 10 at variety of loading frequencies.
2. Crack growth rates measured in air were found to be insensitive to the variation of loading frequency and  $K_{\max}$ , while these two parameters significantly affected the crack growth rate in the near-neutral pH solution.
3. Two distinct regimes of crack growth behavior exist over the range of loading frequency studied. The crack growth rate was found to increase with decreasing loading frequency up to  $10^{-3}$  Hz, while it either remained constant for underload-type variable amplitude cyclic loadings, or decreased slightly for constant amplitude loading when the loading frequency was lower than  $10^{-3}$  Hz. A mechanistic model established based on the hydrogen-assisted crack growth mechanisms successfully predicted the transition of crack growth behavior at about  $10^{-3}$  Hz.

### **7.1.4 Effects of amplitudes of underload and minor cycles on crack growth**

1. The acceleration factor was up to 2.7 and 5.3 for tests in air and in the C2 solution, respectively.
2. The crack growth rate decreased with R ratios of underload and minor cycles for tests both in air and in the C2 solution.
3. A comparison of the crack growth rate in the corrosive C2 solution and in air showed that the corrosive environments could contribute to crack propagation by a factor of up to 11. This was attributed to the synergistic interaction of mechanical loading and hydrogen embrittlement.
4. The R ratio of minor cycles at which the minor cycles do not contribute to crack propagation through load interaction was determined to be 0.982, corresponding to  $0.594 \text{ MPa}\sqrt{m}$  of stress intensity factor range, which is much lower than the threshold determined by constant amplitude fatigue. This critical R ratio could be utilized to demarcate stress corrosion cracking and corrosion fatigue, and improve component/structure design.

### **7.1.5 The role of hydrogen in crack growth in near-neutral pH environments**

1. The crack growth rate for the coated and bare specimens in the near-neutral pH solution was the same, but higher than that in air. These echo the conclusion that it is hydrogen, not corrosion, that contributes to crack growth in near-neutral pH environments. The calculated corrosion rate from crack width in the specimen middle further confirms this conclusion.
2. The fractured surface showed the alternative appearance of striations and quasi-cleavage, and the crack growth rate was found not affected by stress states, which could be explained by both HELP and HEDE.
3. The crack width on the surface was found to be widened by the presence of hydrogen, which can only be explained by HELP. Thus it is believed that HELP governs the cracking behavior of pipeline steel in near-neutral pH environments. The fact that the crack width was not widened under the plane strain state suggests that HELP prevailed in the plane stress state.
4. The process of crack propagation in near-neutral pH environments was illustrated based on the understanding of the HE micro-mechanisms.

### **7.1.6 Practical strategies for avoiding enhanced crack growth**

1. The minimum normal operation pressure should be controlled to as high a level as possible to reduce the amplitude of large cycles (reducing acceleration effect).
2. The pipeline should be operated with a control of mean pressure, rather than the current maximum pressure. This will allow for a certain level of overloading,

- which can both minimize the enhanced crack growth by underload, and on the other hand achieve retarded growth by overload.
3. If shutdown or hydro-tests make underloads unavoidable, the recommendation is to impose a static hold for a period of at least 24 hours following each underload. This will lead to crack tip blunting and thus reduce the magnitude of load interaction and thus the crack growth.
  4. If possible, an overloading can be applied following each underload or after a period of operation.

## **7.2 Research Impact**

1. One of the most important accomplishments in this thesis is the identification and determination of enhanced crack growth caused by underload cycles (depressurization). This finding enables the understanding of crack growth in high pressure gas transmission pipelines, for which pressure fluctuations are often considered to be too benign to cause a significant crack growth through mechanisms of corrosion fatigue.
2. The results obtained from this thesis corroborate various failure scenarios found in the field, including the high frequency of failures at the discharge sections of pipelines and different crack growth characteristics between oil pipelines and gas pipelines, further confirming the importance of the findings.

3. Based on these results, the research group is in the process of developing crack growth software. The software is expected to be a key tool for risk assessment and to ensure that daily operations achieve maximized pipeline service life.

### **7.3 Recommendations**

1. The mechanisms of acceleration effects caused by underload could be studied through the observations of dislocation microstructures in the transmission electron microscope (TEM).
2. Unlike underload, overload can cause a retardation effect in crack growth, which needs to be studied systematically.
3. As well documented, overload can retard the crack growth rate while an underload can accelerate it for many other materials. The crack growth behaviors under the combination of overload and underload for pipeline steels exposed to near-neutral pH environments should be studied: the results can be very useful for pipeline integrity management. In fact, the combined waveform is being performed by a graduate student.
4. Up to now, all the waveforms are performed under symmetric loading cycles. The effects of asymmetric loading, such as quick unloading and slow loading and vice versa, could contribute to a deep understanding of the crack growth behavior under cyclic loadings.
5. As environmental contribution to crack growth is attributed to hydrogen, cathodic potential is another source of hydrogen. A study should be conducted on the effect

of cathodic potential on the crack growth rate under the variable amplitude waveforms.

6. The results obtained are all from the compact tension (CT) specimen, which is characterized by a thickness-through crack. The actual cracks on pipelines are surface cracks. Therefore, specimens with surface cracks should be used to confirm the conclusions from CT specimen. In fact, the testing using surface specimens is being performed by one graduate student in the group.
7. Since crack growth under variable amplitude waveform is significantly different from that under constant amplitude fatigue, further studies should be done to determine whether crack initiation is also affected by the waveform.
8. The above discussions are all based on the observations of laboratory tests, which can be further validated by running on a full-dimension pipe exposed to near-neutral pH environments.
9. The aggressive underload-type of pressure fluctuations may also contribute to crack initiation and propagation for high pH stress corrosion cracking through enhancing film ruptures. This should be studied in detail, in addition to the current understanding of the high pH SCC mechanisms.

## Appendix A<sup>1</sup>

The hydrostatic stress distribution [A.1] near crack tip can be expressed as:

$$\sigma^{hyd}(r, \theta) = \frac{2(1 + \nu)}{3\sqrt{2\pi r}} K_I \cos \frac{\theta}{2} \quad (A.1)$$

where  $K_I$  is the stress intensity near crack tip,  $r$  is the distance to crack tip,  $\nu$  is the Poisson's ratio, and  $\theta$  is the angle between the crack front and the line from specific position to the crack tip. The equilibrium H concentration in the plastic zone,  $c_{eq}$ , can then be expressed as

$$c_{eq} = c_0 \exp\left(\frac{\sigma^{hyd}\Omega}{k_B T}\right) \quad (A.2)$$

where  $k_B$  is the Boltzmann constant,  $T$  is the temperature,  $c_0$  is the atomic ratio of H/Fe away from crack tip, and  $\Omega$  is the partial volume of one H atom. Substituting Eq. (A.1) into Eq. (A.2) [A.2], the equation of  $c_{eq}$  is only a function of  $K_I$  and  $\Theta$ :

$$c_{eq} = c_0 \exp\left(\frac{2(1 + \nu)K_I\Omega}{3k_B T\sqrt{2\pi r}} \cos \frac{\theta}{2}\right) \quad (A.3)$$

The circular region with radius  $r_p$  (the plastic zone size) could be obtained by:

---

<sup>1</sup> This section was performed by Xiao Xing and Dr. Hao Zhang.

$$r_p = \frac{1}{6\pi} \left( \frac{K_{max}}{\sigma_{ys}} \right)^2 \quad (A.4)$$

where  $K_{max}$  is the maximum stress intensity in one cycle and  $\sigma_{ys}$  is the yield strength. The number of hydrogen atoms in an infinitesimal annulus region can be expressed as

$$dN = \frac{c_{eq} 2\pi r l_z}{a_0^3/2} dr \quad (A.5)$$

where  $a_0$  is lattice parameter, and  $l_z$  is the thickness of material. Substitute Eqs. (A.3) and (A.4) into Eq. (A.5) and integrate over distance to obtain

$$N(K_I) = \int_0^{r_p} \frac{c_0 \exp\left(\frac{4(1+\nu)K_I \Omega}{3\pi k_B T \sqrt{2\pi r}}\right) 2\pi r l_z}{a_0^3/2} dr \quad (A.6)$$

Expand Eq. (A.6),

$$N(K_I) = \frac{C}{12} \left[ K_I^3 B^3 \sqrt{r_p} e^{\frac{K_I B}{\sqrt{r_p}}} + K_I^2 B^2 r_p e^{\frac{K_I B}{\sqrt{r_p}}} + 2K_I B r_p^{3/2} e^{\frac{K_I B}{\sqrt{r_p}}} + 6r_p^2 e^{\frac{K_I B}{\sqrt{r_p}}} - K_I^4 B^4 \text{Ei}\left(\frac{K_I B}{\sqrt{r_p}}\right) \right] + \text{constant} \quad (A.7)$$

where  $B = 4(1 + \nu)\Omega/3\pi k_B T\sqrt{2\pi}$ ,  $C = 4\pi l_z c_0/a_0^3$ , and Ei is the exponential integral whose value is close 0 as  $r = r_p$ . As  $r = 0$ ,  $c_{eq}$  would reach the maximum and keep at constant 1 [A.3]. Thus, the lower limit of integral in Eq. (A.6) has been included in the constant in Eq. (A.7). The number of hydrogen atoms needed to saturate circular region with stress can be calculated from  $K_{min}$  to  $K_{max}$  as Eq. (A.7), which is supplied by the annulus region with inner radius  $r_p$  and the outer radius  $R_{eq}$ , therefore,

$$N(K_{max}) - N(K_{min}) = \frac{2\pi c_0 l_z}{a_0^3} (R_{eq} - r_p)^2 = \frac{C}{2} (R_{eq} - r_p)^2 \quad (A.8)$$

Chemical potential driven hydrogen atom diffusion is expressed by Eq. (A.9) [A.4]

$$\mu = \mu_0 + k_B T \ln \frac{c}{1-c} + \sigma^{hyd} \Omega \quad (A.9)$$

where  $\mu$  is the chemical potential and  $\mu_0$  is constant. Since the H concentration,  $c$ , far away from the crack tip has been assumed as a constant value,  $c_0$ , the driving force is only related to the hydrostatic stress  $\sigma^{hyd}$ . The axial velocity of H atom from chemical potential (driving force) and motivation is expressed as [A.3,A.5]

$$V_r = \frac{(1 + \nu)\Omega}{k_B T 3\sqrt{2\pi}} \frac{DK_I \cos \frac{\theta}{2}}{r^{3/2}} \quad (A.10)$$

where  $V_r$  is H atom velocity under specific  $K_I$  and specific position in specimen. The average velocity,  $\bar{V}_r$ , over  $\theta$ , loading and position can be shown as

$$\bar{V}_r = \frac{\int_{r_p}^{R_{eq}} \int_0^\pi \int_{K_{min}}^{K_{max}} V_r dK_I d\theta dr}{\pi(R_{eq} - r_p)(K_{max} - K_{min})} = \frac{2(1 + \nu)\Omega D(K_{max} + K_{min}) \left( \frac{1}{\sqrt{r_p}} - \frac{1}{\sqrt{R_{eq}}} \right)}{\pi(R_{eq} - r_p) k_B T 3\sqrt{2\pi}} \quad (A.11)$$

Hence the minimum time,  $t_{critical}$ , needed to achieve equilibrium hydrogen concentration with  $K_{min}$  to  $K_{max}$  can be approximated with diffusion distance divided by velocity:

$$t_{critical} = \frac{R_{eq} - r_p}{\bar{V}_r} \quad (A.12)$$

Therefore, the critical value of frequency could be expressed

$$f_{critical} = \frac{(1 + \nu)\Omega D(K_{max} + K_{min}) \left( \frac{1}{\sqrt{r_p}} - \frac{1}{\sqrt{R_{eq}}} \right)}{\pi(R_{eq} - r_p)^2 k_B T 3\sqrt{2\pi}} \quad (A.13)$$

According to the testing conditions in current investigation,  $K_{max}=33 \text{ MPa}\sqrt{\text{m}}$ ,  $K_{min}=16.5 \text{ MPa}\sqrt{\text{m}}$ , yield strength of X60 steel is 414 MPa,  $T=303 \text{ K}$ ,  $\nu=0.31$  for steel, and  $\Omega=1.99 \times 10^{-30} \text{ m}^3$ . Diffusivity of H can range from  $1.5 \times 10^{-9}$  to  $2 \times 10^{-9} \text{ m}^2/\text{s}$  with varying stress/strain [A.6]. Then the critical frequency,  $f_{critical}$ , is calculated between  $9.2 \times 10^{-4}$  to  $1.22 \times 10^{-3} \text{ Hz}$ .

## References

- [A.1] T.L. Anderson. Fracture Mechanics, Fundamentals and Applications, Third Edition. Taylors & Francis Group, 2005. pp: 44-45.
- [A.2] R. Matsumoto, S. Taketomi, S. Matsumoto, and N. Miyazaki, “Atomistic simulations of hydrogen embrittlement,” *Int. J. Hydrogen Energy*, vol. 34, no. 23, pp. 9576–9584, Dec. 2009.
- [A.3] Song J, Curtin WA. *Acta Mater* 2011;59(4):1557–1569.
- [A.4] Haftbaradaran H, Song J, Curtin WA, Gao H. *J. Power Sources* 2011;196(1):361–370.
- [A.5] Song J, Curtin WA. *Nat Mater* 2013;12(2):145–51.
- [A.6] Liu, W. Xie, W. Chen, and H. Zhang, “Effects of grain boundary and boundary inclination on hydrogen diffusion in  $\alpha$ -iron,” *J. Mater. Res.*, vol. 26, no. 21, pp. 2735–2743, Sep. 2011.

## References

- [1] B. S. Delanty, J. O'Beirne. Major Field Study Compares Pipeline SCC with Coatings. *Oil & Gas Journal* 15 (1992) 39-44.
- [2] Parkins RN. A review of stress corrosion cracking of high pressure gas pipelines proceedings of corrosion 2000. Paper 00363. Houston, Texas: NACE International; 2000.
- [3] J. A. Beavers and C. E. Jaske. Near-neutral pH SCC in Pipelines: Effects of Pressure Fluctuations on Crack Propagation. *Corrosion: 1999*, NACE International, Paper No.: 98257.
- [4] Weixing Chen and Robert L. Sutherby. Crack Growth Behavior of Pipeline Steel in Near-Neutral pH Soil Environments. *Metallurgical and Materials Transactions A* 2007; 38A; pp.1260-1268.
- [5] W. Chen, Richard Kania, Robert Worthingham, Gregory Van Boven. Transgranular crack growth in the pipeline steel exposed to near-neutral pH soil aqueous solutions: The role of hydrogen. *Acta Materialia* 57 (2009) 6200-6214.
- [6] Alberta Energy Regulator. Report 2013-B: Pipeline Performance in Alberta, 1990-2012.
- [7] National Energy Board (NEB), Focus on Safety and Environment a Comparative Analysis of Pipeline Performance 2000-2007, July 2009.
- [8] R.L. Wenk. Field Investigations of Stress Corrosion Cracking, 5<sup>th</sup> Symposium on Line Pipe Research, American Gas Association, 1974.

- [9] K. Sieradzki and R.C. Newman. Stress-Corrosion Cracking, *J. Physics and Chemistry of Solids*, Vol. 48, No.11, pp. 1101-1113, 1987.
- [10] National Energy Board (NEB), Report of the Inquiry-Stress Corrosion Cracking on Canadian Oil and Gas Pipelines, 1996.
- [11] C. Manfredi, and J.L. Otegui. Failures by SCC in buried pipelines. *Engineering Failure Analysis* 9 (2002) 495-509.
- [12] John A. Beavers, and Brent A. Harle. *Journal of Offshore Mechanics and Arctic Engineering*. 123 (2001). pp.147-151.
- [13] Jones DA. Principles and prevention of corrosion. 2<sup>nd</sup> ed. Upper Saddle River (NJ): Prentice Hall; 1996. pp.291.
- [14] W. Chen, F. King, and E. Vokes. Characteristics of Near-Neutral pH Stress Corrosion Cracks in an X-65 Pipeline. *Corrosion* 2002, Vol. 58, No. 3, pp. 267-275.
- [15] W. Bouaeshi, S. Ironside, and R. Eadie. Research and Cracking Implications from an Assessment of Two Variants of Near-Neutral pH Crack Colonies in Liquid Pipelines. *Corrosion*: July 2007, Vol. 63, No. 7, pp. 648-660.
- [16] Karina Chevil, Abdoulmajid Eslami, Weixing Chen, Reg Eadie, Richard Kania, Robert Worthingham, and Greg Van Boven. Developing Cathodic Protection Based on Disbondment Geometry. Proceedings of 2012 9<sup>th</sup> International Pipeline Conference, Calgary, Alberta, Canada, Sept. 24-28, 2012. Vol. 2, paper No. IPC2012-90675, pp. 583-590.
- [17] Eslami, A., B. Fang, R. Kania, B. Worthingham, J. Been, R. Eadie, and W. Chen. Stress corrosion cracking initiation under the disbonded coating of pipeline steel in near-

neutral pH environment. Corrosion Science, Vol. 52, Issue 11, November 2010. pp.3750-3756.

[18] Karina Chevil, Weixing Chen, Reg Eadie, Richard Kania, Greg Van Boven, and Jenny Been. Correlating Corrosion Field Data with Experimental Findings for the Development of Pipeline Mitigation Strategies. Proceedings of IPC2014, 10<sup>th</sup> International Pipeline conference, Calgary, Alberta, Canada, Sept. 29- Oct. 3, 2014. Paper No. IPC2014-33678.

[19] Abdoulmajid Eslami, Trevor Place, Shamus McDonnell, Chijikoe Ukiwe and Qin You. Landscape Investigation on External Corrosion and SCC of a Tape Coated Enbridge Pipeline. Proceedings of the 2012 9<sup>th</sup> International Pipeline Conference, IPC2012, Sept. 24-28, 2012, Calgary, Alberta, Canada. Paper No. IPC2012-90598.

[20] F. King, Tom Jack, Miroslav Kolar and Robert Worthingham. A Permeable Coating Model for Predicting the Environment at the Pipe Surface under CP-Compatible Coatings. Corrosion 2004, New Orleans, USA, 2004, Paper No. 04158.

[21] Barlo T.J. and Berry W.E.. An assessment of the current criteria for cathodic protection of buried steel pipelines. Materials Performance. Vol. 23:9, 1984,

[22] F. Gan, Z.-W. Sun, G. Sabde, and D.-T. Chin. Cathodic Protection to Mitigate External Corrosion of Underground Steel Pipe Beneath Disbonded Coating. Corrosion: October 1994, Vol. 50, No. 10, pp. 804-816.

[23] R. R. Fessler, A. J. Markworth, and R. N. Parkins. Cathodic Protection Levels under Disbonded Coatings. Corrosion: January 1983, Vol. 39, No.1, pp. 20-25.

- [24] Robert G. Wakelin, Robert A. Gummow, and Sorin Marius Segall. AC Corrosion – Case Histories, Test Procedures, & Mitigation. Corrosion 1998, 22-27 March, San Diego, California. Paper No. NACE-98565.
- [25] X. Chen, X.G. Li, C.W. Du, and Y.F. Cheng. Effect of cathodic protection on corrosion of pipeline steel under disbanded coating. Corrosion Science, Vol. 51, Issue 9, Sept. 2009, pp. 2242-2245.
- [26] Canadian Gas Association OCC-1 Task Force. Recommended Practice OCC-1-2013, Control of External Corrosion on Buried or Submerged Metallic Piping Systems, June 2013.
- [27] O. Vosikovsky, and R.J. Coole. An Analysis of Crack Extension by Corrosion Fatigue in a Crude Oil Pipeline. International Journal of Pressure Vessels and Piping, Vol. 6, Issue 2, March 1978, pp. 113-129.
- [28] T.M. Ahmed, S. B. Sutherby, and A. Plumtree. Cyclic Crack Growth rates of X-60 Pipeline Steel in a Neutral Dilute Solution. Corrosion: July 1997, Vol. 53, No. 7, pp.581-590.
- [29] Baotong Lu, Jingli Luo and Brian McCrady. Near-Neutral pH SCC Initiation and Early Propagation of X70 Pipeline Steel. Proceedings of IPC2002, 4<sup>th</sup> International Pipeline Conference, Sept. 29-Oct. 3, 2002, Calgary, Alberta, Canada. Paper No. IPC2002-27234.
- [30] Weimin Zhao, Yongxing Wang, Timing Zhang, and Tong Wang. Study on the mechanism of high-cycle corrosion fatigue crack initiation in X80 steel. Corrosion Science 57 (2012) 99-103.

- [31] A. Mustapha, E.A. Charles, and D. Hardie. Evaluation of environment-assisted cracking susceptibility of a grade X100 pipeline steel. *Corrosion Science* 54 (2012) 5-9.
- [32] Frand Cheng. *Stress Corrosion Cracking of Pipelines*. A John Wiley & Sons, Inc., Publication, New Jersey, 2013, pp. 73-111.
- [33] Abdoulmajid Eslami. PhD thesis, Near-neutral pH Stress Corrosion Crack Initiation under Simulated Coating Disbondment. University of Alberta, Fall 2012.
- [34] Syed J. Haider, Steven Textor, Aaron Sutton and Yvan Hubert. Managing a New Pressure Cycling Reality in Liquid Pipelines. Proceedings of IPC2014, 10<sup>th</sup> International Pipeline Conference, Sept. 29-Oct. 3, 2014, Calgary, Alberta, Canada. Paper No. IPC2014-33485.
- [35] O. Vosikovsky, and R. J. Cooke. An analysis of crack extension by corrosion fatigue in a crude oil pipeline. *International Journal of Pressure Vessels and Piping*, Vol. 6, Issue 2, March 1978, pp. 113-129.
- [36] R. N. Parkins and B. S. Greenwell. The interface between corrosion fatigue and stress-corrosion cracking. *Metal Science*, Vol. 11, Issue 8-9 (01 August 1977), pp. 405-413.
- [37] Richard W. Hertzber. *Deformation and Fracture Mechanics of Engineering Materials*, Fourth Edition, John Wiley and Sons, Inc., New York, NY, 1989, pp. 591-604.
- [38] P. C. Paris, and F. Erdogan. A Critical Analysis of Crack Propagation Laws. *Journal of Basic Engineering*, Vol. 85, 1960, pp. 528-534.
- [39] J. Been, R. Eadie, and R. Sutherby. Prediction of Environmentally Assisted Cracking on Gas and Liquid Pipelines. Proceedings of IPC2006, 6<sup>th</sup> International Pipeline Conference, Sept. 25-29, 2006, Calgary, Alberta, Canada. Paper No. IPC2006-10345.

- [40] J.A. Beavers, and C.E. Jaske. Effects of Pressure Fluctuations on SCC Propagation". PRCI Report on Contract PR-186-9706, Arlington, Virginia 2004.
- [41] R. L. Eadie, K.E. Szklarz, and R. L. Sutherby. Corrosion Fatigue and Near-Neutral pH Stress Corrosion Cracking of Pipeline Steel and the Effect of Hydrogen Sulfide. Corrosion: February 2005, Vol. 61, No. 2, pp.167-173.
- [42] Afolabi Egbewande, Weixing Chen, Reg Eadie, Richard Kania, Greg Van Boven, Robert Worthingham and Jenny Been. Transgranular crack growth in the pipeline steel exposed to near-neutral pH soil aqueous solutions: Discontinuous crack growth mechanism. Corrosion Science, Vol. 83, June 2014, pp. 343-354.
- [43] P.S. Pao and R.A. Bayles. Effect of Ripple Loads on Stress-Corrosion Cracking in Structural Steel. Technical Report, Report No. NRL ser 6310/003, May 30, 1995.
- [44] T.L. Anderson. Fracture Mechanics, Fundamentals and Applications, Third Edition. Taylors & Francis Group, 2005. pp: 464-473.
- [45] S. Srivatsan, and T.S. Sudarshan. Mechanisms of fatigue crack initiation in metals: role of aqueous environments. Journal of Materials Science, May 1988, Vol. 23, Issue 5, pp. 1521-1533.
- [46] Weixing Chen, and Robert Sutherby. Laboratory Simulation of Hydrostatic Test in Near-Neutral pH Soil Environments. Proceedings of IPC2006, 6<sup>th</sup> International Pipeline Conference, Sept. 25- 29, 2006, Calgary, Alberta, Canada. Paper No. IPC2006-10477.
- [47] T.L. Anderson. Fracture Mechanics, Fundamentals and Applications, Third Edition. Taylors & Francis Group, 2005. pp: 529-537.

- [48] R. E. Ricker, and D. J. Duquette. The role of hydrogen in corrosion fatigue of high purity Al-Zn-Mg exposed to water vapor. *Metallurgical Transactions A*, Vol. 19A, July 1988, pp. 1775-1783.
- [49] Roy Johnsen, Bård Nyhus and Stig Wästberg. Hydrogen Induced Stress Cracking (HISC) of Stainless Steel under Cathodic Protection in Seawater: Presentation of a New Test Method. Proceedings of the ASME 2009 28<sup>th</sup> International Conference on Ocean, Offshore and Arctic Engineering, OMAE2009, May 31- June 5, 2009, Honolulu, Hawaii, USA.
- [50] N. Nanninga, A. Slifka, Y. Levy, and C. White. A Review of Fatigue Crack Growth for Pipeline Steel Exposed to Hydrogen. *Journal of Research of the National Institute of Standards and Technology*, Vol. 115, No. 6, Nov. - Dec. 2010, pp. 437-452.
- [51] Arnaud Macadre, Maxim Artamonov, Saburo Matsuoka, and Jader Furtado. Effects of hydrogen pressure and test frequency on fatigue crack growth properties of Ni-Cr-Mo steel candidate for a storage cylinder of a 70 MPa hydrogen filling station. *Engineering Fracture Mechanics* 78 (2011) 3196-3211.
- [52] Z. Sun, C. Moriconi, G. Benoit, D. Halm, and G. Henaff. Fatigue Crack Growth under High Pressure of Gaseous Hydrogen in a 15-5PH Martensitic Stainless Steel: Influence of Pressure and Loading Frequency. *Metallurgical and Materials Transactions A*, March 2013, Vol. 44, No. 3, pp. 1320-1330.
- [53] D. X. He, W.X. Chen, and J.L. Luo. Effect of cathodic potential on hydrogen content in a pipeline steel exposed to NS4 near-neutral pH soil solution. *Corrosion* 2004;60(8):778-786.

- [54] W. Chen, S.-H Wang, F. King, T. R. Jack, M. J. Wilmott. Hydrogen Permeation Behavior of X-70 Pipeline Steel in a Near-Neutral pH Soil Environment. Proceedings of IPC2000, 3<sup>rd</sup> International Pipeline Conference, Vol. 2, New York, NY: ASME International, 2000, pp. 953-960.
- [55] D.X. He, W. Chen, and J.L. Luo. Effect of Cathodic Potential on Hydrogen Content in a Pipeline Steel Exposed to NS4 Near-Neutral pH Soil Solution. Corrosion 2004;60(8):778-786.
- [56] Y.F. Cheng. Fundamentals of hydrogen evolution reaction and its implications on near-neutral pH stress corrosion cracking of pipeline. Electrochimica Acta 52 (2007) 2661-2667.
- [57] Z.Y. Liu, X.G. Li, Y.F. Cheng. Mechanistic aspect of near-neutral pH stress corrosion cracking of pipelines under cathodic polarization. Corrosion Science 55 (2012) 54-60.
- [58] Lisa M. Young, Peter L. Andresen, and Thomas M. Angeliu. Crack tip Strain Rate: Estimates Based on Continuum Theory and Experimental Measurement. Corrosion 2001, March 11-16, 2001, NACE, Houston, TX, 2001, paper No. 01131.
- [59] R.N. Parkins and J.A. Beavers. Some Effects of Strain Rate on the Transgranular Stress Corrosion Cracking of Ferritic Steel in Dilute Near-Neutral pH Solutions. Corrosion: March 2003, Vol. 59, No. 3, pp. 258-273.
- [60] T. L. Anderson. Fracture Mechanics, Fundamentals and Applications, Third Edition. Taylor & Francis Group, 2005. pp: 538-545.
- [61] S. B. Lambert, J.A. Beavers, B. Delanty, R. Sutherby, and A. Plumtree. Mechanical factors affecting stress corrosion cracking growth rates in buried pipelines.

Proceedings of International Pipeline conference, IPC2000, ASME, Calgary, Canada, pp. 961-966.

[62] G. Van Boven, R. Sutherby, and F. King. Characterizing Pressure Fluctuations on Buried Pipelines in Terms Relevant to Stress Corrosion Cracking. Proceedings of IPC2002, 4<sup>th</sup> International Pipeline Conference, Sept. 29- Oct. 3, 2002, Calgary, Alberta, Canada. Paper No. IPC2002-27149.

[63] Jenny Been, Raymond R. Fessler, Sean Keane, and Walter Kresic. History of Pressure Fluctuations Related to Severity of Near-Neutral pH SCC. Proceedings of IPC2006, 6<sup>th</sup> International Pipeline Conference, Sept. 25- 29, 2006, Calgary, Alberta, Canada. Paper No. IPC2006-10412.

[64] ASTM E1049 – 85 (reapproved 2011)<sup>E1</sup>. Standard Practices for Cycle Counting in Fatigue Analysis. American Society for Testing and Materials, West Conshohocken, PA, 2011.

[65] G. Van Boven, R. Sutherby, and F. King. Characterizing Pressure Fluctuations on Buried Pipelines in Terms Relevant to Stress Corrosion Cracking. Proceedings of IPC2002, 4<sup>th</sup> International Pipeline Conference, Sept. 29- Oct. 3, 2002, Calgary, Alberta, Canada. Paper No. IPC2002-27149.

[66] M. Skorupa. Load Interaction Effects During Fatigue Crack Growth under Variable Amplitude loading- a Literature Review. Part I: Empirical Trends. Fatigue & Fracture of Engineering Materials & Structures 1998; 21: 987-1006.

[67] M. Skorupa. Load Interaction Effects During Fatigue Crack Growth under Variable Amplitude loading- a Literature Review. Part II: Qualitative explanation. Fatigue & Fracture of Engineering Materials & Structures 1999; 22: 905-926.

- [68] Vasilios Zitounis. Fatigue Crack Growth Rates under Variable Amplitude Load Spectra Containing Tensile Underloads. PhD thesis, Cranfield University, 28 October 2003.
- [69] Stephan M. Russ. Effect of Underloads on Fatigue Crack Growth of Ti-17. PhD thesis, Georgia Institute of Technology, October 2003.
- [70] Fowler, K.R. and Watanabe, R.T.. Development of Jet Transport Airframe Fatigue Test Spectra, Development of Fatigue Loading Spectra, ASTM STP 1006, J. M. Potter and R. T. Watanabe, Eds., American Society for Testing and Materials, Philadelphia, 1989, pp. 36-64.
- [71] Sunder, R. Contribution of Individual Load Cycles to Crack Growth under Aircraft Spectrum Loading, Advances in Fatigue Lifetime Predictive Techniques, ASTM STP 1122, M. R. Mitchell and R. W. Landgraf, Eds., American Society for Testing and Materials, Philadelphia, 1992, pp. 176-190.
- [72] T. L. Anderson. Fracture Mechanics, Fundamentals and Applications, Third Edition. Taylors & Francis Group, 2005. pp: 473-488.
- [73] Henning Agerskov. The Fatigue Behavior of Steel Structures under Random Loading. Key Engineering Materials, Vols. 378-379 (2008) pp.3-16.
- [74] Yan-Hui Zhang, and S.J. Maddox. Investigation of fatigue damage to welded joints under variable amplitude loading spectra. International Journal of Fatigue 31 (2009) 138-152.
- [75] N.A. Fleck. Fatigue Crack Growth due to Periodic Underloads and Overloads. Acta Metallurgica, Vol. 33, No. 7, July 1985, pp. 1339-1354.

- [76] Colin MacDougall, and T.H. Topper. The influence of variable amplitude loading on crack closure and notch fatigue behavior. *International Journal of Fatigue*, Vol. 19, No. 5, pp. 389-400, 1997.
- [77] M. El-Zeghayar, T.H. Topper, F.A. Conle, and J.J. F. Bonnen. Modeling crack closure and damage in variable amplitude fatigue using smooth specimen fatigue test data. *International Journal of Fatigue*, Vol. 33, No. 2, Feb. 2011, pp. 223-231.
- [78] J. C. Newman, Jr. and E.P. Phillips. Prediction of Crack Growth Under Variable-Amplitude and Spectrum Loading in a Titanium Alloy. *Fatigue Testing and Analysis under Variable Amplitude Loading Conditions*, ASTM STP 1439, Peter C. McKeighan, and Narayanaswami Ranganathan, American Society for Testing and Materials, Philadelphia, 2005, pp. 232-250.
- [79] N. Ohrloff, A. Gysler and G. Lütjering. *Journal DE Physique*, Colloque C3, supplement au n°9, Tome 48, Sept. 1987, C3-801.
- [80] M. Krkoska, S.A. Barter, R.C. Alderliesten, P. White, R. Benedictus. Fatigue crack paths in AA2024-T3 when loaded with constant amplitude and simple underload spectra. *Engineering Fracture Mechanics*, Vol. 77, No. 11, July 2010, pp. 1857-1865.
- [81] Richard W. Hertzberg. *Deformation and Fracture Mechanics of Engineering Materials*, Fourth Edition, John Wiley & Sons, Inc., 1996, pp. 634-641.
- [82] Kentaro Yamada, Qiuliang Cao, Yuji Okuhara and Xiaohua Cheng. Fatigue Crack Growth Behavior of Various Structural Steel after Single and Periodic Overloads. *Structural Eng./Earthquake Eng., JSCE*, Vol. 15, No. 2, 191s-200s, 1998 July. pp. 37-46.

- [83] J. Schijve, F. A. Jacobs, and P. J. Tromp. Crack propagation in 2024-T3Al cald under flight-simulation loading effect of truncating high gust loads. National Aerospace Laboratory, NLR, The Netherlands, NLR TR-69050-U, June 1969.
- [84] Raymond R. Fessler and Steve Rapp. Method for Establishing Hydrostatic Re-Test Intervals for Pipelines with Stress-Corrosion Cracking. Proceedings of IPC2006, 6<sup>th</sup> International Pipeline Conference, Sept. 25- 29, 2006, Calgary, Alberta, Canada. Paper No. IPC2006-10163, pp. 259-263.
- [85] Weixing Chen, Yongwang Kang, Reg Eadie, Richard Kania, Greg Van Boven, and Robert Worthingham. Proceedings of the 2012 9<sup>th</sup> International Pipeline Conference, IPC2012, Sept. 24- 28, 2012, Calgary, Alberta, Canada. Paper No. IPC2012-90635.
- [86] Yongwang Kang, Weixing Chen, Richard Kania, Gregory Van Boven, Robert Worthingham. Simulation of crack growth during hydrostatic testing of pipeline steel in near-neutral pH environment. Corrosion Science 53 (2011) 968-975.
- [87] Jian Li, M. Elboujdaini, M. Gao, R. W. Revie. Investigation of plastic zones near SCC tips in a pipeline after hydrostatic testing. Materials Science and Engineering A 486 (2008) 496-502.
- [88] Ryoichi Koterazawa, and Takayoshi Noshō. Acceleration of Crack Growth under Intermittent Overstressing in Different Environments. Fatigue & Fracture of Engineering Materials & Structures. Vol. 15, No. 1, pp. 103-113, 1992.
- [89] T. L. Anderson. Fracture Mechanics, Fundamentals and Applications, Third Edition. Taylors & Francis Group, 2005. pp: 457-464.
- [90] Eric F. J. von Euw. Effect of Overload Cycle(s) on Subsequent Fatigue Crack Propagation in 2024-T3 Aluminum Alloy. PhD Dissertation, Lehigh University, 1971.

- [91] Asok Ray, and Ravindra Patankar. Fatigue crack growth under variable-amplitude loading: Part I – Model formulation in state-space setting. *Applied Mathematical Modelling* 25 (2001) 979-994.
- [92] T. L. Anderson. *Fracture Mechanics, Fundamentals and Applications*, Third Edition. Taylors & Francis Group, 2005. pp: 473-488.
- [93] Soo Yeol Lee. *Effects of Overload and Underload on Internal Strains/Stresses and Crack Closure during Fatigue-Crack Propagation*. Doctoral Dissertations, University of Tennessee - Knoxville, December, 2009.
- [94] J. Schijve. The Effect of Pre-strain on Fatigue Crack Growth and Crack Closure. *Engineering Fracture Mechanics*, 1976, Vol. 8, pp. 575-581.
- [95] S. Suresh. *Fatigue of Materials*. Cambridge University Press, Cambridge, New York Port Chester, Melbourne Sydney, 1991, pp:113.
- [96] K. Katagiri, R. Koterazawa, T. Yamada, and T. Tsuboi. Changes in dislocation structures adjacent to fatigue crack tips induced by intermittent overstraining. *Metal Science*, Vol. 17, November 1983, pp:556-562.
- [97] Canadian Energy Pipeline Association (CEPA). *Stress Corrosion Cracking Recommended Practices*, 2<sup>nd</sup> Edition, An industry leading document detailing the management of transgranular SCC, December 2007, pp.5-5.
- [98] TransCanada Pipeline (1996) Response to National Energy Board Information Request 2 of Proceeding MH-2-5, TCP, Calgary, Alberta, Canada, pp.3.
- [99] B. W. Williams, S. B. Lamber, R. Sutherby, A. Plumtree. Environmental Crack Growth under Variable Amplitude Loading of Pipeline Steel. *Corrosion*: January 2004, Vol. 60, No.1, pp. 95-103.

[100] J. A. Beavers, C. J. Maier, and C. E. Jaske. Methodology for Ranking SCC Susceptibility of Pipeline Segments Based on the Pressure Cycle history. Corrosion 2007, Paper No. 07128.

[101] Brett Conrad, Weixing Chen, Reg Eadie, Richad Kania, Greg Van Boven, Robert Worthingham. Developing a Predictive Model of Near Neutral pH Stress Corrosion Cracking of Underground Pipelines. Proceedings of IPC 2012, 9<sup>th</sup> International Pipeline conference, Sept. 24-28, 2012, Calgary, Alberta, Canada. Paper No.: IPC2012-90629, pp: 559-567.

[102] Weixing Chen, Achieving Maximum Crack Remediation Effect from Optimized Hydrotesting, Final Report Prepared for US Department of Transportation PHMSA, Client Contract Number: DTPH56-08-T-000008-WP#355, June 15, 2011, total pages: 93.

[103] R.W. Staehle. R.W. Staehle, et al., editors. Stress corrosion cracking and hydrogen embrittlement of iron base alloys, NACE-5. Houston (TX): NACE; 1977. p. 193.

[104] S. Srivatsan, T.S. Sudarshan. Mechanisms of fatigue crack initiation in metals: role of aqueous environments. Journal of Materials Science, 1988;23:1521-1533.

[105] Sheng-Hui Wang, Weixing Chen. A Study on the pre-cyclic load-induced burst of creep deformation of a pipeline steel under subsequent static load. Materials Science and Engineering A, 2002;A325:144-151.

[106] Sheng-Hui Wang, Yonggang Zhang, Weixing Chen. Room temperature creep and strain-rate-dependent stress-strain behavior of pipeline steel. Journal of Materials Science, 2001;36:1931-1938.

- [107] Sheng-Hui Wang, Weixing Chen. Room temperature creep deformation and its effect on yielding behavior of a line pipe steel with discontinuous yielding. *Materials Science and Engineering A* 2001;301:147-153.
- [108] Kamel Makhlouf, J.W. Jones. Effects of temperature and frequency on fatigue crack growth in 18% Cr ferritic stainless steel. *International Journal of Fatigue*, 1993;15(3):163-171.
- [109] Lambert SB, Beavers JA, Delanty B, Sutherby R, Plumtree A. Mechanical factors affecting stress corrosion cracking growth rates in buried pipelines. In: *Proceedings of 3rd International Pipeline Conference*; 2000, Calgary. p.961-965.
- [110] Zhao J, Chen W, Boven GV, Keane S, Been J. Development and Validation of Load-Interaction Based Models for Crack Growth Prediction. In: *Proceedings of 10th International Pipeline Conference*; 2014, Calgary. Paper No.: IPC2014-33325.
- [111] T.M. Ahmed, S.B. Lambert, R. Sutherby, A. Plumtree. Cyclic crack growth rates of X-60 pipeline steel in a neutral dilute solution. *Corrosion* 1997;53(7):581-590.
- [112] C.D. Beachem. A new model for hydrogen-assisted cracking (hydrogen “embrittlement”). *Metallurgical Transactions*, 1972;3(2):437-451.
- [113] P.J. Ferreira, I.M. Robertson, H.K. Birnbaum. Hydrogen effects on the character of dislocations in high-purity aluminum. *Acta Mater* 1999;47(10):2991-2998.
- [114] Zhao J *et al.* Statistical analysis on pipeline spectra, in preparation.
- [115] D.L. Davidson, J. Lankford. Fatigue crack growth in metals and alloys: mechanisms and micromechanics. *International Materials Reviews*, 1992;37(2):45-74.

- [116] Ryosuke Matsumoto, Shinya Taketomi, Sohei Matsumoto, Noriyuki Miyazaki. Atomistic simulations of hydrogen embrittlement. *International Journal of Hydrogen Energy*, 2009;34(23):9576–9584.
- [117] Xiaoyang Liu, Wenbo Xie, Weixing Chen, Hao Zhang. Effects of grain boundary inclination on hydrogen diffusion in  $\alpha$ -iron. *Journal of Materials Research*, 2011;26(21):2735–2743.
- [118] Alexander Troiano. The role of hydrogen and other interstitials in the mechanical behavior of metals. *Trans. ASM* 52.1 (1960):54-80.
- [119] H.K. Birnbaum, P. Sofronis. Hydrogen-enhanced localized plasticity—a mechanism for hydrogen related fracture. *Materials Science and Engineering A* 176 (1994) 191–202.
- [120] T. Doshida, M. Nakamura, H. Saito, T. Sawada, K. Takai. Hydrogen-enhanced lattice defect formation and hydrogen embrittlement of cyclically prestressed tempered martensitic steel. *Acta Mater* 61 (2013) 7755-7766.
- [121] Afolabi Egbewande, Weixing Chen, Reg Eadie, Richard Kania, Greg Van Boven, Robert Worthingham, Jenny Been. Transgranular crack growth in the pipeline steel exposed to near-neutral pH soil aqueous solutions: discontinuous crack growth mechanism. *Corrosion Science* 2014;83:343-354.
- [122] M. Baker Jr. (2004), *Stress Corrosion Cracking Studies*, Integrity Management Program DTRS56-02-D-70036, Department of Transportation, Office and Pipeline Safety.
- [123] R. Koterazawa (1981). Fatigue crack propagation under periodic overstressing. In: *Proc. Fatigue '81, SEE Fatigue Group Conf.* Warwick Univ. England (edited by F. Sherratt and J. B. Sturgeon), 318-327. Westbury House, Guildford, England.

- [124] V. M. Pleskach and P. A. Averchenko. Effect of gaseous erosion on a decrease of the fatigue strength of specimens of titanium alloy VT8. Plenum Publishing Corporation, 1976, No. 8, pp.118-119.
- [125] H.-J. Christ, A. Jung, H.J. Maier and R. Teteruk. Thermomechanical fatigue-damage mechanisms and mechanism-based life prediction methods. *Sadhana*, Vol. 28, Parts 1 & 2, February-April 2003, pp. 147–165.
- [126] B.L. Boyce and R.O. Ritchie. Effects of load ratio and maximum stress intensity on the fatigue threshold in Ti-6Al-4V. *Engineering Fracture Mechanics*, Vo.68, Issue 2, 2001:129-147.
- [127] M. O. Speidel, S.E. Stanzl and E. Tschegg. Fatigue crack growth in a 13% Cr steel at frequencies from  $10^{-3}$  Hz to  $10^4$  Hz determination of the threshold stress intensity  $\Delta K_0$  by ultrasonic fatigue. *Materials Science and Engineering Technology*. 1980, 11, 305-308.
- [128] Kamel Makhlof and J.W. Jones. Effects of temperature and frequency on fatigue crack growth in 18% Cr ferritic stainless steel. *International Journal of Fatigue*. Vol. 15, No. 3,1993, pp.163-171.
- [129] Elber, Wolf. Fatigue crack closure under cyclic tension. *Engineering Fracture Mechanics*, Vol. 2, No. 1, 1970, pp.37-44.
- [130] A.K. Vasudevan, K. Sadananda, G. Glinka. Critical parameters for fatigue damage. Vol. 23, 2001, pp. 39-53.
- [131] C. Manfredi and J.L. Otegui. Failures by SCC in buried pipelines. *Engineering Failure Analysis*, Vol. 9, 2002, pp. 495-509.

- [132] Fowler, K.R. and Watanabe, R.T.. Development of Jet Transport Airframe Fatigue Test Spectra, Development of Fatigue Loading Spectra, ASTM STP 1006, J. M. Potter and R. T. Watanabe, Eds., American Society for Testing and Materials, Philadelphia, 1989, pp. 36-64.
- [134] Richard W. Hertzber. Deformation and Fracture Mechanics of Engineering Materials, Fourth Edition, John Wiley and Sons, Inc., New York, NY, 1989, pp. 521-586.
- [135] Yan-Hui Zhang, and S.J. Maddox. Fatigue life prediction for toe ground welded joints. *International Journal of Fatigue*, 31 (2009):138-152.
- [136] C.F. Dong, Z.Y. Liu, X.G. Li and Y.F. Cheng. Effects of hydrogen-charging on the susceptibility of X100 pipeline steel to hydrogen-induced cracking. *International Journal of Hydrogen Energy*, 34 (2009): 9879-9884.
- [137] R. Sunder, W. J. Porter and N. E. Ashbaugh. The role of air in fatigue load interaction. *Fatigue & Fracture of Engineering Materials & Structures*, Vol. 26, Issue 1, Jan. 2003: 1-16.
- [138] L. Raymond. Hydrogen Embrittlement: Prevention and Control, ASTM STP 962, L. Raymond, Ed., American Society for Testing and Materials, Philadelphia, 1988, pp. 10-16.
- [139] M.A.V. Devanathan, Z. Stachurski, W. J. Beck. A technique for the evaluation of hydrogen embrittlement characteristics of electroplating baths. *Journal of the Electrochemical Society*, 1963 Vol. 110, Issue 8, 886-890.
- [140] D. Hardie, E.A. Charles, A.H. Lopez. Hydrogen embrittlement of high strength pipeline steel. *Corrosion Science*, 48 (2006) 4378-4385.

- [141] J.L. Gillette, R.L. Kolpa. Overview of interstate hydrogen pipeline systems. Report No. : ANL/EVS/TM/08-2, TRN: US0802253, Feb. 2008.
- [142] W.H. Johnson. On some remarkable changes produced in iron and steel by the action of hydrogen and acids. *Nature*, Vo. 11, Issue 281, 1875: 393.
- [143] R.P. Gangloff, R.P. Wei. Gaseous hydrogen embrittlement of high strength steel. *Metallurgical Transactions A*, Vol.8, Issue 7, 1977, 1043-1053.
- [144] R. A. Oriani. Hydrogen embrittlement of steel. *Annual Review of Materials Science*, 1978.8:327-357.
- [145] John P. Hirth. Effects of hydrogen on the properties of iron and steel. *Metallurgical Transactions A*, Vol. 11, Issue 6, 1980: 861-890.
- [146] A. Nagao, C.D. Smith, M. Dadfarnia, P. Sofronis, I.M. Robertson. The role of hydrogen in hydrogen embrittlement fracture of lath martensitic steel. *Acta Mater.* 60 (2012) 5182-5189.
- [147] S. Ohmiya, H. Fujii. Effects of Ni and Cr contents on fatigue crack growth properties of SUS316-based stainless steel in high-pressure gaseous hydrogen. *The Iron and Steel Institute of Japan (ISIJ) International*, 52 (2) (2012) 247-254.
- [148] J. Zhao, Z. Jiang, C.S. Lee. Effects of tungsten on the hydrogen embrittlement behavior of microalloyed steel. *Corrosion Science*, 82 (2014) 380-391.
- [149] V. Venegas, F. Caleyó, T. Baudin, J.H. Espina-Hernández, J.M. Hallen. On the role of crystallographic texture in mitigating hydrogen-induced cracking in pipeline steel. *Corrosion Science*, 53 (2011) 4204-4212.

- [150] S. Chen, M. Zhao, L. Rong. Effect of grain size on the hydrogen embrittlement sensitivity of a precipitation strengthened Fe-Ni based alloy. *Materials Science and Engineering A*, 594 (2014) 98-102.
- [151] O.M.I. Todoshchenko, Y. Yagodzinsky, T. Saukkonen, H. Hänninen. Role of nonmetallic inclusions in hydrogen embrittlement of high-strength carbon steel with different microalloying. *Metallurgical and Materials Transactions A*, 45 (11) (2014) 4742-4747.
- [152] O. Takakuwa, T. Ohmi, M. Nishikawa, A. Toshimitsu Yokobori Jr. and H. Soyama. Suppression of fatigue crack propagation with hydrogen embrittlement in stainless steel by cavitation peening. *Strength, Fracture and Complexity*, 7 (2011) 79-85.
- [153] K. Takai, H. Shoda, H. Suzuki, M. Nagumo. Lattice defects dominating hydrogen-related failure of metals. *Acta Mater.* 56 (2008) 5158-5167.
- [154] Y. Murakami. The effect of hydrogen on fatigue properties of metals used for fuel cell system. *Advances in Fracture Research*, 2006, p.167-195.
- [155] J.J. DeLuccia. *Hydrogen Embrittlement: Prevention and Control*, ASTM STP 962, L. Raymond, Ed., American Society for Testing and Materials, Philadelphia, 1988, pp. 17-34.
- [156] M.R. Louthan. Hydrogen embrittlement of metals: a primer for the failure analyst. *Journal of Failure Analysis and Prevention*, (2008) 8:289-307.
- [157] H.D. Fleming, R. G. Ide. Determination of volatile hydride-forming metals in steel by atomic absorption spectrometry. *Analytica Chimica Acta*. 83 (1976) 67-82.
- [158] A. Troiano. The role of hydrogen and other interstitials in the mechanical behavior of metals. *Trans. ASM* 52 (1960) 147-157.

- [159] R.A. Vennett, G.S. Ansell. The effect of high-pressure hydrogen upon the tensile properties and fracture behavior of 304 L stainless steel. *Transactions of American Society for Metals*, 60 (1967) 242-251.
- [160] Z.T. Liu, X.G. Li, Y.F. Cheng. Mechanistic aspect of near-neutral pH stress corrosion cracking of pipelines under cathodic polarization. *Corrosion Science* 55 (2012) 54-60.
- [161] I.M. Robertson, H.K. Birnbaum. Chapter 91 Hydrogen effects on plasticity. *Dislocations in Solids*, 15 (2009) 249–293.
- [162] S. Wang, M.L. Martin, P. Sofronis, S. Ohnuki, N. Hashimoto, I.M. Robertson. Hydrogen-induced intergranular failure of iron. *Acta Mater.* 69 (2014) 275-282.
- [163] T. Neeraj, R. Srinivasan, Ju Li. Hydrogen embrittlement of ferritic steel: observations on deformation microstructure, nanoscale dimples and failure by nanovoiding. *Acta Materialia* 60 (2012) 5160–5171.
- [164] X. Chen, T. Foecke, M. Lii, Y. Katz, W.W. Gerberich. The role of stress state on hydrogen cracking in Fe-Si single crystals. *Engineering Fracture Mechanics*. Vol. 35, No. 6, pp. 997-1017, 1990.
- [165] E. Hörnlund, J.K.T. Fossen, S. Hauger, C. Haugen, T. Havn, T. Hemmingsen. Hydrogen diffusivities and concentrations in 520M carbon steel under cathodic protection in 0.5 M NaCl and the effect of added sulphite, dithionite, thiosulphate, and sulphide. *International Journal of Electrochemical Science*, 2 (1) (2007) 82-92.
- [166] J. Song, W.A. Curtin. A nanoscale mechanism of hydrogen embrittlement in metals. *Acta Mater* 2011;59(4):1557–1569.

- [167] Haftbaradaran H, Song J, Curtin WA, Gao H. J. Continuum and atomistic models of strongly coupled diffusion, stress, and solute concentration. *Journal of Power Sources*, 2011;196(1):361–370.
- [168] J. Song, W.A. Curtin. Atomic mechanism and prediction of hydrogen embrittlement in iron. *Nature Materials*, 2013;12(2):145–51.
- [169] Shyyuan-Fang Chen, Robert P Wei. Environmentally assisted crack growth in a Ni-18Cr-18Fe ternary alloy at elevated temperatures. *Materials Science and Engineering A*, Vol. 256, Issue 1-2, 1998, pp. 197-207.
- [170] T. Bellahcene, J. Capelle, M. Aberkane, Z. Azari. Effect of hydrogen on mechanical properties of pipeline API 5L X70 steel. *Applied Mechanics and Materials*, Vol. 146 (2012) pp. 213-225.
- [171] Zuhair Mattoug Gasem. Frequency dependent environmental fatigue crack propagation in the 7XXX alloy/aqueous chloride system. PhD thesis, University of Virginia, May 1999.